UNIVERSITY OF CALIFORNIA,
IRVINE

Structural and functional consequences of PTEN deletion in mature circuits of the adult central nervous system

DISSERTATION

submitted in partial satisfaction of the requirements
for the degree of

DOCTOR OF PHILOSOPHY

in Biomedical Sciences

by

Jennifer Marie Yonan

Dissertation Committee:
Professor Oswald Steward, Chair
Professor Christine Gall
Associate Professor Robert Hunt
Professor Richard T. Robertson
Professor Marcelo Wood
Professor Karina Cramer

2022

DEDICATION

To

My loving parents, amazing husband, incredible brother, and wonderful family and friends.

In recognition of your unconditional support,
enthusiastic encouragement,
and unmatched belief in my dreams and aspirations.

You are my strength and my happiness.

For

Nana Agustina Luevano & Nana Juliet Yonan

TABLE OF CONTENTS

LIST OF FIGURES

LIST OF TABLES

ACKNOWLEDGMENTS

I would like to express my deepest appreciation and gratitude to my mentor and committee chair, Oswald Steward. To say that you are the reason I am able to pursue my dreams is an understatement. Thank you for your unwavering support since the very beginning. Your mentorship and enthusiastic approach to science is unmatched. Whether it's writing an abstract or manuscript, preparing for a presentation, designing an experiment, or simply looking at slides at the microscope, your passion and curiosity for science and teaching always shines through. You have made my graduate experience amazing. Thank you for helping me become a better scientist. It is an honor to have worked with you. Thank you for taking a chance on me, I hope to make you proud in the years to come.

I would like to thank my committee members Professor Christine Gall, Associate Professor Robert Hunt, Professor Richard T. Robertson, Professor Marcelo Wood, and Professor Karina Cramer. Thank you for your valuable input, hard hitting questions, and thought-provoking discussions throughout my graduate training. Each of your unique perspectives and expertise has expanded my breadth of knowledge and helped me become a better scientist.

Additionally, thank you to my collaborator, Professor Tallie Z. Baram. Your enthusiastic help during my graduate training afforded me the opportunity to extend my research beyond what was initially possible. Thank you for your valuable input and guidance.

I would also like to thank Dr. Marlene de la Cruz from UCI's Minority Science Programs. Your constant support throughout my undergraduate and graduate years has helped me to see that my dreams of a higher education were possible.

Thank you to my parents, Hamlet and Eva, for always believing in me. Thank you for always encouraging my educational pursuits and being the strongest support system that anyone could ever ask for. There is no way that I could have made it to this point without your love and dedication. It is your drive and determination that I look to as an example for my own life. Thank you to my older brother, David, for always challenging and believing in me. You are one of the most hard-working and intelligent people I know. I will always look up to you. Thank you to my grandmothers, Augustina Luevano and Juliet Yonan, who are hands down the strongest and most courageous women out there. Our family would not have had this incredible life or opportunity to pursue our dreams had it not been for your bravery.

Finally, thank you to my husband, Greg, who has been by my side from start to finish throughout this process. Thank you for your constant support and encouragement. You have seen me through all the highs and lows, celebrations and tears. Thank you for being my rock. Thank you for being my best friend. I'm excited to see what the future has in store for us.

This work was supported in part by a T32 Epilepsy Training grant (5T32 NS045540), an R01 Diversity Supplemental (R01 NS108189), and the Graduate Dean's Dissertation Fellowship.

VITA

Jennifer Marie Yonan

EDUCATION

2022 **Doctor of Philosophy · Biomedical Sciences**
Department of Anatomy and Neurobiology
University of California, Irvine

2018 **Master of Science · Neuroscience**
Neuroscience Graduate Program
University of California, Riverside

2011 **Bachelor of Science · Biological Sciences**
University of California, Irvine

2007 **High School Diploma**
Salesian High School, Richmond, California

RESEARCH EXPERIENCE

2019 – 2022 **Ph.D. Graduate Student Researcher**
Department of Anatomy and Neurobiology · University of California, Irvine
Principle Investigator: Oswald Steward, Ph.D.
Thesis: Structural and functional consequences of PTEN deletion in mature circuits of the adult central nervous system

2014 – 2018 **M.S. Graduate Student Researcher**
Neuroscience Graduate Program · University of California, Riverside
Principle Investigator: Devin Binder, M.D., Ph.D.
Project title: Functional role of edema formation following spinal cord injury

2016 **Spinal Cord Injury Training Program (SCITP) Research Trainee**
Ohio State University Wexner Medical Center

2011 – 2014 **Research Assistant**
Reeve Irvine Research Center · University of California, Irvine
Principle Investigator: Oswald Steward, Ph.D.
Research topic: Spinal cord injury and regeneration.

2010 – 2011 **Undergraduate Researcher**
Department of Anatomy and Neurobiology • University of California, Irvine
Principle Investigator: Oswald Steward, Ph.D.
Mentor: Melissa K. Strong, Ph.D.
Project title: Resistance to excitotoxic cell death in FVB/N mice carrying a Huntington's Disease transgene

FELLOWSHIPS AND SCHOLARSHIPS

2022 **Graduate Dean's Dissertation Fellowship**
University of California, Irvine

2020 – 2022 **R01 Diversity Supplemental Fellowship**
Grant R01 NS108189
University of California, Irvine

2019 – 2020 **T32 Epilepsy Training Fellowship**
Grant 5T32 NS045540
University of California, Irvine

2014 - 2016 **Eugene Cota-Robles Diversity Fellowship**
University of California, Riverside

2010 - 2011 **Minority Access for Research Careers (MARC) Scholar**
National Institute of Health (NIH) Diversity funded Scholarship
University of California, Irvine

2010 **Minority Biomedical Research Support (MBRS) Scholar**
National Institute of Health (NIH) Diversity funded Scholarship
University of California, Irvine

TEACHING AND MENTORING EXPERIENCE

2020 **Undergraduate Research Mentor**
Minority Science Program, Bridges to Baccalaureate
University of California, Irvine
Rosanna Burgos Pujols

2019 **Undergraduate Research Mentor**
Minority Science Program, Bridges to Baccalaureate
University of California, Irvine
Jennifer Aranda

2018 **Undergraduate Research Mentor**
University of California, Riverside
Terese Garcia

2017 – 2018 **Undergraduate Research Mentor**
University of California, Riverside
Raymond Smith

2016 – 2017 **Undergraduate Research Mentor**
University of California, Riverside
Kristina Rodriguez

LEADERSHIP & COMMITTEE MEMBERSHIP

2019 – 2022 **Brews & Brains Science Communication Group**
University of California, Irvine
Leadership team

2017- 2018 **Neuroscience Graduate Student Association**
University of California, Riverside
Vice President

2015- 2017 **Neuroscience Graduate Student Association**
University of California, Riverside
Outreach Chair

2015 **Association for Women in Science (AWIS)**
University of California, Riverside
Outreach Committee

2014 – 2015 **Neuroscience Graduate Student Association**
University of California, Riverside
Member

PUBLICATIONS

Steward, O., **Yonan, J.M.**, Falk, P.M., The curious anti-pathology of the *Wld^S* mutation: paradoxical postsynaptic spine growth accompanies delayed presynaptic Wallerian degeneration. Frontiers in Molecular Neuroscience. 2021; 14: 735919.

Steward, O., Coulibay, A.P., Metcalfe, M., **Yonan, J.M.**, and Yee, K.M. AAVshRNA-mediated PTEN knockdown in adult neurons attenuates activity-dependent kinase activation and immediate early gene induction. Experimental Neurology. 2020; 326: 113098.

Yonan, J.M.*, Hale, C.*, Batarseh, R., Chaar, R., Jonak, C.R., Ge, S., Binder, D.K., Rodgers, V.G.J. Implantable osmotic transport device can reduce edema after severe contusion spinal cord injury. Front Bioeng Biotechnol. 2020; 8: 806.

Hale, C., Bhakta, H.C., Jonak, C.R., **Yonan, J.M.**, Binder, D.K., Grover, W.H., and Rodgers, V.G.J. Differential densimetry: a method for determining ultra-low fluid flux and tissue permeability. AIP Advances. 2019; 9: 1-7.

Hubbard, J.A., Szu, J.I., **Yonan, J.M.**, and Binder, D.K. Regulation of astrocytic glutamate transporter-1 (GLT1) and aquaporin-4 (AQP4) expression in a model of epilepsy. Experimental Neurology. 2016; 283: 85-96.

Yonan, J.M., and Binder, D.K. Aquaporin-4 and spinal cord injury. World Journal of Neurology. 2016; 6(1):1-13.

Strong, M.K., Southwell, A.L., **Yonan, J.M.**, Hayden, M.R., MacGregor, G.R., Thompson, L.M., and Steward, O. Age-dependent resistance to excitotoxicity in Htt CAG140 mice and the effect of strain background. Journal of Huntington's Disease. 2012; 221-241.

Yonan, J.M. Resistance to excitotoxic cell death in FVB/N mice carrying a Huntington's Disease transgene. University of California, Irvine Journal of Undergraduate Research. 2011.

ABSTRACTS AND POSTERS

Yonan, J.M., Chen, K., Baram, T.Z., Steward, O., Conditional PTEN deletion in the adult dentate gyrus triggers robust *de novo* growth of granule cells and the formation of a seizure prone circuit. Poster, Society for Neuroscience Annual Conference. Virtual Conference. November 8-16, 2021.

Pujols, R.B., **Yonan, J.M.**, Steward, O., Effects of vector-mediated PTEN deletion on neurogenesis in the adult dentate gyrus. Poster, ABRCMS Annual Conference. Virtual conference. November 10-13, 2021.

Yonan, J.M., Steward, O. AAV-mediated conditional PTEN deletion in adult dentate granule cells triggers robust *de novo* growth without disruption of connectional specificity. Poster, Society for Neuroscience Global Connectome. Virtual conference. January 11-13, 2021.

Yonan, J.M., Yee, K.M., Steward, O. *De novo* growth of adult dentate granule neurons triggered by PTEN deletion does not lead to disruption of connectional specificity. Poster, Cold Spring Harbor Molecular Mechanisms of Neuronal Connectivity Conference. Virtual conference. September 8-11, 2020.

Yonan, J.M., Metcalfe, M., Yee, K.M., Steward, O. Retrograde transfection and PTEN deletion in adult cortical motoneurons results in rapid *de novo* neuronal growth. Poster, International Symposium on Neural Regeneration Annual Conference. Asilomar, California. January 26-30, 2020.

Yonan, J.M., Yee, K.M., Steward, O. Vector-mediated PTEN deletion in adult dentate granule cells triggers de novo growth without apparent adverse consequences. Poster, Society for Neuroscience Annual Conference. Chicago, Illinois. October 19-23, 2019.

Luo, J. Yee, K.M., Mizufuka, J., **Yonan, J.M.**, Metcalfe, M., Gunawan, A. Steward, O. Selective activation of the cells of origin in the corticospinal tract using a 2-vector system for selective expression of DREADDS. Poster, Society for Neuroscience Annual Conference. Chicago, Illinois. October 19-23, 2019.

Yonan, J.M. and Steward, O. Harnessing retrograde AAV to assess *de novo* growth of adult cortical neurons following PTEN deletion. Poster, National Neurotrauma Society Symposium, Pittsburgh, Pennsylvania. June 29 - July 3, 2019.

Yonan, J.M. and Steward, O. Harnessing retrograde AAV to assess *de novo* growth of adult cortical neurons following PTEN deletion. Poster, EpiCenter Symposium, University of California, Irvine. February 26, 2019.

Yonan, J.M., Hale, C. Rodgers, V., Binder, D.K. Direct osmotherapy for the reduction of edema following spinal cord injury. Poster, Center for Glial and Neuronal Interactions Annual Symposium. Riverside, California. March 28, 2018.

Yonan, J.M., Hale, C. Rodgers, V., Binder, D.K. Direct osmotherapy for the reduction of edema following spinal cord injury. Poster, Society for Neuroscience Annual Conference. Washington D.C. November 11-15, 2017.

Hale, C., **Yonan, J.M.,** Binder, D.K., and Rodgers, V. Osmotic transport device to alleviate tissue swelling following spinal cord injury. Poster, Biomedical Engineering Society Annual Meeting. Pheonix, Arizona. October 11-14, 2017.

Hubbard, J. A., Szu, J.L., **Yonan, J.M.,** and Binder, D.K. Regulation of astrocyte glutamate reporter-1 (GLT-1) and aquaporin-4 (AQP4) expression in a model of epilepsy. Poster, Center for Glial and Neuronal Interactions Annual Symposium. University of California, Riverside. January 8, 2016.

Hubbard, J. A., Szu, J.L., **Yonan, J.M.,** and Binder, D.K. Astrocytic cell changes in a model of epilepsy. Poster, Annual Biochemistry and Molecular Biology Symposium. University of California, Riverside. September 18, 2015.

Hubbard, J. A., Szu, J.L., **Yonan, J.M.,** and Binder, D.K. Regulation of hippocampal glutamate transporter-1 (GLT-1) expression in the intrahippocampal kainic acid model

of epileptogenesis. Poster, Center for Glial and Neuronal Interactions Annual Symposium. University of California, Riverside. January 9, 2015.

Strong, M.K., **Yonan, J.M.**, and Steward, O. Resistance to excitotoxic cell death in the CAG140 mouse model on a vulnerable strain background: changes in gene expression. Poster, Gordon Research Seminar and Gordon Research Conference: CAG Triplet Repeat Disorders. June 4-10, 2011.

Yonan J.M. Resistance to excitotoxic cell death in FVB/N mice carrying a Huntington's Disease transgene. Poster and Presentation, Excellence in Research Symposium. University of California, Irvine. May 2011.

Yonan, J.M., Strong, M.K., and Steward, O. Time course of neuronal death following quinolinic acid treatment in mice carrying a Huntington's disease transgene. Poster, AAAS National Conference, Washington D.C. February 17-21, 2011.

Strong, M.K., **Yonan, J.M.**, and Steward, O. Cell intrinsic mechanism of resistance to excitotoxicity induced neurodegeneration in aged FVB/N mice carrying a Huntington's disease transgene. Poster, Society for Neuroscience Annual Meeting. San Diego, California, November 13-17, 2010.

Yonan, J.M., Strong, M.K, and Steward, O. Time course of neuronal death following quinolinic acid treatment in mice carrying a Huntington's disease transgene. Poster, Sigma Xi Conference. Raleigh, North Carolina. November 11-14, 2010.

Strong, M.K., **Yonan, J.M.**, and Steward, O. Resistance to kainic acid induced neurodegeneration in FVB/n mice carrying a Huntington's disease transgene. Poster, EpiCenter meeting, University of California, Irvine. April 27, 2010

PROFESSIONAL AFFILIATIONS

Since 2014 **Society for Neuroscience**

Since 2010 **Sigma Xi: The Scientific Research Society**

Since 2010 **Minority Sciences Program**
University of California, Irvine

HONORS & AWARDS

2022 **Latino Excellence and Achievement Award (LEAD)**
School of Medicine Awardee
University of California, Irvine

2020 **Anatomy & Neurobiology Grad Day 2020 Best Presentation**
University of California, Irvine

2019 **School of Medicine Ph.D. Student Travel Stipend Award**
University of California, Irvine

2019 **School of Medicine Grad Day 2019 Travel Award**
University of California, Irvine

2019 **Diversity Travel Grant Award**
National Neurotrauma Society Symposium

2011 **Excellence in Research**
University of California, Irvine

2010 **Sigma Xi - Superior Presenter**
Student Poster Competition
Sigma Xi: The Scientific Research Society

Spring 2008 **Dean's Honor List**
University of California, Irvine

Spring 2010 **Dean's Honor List**
University of California, Irvine

Spring 2011 **Dean's Honor List**
University of California, Irvine

TEACHING AND OUTREACH

2011 – 2014 **Meet the Scientist** · Reeve-Irvine Research Center
2019 – 2022 Aided in the execution of tours and data presentations provided to the public in order to introduce those interested to current and future research regarding spinal cord injury and therapeutic means of intervention.

2016 – 2018 **MECCA Project** · University of California, Riverside
Mentor and tutor high school students from Thermal, California, a school district with one of the lowest graduation rates and number of students attending college.

2015 – 2018 **Brain Awareness Day** · University of California, Riverside
An interactive day for local high students and undergraduates to be introduced to the Neuroscience field: includes poster presentations and hands on demonstrations of current research being conducted at UCR.

July 2013 **Summer Trek Camp** · Reeve-Irvine Research Center
Assisted with an all-day interactive experience for 30 high school girls interested in future careers in science.

July 2013 **Summer Trek Camp** · Reeve-Irvine Research Center
Assisted in teaching a class of pre-med high school students about research design in the context of spinal cord injury research. Topics included: brain and spinal cord anatomy, genetic and pharmacological interventions, and robotic devices for rehabilitation.

April 2005 **El Oratorio Salesiano** · Tijuana, Mexico
Traveled to impoverished schools and orphanages over a two-week period remodeling classrooms and teaching young children math and English

ABSTRACT OF THE DISSERTATION

Structural and functional consequences of PTEN deletion in mature circuits of the adult central nervous system

By

Jennifer Marie Yonan

Doctor of Philosophy in Biomedical Sciences

University of California, Irvine, 2022

Professor Oswald Steward, Chair

Phosphatase and tensin homolog (PTEN) is an important negative regulator of the mechanistic target of rapamycin (mTOR) pathway responsible for cell growth during development. Previous studies have documented that both embryonic and early postnatal PTEN deletion results in neuronal hypertrophy, formation of aberrant circuitry, seizures, and high mortality rates. We have recently documented that intracortical PTEN deletion in uninjured adult neurons triggers progressive growth of cell bodies and dendrites, without any obvious adverse consequences. In Chapter 2, we expand these results to include increases in cell and nuclear sizes following targeted PTEN deletion in thousands of mature cortical motoneurons utilizing a novel retrograde vector that, when injected into the spinal cord, is transported back to the cell bodies of neurons that give rise to the corticospinal tract. Still, the consequences of PTEN deletion, persistent mTOR activation, and growth of mature neurons within established circuits of the adult brain are not fully understood.

The present study explores the structural, circuit, and functional consequences of PTEN deletion in mature granule cells of the dentate gyrus in adult mice. The dentate gyrus and

hippocampus are an ideal model to study such effects due to its precise organization and highly specific laminar pattern of its inputs and outputs. PTEN was deleted in adult PTEN-floxed, ROSA-reporter mice through unilateral, intra-dentate injections of AAV-Cre. In this model, Cre transduces granule cells focally, resulting in PTEN deletion and tdTomato expression in the same cells. Focal PTEN deletion in this model is advantageous as it allows for targeted PTEN deletion in granule cells, while preserving PTEN expression in granule cell input neurons and target cells.

In Chapter 3, we show that cell body size of PTEN deleted granule cells increased gradually by 2 months after injection and progressed out to 6 months, with significant growth occurring sooner in more densely transduced regions. Increases in soma size was accompanied by increases in molecular layer thickness by 4 and 6 months after AAV-Cre injection. Quantitative assessment of Golgi-stained granule cells at 6 months post deletion revealed increases in dendritic length, dendrite caliber, and spine densities in the inner, middle, and outer molecular layers, with many spines exhibiting an immature morphology. Thus, postsynaptic dendritic growth was sufficient to trigger the formation of new synapses by input pathways in which PTEN expression was preserved. Despite substantial growth of apical dendrites, tract tracing of perforant path and commissural projections from the entorhinal cortex and contralateral hippocampus to PTEN deleted granule cells revealed that the laminated pattern of input to the inner and middle molecular layers was maintained. Additionally, axonal projections from PTEN-deleted granule cells appropriately projected to, but expanded their terminal field in the CA3, suggesting increased connectivity onto PTEN expressing target neurons. Supra-granular mossy fibers were seen in some mice at long post-injection time points.

Chapter 4 present experiments that assess if the initiation and maintenance of progressive growth in mature neurons is dependent on sustained mTOR activity. Prolonged rapamycin treatment reduced the phosphorylation of ribosomal protein S6 in PTEN deleted granule cells, suggesting effective inhibition of downstream mTOR activity. Rapamycin administration during the acute period after PTEN deletion (0-2 months) prevented growth of cell bodies, while delayed rapamycin administration from 2 to 4 months after AAV-Cre injection prevented dendritic and axonal growth, prevented the occurrence of supragranular mossy fibers, and reversed increases in soma size.

To assess for altered function in mice with Cre-mediated PTEN deletion in adulthood, in Chapter 5 mice underwent continuous video electroencephalogram (EEG) recordings. Monitoring revealed onset of electrographic and behavioral seizures beyond 2 months after PTEN deletion, suggesting a critical period for circuit modification, with evidence of occasional death during a seizure. Our results indicate that PTEN deletion in mature granule cells triggers a dramatic growth phenotype that is dependent on mTOR activation, that growth of granule cell processes is sufficient to increase connectivity with PTEN expressing inputs and target cells, that the fundamental specificity of hippocampal connectivity is largely maintained, and that even unilateral focal deletion of PTEN in the dentate gyrus of adult mice is sufficient to result in the development of spontaneous seizures. Together, these results reveal the potential of PTEN deletion to induce plasticity in mature neuronal populations and established brain circuits, and that loss of PTEN can influence functional outcomes in the adult central nervous system.

Chapter 1:

Introduction

"Once the development was ended, the founts of growth and regeneration of the axons and dendrites dried up irrevocably. In the adult centers, the nerve paths are something fixed, ended, and immutable. Everything may die, nothing may be regenerated. It is for the science of the future to change, if possible, this harsh decree." *-Ramón y Cajal, 1914*

For many years, it was believed that the adult brain was fixed and that mature neurons in the central nervous system (CNS) were incapable of growth or recovery following injury or disease. This was in stark contrast to the regenerative ability of younger neurons and neural networks. In the case of spinal cord injury, it is well established that neurons have a limited ability to regenerate due to both a non-permissive extrinsic environment that arises after injury and a loss of intrinsic regenerative ability that occurs after development (Kaplan et al., 2015). Methods used to recapitulate development in mature systems have proven to be advantageous for recovery. In 2008, a paper by Dr. Zhigang He and collogues was the first to report that genetic deletion of the phosphatase and tensin homolog (PTEN) gene in an optic nerve crush model led to increased neuronal survival and striking regeneration of retinal ganglion cells following injury in young adult mice (Park et al., 2008).

PTEN is protein and lipid phosphatase that has been identified as an important negative regulator of the mechanistic target of rapamycin (mTOR) pathway responsible for cell growth and proliferation during development. As a serine-threonine kinase, mTOR functions

in response to intracellular and extracellular stimuli to target components of translational machinery, eIF4E binding protein 1 (4EBP1) and ribosomal protein S6 kinase 1 (S6K1), and regulate critical protein translation (Ma & Blenis, 2009). PTEN functions upstream of mTOR in opposition to phosphoinositide 3 kinase (PI3K) activity, influencing the activity of other downstream effectors including AKT, and preventing downstream activation of mTOR (Switon et al., 2017). Deletion of PTEN therefore results in activation of the mTOR pathway.

Since the initial report in retinal ganglion cells, both our lab and others have shown that PTEN deletion and knockdown in cortical motoneurons triggers notable axon regeneration and functional improvements following both cervical and thoracic spinal cord injury. Early postnatal PTEN deletion and knockdown in the cortex at one day after birth in mice has been reported to result in extensive axon regeneration following spinal cord injury in adulthood (Liu et al., 2010; Zukor et al., 2013). Along similar lines, short hair pin ribonucleic acid (shRNA)-mediated PTEN knockdown in adult rats done days before an injury produced axon regeneration and forelimb functional recovery (Lewandowski & Steward, 2014). In these cases, mTOR activation at early postnatal periods, or even prior to an injury, might be expected to prime the system for later recovery.

Testing the potential of PTEN deletion as a therapeutic intervention, deletion immediately after an injury showed similar therapeutic benefits (Danilov & Steward, 2015). Even delayed PTEN deletion out to one year after injury had regenerative effects on corticospinal tract axons, although functional outcomes in this study were not assessed (Du et al., 2015).

Together, these approaches function to re-engage the intrinsic growth capacity of mature neurons in adulthood.

While PTEN deletion in cortical motoneurons and subsequent mTOR activation at early postnatal periods and in adulthood have proven beneficial in spinal cord injury animal models, one must not forget that appropriately balanced mTOR signaling is important for normal brain development in humans. Mutations in genes involved in mTOR signaling during development have been implicated in various neurological disorders, termed TORopathies (Switon et al., 2017). These mutations often involve dysregulation of upstream mTOR effectors, like PTEN. Features of inherited or embryonic PTEN mutations in humans include focal cortical dysplasia, macrocephaly, autism, seizures, and reduced mental capability (Adachi et al., 2018; Conti et al., 2012; Jansen et al., 2015; Ronzano et al., 2022; Tilot et al., 2015; Zahedi Abghari et al., 2019).

Various developmental models have been established in rodents to recapitulate and understand the development of disease in humans. In initial studies, it was discovered that PTEN is critical for embryonic development, where complete loss of PTEN results in embryonic lethality (Di Cristofano et al., 1998). Germline PTEN haploinsufficient mice have further shown brain-wide macrocephaly with behavioral outcomes reminiscent to those found in autism spectrum disorders, including impaired social interactions, anxiety, mood disorders, and learning and memory deficits (Clipperton-Allen & Page, 2014). This same study performed *in situ* hybridization to examine PTEN expression across brain regions and throughout development in both mouse and human tissue. In either case, PTEN expression

was fairly similar across all major brain regions and was highly expressed at both embryonic and postnatal periods. These results emphasize the importance of PTEN's role throughout development and during aging.

Transgenic mouse models that allow for promoter-driven, Cre/Lox-mediated PTEN deletion at various embryonic and postnatal stages during development have allowed for better delineation of cause and effect in broader (Table 1.1) and more targeted (Table 1.2 and 1.3) neuronal populations. Among the first models were those that utilized glial fibrillary acidic protein (GFAP) and neuron specific (NS) promotor-driven Cre expression in PTEN-floxed mice. These models result in broad PTEN deletion in neurons of the hippocampus, cortex, and cerebellum (Backman et al., 2001; Kwon et al., 2003; Kwon et al., 2001; Lugo et al., 2014; Sunnen et al., 2011), as well as in astrocytes throughout multiple brain regions (Fraser et al., 2008; Fraser et al., 2004). While the identified timing of either Cre expression or PTEN deletion varied across studies (embryonic vs. postnatal periods), the earliest report of Cre expression was documented at embryonic day (E) 14.5 (Fraser et al., 2004) and GFAP expression has been reported as early as E13.5 (Brenner et al., 1994), suggesting that GFAP/NS-driven deletion represents a model of embryonic PTEN deletion. Collectively, these studies report macrocephaly, neuronal hypertrophy, and altered lamination within the three regions. Common across all studies was the prevalence of progressive seizures in PTEN deleted mice developing between 4- and 10- weeks of age, resulting in high mortality rates.

Further multi-structure PTEN deletion has been investigated using neuron specific enolase (Nse)-driven Cre expression for targeting of differentiated neurons in the cortex and

hippocampus (Haws et al., 2014; Kwon et al., 2006; Ogawa et al., 2007; Takeuchi et al., 2013; Zhou et al., 2009). Again, while the earliest period of PTEN deletion was reported by 2 weeks of age (Kwon et al., 2006), Nse expression has been documented as soon as E12.5 (Forss-Petter et al., 1990). Like results found in GFAP/NS models, embryonic PTEN deletion triggered macrocephaly, hypertrophy of neuronal cell bodies, and seizures. These reports expand these results to include hypertrophy of dendrites and mossy fiber axons on granule cells within the dentate gyrus, the presence of ectopic processes within the hilus, and increased spine densities along dendritic arbors. Physiological consequences include age-related impairments in synaptic plasticity (long term potentiation and depression) at perforant path projections from the entorhinal cortex to the dentate gyrus that are suggested to underly abnormal behavioral outcomes (Takeuchi et al., 2013). As a results of these studies, the hippocampus, and especially the proliferation of granule cells within the dentate gyrus have become a major focus for further investigation.

At early postnatal periods (Table 1.2), promotor-driven PTEN deletion specifically in young adult neural stem cells (Amiri et al., 2012) and collections of newborn progenitors and immature neurons (Matsushita et al., 2016) within the hippocampus exhibit enlarged hippocampi, altered excitatory-inhibitory balance, disrupted proliferation and differentiation, and seizures. Inducible methods to delete PTEN in newborn neurons using direct retroviral-Cre injections into the dentate gyrus (Table 1.3) have also reported hypertrophic effects on neuronal cell bodies and processes (Getz et al., 2016; Skelton et al., 2019; Williams et al., 2015). Williams et al. assessed the morphological and physiological consequences of PTEN deletion following injections of retroviral-Cre at p7 and collection at

various time points within a month after injection. This timepoint is critical as it signifies a period of elevated granule cell neurogenesis in the postnatal period (Bond et al., 2020). In addition to neuronal hypertrophy, this study reports increases in membrane capacitance and reduced input resistance that would otherwise be expected to lower the responsiveness of larger cells. Studies of perforant path stimulation revealed that while more current was required to trigger an action potential in granule cells, this occurred at more hyperpolarized membrane potentials compared to PTEN expressing cells. The authors suggest that this increased sensitivity to synaptic input could be attributed to the notable increases in mushroom spine density and synapse number along more complex dendritic arbors (Williams et al., 2015).

In a similar paradigm, Skelton et al. report increases in spine densities and number of presynaptic partners that are dependent on the density of PTEN deletion. Specifically, the more sparse the deletion the greater the increase in dendritic spines on PTEN deleted cells. This is attributed to reduced competition for connectivity experienced by newborn, PTEN deleted granule cells when developing amongst neighboring wild type granule cells compared to the competition that might occur for synaptic partners in more densely PTEN deleted regions (Skelton et al., 2019).

Recent studies from Dr. Steve Danzer and collogues (Table 1.2) have reported that tamoxifen-induced PTEN deletion at postnatal day 14 specifically in Gli1-expressing, adult-born granule cells of the dentate gyrus are sufficient to cause neuronal hypertrophy, aberrant hyperexcitable circuitry, and morphological features reminiscent of temporal lobe

epilepsy (Arafa et al., 2019; LaSarge et al., 2016; LaSarge et al., 2015; Pun et al., 2012; Santos et al., 2017). These studies proposed that a minimum of 9% PTEN deletion in granule cells is all that is required to cause epilepsy and increased mortality *in vivo*. Further physiological assessment revealed that perforant path stimulation in PTEN knockout slices results in increased field excitatory post-synaptic potentials (fEPSP), decreased inhibition, reduced population spike thresholds, a propensity to produce multiple population spikes, and impaired facilitation to paired pulses (LaSarge et al., 2016; Santos et al., 2017). They were also among the first to propose a link between the extend of PTEN deletion and the severity of resulting morphological and behavioral outcomes. Together these data indicate that, in early life, promotor-driven models, PTEN deletion in newborn and immature neurons results in alterations to network connectivity that trigger increased excitability within the developing dentate gyrus.

In contrast to developmental PTEN deletion, less is known about the consequences of PTEN deletion in fully mature neurons. Luikart et al. were the first to directly address this gap using shRNA-mediated PTEN knockdown in mice at p7 and in adulthood (Luikart et al., 2011). Early postnatally injected mice were assessed at 14 days and 4 months post injection. Anatomical assessment was in agreement with previous reports, including enlarged somata, increased dendrite caliber, and increased spine densities within two weeks after injection. Curiously, these granule cells presented with thinner, filopodia-like protrusions. By 4 months post injection, the authors report maintenance of the aforementioned features, and including increased mossy fiber axon thickness and bouton volume. In a second cohort of mice, injections occurred between 6 and 8 weeks of age, followed by histological analysis at

14 days and 4 months post injection. In contrast to early postnatal PTEN deletion, anatomical changes were not noted until later timepoints, suggesting slower onset of morphological change in adulthood. Again, larger cells presented with increased capacitance and reduced input resistance. Similar to anatomical timelines, physiological alterations were more delayed in adults compared to young mice, showing increases in excitatory postsynaptic currents, with no difference in measures of inhibitory postsynaptic currents.

Similarly, Haws et al. knocked down PTEN expression in neurons of the basolateral amygdala of 7-week-old mice (Haws et al., 2014). At 3 weeks post injection, the authors report increases in soma sizes without any changes to dendrite length. In vast contrast to previous reports, Haws et al. report a decrease in spine densities along dendrite arbors. More detailed morphological assessments instead revealed increases in the number of more mature, mushroom shaped spines and decreases in thin spine number. Additionally, no behavioral abnormalities were noted in these mice. These results are curious and may perhaps be attributed to the brief post-inject period at which they completed their assessments. While both Luikart et al. and Haws et al. provide important information regarding anatomical changes and synaptic function in more mature brain structures, they do not directly assess alterations to local and long-distance connectivity, nor how such changes might affect whole circuit function.

Given the therapeutic potential of PTEN deletion following injury to the mature central nervous system, our lab sought out to investigate the long-term consequences of PTEN loss in the brain. In the first round of investigation, mice received injections of AAV-Cre into the

sensorimotor cortex at postnatal day 1 for vector-mediated PTEN deletion in cortical motoneurons of PTEN-floxed mice. At 18 months post deletion, anatomical assessments revealed that PTEN deleted neurons exhibited dramatic growth of cell bodies, with no effect on mortality or obvious neuropathology (Gutilla et al., 2016).

As a follow up, the same model of vector-mediated PTEN deletion done in the mature, fully developed motor cortex elicited a new wave of neuronal growth characterized by progressive increases in soma size and dendritic complexity as far as 15 months after deletion, with improvements in motor learning over time (Gallent & Steward, 2018). Growth was notably slower than that documented in previously discussed developmental PTEN deletion models, suggesting a reduced ability for growth in mature systems. This time course of morphological change in young vs. adult systems is in agreement with that suggested by (Luikart et al., 2011). More recently, we have expanded these results to include growth of cortical motoneuron cell bodies and nuclei in the adult rat following shRNA-mediated PTEN knockdown (Steward et al., 2020). These results are further extended on in Chapter 2 utilizing a novel retrograde virus injected into the spinal cord of adult PTEN-floxed mice for more targeted PTEN deletion in mature layer V cortical motoneurons. Collectively, these studies have revealed that modulation of PTEN expression in cortical motoneurons at both developmental and mature stages does result in neuronal growth but does not appear to negatively alter lifespan or function. Similar to previously described models of PTEN deletion in the adult brain, we did not directly assess alterations to connectivity or function in mature systems using our vector-mediated approach.

The possibility of growth in mature neural networks goes against the initial notion of a "fixed" and "immutable" system that was once the standard. It is now more accepted that the adult brain has the potential for substantial change given appropriate intervention. Still, the consequences of PTEN deletion, long term mTOR activation, and growth of mature neurons is largely unexplored.

The proposed dissertation aims to investigate the structural, circuit, and functional consequences of PTEN deletion in the mature central nervous system. Specifically, we investigate the effects of vector-mediated PTEN deletion in the hippocampal dentate gyrus of adult mice. The dentate gyrus and hippocampus are an ideal model to study such effects due to their precise organization and highly specific laminar pattern of its inputs and outputs. Additionally, focal PTEN deletion in the mature dentate gyrus allows for preservation of PTEN expression in granule cell input neurons and target cells.

In Chapter 3 we show that PTEN deletion in mature granule cells of the dentate gyrus triggers progressive growth of cell bodies, dendrites, and axons. This reveals that PTEN loss initiates a growth program in mature neurons regardless of cell type. Increases in dendrite length and spine densities as well as expansion of mossy fiber axons suggest increased connectivity with PTEN expressing pre- and postsynaptic partners. Despite striking growth of neuronal processes, patterns of local and long-distance connectivity to and from the dentate gyrus are maintained. The studies in Chapter 4 provide evidence for the reliance of initiation and maintenance of growth of mature neurons on sustained mTOR activation. Results show that chronic administration of the mTOR inhibitor, rapamycin, can prevent and reverse several

aspects of PTEN deletion-induced growth. Finally, the studies in Chapter 5 investigate the functional outcomes of PTEN deletion in mature circuits. Specifically, long term video and electroencephalogram (EEG) recordings reveal that unilateral PTEN deletion in mature granule cells is sufficient to trigger the formation of a seizure-prone circuit in adulthood. Together, these results uncover the potential plasticity of mature neuronal populations and established brain circuits, and reveal that loss of PTEN can influence functional outcomes in the adult central nervous system.

Table 1.1:

Embryonic & early postnatal promoter-driven, multi-structure PTEN deletion models

References	Strain/ Promoter	Target structure/ cell type	Average survival	Morphological changes	Physiological Changes	Behavior
Backman et al. 2001	$PTEN^{f/f}$ x GFAP-Cre (report PTEN deletion at 4 weeks)	DG, cortex, cerebellum (neurons)	3-29 weeks	Macrocephaly, Dysplasia in cerebellum and dentate gyrus, ↑ Soma size		Seizures and ataxia by 9 weeks
Kwon et al. 2001	$PTEN^{f/f}$ x GFAP-Cre (report Cre at p5-14)	DG, cortex, cerebellum (neurons)	9-48 weeks	Macrocephaly, Altered cerebellar lamination, ↑ Soma size in dentate gyrus and cerebellum		Seizures by 7-10 weeks
Kwon et al. 2003	$PTEN^{f/f}$ x GFAP-Cre	DG, cortex, cerebellum (neurons)	8 weeks	↑ Soma and nuclear size in dentate gyrus and cerebellum		Seizures
Fraser et al. 2004	$PTEN^{f/f}$ x GFAP-Cre (report Cre expression in astrocytes at E14.5)	DG, cortex, cerebellum (neurons and astrocytes)	40% died by p50	Macrocephaly, Altered lamination in hippocampus and cerebellum, ↑ Soma and nuclear size in cortex, hippocampus and cerebellum, ↑ Astrocyte proliferation		Seizures by 10 weeks in 20% of mice, Ataxia
Fraser et al. 2008	$PTEN^{f/f}$ x GFAP-Cre	DG, cortex, cerebellum (neurons and astrocytes)	10+ weeks old	↑ Soma and nuclear size, ↑ Mitochondrial size, ↑ Ribosome density, ↑ Nucleolar size, ↑ Dendrite caliber, ↑ Spine density, ↑ Presynaptic terminal size with more vesicles, ↑ Axon size and myelin thickness	CA3-CA1 synapses: Impaired fEPSPs, normal PPR, decreased LTP	

Ljungberg et al. 2009	PTEN$^{f/f}$x GFAP/NS-Cre	DG, cortex, cerebellum (neurons)	Premature mortality in hom., normal in het.	Macrocephaly, ↑ Soma size in cortex		Seizures by 6 weeks
Sunnen et al. 2011	PTEN$^{f/f}$x GFAP/NS-Cre	DG, cortex, cerebellum (neurons)	7-25 weeks	Supragranular mossy fibers		Seizures by 4 weeks
Lugo et al. 2014	PTEN$^{f/f}$x GFAP/NS-Cre	DG, cortex, cerebellum (neurons)	Survived to endpoint (8-9 weeks)		↓ mGluR5 and Kv4.2, ↑ FMRP	↓ Social interaction, Repetitive behavior deficits, Hyperactivity, ↓ Anxiety
Kwon et al. 2006	PTEN$^{f/f}$x Nse-Cre (report PTEN deletion at 2 weeks)	Cortex, CA3, dentate gyrus (differentiated neurons)	Normal lifespan up to 10 months	Macrocephaly, ↑ Soma size in cortex, DG and CA3 ↑ Mossy fiber track thickness, Supragranular mossy fibers (w/ more presynaptic vesicles), ↑ Length and caliber of dendrites in DG, ↑ Spine density, Ectopic processes in hilus		Seizures, ↓ Social interaction, maternal care, and learning, ↑ Activity under stress, Anxiety
Ogawa et al. 2007	PTEN$^{f/f}$x Nse-Cre	Cortex, CA3, dentate gyrus (differentiated neurons)	Survived to endpoint (13-33 weeks old)	Macrocephaly, ↑ Soma size, DG granule cell dispersion		Seizures, ↑ Irritability/ aggression, ↑ Locomotion and wheel running
Zhou et al. 2009	PTEN$^{f/f}$x Nse-Cre (report Cre activity between 2-4 weeks)	Cortex, CA3, dentate gyrus (differentiated neurons)	Survived to endpoint (10-18 weeks old)	Macrocephaly, ↑ Soma and nuclear size, ↑ Axon thickness and dendritic length, Supragranular mossy fibers, ↑ Spine density		Seizures, ↑ Anxiety, ↓ Social interaction

Takeuchi et al. 2013	PTEN$^{f/f}$x Nse-Cre (report Cre activity by 4 weeks)	Cortex, CA3, dentate gyrus (differentiated neurons)	Survived to endpoint (8-30 weeks)	↑ Spine density at middle age, ↑ Soma size, ↑ Mossy fiber axon thickness	MPP to DG synapses: Normal input/output (fEPSP vs. stimulus intensity) in young and old, increased in middle age, Normal PPR in young and old, decreased in middle age, ↑ LTP in young but impaired in middle age and old, impaired LTD at all ages, CA3-CA1 synapses: Normal basal transmission, Impaired LTP in middle age, Normal LTD	
Haws et al. 2014	PTEN$^{f/f}$x Nse-Cre	Cortex, CA3, dentate gyrus (differentiated neurons)	Survived to endpoint (6months)	↑ Dendrite diameter, ↑ Spine head diameter, No change in spine density, ↑ Mushroom spine number		
Chow et al. 2009	PTEN$^{f/f}$x CamKII-Cre	Cortical layer II/III	Survived to endpoint (4 months)	↑ Apical dendrite length and tortuosity, Normal spine density, Normal basal dendrites, Normal layer V dendrites		
Sperow et al. 2012	PTEN$^{f/f}$x CamKII-Cre (report PTEN deletion by p14)	Hippocampus	9-11 weeks	No change in soma, nuclear, or dendritic sizes at 8 weeks, No change in spine density, synapse morphology, or vesicle numbers	CA3-CA1 synapse at 8 wks: Normal basal synaptic transmission (normal fEPSP, PPR), ↓ LTP and LTD Normal AMPAR/NMDAR ratio and mEPSCs	Normal spatial learning, ↓ Spatial memory
Kazdoba et al. 2012	PTEN$^{f/f}$x NEX-Cre	Cortex, hippocampus (early postmitotic excitatory neurons)	Normal lifespan in het out to 2 weeks, hom. died by 1 week	Macrocephaly, ↑ Soma size		

Note: GFAP expression begins around E13.5 (Brenner et al., 1994), Nse expression begins around E12.5 (Forss-Petter et al., 1990), CamKII expression begins around p4 (Burgin et al., 1990), and NEX expression begins around E11.5 (Goebbels et al., 2006)

Table 1.2:

Early postnatal promoter-driven, cell type-specific PTEN deletion models

References	Strain/ Promoter	Target structure/ cell type	Average Survival	Morphological changes	Physiological Changes	Behavior
Amiri et al. 2012	$PTEN^{f/f}$ x Nestin-CreERT2 (tamoxifen at 1 month)	Dentate gyrus (postnatal/ young adult NSC)	Survived to endpoint (4-7 months)	↑ Soma size, Disorganized dentate gyrus, ↑ Mossy fiber tract thickness, ↑ Dendrite length, ↑ Proliferation, Accelerated differentiation		Seizures, ↓ Social interaction
Matsushita et al. 2016	$PTEN^{f/f}$ x Pomc-Cre	Dentate gyrus (newborn progenitors and immature neurons)	10 weeks	↑ Size of dentate gyrus, No change in proliferation but disrupted differentiation, ↑ Soma size, ↑ Dendritic length, Supragranular mossy fibers	↑ cFOS, ↑ Excitatory synapse markers, ↓ Inhibitory neuron markers	Seizures by 8 weeks, Rigid posture, ↑ Startle response
Pun et al. 2012	$PTEN^{f/f}$ x Gli1-CreERT2 (tamoxifen at p14)	Dentate gyrus (adult born granule cells)	2.2 months	↑ Soma size, Basal dendrites, ↑ Spine density, Ectopic cells, Supragranular mossy fibers		Seizures within 4 weeks of tamoxifen
La Sarge et al. 2015	$PTEN^{f/f}$ x Gli1-CreERT2 (tamoxifen at p14)	Dentate gyrus (adult born granule cells)	Survived to endpoint (6 weeks – 9 months)	↑ Mossy fiber thickness, Dual axon collaterals to CA3, Normal bouton volume, More boutons with greater spacing		
La Sarge et al. 2016	$PTEN^{f/f}$ x Gli1-CreERT2 (tamoxifen at p14)	Dentate gyrus (adult born granule cells)	Survived to endpoint (2-5 months)	Supragranular mossy fibers (not required for functional outcomes)	↑ fEPSP, ↑ Evoked population spikes, Multiple population spikes, Impaired paired pulse facilitation	

Santos et al. 2017	$PTEN^{f/f}$ x Gli1-CreERT2 (tamoxifen at p14)	Dentate gyrus (adult born granule cells)	Survived to endpoint (2-6 months)	↑ Soma size, ↑ Dendrite length and branching, Basal dendrites, Basal dendrite-originating axons	↓ Input resistance, No change in inward and outward currents (Na and K currents unchanged at soma), ↑ Burst firing, ↑ EPSCs, ↓ IPSCs, Multiple population spikes	
Arafa et al. 2019	$PTEN^{f/f}$ x Gli1-CreERT2 (tamoxifen at p21)	Dentate gyrus (adult born granule cells)	Survived to endpoint (2-5 months)	↑ Soma size, ↑ Apical dendrite length and complexity, Basal dendrites		

Table 1.3:

Early postnatal and adult vector-mediated PTEN deletion models

References	Strain/ Vector	Target structure/ cell type	Average Survival	Morphological changes	Physiological Changes	Behavior
Williams et al. 2015	$PTEN^{f/f}$, Retro-Cre (injected at p7)	Dentate gyrus (newborn neurons)	Survived to endpoint (7.5-24.5 days post Cre)	↑ Soma size, ↑ Dendrite length, caliber and complexity, ↑ Spine density (mushroom spines), ↑ Synapse number	↑ Neuronal activity (pS6, cFOS), ↑ Capacitance, ↓ Input resistance, More current to reach AP but at more hyperpolarized membrane potentials, ↑ Sensitivity to PP stimulation, ↑ EPSC, normal IPSC, normal PPR	
Getz et al. 2016	$PTEN^{f/f}$, Retro-Cre (injected at p7)	Dentate gyrus (newborn neurons)	Survived to endpoint (7.5-24.5 days post Cre)	↑ Migration of newborn neurons into granule cell layer, ↑ Soma size		
Skelton et al. 2019	$PTEN^{f/f}$, AAV-Cre or Retro-Cre (injected at p7)	Dentate gyrus (granule cells and/or newborn neurons)	Survived to endpoint (24 days post Cre)	↑ Soma size, ↑ Dendrite branching, ↑ Migration into granule cell layer, ↑ Spine density (higher in sparse vs. dense deletion), Basal dendrites in dense deletion, Normal presynaptic bouton density from entorhinal cortex, ↑ Presynaptic partners	↑ mEPSC in sparse deletion, ↑ Light evoked EPSCs from entorhinal cortex and contralateral hilus	
Luikart et al. 2011	C57Bl/6, LV-shPTEN (injected at p7 and 6-8 weeks)	Dentate gyrus (neurons)	Survived to endpoint (14 days – 4 months post shPTEN)	↑ Soma size, ↑ Dendrite diameter and spine densities (thin), ↑ Mossy fiber axon thickness and bouton volume, Slower onset in adult mice	↑ Capacitance, ↓ Input resistance, ↑ sEPSC and mEPSC, normal sIPSC and mIPSC	

Xiong et al. 2012	PTEN$^{f/f}$, AAV-Cre (injected at p18-21)	Auditory cortex (layer II-VI pyramidal neurons)	Survived to endpoint (p30-45)	↑ Dendrite length and branching, ↑ Spine density	Normal resting membrane potential and spike threshold, ↓ Input resistance, ↑ Local and long-distance inputs (light evoked EPSCs)	
Haws et al. 2014	C57Bl/6, AAV-shPTEN (injected at 7 weeks)	Basolateral amygdala (neurons)	Survived to endpoint (10 weeks)	↑ Soma size, Normal dendrite length, ↑ Dendrite diameter, No change in spine density, ↑ Mushroom spine number and head diameter	↑ mEPSC	Normal anxiety, social interaction, learning and locomotion
Gutilla et al. 2016	PTEN$^{f/f}$, AAV-Cre (injected at p1)	Cortex (neurons)	Survived to endpoint (14 months)	↑ Cortical thickness, ↑ Soma size		Normal function on rotorod and open field
Gallent and Steward, 2018	PTEN$^{f/f}$, AAV-Cre (injected at 8+ weeks)	Cortex (neurons)	Survived to endpoint (3-15 months post Cre)	↑ Soma size, ↑ Dendrite arborization and caliber, ↑ Axon diameter		Impaired coordination with unilateral deletion, Improved motor learning with bilateral deletion (rotorod)

REFERENCES

Adachi, T., Takigawa, H., Nomura, T., Watanabe, Y., & Kowa, H. (2018, Jan 1). Cowden Syndrome with a Novel PTEN Mutation Presenting with Partial Epilepsy Related to Focal Cortical Dysplasia. *Intern Med, 57*(1), 97-99. https://doi.org/10.2169/internalmedicine.9052-17

Amiri, A., Cho, W., Zhou, J., Birnbaum, S. G., Sinton, C. M., McKay, R. M., & Parada, L. F. (2012, Apr 25). Pten deletion in adult hippocampal neural stem/progenitor cells causes cellular abnormalities and alters neurogenesis. *J Neurosci, 32*(17), 5880-5890. https://doi.org/10.1523/JNEUROSCI.5462-11.2012

Arafa, S. R., LaSarge, C. L., Pun, R. Y. K., Khademi, S., & Danzer, S. C. (2019, Jan). Self-reinforcing effects of mTOR hyperactive neurons on dendritic growth. *Exp Neurol, 311*, 125-134. https://doi.org/10.1016/j.expneurol.2018.09.019

Backman, S. A., Stambolic, V., Suzuki, A., Haight, J., Elia, A., Pretorius, J., Tsao, M. S., Shannon, P., Bolon, B., Ivy, G. O., & Mak, T. W. (2001, Dec). Deletion of Pten in mouse brain causes seizures, ataxia and defects in soma size resembling Lhermitte-Duclos disease. *Nat Genet, 29*(4), 396-403. https://doi.org/10.1038/ng782

Bond, A. M., Berg, D. A., Lee, S., Garcia-Epelboim, A. S., Adusumilli, V. S., Ming, G. L., & Song, H. (2020, Nov 26). Differential Timing and Coordination of Neurogenesis and Astrogenesis in Developing Mouse Hippocampal Subregions. *Brain Sci, 10*(12). https://doi.org/10.3390/brainsci10120909

Brenner, M., Kisseberth, W. C., Su, Y., Besnard, F., & Messing, A. (1994, Mar). GFAP promoter directs astrocyte-specific expression in transgenic mice. *J Neurosci, 14*(3 Pt 1), 1030-1037. https://www.ncbi.nlm.nih.gov/pubmed/8120611

Burgin, K. E., Waxham, M. N., Rickling, S., Westgate, S. A., Mobley, W. C., & Kelly, P. T. (1990, Jun). In situ hybridization histochemistry of Ca2+/calmodulin-dependent protein kinase in developing rat brain. *J Neurosci, 10*(6), 1788-1798. https://www.ncbi.nlm.nih.gov/pubmed/2162385

Chow, D. K., Groszer, M., Pribadi, M., Machniki, M., Carmichael, S. T., Liu, X., & Trachtenberg, J. T. (2009, Feb). Laminar and compartmental regulation of dendritic growth in mature cortex. *Nat Neurosci, 12*(2), 116-118. https://doi.org/10.1038/nn.2255

Clipperton-Allen, A. E., & Page, D. T. (2014, Jul 1). Pten haploinsufficient mice show broad brain overgrowth but selective impairments in autism-relevant behavioral tests. *Hum Mol Genet, 23*(13), 3490-3505. https://doi.org/10.1093/hmg/ddu057

Conti, S., Condo, M., Posar, A., Mari, F., Resta, N., Renieri, A., Neri, I., Patrizi, A., & Parmeggiani, A. (2012, Mar). Phosphatase and tensin homolog (PTEN) gene mutations and autism: literature review and a case report of a patient with Cowden syndrome, autistic disorder, and epilepsy. *J Child Neurol, 27*(3), 392-397. https://doi.org/10.1177/0883073811420296

Danilov, C. A., & Steward, O. (2015, Apr). Conditional genetic deletion of PTEN after a spinal cord injury enhances regenerative growth of CST axons and motor function recovery in mice. *Exp Neurol, 266*, 147-160. https://doi.org/10.1016/j.expneurol.2015.02.012

Di Cristofano, A., Pesce, B., Cordon-Cardo, C., & Pandolfi, P. P. (1998). Pten is essential for embryonic development and tumour suppression. *Nature Genetics, 19*(4), 348-355. https://doi.org/10.1038/1235

Du, K., Zheng, S., Zhang, Q., Li, S., Gao, X., Wang, J., Jiang, L., & Liu, K. (2015, Jul 1). Pten Deletion Promotes Regrowth of Corticospinal Tract Axons 1 Year after Spinal Cord Injury. *J Neurosci, 35*(26), 9754-9763. https://doi.org/10.1523/JNEUROSCI.3637-14.2015

Forss-Petter, S., Danielson, P. E., Catsicas, S., Battenberg, E., Price, J., Nerenberg, M., & Sutcliffe, J. G. (1990, Aug). Transgenic mice expressing beta-galactosidase in mature neurons under neuron-specific enolase promoter control. *Neuron, 5*(2), 187-197. https://doi.org/10.1016/0896-6273(90)90308-3

Fraser, M. M., Bayazitov, I. T., Zakharenko, S. S., & Baker, S. J. (2008, Jan 24). Phosphatase and tensin homolog, deleted on chromosome 10 deficiency in brain causes defects in synaptic structure, transmission and plasticity, and myelination abnormalities. *Neuroscience, 151*(2), 476-488. https://doi.org/10.1016/j.neuroscience.2007.10.048

Fraser, M. M., Zhu, X., Kwon, C. H., Uhlmann, E. J., Gutmann, D. H., & Baker, S. J. (2004, Nov 1). Pten loss causes hypertrophy and increased proliferation of astrocytes in vivo. *Cancer Res, 64*(21), 7773-7779. https://doi.org/10.1158/0008-5472.CAN-04-2487

Gallent, E. A., & Steward, O. (2018, May). Neuronal PTEN deletion in adult cortical neurons triggers progressive growth of cell bodies, dendrites, and axons. *Exp Neurol, 303*, 12-28. https://doi.org/10.1016/j.expneurol.2018.01.005

Getz, S. A., DeSpenza, T., Jr., Li, M., & Luikart, B. W. (2016, Sep). Rapamycin prevents, but does not reverse, aberrant migration in Pten knockout neurons. *Neurobiol Dis, 93*, 12-20. https://doi.org/10.1016/j.nbd.2016.03.010

Goebbels, S., Bormuth, I., Bode, U., Hermanson, O., Schwab, M. H., & Nave, K. A. (2006, Dec). Genetic targeting of principal neurons in neocortex and hippocampus of NEX-Cre mice. *Genesis, 44*(12), 611-621. https://doi.org/10.1002/dvg.20256

Gutilla, E. A., Buyukozturk, M. M., & Steward, O. (2016, May). Long-term consequences of conditional genetic deletion of PTEN in the sensorimotor cortex of neonatal mice. *Exp Neurol, 279*, 27-39. https://doi.org/10.1016/j.expneurol.2016.02.013

Haws, M. E., Jaramillo, T. C., Espinosa, F., Widman, A. J., Stuber, G. D., Sparta, D. R., Tye, K. M., Russo, S. J., Parada, L. F., Stavarache, M., Kaplitt, M., Bonci, A., & Powell, C. M. (2014, Apr 1). PTEN knockdown alters dendritic spine/protrusion morphology, not density. *J Comp Neurol, 522*(5), 1171-1190. https://doi.org/10.1002/cne.23488

Jansen, L. A., Mirzaa, G. M., Ishak, G. E., O'Roak, B. J., Hiatt, J. B., Roden, W. H., Gunter, S. A., Christian, S. L., Collins, S., Adams, C., Riviere, J. B., St-Onge, J., Ojemann, J. G., Shendure, J., Hevner, R. F., & Dobyns, W. B. (2015, Jun). PI3K/AKT pathway mutations cause a spectrum of brain malformations from megalencephaly to focal cortical dysplasia. *Brain, 138*(Pt 6), 1613-1628. https://doi.org/10.1093/brain/awv045

Kaplan, A., Ong Tone, S., & Fournier, A. E. (2015). Extrinsic and intrinsic regulation of axon regeneration at a crossroads. *Front Mol Neurosci, 8*, 27. https://doi.org/10.3389/fnmol.2015.00027

Kazdoba, T. M., Sunnen, C. N., Crowell, B., Lee, G. H., Anderson, A. E., & D'Arcangelo, G. (2012). Development and characterization of NEX- Pten, a novel forebrain excitatory neuron-specific knockout mouse. *Dev Neurosci, 34*(2-3), 198-209. https://doi.org/10.1159/000337229

Kwon, C. H., Luikart, B. W., Powell, C. M., Zhou, J., Matheny, S. A., Zhang, W., Li, Y., Baker, S. J., & Parada, L. F. (2006, May 4). Pten regulates neuronal arborization and social interaction in mice. *Neuron, 50*(3), 377-388. https://doi.org/10.1016/j.neuron.2006.03.023

Kwon, C. H., Zhu, X., Zhang, J., & Baker, S. J. (2003, Oct 28). mTor is required for hypertrophy of Pten-deficient neuronal soma in vivo. *Proc Natl Acad Sci U S A, 100*(22), 12923-12928. https://doi.org/10.1073/pnas.2132711100

Kwon, C. H., Zhu, X., Zhang, J., Knoop, L. L., Tharp, R., Smeyne, R. J., Eberhart, C. G., Burger, P. C., & Baker, S. J. (2001, Dec). Pten regulates neuronal soma size: a mouse model of Lhermitte-Duclos disease. *Nat Genet, 29*(4), 404-411. https://doi.org/10.1038/ng781

LaSarge, C. L., Pun, R. Y., Muntifering, M. B., & Danzer, S. C. (2016, Dec). Disrupted hippocampal network physiology following PTEN deletion from newborn dentate granule cells. *Neurobiol Dis, 96*, 105-114. https://doi.org/10.1016/j.nbd.2016.09.004

LaSarge, C. L., Santos, V. R., & Danzer, S. C. (2015, Mar). PTEN deletion from adult-generated dentate granule cells disrupts granule cell mossy fiber axon structure. *Neurobiol Dis, 75*, 142-150. https://doi.org/10.1016/j.nbd.2014.12.029

Lewandowski, G., & Steward, O. (2014, Jul 23). AAVshRNA-mediated suppression of PTEN in adult rats in combination with salmon fibrin administration enables regenerative growth of corticospinal axons and enhances recovery of voluntary motor function after cervical spinal cord injury. *J Neurosci, 34*(30), 9951-9962. https://doi.org/10.1523/JNEUROSCI.1996-14.2014

Liu, K., Lu, Y., Lee, J. K., Samara, R., Willenberg, R., Sears-Kraxberger, I., Tedeschi, A., Park, K. K., Jin, D., Cai, B., Xu, B., Connolly, L., Steward, O., Zheng, B., & He, Z. (2010, Sep). PTEN deletion enhances the regenerative ability of adult corticospinal neurons. *Nat Neurosci, 13*(9), 1075-1081. https://doi.org/10.1038/nn.2603

Ljungberg, M. C., Sunnen, C. N., Lugo, J. N., Anderson, A. E., & D'Arcangelo, G. (2009, Jul-Aug). Rapamycin suppresses seizures and neuronal hypertrophy in a mouse model of cortical dysplasia. *Dis Model Mech, 2*(7-8), 389-398. https://doi.org/10.1242/dmm.002386

Lugo, J. N., Smith, G. D., Arbuckle, E. P., White, J., Holley, A. J., Floruta, C. M., Ahmed, N., Gomez, M. C., & Okonkwo, O. (2014). Deletion of PTEN produces autism-like behavioral deficits and alterations in synaptic proteins. *Front Mol Neurosci, 7*, 27. https://doi.org/10.3389/fnmol.2014.00027

Luikart, B. W., Schnell, E., Washburn, E. K., Bensen, A. L., Tovar, K. R., & Westbrook, G. L. (2011, Mar 16). Pten knockdown in vivo increases excitatory drive onto dentate granule cells. *J Neurosci, 31*(11), 4345-4354. https://doi.org/10.1523/JNEUROSCI.0061-11.2011

Ma, X. M., & Blenis, J. (2009, May). Molecular mechanisms of mTOR-mediated translational control. *Nat Rev Mol Cell Biol, 10*(5), 307-318. https://doi.org/10.1038/nrm2672

Matsushita, Y., Sakai, Y., Shimmura, M., Shigeto, H., Nishio, M., Akamine, S., Sanefuji, M., Ishizaki, Y., Torisu, H., Nakabeppu, Y., Suzuki, A., Takada, H., & Hara, T. (2016, Mar 10). Hyperactive mTOR signals in the proopiomelanocortin-expressing hippocampal neurons cause age-dependent epilepsy and premature death in mice. *Sci Rep, 6*, 22991. https://doi.org/10.1038/srep22991

Ogawa, S., Kwon, C. H., Zhou, J., Koovakkattu, D., Parada, L. F., & Sinton, C. M. (2007, Sep 7). A seizure-prone phenotype is associated with altered free-running rhythm in Pten mutant mice. *Brain Res, 1168*, 112-123. https://doi.org/10.1016/j.brainres.2007.06.074

Park, K. K., Liu, K., Hu, Y., Smith, P. D., Wang, C., Cai, B., Xu, B., Connolly, L., Kramvis, I., Sahin, M., & He, Z. (2008, Nov 7). Promoting axon regeneration in the adult CNS by modulation of the PTEN/mTOR pathway. *Science, 322*(5903), 963-966. https://doi.org/10.1126/science.1161566

Pun, R. Y., Rolle, I. J., Lasarge, C. L., Hosford, B. E., Rosen, J. M., Uhl, J. D., Schmeltzer, S. N., Faulkner, C., Bronson, S. L., Murphy, B. L., Richards, D. A., Holland, K. D., & Danzer, S. C. (2012, Sep 20). Excessive activation of mTOR in postnatally generated granule cells is sufficient to cause epilepsy. *Neuron, 75*(6), 1022-1034. https://doi.org/10.1016/j.neuron.2012.08.002

Ronzano, N., Scala, M., Abiusi, E., Contaldo, I., Leoni, C., Vari, M. S., Pisano, T., Battaglia, D., Genuardi, M., Elia, M., Striano, P., & Pruna, D. (2022, Aug). Phosphatase and tensin homolog (PTEN) variants and epilepsy: A multicenter case series. *Seizure, 100*, 82-86. https://doi.org/10.1016/j.seizure.2022.06.013

Santos, V. R., Pun, R. Y. K., Arafa, S. R., LaSarge, C. L., Rowley, S., Khademi, S., Bouley, T., Holland, K. D., Garcia-Cairasco, N., & Danzer, S. C. (2017, Dec). PTEN deletion increases hippocampal granule cell excitability in male and female mice. *Neurobiol Dis, 108*, 339-351. https://doi.org/10.1016/j.nbd.2017.08.014

Skelton, P. D., Frazel, P. W., Lee, D., Suh, H., & Luikart, B. W. (2019, Nov). Pten loss results in inappropriate excitatory connectivity. *Mol Psychiatry, 24*(11), 1627-1640. https://doi.org/10.1038/s41380-019-0412-6

Sperow, M., Berry, R. B., Bayazitov, I. T., Zhu, G., Baker, S. J., & Zakharenko, S. S. (2012, Feb 15). Phosphatase and tensin homologue (PTEN) regulates synaptic plasticity independently of its effect on neuronal morphology and migration. *J Physiol, 590*(4), 777-792. https://doi.org/10.1113/jphysiol.2011.220236

Steward, O., Coulibaly, A. P., Metcalfe, M., Yonan, J. M., & Yee, K. M. (2020, Apr). AAVshRNA-mediated PTEN knockdown in adult neurons attenuates activity-dependent immediate early gene induction. *Exp Neurol, 326*, 113098. https://doi.org/10.1016/j.expneurol.2019.113098

Sunnen, C. N., Brewster, A. L., Lugo, J. N., Vanegas, F., Turcios, E., Mukhi, S., Parghi, D., D'Arcangelo, G., & Anderson, A. E. (2011, Nov). Inhibition of the mammalian target of rapamycin blocks epilepsy progression in NS-Pten conditional knockout mice. *Epilepsia, 52*(11), 2065-2075. https://doi.org/10.1111/j.1528-1167.2011.03280.x

Switon, K., Kotulska, K., Janusz-Kaminska, A., Zmorzynska, J., & Jaworski, J. (2017, Jan 26). Molecular neurobiology of mTOR. *Neuroscience, 341*, 112-153. https://doi.org/10.1016/j.neuroscience.2016.11.017

Takeuchi, K., Gertner, M. J., Zhou, J., Parada, L. F., Bennett, M. V., & Zukin, R. S. (2013, Mar 19). Dysregulation of synaptic plasticity precedes appearance of morphological defects in a Pten conditional knockout mouse model of autism. *Proc Natl Acad Sci U S A, 110*(12), 4738-4743. https://doi.org/10.1073/pnas.1222803110

Tilot, A. K., Frazier, T. W., 2nd, & Eng, C. (2015, Jul). Balancing Proliferation and Connectivity in PTEN-associated Autism Spectrum Disorder. *Neurotherapeutics, 12*(3), 609-619. https://doi.org/10.1007/s13311-015-0356-8

Williams, M. R., DeSpenza, T., Jr., Li, M., Gulledge, A. T., & Luikart, B. W. (2015, Jan 21). Hyperactivity of newborn Pten knock-out neurons results from increased excitatory synaptic drive. *J Neurosci, 35*(3), 943-959. https://doi.org/10.1523/JNEUROSCI.3144-14.2015

Xiong, Q., Oviedo, H. V., Trotman, L. C., & Zador, A. M. (2012, Feb 1). PTEN regulation of local and long-range connections in mouse auditory cortex. *J Neurosci, 32*(5), 1643-1652. https://doi.org/10.1523/JNEUROSCI.4480-11.2012

Zahedi Abghari, F., Moradi, Y., & Akouchekian, M. (2019). PTEN gene mutations in patients with macrocephaly and classic autism: A systematic review. *Med J Islam Repub Iran, 33*, 10. https://doi.org/10.34171/mjiri.33.10

Zhou, J., Blundell, J., Ogawa, S., Kwon, C. H., Zhang, W., Sinton, C., Powell, C. M., & Parada, L. F. (2009, Feb 11). Pharmacological inhibition of mTORC1 suppresses anatomical, cellular, and behavioral abnormalities in neural-specific Pten knock-out mice. *J Neurosci, 29*(6), 1773-1783. https://doi.org/10.1523/JNEUROSCI.5685-08.2009

Zukor, K., Belin, S., Wang, C., Keelan, N., Wang, X., & He, Z. (2013, Sep 25). Short hairpin RNA against PTEN enhances regenerative growth of corticospinal tract axons after spinal cord injury. *J Neurosci, 33*(39), 15350-15361. https://doi.org/10.1523/JNEUROSCI.2510-13.2013

CHAPTER 2:

Intraspinal injection of retrograde AAV vectors to delete PTEN in uninjured adult cortical motoneurons triggers dramatic neuronal growth, but fails to transduce injured CST axons

Data on cortical motoneuron growth in rats (Figure 2) were included in a paper published in *Experimental Neurology* in 2020 as: Oswald Steward, Aminata P. Coulibaly, Mariajose Metcalfe, Jennifer M. Yonan, Kelly M. Yee. "AAV-shRNA-mediated PTEN knockdown in adult neurons attenuates activity-dependent immediate early gene induction." *Experimental Neurology.* 326 (2020): 113098.

ABSTRACT

Phosphatase and tensin homolog (PTEN) is a key negative regulator of the mechanistic target of rapamycin (mTOR) pathway responsible for cell growth and proliferation during development. Modulation of PTEN expression using intracortical vector-mediated approaches has been shown to trigger axon regeneration and improve functional recovery after spinal cord injury, while inducing cell growth of uninjured neurons in adulthood. One caveat is the focal nature of intracortical injections which result in transduction of various cells throughout cortical laminae and limited transduction of target layer V cortical

motoneurons throughout the sensorimotor cortex that project to the corticospinal tract. Here we explore the ability of a novel retrograde vector to specifically transduce cortical motoneurons and assess alterations to neuronal morphology in uninjured and injured neurons. PTEN deletion was accomplished by injecting retrograde AAV-Cre into the spinal cord of double transgenic mice with lox-P sites flanking exon 5 of the PTEN gene and stop/flox tdTomato in the Rosa locus ($PTEN^{f/f}/ROSA^{tdTomato}$). In uninjured mice, transduction resulted in targeted PTEN deletion in layer V cortical motoneurons, progressive increases in neuronal and nuclear size, and increased dendritic caliber. Surprisingly, assessment of transduced neurons from control mice injected with retrograde AAV-Cre immediately after a spinal cord injury showed a lack of injury-induced neuronal atrophy. Further investigation revealed that our retrograde vector is taken up by uninjured axons that terminate rostral to the injury site, but not by transected axons exposed to the vector at the time of injury. These findings document that retrograde deletion of PTEN in uninjured mature cortical motoneurons triggers a wave of targeted neuronal growth, but also highlight unexpected limitations of AAV-retro for targeting cortical neurons whose axons were damaged by a spinal cord injury.

INTRODUCTION

Neurons in the mature central nervous system (CNS) have a limited ability to regenerate and recover following a traumatic event, such as spinal cord injury. This is thought to be due to both a non-permissive extrinsic environment that arises after injury and a loss of intrinsic

regenerative ability that occurs after development (Kaplan et al., 2015). Efforts to identify therapeutic strategies to combat this lack of regeneration have identified the phosphatase and tensin homolog (PTEN) gene as a therapeutic target to enhance intrinsic growth capacity to enable axon regeneration. PTEN is a key negative regulator of the mechanistic target of rapamycin (mTOR) pathway responsible for cell growth and proliferation during development.

In 2008, a study by Zhigang He and collogues was the first to report that conditional genetic deletion of PTEN in an optic nerve crush model led to regeneration of retinal ganglion cells following injury (Park et al., 2008). Since then, intracortical vector-mediated PTEN deletion and knockdown in cortical motoneurons at various time points before and after injury has resulted in notable axon regeneration and functional recovery following both cervical and thoracic spinal cord injury (Danilov & Steward, 2015; Du et al., 2015; Lewandowski & Steward, 2014; Liu et al., 2010; Zukor et al., 2013). Recently, our lab has shown that direct cortical PTEN deletion in adult mice also triggers growth of uninjured cortical neuron cell bodies and increases dendritic arborization, without any obvious long term adverse consequences (Gallent & Steward, 2018). It was previously unknown whether mature neurons that have already undergone normal development could undergo further modification at mature stages.

While the resulting neuronal growth, regeneration, and functional improvements following intracortical vector-mediated PTEN deletion methods are impressive, there are several caveats to this approach. Intracortical injections: 1) can result in cortical injury during

surgery, 2) result in transduction of multiple cell types across all cortical laminae, and 3) transduce only a small number of cortical layer V motoneurons due to the focal nature of injection. Additionally, such approaches only allow for targeting of a single motor pathway at a time, despite the fact that spinal cord injury interrupts many descending and ascending functional and sensory pathways (Metcalfe et al., 2022).

Recently, our lab and others have shown that advances in AAV technology provide a platform to more precisely target multiple spinal pathways. Specifically, intraspinal injections of retrograde AAV-Cre have resulted in impressive and selective transduction of cortical and subcortical motoneurons, dependent on the level of injection (Metcalfe et al., 2022; Steward et al., 2021). This approach allows us to: 1) determine how selective PTEN deletion in uninjured layer V cortical motoneurons influences neuronal morphology and connectivity at the cortical level, 2) characterize how axonal injury influences neuronal cell body structure, 3) determine if PTEN deletion-induced neuronal growth can attenuate spinal cord injury-induced neuronal atrophy, and 4) determine if targeting of multiple descending and ascending neuronal pathways can improve outcomes after spinal cord injury. This report aims to address the first three points.

To address this, we first characterize alterations to neuron morphology using a model with shRNA-mediated PTEN knockdown in adult rats. These published data are included in this chapter because they solidify the concept of inducible growth of adult neurons to include knockdown of PTEN expression rather than deletion, specifically in a rat model. Additionally,

these data serve to highlight some of the caveats that result from intracortical injections previously discussed.

Further, we utilized a remarkable new technology involving AAV vectors that are transported retrogradely from axons within the spinal cord to neuronal cell bodies in the cortex to specifically target cortical motoneurons that give rise to the corticospinal tract (CST). Here, retrograde AAV-Cre was injected into the spinal cord at cervical level 5 (C5) in adult transgenic mice with floxed PTEN and a Cre-dependent reporter gene, stop-flox tdTomato (tdT), referred to as PTEN/tdT mice. Controls were transgenic tdT reporter mice. In both strains, thousands of cortical motoneurons are transduced as evidenced by expression of tdT. Immunostaining revealed effective deletion of PTEN in retrogradely transduced neurons in PTEN/tdT mice with continued PTEN expression in tdT controls. Here, we extend previous observations by reporting that selective PTEN deletion in cortical motoneurons triggers growth of uninjured, mature cortical motoneuron cell bodies, nuclei, and dendrites within the cortex.

Finally, we sought to assess how PTEN deletion-induced neuronal growth influences injury-induced atrophy of cortical motoneurons following spinal cord injury. Surprisingly, we discovered that injections of retrograde AAV-Cre performed immediately rostral to an injury are not taken up by transected axons in either experimental mice or controls, but are instead taken up by uninjured axons that naturally terminate above the lesion. These results point to a need for clearer understanding of the mechanism and capabilities of retrograde vector technology and investigation into the use of novel vector approaches or treatment

paradigms within an injury setting. Further characterization will allow for better understanding of the role of PTEN in neuronal morphology and plasticity and insights into the therapeutic potential of this intervention following injury.

MATERIALS AND METHODS

AAV-shRNA injection into the sensorimotor cortex of adult rats

The AAV-shPTEN vector (serotype AAV2/9) used in the following rat experiments expresses shRNA-PTEN driven by the human U6 promoter and a GFP reporter protein under the CMV promoter (Lewandowski & Steward, 2014; Steward et al., 2020). The vector was constructed by the University of Pennsylvania Vector Core, details on original vector design can be found in (Lewandowski & Steward, 2014).

Experimental animals were adult Fisher 344 rats (n=3). All experimental procedures were approved by the Institutional Animal Care and Use Committee (IACUC) at the University of California, Irvine. For all surgical procedures, rats were anesthetized with Isoflurane (2-3%) and surgical duration was noted. Anesthetized rats were placed in a stereotaxic device. Eyes were covered with Vaseline and the skin above the incision site was shaved and disinfected with Betadine. A scalp incision was made to expose the skull. Small burr holes were created above each injection site. Using a 10µl Hamilton syringe with a pulled glass pipette tip, five separate unilateral AAV-shPTEN-GFP injections were made at +2.5(M/L)/+2.0(A/P), +2.5(M/L)/+1.0(A/P), +2.5(M/L)/0.0(A/P), +3.2(M/L)/+1.0(A/P), and +3.2(M/L)/0.0(A/P)

from bregma at a depth of 0.8mm from the cortical surface. Each injection was 1.0µl in volume (total of approximately 10^9 genome copies). After injection, the incision site was sutured and rats were allowed to recover in a cage placed on top of a 37°C heating pad. Rats survived for 4 months following AAV-shRNA injection.

Tissue preparation and immunohistochemistry for rat studies

At the designated endpoint, rats were euthanized with Fatal Plus and were transcardially perfused with 4% paraformaldehyde. Brains were post-fixed then cryoprotected in 27% sucrose. Coronal brain sections at 480µm intervals were collected using a cryostat. Sections were washed in 1xTBS (100mM Tris, pH 7.4 and 150mM NaCl) then quenched for endogenous peroxidase activity by incubation in 3% H_2O_2 in 1xTBS for 15 minutes. Sections were then washed in 1xTBS and blocked in blocking buffer (1xTBS, 0.3% triton X-100, 5% NDS) for 2 hours at room temperature. Sections were then incubated overnight at room temperature in buffer containing primary antibodies for rabbit anti-PTEN (1:250, Cell Signaling Technology AB-390810), rabbit anti-pS6 Ser235/236 (1:250, Cell Signaling Technology 4858), and mouse anti-NeuN (1:200, Millipore MAB377). Sections were then washed in 1xTBS, incubated for 2 hours in buffer containing biotinylated donkey anti-rabbit IgG (1:250, Jackson ImmunoResearch 711-065-152) and donkey anti-mouse Alexa 555 (1:250, Invitrogen A31570), then washed again. PTEN detection was accomplished through incubation in ABC reagent (Vectastain Elite kit, catalog #PK-6100; Vector Laboratories) and Tyramide-FITC (1:250). Sections stained for rabbit anti-GFP (1:1500, Novus NB600-308) were visualized using Alexa fluor-488 (1:250, Invitrogen A21206). Sections were then

mounted on 0.5% gelatin coated slides and counterstained with Hoechst (1μg/mL). For PTEN and pS6 detection by DAB, sections were incubated in 3,3'-diaminobenzidine (DAB substrate kit, Vector Laboratories, SK-4100), dehydrated through graded ethanols, cleared in xylene, and cover slipped with DPX.

Cortical motoneuron cell size measurements

Three consecutive sections spaced 480μm apart were taken for assessment of cortical motor neuron cross sectional area. Images were taken at 10x on an Olympus AX80 microscope and images were imported into Image J. Sampling was done by identifying a 400x300μm region of interest (ROI) in layer V of the motor cortex within the area of PTEN knockdown. PTEN deletion was confirmed by a lack of co-labeling of PTEN with NeuN. The cross-sectional area of cell bodies and corresponding nuclear size were manually traced beginning at the top left end of the ROI, moving medially until 25 cells were collected. Only neurons with a pyramidal cell shape were included, and whose soma and nuclear borders could be distinguished from surrounding cells. As an intra-animal control, 25 PTEN-expressing cells and their corresponding nuclei were measured on the contralateral cortex using comparable methods. In total, 75 PTEN-deleted and 75 PTEN-expressing neurons were assessed per animal.

Experimental mouse model

Experimental mice were adult $PTEN^{f/f}Rosa^{tdTomato}$ and $Rosa^{tdTomato}$ control mice. Mice were generated by crossing PTEN-floxed mice (RRID: IMSR_JAX:004597) with ROSA reporter mice

with a lox-P flanked STOP cassette in the Rosa locus upstream of a tandem dimer tomato (tdT) fluorescent protein sequence (RRID: IMSR_JAX:007905). The double transgenic strain is designated $PTEN^{f/f}/Rosa^{tdTomato}$. Control mice ($Rosa^{tdTomato}$) only contain the floxed stop cassette before the tdT sequence. All studies involved mice that were homozygous at the transgenic loci. For simplicity, mice will be referred to as PTEN/tdT and tdT, respectively.

AAV-retro/Cre injection into the spinal cord of uninjured adult mice

For all surgical procedures, mice were anesthetized with Isoflurane (2-3%) and surgical duration was noted. Anesthetized mice were placed on a heating pad through the duration of the procedure. Eyes were covered with Vaseline and the skin above the incision site was shaved and disinfected with Betadine. An incision was made above the cervical spinal column and a laminectomy was performed at cervical level 5 (C5). Mice received bilateral injections of AAV-retro/Cre (Addgene viral prep #24593-AAVrg) into the spinal cord at 0.5mm lateral to midline and 0.5mm deep. Each injection was 0.3µl in volume. After injection, the incision site was sutured, and mice were allowed to recover in a cage placed on top of a 37°C heating pad. Mice were allowed to survive for periods of time ranging from 1 month and 1 year post injection (Table 2.1).

Spinal cord injury

For mice undergoing simultaneous spinal cord injury and AAV-retro/Cre injections into the dorsal spinal column, mice were anesthetized under isoflurane, as above. The animals' back

was shaved and disinfected with Betadine and a 1-2cm incision was made above the cervical spinal column. The C5 vertebra was exposed and removed for visualization of the spinal cord. A feather needle (15 degree) was then used to perform a hemisection of the dorsal column for transection of the descending cortical spinal tract. Following injury, animals received injections of AAV-retro/Cre at 1mm rostral to the injury site, as previously described, and allowed to survive for 84 days post SCI and injection (Table 2.2).

A second set of animals underwent a dorsal over hemisection, followed by placement of a gelfoam soaked in 4% Fluorogold (1.0µl) and retrograde AAV-Cre (0.6µl) directly into the transection site. Animals were allowed to survive for 5-7 days post injury before tissue collection (Table 2.2).

Tissue processing and immunohistochemistry

At the designated endpoint, mice were euthanized with Fatal Plus and were transcardially perfused with 4% paraformaldehyde. Brains were post-fixed then cryoprotected in 27% sucrose. Coronal brain sections at 360µm intervals were collected using a cryostat. Sections were washed in 1xTBS (100mM Tris, pH 7.4 and 150mM NaCl) then quenched for endogenous peroxidase activity by incubation in 3% H_2O_2 in 1xTBS for 15 minutes. Sections were then washed in 1xTBS and blocked in blocking buffer (1xTBS, 0.3% triton X-100, 5% NDS) for 2 hours at room temperature. Sections were then incubated overnight at room temperature in buffer containing primary antibodies for rabbit anti-PTEN (1:250, Cell Signaling Technology 9188, RRID: AB_2253290), mouse anti-pS6 (1:250, Cell Signaling

Technology 4858, RRID: AB_916156), or rabbit anti-RFP (1:1000, Rockland 35868). Sections were then washed in 1xTBS, incubated for 2 hours in buffer containing biotinylated donkey anti-rabbit IgG (1:250, Jackson ImmunoResearch 711-065-152), then washed again. PTEN and pS6 detection was accomplished through incubation in ABC reagent (Vectastain Elite kit, catalog #PK-6100; Vector Laboratories) and Tyramide-FITC (1:250). Sections were then mounted on 0.5% gelatin coated slides and counterstained with Hoechst (1μg/mL). For PTEN and pS6 detection by DAB IHC, sections were incubated in 3,3'-diaminobenzidine (DAB substrate kit, Vector Laboratories, SK-4100), dehydrated through graded ethanols, cleared in xylene and cover slipped with DPX.

Cortical motoneuron and nuclear size measurements

Cortical motoneuron soma and nuclear size were assessed in sections using native tdT expression (no IHC) and Hoechst. Images were taken at 10x on an Olympus AX80 microscope and imported into ImageJ FIJI. For the time course study, sampling was done by starting at the lateral end of transduction and moving medially until 50 tdT expressing cells had been measured with their corresponding nuclei. Twenty neurons from experimental mice were selected for quantification of apical dendrite caliber at 1- and 12-months post injection. For the neuronal atrophy study after SCI, a total of 30 cells and their corresponding nuclei were measured. The mean cross-sectional area for PTEN deleted and control groups was determined by first averaging cell size measurements in individual mice, then averaging at each time point within each group so "n" for statistical purposes is number of animals.

Statistical analysis

All data were imported into Graphpad Prism software. Cell body and nuclear sizes were analyzed separately by one way analysis of variance (ANOVA). Combined comparisons were done using two-way ANOVA. Post hoc comparisons were accomplished by Tukey multiple comparisons test.

RESULTS

Successful PTEN knockdown in rats following shPTEN injections into the sensory motor cortex

Unilateral injection of AAV-shPTEN-GFP into the motor cortex of adult rats resulted transduction of the local neuronal population that spanned several laminae within the cortex, including layer V cortical motoneurons as evidence by GFP expression (Fig. 2.1A). Immunohistochemistry confirmed suppression, or knockdown, of PTEN expression within the area of injection and GFP expression compared to the contralateral cortex (Fig. 2.1B). Within the cortex, PTEN-negative "ghost cells" devoid of any labeling were evident within the surrounding neurophil (arrows in Fig. 2.1D vs. PTEN expressing cells in the contralateral cortex, Fig. 2.1C). Immunolabeling for the phosphorylated form of ribosomal protein S6, an indicator of mTOR activation, revealed increased phosphorylation within the area of PTEN deletion (contralateral cortex, arrowheads in Fig. 2.1E vs. ipsilateral cortex, arrows in Fig. 2.1F). This result suggests successful activation of the mTOR pathway in transduced, PTEN-deleted cells.

PTEN knockdown triggers growth of cell bodies of cortical neurons and nuclear enlargement

To determine whether PTEN knockdown via AAV-shPTEN induces neuronal growth in the same way as intra-cortical injections of AAV/Cre in PTEN-floxed mice (Gallent & Steward, 2018), we measured cell body size in three rats at 4 months post AAV-shPTEN injection (AAVshPTEN-GFP). In sections co-stained for PTEN, NeuN and Hoechst, NeuN-positive neurons on the side contralateral to the injection were PTEN-positive (Fig. 2.2A). On the side of the AAV-shPTEN injection, the area of PTEN deletion was evident by the absence of PTEN immunofluorescence with preserved NeuN staining (Fig. 2.2B). Insets show high magnification images of a single NeuN positive neuron expressing PTEN (Fig. 2.2A, inset) and PTEN-depleted, NeuN positive neuron (Fig. 2.2B, inset). The average soma area for PTEN-depleted neurons was almost 2-fold higher than PTEN-expressing neurons (500.12 ± 93.13μm^2 for PTEN-depleted neurons vs. 257.96 ± 37.98μm^2 for PTEN-positive neurons, Fig. 2.2C). There were corresponding increases in average nuclear area (204.13 ± 31.31μm^2 for PTEN-depleted neurons vs. 141.25 ± 20.15μm^2 for PTEN-positive neurons, Fig. 2.2D). Two-way ANOVA revealed an overall significant difference between PTEN-depleted and PTEN-expressing neurons [$F(1,8) = 109$, $p<.0001$]. A plot of soma vs. nuclear size (Fig. 2.2E) reveals clear separation and clustering of PTEN-depleted vs. PTEN expressing neurons. These results confirm that AAVshRNA-mediated PTEN knockdown in rats triggers growth of mature neuronal cell bodies and nuclei.

Retrograde AAV-Cre results in selective transduction of cortical motoneurons

Our lab has recently reported that injection of AAV-Cre unilaterally into the motor cortex of PTEN/tdT mice results in effective deletion of PTEN and expression of tdT in transduced cells (Gallent & Steward, 2018). Similarly, injection of our novel retrograde AAV-Cre into the spinal cord of the same mouse strain results in impressive transduction and tdT expression in a large number of cortical layer V neurons (Metcalfe et al., 2022; Steward et al., 2021).

Figure 2.3 illustrates an example of targeted retrograde transduction of layer V cortical motoneurons following AAV-retro/Cre injections into C5 of the spinal cord in PTEN/tdT (Fig. 2.3D) and tdT control mice (Fig. 2.3A). Although not shown, tdT epifluorescence was evident throughout the sensorimotor cortex. Previous work suggests that injections of this kind are capable of transducing thousands of motoneurons (Steward et al., 2021). Details on patterns of transduction of cortical and subcortical regions following cervical, thoracic, and lumbar injections have been previously described (Metcalfe et al., 2022; Steward et al., 2021).

Effective PTEN deletion and mTOR activation in transduced cortical motoneurons

Retrograde transduction of cortical motoneurons through intraspinal injections of AAV-retro/Cre resulted in bilateral PTEN deletion in PTEN/tdT mice. Immunostaining for PTEN revealed a lack of PTEN expression in tdT positive cells, termed “ghost cells (Fig. 2.3E,F, Fig. 2.4C, see arrows in high magnification panels). PTEN expression was preserved in transduced cortical motoneurons from tdT controls (Fig. 2.3B,C arrow heads in high magnification panels, Fig. 2.4A).

Immunostaining for the phosphorylation of ribosomal protein S6 is used as a downstream marker of mTOR activation. Phosphorylation levels of S6 were increased in layer V cortical motoneurons of PTEN/tdT mice (Fig. 2.4D, see arrowheads in high magnification image) but remained at baseline levels in tdT control mice (Fig. 2.4B). Together, these results confirm that this technique allows for targeted PTEN deletion and mTOR activation specifically in layer V neurons that project to the corticospinal tract.

PTEN deletion in adult cortical motoneurons results in selective growth of somata, nuclei and dendrites

PTEN deletion via AAV-retro/Cre resulted in dramatic and progressive increases in cell body size (see Fig. 2.5A,C vs. 2.5D,F of tdT control and experimental animals collected at 12 months post AAV-retro/Cre injection), in accordance with our previous intracortical PTEN deletion models (Gallent & Steward, 2018). To quantify this, we measured the cross-sectional area of tdT positive cells from PTEN/tdT and tdT control mice at 1, 1.5, 4, and 12 months after AAV-retro/Cre injection (Fig. 2.5G). Measurements from control mice were comparable across time and were therefore combined (353.3 +/- 15.78μm^2). Average cell size was not significantly different from controls at 1 month post injection but was significantly increased by 1.5 (458.3 +/- 21.43μm^2), 4 (511.6 +/- 41.52μm^2), and 12 months (517.8μm^2) post injection. One-way ANOVA revealed a significant difference between groups [$F(4,9) = 29.22$, $p<0.0001$] and Tukey post hoc comparisons were significant from 1.5 to 12 months after injection (see Figure 2.5 legend for details on statistics).

In addition to increases in soma size over time, nuclear sizes were also larger following PTEN deletion compared to nuclei from PTEN-expression cortical motoneurons (Fig. 2.5B vs. 2.5E). Measurements for control nuclei were 161.2 +/- 14.12μm^2 collectively across time. Nuclear sizes were significantly increased at 1.5 (205.5 +/- 6.806μm^2) and 4 months (230.7 +/- 8.403μm^2) after PTEN deletion. Again, one-way ANOVA revealed a significant difference between groups [F (4,9) = 19.67, p=0.0002] and Tukey post hoc comparisons were significant at 1.5 and 4 months after injection (see Figure 2.5 legend for details on statistics). A plot of soma vs. nuclear size (Fig. 2.5I) revealed clear separation of tdT positive cells from PTEN/tdT and control mice.

Increases in cell body and nuclear sizes were accompanied by increased caliber of apical dendrites measured in PTEN/tdT mice collected at one (Fig. 2.6A) and 12 months (Fig. 2.6B) following PTEN deletion. Dendrite caliber was 4.068 +/- 0.654μm at 1 month and increased to 6.736 +/- 1.117μm by 12 months following PTEN deletion (Fig. 2.6C, t-test: df=38, t=9.218, p<0.0001). Importantly, due to the density of cortical labeling with intraspinal injections of retrograde AAV-Cre, measurements on dendritic arborization in this tissue were difficult. Previous reports with intracortical PTEN deletion in adults document increased dendritic complexity of layer II/III pyramidal cells (Gallent & Steward, 2018). It is therefore plausible that similar results are expected with specific layer V PTEN deletion, assuming there are no cell type-specific effects of PTEN deletion in this model.

Injections of AAV-retro/Cre rostral to an injury do not transduce injured axons

Previous studies from our lab suggest that spinal cord injury triggers atrophy of cortical motoneurons between 1 and 4 weeks after injury (Nielson et al., 2011). We were therefore curious whether PTEN deletion induced growth of cortical motoneurons could attenuate injury-induced neuronal atrophy. Accordingly, PTEN/tdT and tdT control mice received injections of AAV-retro/Cre rostral to a C5 dorsal hemisection, immediately after injury (Fig. 2.7A). Mice were then collected at nearly 3 months following injury and injection (Fig. 2.7B), well within the ranges of previously documented cell body growth and atrophy.

Figures 2.7C and 2.7D illustrate examples of tdT labeled cortical motoneurons and DAPI labeled nuclei from PTEN/tdT and tdT control mice, respectively. Unexpectedly, there were no notable quantitative differences between either cell or nuclear sizes between groups, suggesting a surprising lack of atrophy or growth in either group. Measurements from control and experimental animals confirmed this conclusion (Fig. 2.7E) and two-way ANOVA confirmed a lack of significance between groups [$F(1,14) = 0.2715$, $p=0.6104$].

In uninjured animals, intraspinal injections of AAV-retro/Cre are taken up by axon terminals and collaterals that terminate at the spinal injection level (Metcalfe et al., 2022; Steward et al., 2021). Our surprising result led us to wonder whether: 1) transected axons take up viral vectors at the lesion site, or: 2) if AAV-retro/Cre injection rostral to a spinal cord injury is instead solely taken up by axons that normally terminate above the level of the lesion. If so, our measurements showing a lack of atrophy of tdT-positive cortical motoneurons may be

due to the fact that axons from transduced neurons were actually not damaged by the injury because they may have been from uninjured neurons that terminate rostral to the lesion.

To assess these possibilities, we compared retrograde transduction at the injury site by AAV-retro/Cre vs. fluorogold, which is known to be taken up by cut axons. Mice underwent a C5 dorsal over hemisection followed by immediate placement of gelfoam soaked in fluorogold and AAV-retro/Cre directly into the lesion (Fig. 2.8A). Mice were then allowed to survive for 5-7 days following injury (Fig. 2.8B), a time point which has been previously confirmed to show transduction of cortical motoneurons following intraspinal injections of retrograde AAV-Cre (Metcalfe et al., 2022). Remarkably, large numbers of cortical motoneurons were effectively labeled with fluorgold (Fig. 2.8C), but there were no tdT-positive neurons indicating any retrograde transduction by AAV-retro/Cre (Fig. 2.8D). These results provide strong evidence that AAV-retro/Cre is minimally effective at transducing cut axons at an injury site.

DISCUSSION

The goal of this study was to determine whether intraspinal injections of retrograde AAV-Cre would transduce cortical motoneurons with high specificity, characterize how targeted PTEN deletion would alter morphology of a single neuronal population, define how spinal cord injury affects neuronal structure in the brain, and determine if PTEN deletion in injured neurons could attenuate injury-induced cell body atrophy. These objectives were based on

previous reports describing effective retrograde transduction and mapping of cortical and subcortical spinal pathways (Steward et al., 2021; Z. Wang et al., 2018) and successful retrograde transport of gene-modifying vectors (Metcalfe et al., 2022) dependent on the spinal level at which injections were performed. Here, retrograde AAV-Cre was injected into the spinal cord of adult double transgenic PTEN-floxed, ROSA-reporter mice with and without spinal cord injury. Using this model, we first show that retrograde vectors selectively transduce a large population of layer V cortical motoneurons and that PTEN deletion in uninjured neurons triggers progressive growth of cell bodies, nuclei, and dendrites. Further, we document a surprising finding that retrograde AAV-Cre fails to transduce transected axons from injured neurons when injected near the injury site immediately after a spinal cord injury. This latter finding reveals an unanticipated major limitation of AAV-retro/Cre for potential applications to enable regeneration of cut axons with injections in a therapeutically relevant time frame (after an injury).

Intracortical injections target a small population of cortical motoneurons

Intracortical injections of AAV-shRNA into rats has been shown to improve regeneration and functional recovery after spinal cord injury (Lewandowski & Steward, 2014), and here, we document a new feature, that PTEN knockdown in uninjured adult rats results in increased soma and nuclear size. Increases in cell body size in the cortex of adult mice has previously been reported by our lab following intracortical PTEN deletion via intracortical injection of AAV-Cre in PTEN-floxed mice (Gallent & Steward, 2018), but increases in nuclear size, to our knowledge, have only been reported in a model of developmental, brain-wide PTEN deletion

(Fraser et al., 2008). Our initial unpublished observations of gross chromatin structure in nuclei from PTEN expressing granule cells in the adult rat dentate gyrus reveal a euchromatin core surrounded by a heterochromatin border with chromocenters scattered throughout. Conversely, enlarged nuclei in PTEN deleted granule cells show an increased presence of euchromatin that extends to nuclear borders, a reduction in heterochromatin and chromocenters, and increased nucleolar size. These initial observations suggest possible chromatin reorganization in enlarged nuclei following PTEN deletion and probable increased gene expression due to PTEN deletion and mTOR activation that require further investigation.

While intracortical injections of both AAV-Cre in PTEN-floxed mice and AAV-shRNA in rats have been reported to enhance regeneration and motor recovery following spinal cord injury, we highlight several caveats to this approach. We show that focal intracortical injections non-specifically transduce neurons across cortical laminae and only target a small population of layer V cortical motoneurons within the motor cortex. These patterns of transduction emphasize the need for more targeted approaches for spinal cord injury.

Selective transduction and PTEN deletion in cortical motoneurons with intraspinal injection of retrograde AAV-Cre

Injections of retrograde AAV-Cre into the spinal cord of ROSA-reporter mice led to effective and highly targeted transduction of layer V cortical motoneurons. The distribution of transductions is as previously described (Metcalfe et al., 2022; Steward et al., 2021), having

dense labeling in the primary and secondary motor cortices, as well as the primary somatosensory cortex. Delivery of the same viral cargo in PTEN/tdT mice, resulted in selective PTEN deletion in transduced cells, highlighting the potential for targeted, population-specific genetic modification.

Enlargement of cortical motoneuron cell body and nuclear size

The time course of growth reported after targeted PTEN deletion seen here follows a similar time course to our previously documented intracortical PTEN deletion methods (Gallent & Steward, 2018). PTEN deleted pyramidal cells were nearly 150% larger than PTEN expressing pyramidal cells measured from controls at 12 months after transductions. We again document a new feature – that enlargement of cell body size is accompanied by corresponding increases in nuclear size. Nuclear sizes after PTEN deletion increased by roughly 130% at the same timepoint. These results emphasize that regardless of PTEN deletion method, mature neuronal populations are capable of pronounced growth long after development.

Growth of apical dendrites in PTEN-deleted pyramidal neurons

In addition to increases in cell body and nuclear sizes, we document dramatic increases in dendritic caliber. Previous reports from our lab in mature layer II/III cortical motoneurons have shown increased dendritic complexity after intracortical PTEN deletion, even negating the dendritic atrophy that occurs naturally with age (Gallent & Steward, 2018). Due to the

density of labeling that results from retrograde transduction, we were unable to assess dendritic arborization in this model. Injection parameters that result in more diffuse cortical motoneuron labeling or postmortem labeling of individual neurons with biocytin would be required for such morphological assessment. Curiously, in a model of CamKIIa promotor driven PTEN deletion in developing neurons, increases in dendrite length and complexity were also noted in layer II/III pyramidal neurons within the cortex, but not in neurons located in layer V (Chow et al., 2009), suggesting cell type-specific regulation of dendritic architecture during development and circuit organization. Conversely, vector-mediated PTEN deletion in the juvenile mouse auditory cortex revealed increases in dendritic length, branching, and spine numbers in layer V pyramidal cells possibly resulting in the reportedly increased synaptic activity (Xiong et al., 2012).

While the effects of PTEN deletion on cell body growth in otherwise uninjured neurons at any age appear to be universal, the consequences of PTEN deletion on dendritic growth may be specific to PTEN deletion method, neuronal age, or cell type. It will be of importance to determine this in our model of targeted retrograde transduction of layer V cortical motoneurons in adulthood. Especially in instances of disease, like spinal cord injury, where cell bodies and dendrites are subject to injury-induced atrophy (Nielson et al., 2011; Y. Wang et al., 2018), having the ability to attenuate or reverse neuronal atrophy could be beneficial to functional recovery. Additionally, it will be important to determine the implications of dendritic growth in uninjured and injured neurons on local and long-distance connectivity in the brain.

Possible limitations of retrograde transport in injured axons

Initial studies utilizing retrograde vector technology following spinal cord injury report effective labeling of neurons in the spinal cord and brain when delivered rostral to the injury site (Klaw et al., 2013). This report, however, did not directly confirm transduction of neurons in the cortex, investigate whether transduced cells of origin were in fact from injured axons, or determine the efficacy of cargo delivery in an injury setting.

Our initial intentions when designing this study was to investigate whether or not PTEN deletion would attenuate or prevent injury-induced atrophy of cortical motoneurons after spinal cord injury. While injections rostral to the injury did label many neurons in the cortex, we surprisingly found that measurements of cell body and nuclear sizes between PTEN-floxed and control mice did not differ. Instead, measurements from each were similar to those taken from uninjured controls. This led us to consider if transduced axons were from uninjured neurons that terminate above the injury and not from transected axons that would terminate at or beyond the lesion.

Accordingly, placement of a retrograde fluorescent tracer in combination with our retrograde vector directly into the lesion site confirmed our suspicions. Here, cortical motoneurons were labeled with fluorogold which has previously been shown to successfully label cell bodies from injured axons, but there was no evidence of tdTomato labeling in the cortex. Our lab's investigation into transduction efficacy in the uninjured setting suggested that intraspinal injections were favorably taken up by axon terminals in the grey matter and not by caudally projecting, myelinated axons in the white matter (Metcalfe et al., 2022).

What remained unclear was whether this was due to a lack of viral diffusion or mechanisms of viral uptake. Our current results suggest the later. Further, we expand this concept to include a new caveat - where uptake of retrograde vectors is limited to intact axon terminals, and not transected axons. It will be important to determine if this remains true at more delayed, therapeutically relevant periods after injury, or if this phenomenon is vector serotype specific. Further characterization will allow for better understanding of the mechanisms of retrograde viral transduction and identify appropriate novel approaches for therapeutic treatments following spinal cord injury.

Table 2.1:

Uninjured mice used for cell and nuclear size measurements

Time post AAV-retro/Cre	Age at time of injection	# PTEN/tdT mice	# tdT mice
1 month	3-9 months	n=2 (2F)	n=2 (2M)
1.5 months	3 months	n=2 (2M)	
4 months	3 months	n=3 (3M)	n=3 (3M)
12 months	3 months	n=1 (1M)	n=1 (1M)

Table 2.2:

Injured mice used for cell measurements and transduction efficacy

Group	Method	Endpoint	Age at time of injection/ injury	# PTEN/tdT mice	# tdT mice
Cell size measurements	Intraspinal injection rostral to injury	84 days	9-10 months	n=6 (3M, 3F)	n=3 (3 F)
Transduction efficacy	Gel foam into lesion	5-7 days	16 months	n=5 (2M, 3F)	

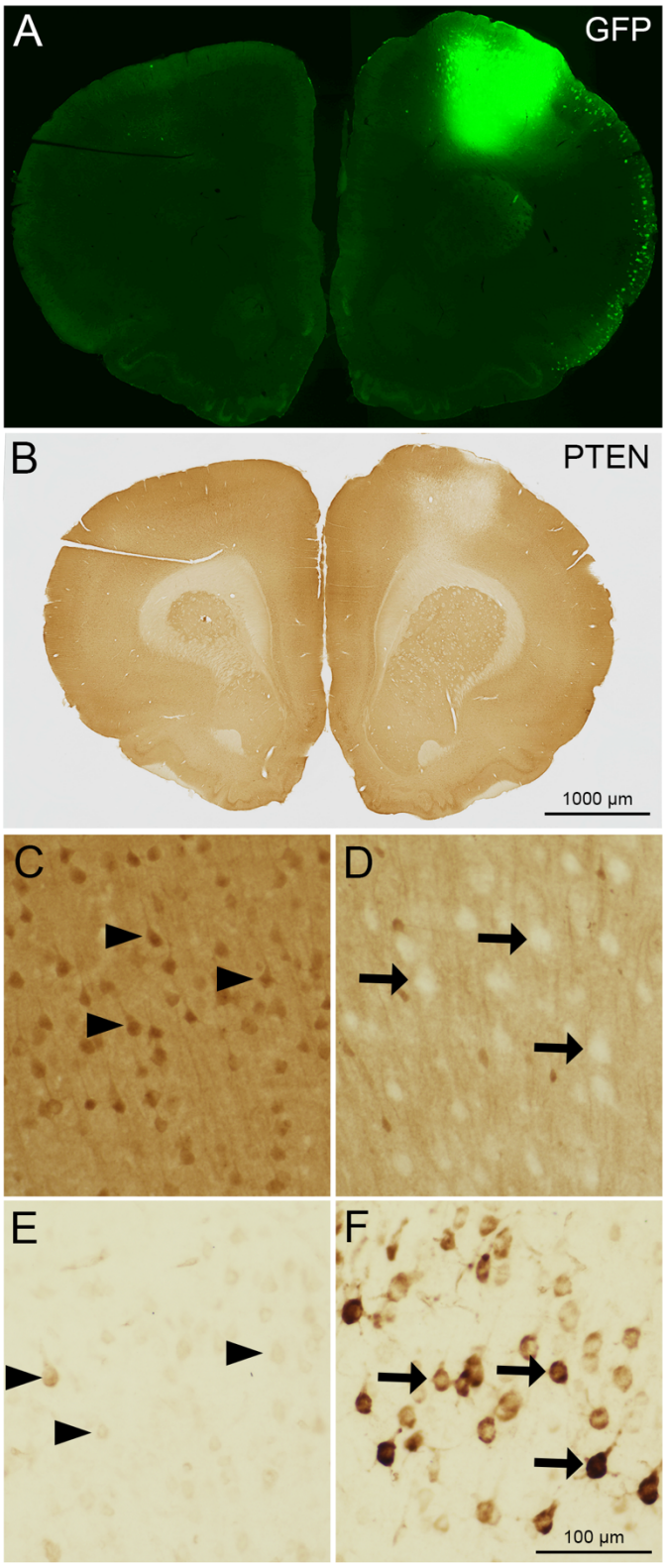
A
GFP
B
PTEN
1000 µm
C
D
E
F
100 µm

Figure 2.1. PTEN knockdown and phosphorylation of ribosomal protein S6 following unilateral injection of AAV-shPTEN into the cortex of adult rats.

A) Area of neuronal transduction by AAV-shPTEN within the cortex expressing GFP. B) PTEN immunostained section showing PTEN knockdown in transduced cells and preservation of PTEN expression in the contralateral cortex. C) High magnification image of the contralateral cortex. Arrowheads denote PTEN expressing cortical motoneurons. D) High magnification image of the ipsilateral, PTEN-deleted cortex. Arrows denote "ghost cells" within the cortex that lack PTEN expression. E) High magnification image of pS6 immunostaining in the contralateral cortex. F) pS6 immunostaining showing area of increased phosphorylation of ribosomal protein S6 within the ipsilateral cortex in PTEN-deleted cells.

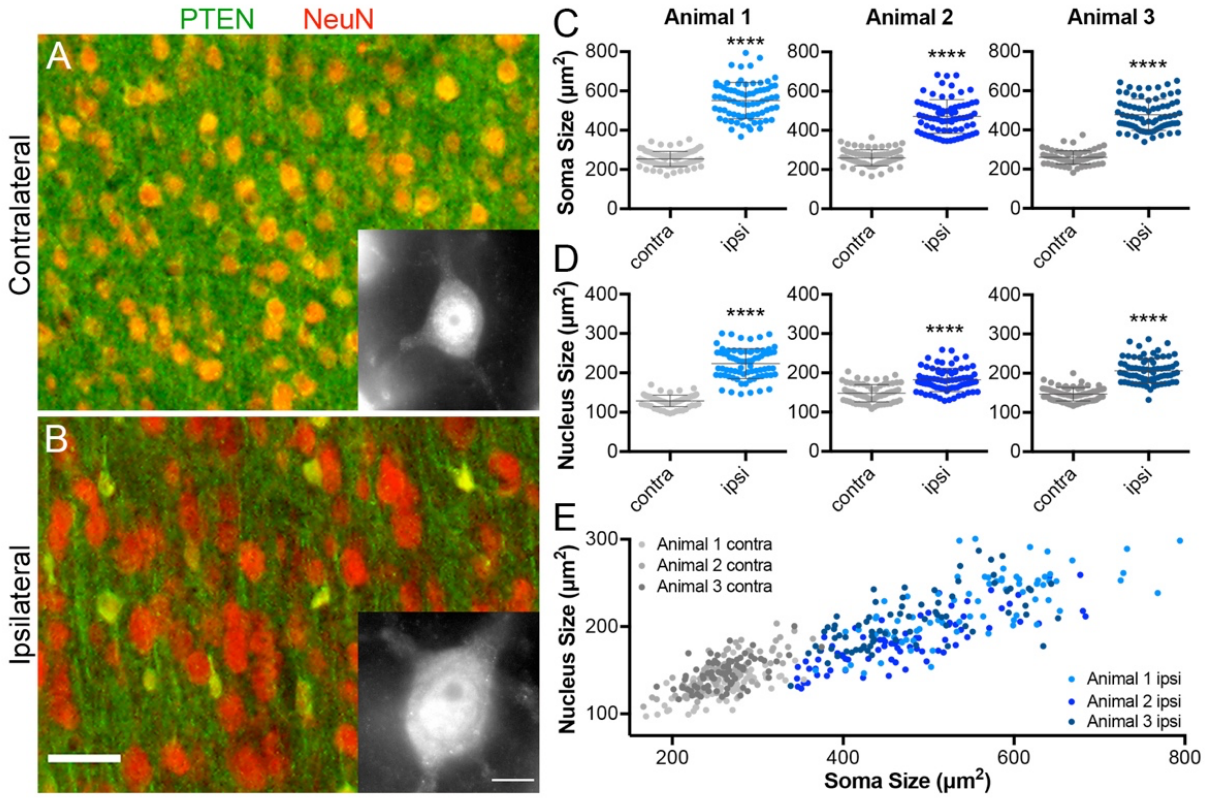
PTEN
NeuN
A
B
Contralateral
Ipsilateral
C
Animal 1
Animal 2
Animal 3
Soma Size (µm²)
****
contra
ipsi
D
Nucleus Size (µm²)
E
Animal 1 contra
Animal 2 contra
Animal 3 contra
Animal 1 ipsi
Animal 2 ipsi
Animal 3 ipsi
Nucleus Size (µm²)
Soma Size (µm²)

Figure 2.2. Enlargement of cortical neuronal cell bodies and nuclei with PTEN knockdown.

A) Immunofluorescence for PTEN (green) and NeuN (red) in the cortex contralateral to AAV-shPTEN injection. Neurons show co-localization with PTEN immunostaining. Inset represents a higher magnification image of a single PTEN-expressing neuron. B) Immunofluorescence for PTEN (green) and NeuN (red) in the area of PTEN deletion identified by the absence of immunofluorescence for PTEN. Note that all NeuN-positive neurons are PTEN-negative. Inset represents a higher magnification image of a single PTEN-depleted neuron. C) Scatter plots of soma cross-sectional areas of PTEN-depleted and PTEN-expressing neurons in three cases. D) Scatter plots of nuclear cross-sectional area of PTEN-depleted and PTEN-expressing neurons in the three cases shown in C. Paired t-test comparing contralateral vs. ipsilateral side in individual rats [$p<.0001$]. Two-way ANOVA comparing PTEN-depleted and PTEN-expressing neurons in all rats [$F(1,8)= 109, p<.0001$]. E) Plot of soma vs. nuclear size in the same three cases showing clear separation between PTEN-expressing and PTEN-depleted cortical neurons. Data points for each individual rat are shown in different shades of gray (for contralateral, PTEN-expressing neurons) and blue (for ipsilateral, PTEN-depleted neurons). Scale bar= 50μm, inset=10μm.

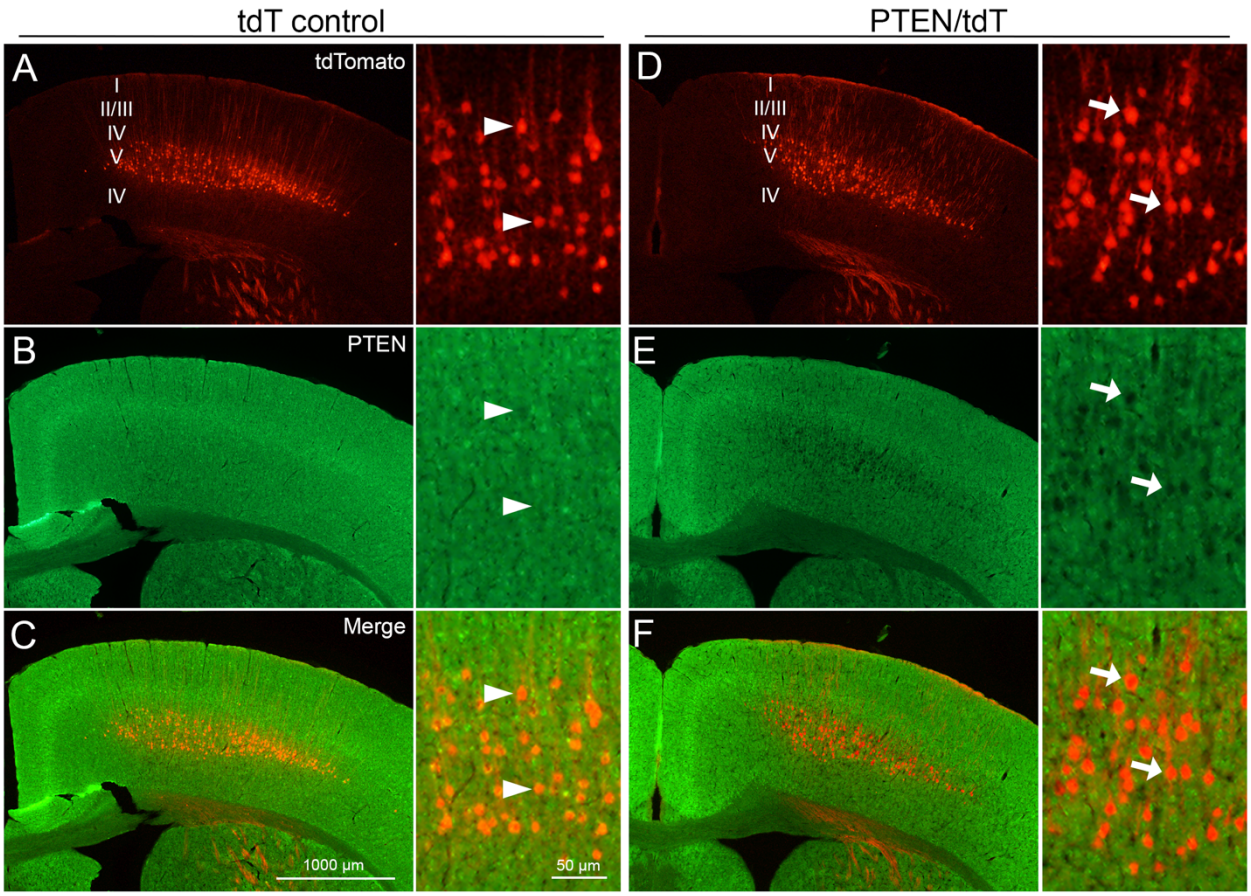
tdT control
PTEN/tdT
A
tdTomato
I
II/III
IV
V
IV
D
B
PTEN
E
C
Merge
F
1000 µm
50 µm

Figure 2.3. Transduction of cortical motoneurons and area of PTEN deletion following bilateral retrograde AAV-Cre injection into C5 of the spinal cord.

A) Native tdTomato expression in a tdT control mouse following retrograde AAV-Cre injection into C5 of the spinal cord. B) PTEN immunostain in the same control mouse. C) Overlay of native tdT and PTEN immunostain showing preservation of PTEN expression in transduced cells. D) Native tdT expression in a PTEN/tdT experimental mouse following retrograde AAV-Cre injection. E) PTEN immunostain showing "ghost cells" in layer V of the cortex. F) Overlay of native tdT and PTEN immunostain showing a lack of PTEN expression in tdT positive neurons, indicative of successful PTEN deletion. Right panels show higher magnification images of each respective section with arrow heads denoting transduced cells with preserved PTEN expression in controls and arrows identifying PTEN deleted neurons in PTEN/tdT mice.

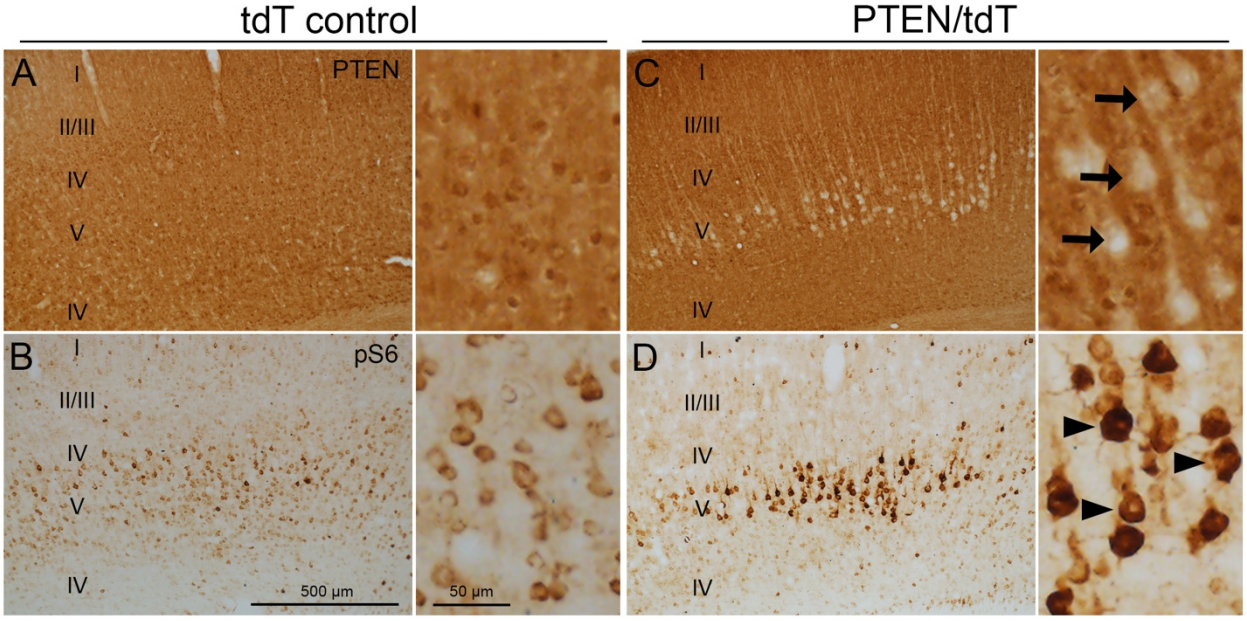
tdT control
PTEN/tdT
A
PTEN
I
II/III
IV
V
IV
C
B
pS6
500 µm
50 µm
D

Figure 2.4. Area of PTEN deletion and phosphorylation of ribosomal protein S6 in cortical layer V pyramidal neurons following retrograde AAV-Cre injection.

A) Preservation of PTEN expression in tdT control mice following retrograde AAV-Cre injection. B) Ribosomal protein S6 immunostain in the same control mouse. C) PTEN expression in an experimental PTEN/tdT mouse following retrograde AAV-Cre injection showing "ghost cells" lacking PTEN expression in layer V of the cortex. D) Ribosomal protein S6 immunostaining in the same experimental animal showing increased phosphorylation, indicative of mTOR activation. Right panels show higher magnification images of each respective section. Arrows denote ghost cells lacking PTEN expression and arrow heads indicate PTEN deleted cells with increased phosphorylation of ribosomal protein S6.

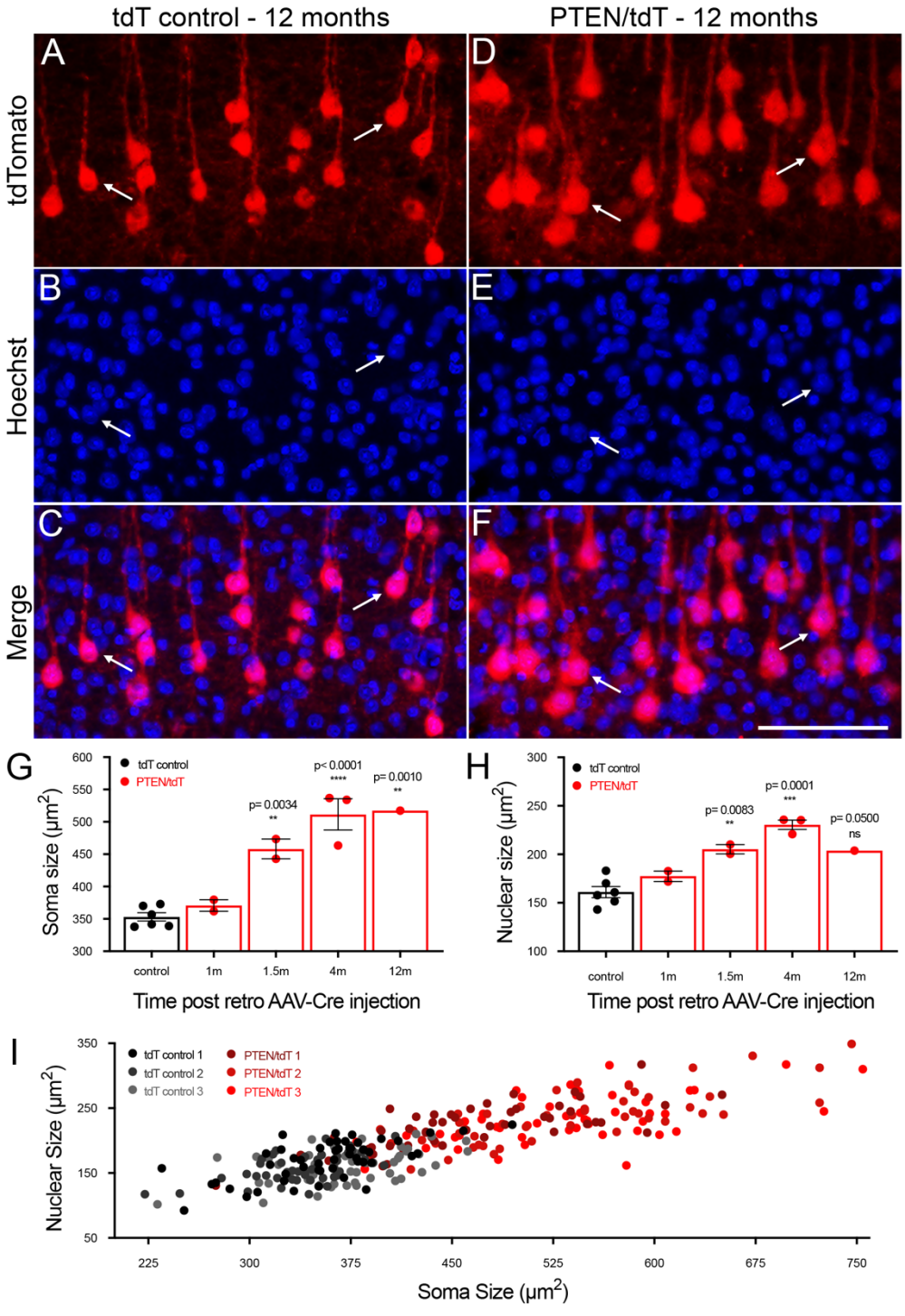
tdT control - 12 months
PTEN/tdT - 12 months
A
D
tdTomato
B
E
Hoechst
C
F
Merge
G
tdT control
PTEN/tdT
Soma size (µm2)
p= 0.0034
**
p< 0.0001
****
p= 0.0010
**
control
1m
1.5m
4m
12m
Time post retro AAV-Cre injection
H
tdT control
PTEN/tdT
Nuclear size (µm2)
p= 0.0083
**
p= 0.0001
***
p= 0.0500
ns
control
1m
1.5m
4m
12m
Time post retro AAV-Cre injection
I
tdT control 1
tdT control 2
tdT control 3
PTEN/tdT 1
PTEN/tdT 2
PTEN/tdT 3
Nuclear Size (µm2)
Soma Size (µm2)

Figure 2.5. Quantification of soma and nuclear size in PTEN expressing and PTEN deleted cortical motoneurons following retrograde AAV-Cre injection.

A-C) Representative images of somata and nuclei from a tdT control mouse at 12 months following retrograde AAV-Cre injection. D-F) Representative images of somata and nuclei from an experimental PTEN/tdT mouse at 12 months after retrograde AAV-Cre injection and PTEN deletion. Note enlarged cell and nuclear size after PTEN deletion. G) Time course of soma size from control and experimental mice at 1, 1.5, 4, and 12 months following retrograde AAV-Cre injection. Tukey post hoc comparisons vs. controls: 1.5 month ($p=0.0034$), 4 months ($p<0.0001$), and 12 months ($p=0.0010$). H) Time course of nuclear size from the same animals shown in G. Tukey post hoc comparisons vs. controls: 1.5 month ($p=0.0083$) and 4 months ($p=0.0001$). I) Plot of soma vs. nuclear size in three control and experimental cases showing clear separation between PTEN-expressing and PTEN-depleted cortical neurons at 4 months after AAV-Cre injection. Data points for each individual mouse are shown in different shades of black and gray (for contralateral, PTEN-expressing neurons) and red (for ipsilateral, PTEN-depleted neurons). A total of 50 cells and their corresponding nuclei were measured for each animal.

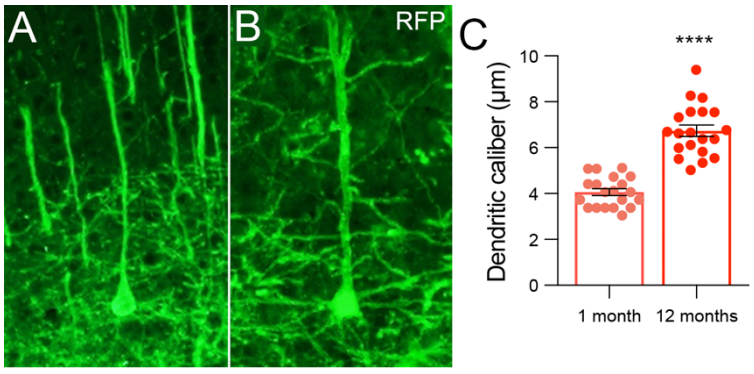
A
B
RFP
C
****
Dendritic caliber (µm)
10
8
6
4
2
0
1 month
12 months

Figure 2.6. Apical dendrite caliber following PTEN deletion.

A) Red fluorescent protein (RFP)-labeled cortical motoneuron at 1 month after PTEN deletion. B) RFP-labeled cortical motoneuron at 12 months after PTEN deletion, note the enlarged soma and apical dendrite. C) Scatter plot of apical dendrite caliber measured 200-250μm below the cortical surface reveals a significant increase in dendrite caliber between 1- and 12-months post PTEN deletion ($p<0.0001$).

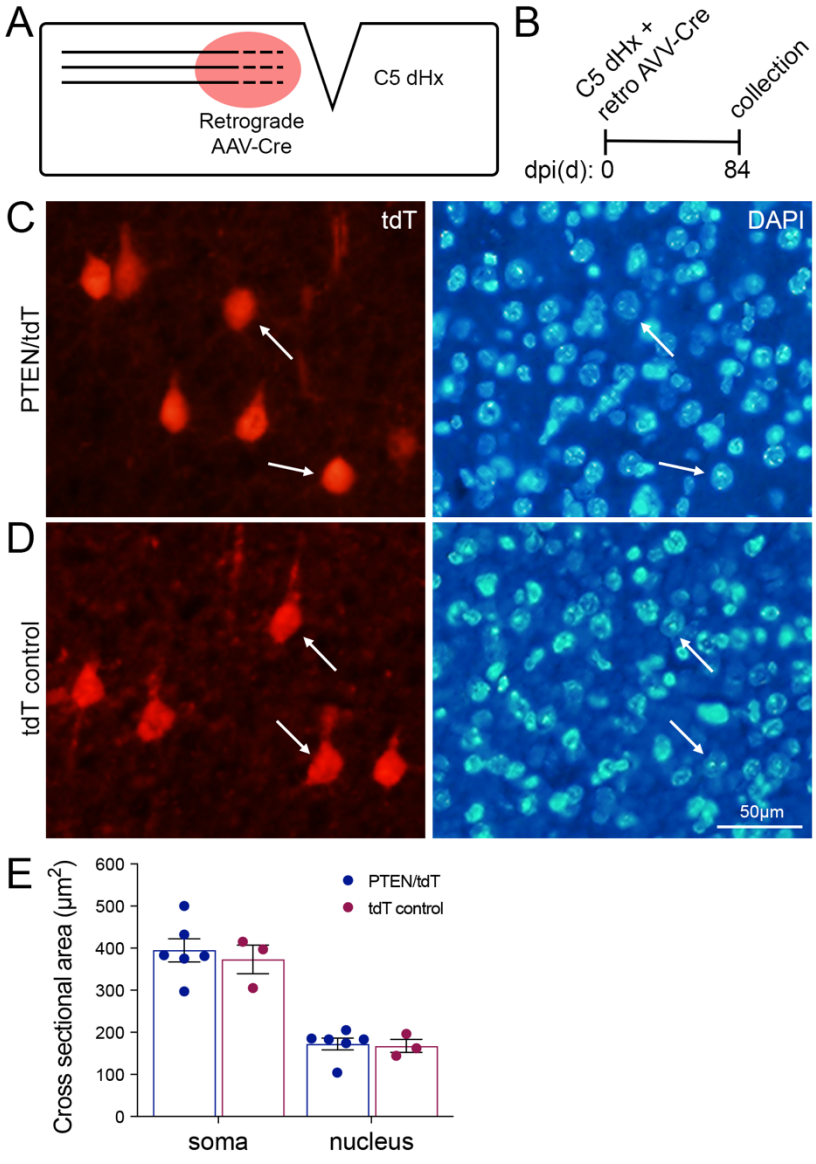
A
C5 dHx
Retrograde
AAV-Cre
B
C5 dHx +
retro AVV-Cre
collection
dpi(d): 0
84
C
tdT
DAPI
PTEN/tdT
D
tdT control
50μm
E
Cross sectional area (μm2)
600
500
400
300
200
100
0
PTEN/tdT
tdT control
soma
nucleus

Figure 2.7. Cortical motoneuron size following injections of retrograde AAV-Cre rostral to a C5 dorsal hemisection.

A-B) Schematic of experimental design. Mice underwent injections of retrograde AAV-Cre rostral to the injury site, immediately after a C5 dorsal hemisection. Mice were perfused 84 days after surgical procedures for histological assessments. C) Representative images of somata (left) and nuclei (right) from a PTEN/tdT mouse. D) Representative images from a tdT control mouse that underwent a similar experimental paradigm. E) Measurements of soma and nuclear sizes from PTEN/tdT and tdT control mice showing a lack of atrophy following C5 dorsal hemisection. A total of 30 cells and their corresponding nuclei were measured for each mouse.

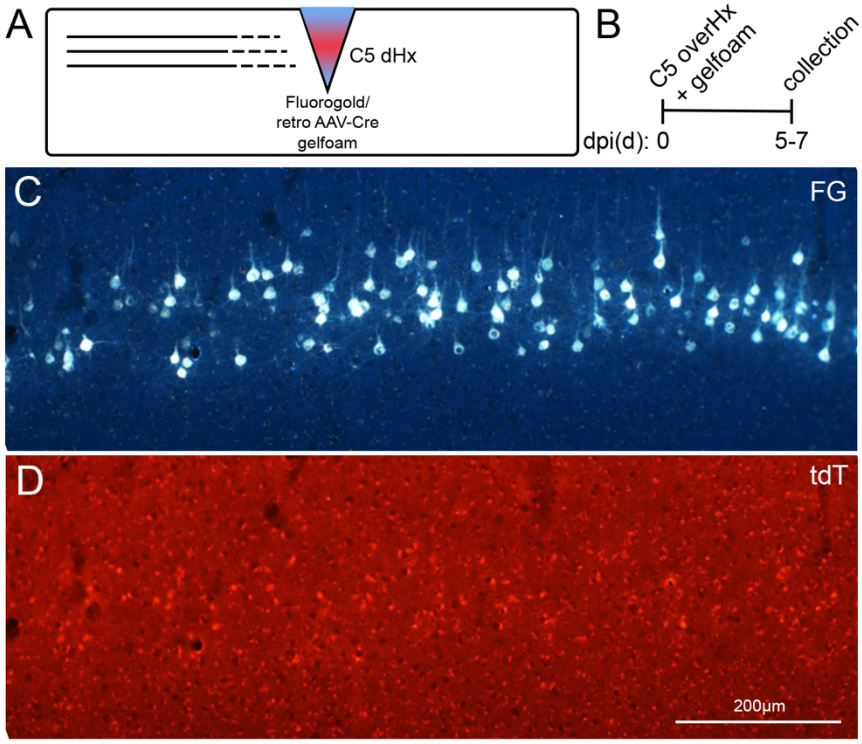
A
C5 dHx
Fluorogold/
retro AAV-Cre
gelfoam
B
C5 overHx
+ gelfoam
collection
dpi(d): 0
5-7
C
FG
D
tdT
200μm

Figure 2.8. Lack of viral uptake by transected CST axons.

A-B) Schematic of surgical and experimental design. Animals underwent a C5 dorsal over hemisection followed by placement of gelfoam soaked in Fluorogold and retrograde AAV-Cre into the lesion cavity. Tissue was collected between 5-7 days after surgery. C) Evidence of fluorogold labeling in layer V cortical motoneurons suggesting uptake by transected axons. D) Lack of tdTomato labeling in the cortex suggests that retrograde AAV-Cre is not efficiently taken up at the spinal cord injury site.

REFERENCES

Chow, D. K., Groszer, M., Pribadi, M., Machniki, M., Carmichael, S. T., Liu, X., & Trachtenberg, J. T. (2009, Feb). Laminar and compartmental regulation of dendritic growth in mature cortex. *Nat Neurosci, 12*(2), 116-118. https://doi.org/10.1038/nn.2255

Danilov, C. A., & Steward, O. (2015, Apr). Conditional genetic deletion of PTEN after a spinal cord injury enhances regenerative growth of CST axons and motor function recovery in mice. *Exp Neurol, 266*, 147-160. https://doi.org/10.1016/j.expneurol.2015.02.012

Du, K., Zheng, S., Zhang, Q., Li, S., Gao, X., Wang, J., Jiang, L., & Liu, K. (2015, Jul 1). Pten Deletion Promotes Regrowth of Corticospinal Tract Axons 1 Year after Spinal Cord Injury. *J Neurosci, 35*(26), 9754-9763. https://doi.org/10.1523/JNEUROSCI.3637-14.2015

Fraser, M. M., Bayazitov, I. T., Zakharenko, S. S., & Baker, S. J. (2008, Jan 24). Phosphatase and tensin homolog, deleted on chromosome 10 deficiency in brain causes defects in synaptic structure, transmission and plasticity, and myelination abnormalities. *Neuroscience, 151*(2), 476-488. https://doi.org/10.1016/j.neuroscience.2007.10.048

Gallent, E. A., & Steward, O. (2018, May). Neuronal PTEN deletion in adult cortical neurons triggers progressive growth of cell bodies, dendrites, and axons. *Exp Neurol, 303*, 12-28. https://doi.org/10.1016/j.expneurol.2018.01.005

Kaplan, A., Ong Tone, S., & Fournier, A. E. (2015). Extrinsic and intrinsic regulation of axon regeneration at a crossroads. *Front Mol Neurosci, 8*, 27. https://doi.org/10.3389/fnmol.2015.00027

Klaw, M. C., Xu, C., & Tom, V. J. (2013, Jul 23). Intraspinal AAV Injections Immediately Rostral to a Thoracic Spinal Cord Injury Site Efficiently Transduces Neurons in Spinal Cord and Brain. *Mol Ther Nucleic Acids, 2*, e108. https://doi.org/10.1038/mtna.2013.34

Lewandowski, G., & Steward, O. (2014, Jul 23). AAVshRNA-mediated suppression of PTEN in adult rats in combination with salmon fibrin administration enables regenerative growth of corticospinal axons and enhances recovery of voluntary motor function after cervical spinal cord injury. *J Neurosci, 34*(30), 9951-9962. https://doi.org/10.1523/JNEUROSCI.1996-14.2014

Liu, K., Lu, Y., Lee, J. K., Samara, R., Willenberg, R., Sears-Kraxberger, I., Tedeschi, A., Park, K. K., Jin, D., Cai, B., Xu, B., Connolly, L., Steward, O., Zheng, B., & He, Z. (2010, Sep). PTEN deletion enhances the regenerative ability of adult corticospinal neurons. *Nat Neurosci, 13*(9), 1075-1081. https://doi.org/10.1038/nn.2603

Metcalfe, M., Yee, K. M., Luo, J., Martin-Thompson, J. H., Gandhi, S. P., & Steward, O. (2022, Apr). Harnessing rAAV-retro for gene manipulations in multiple pathways that are interrupted after spinal cord injury. *Exp Neurol, 350*, 113965. https://doi.org/10.1016/j.expneurol.2021.113965

Nielson, J. L., Strong, M. K., & Steward, O. (2011, Oct 1). A reassessment of whether cortical motor neurons die following spinal cord injury. *J Comp Neurol, 519*(14), 2852-2869. https://doi.org/10.1002/cne.22661

Park, K. K., Liu, K., Hu, Y., Smith, P. D., Wang, C., Cai, B., Xu, B., Connolly, L., Kramvis, I., Sahin, M., & He, Z. (2008, Nov 7). Promoting axon regeneration in the adult CNS by modulation of the PTEN/mTOR pathway. *Science, 322*(5903), 963-966. https://doi.org/10.1126/science.1161566

Steward, O., Coulibaly, A. P., Metcalfe, M., Yonan, J. M., & Yee, K. M. (2020, Apr). AAVshRNA-mediated PTEN knockdown in adult neurons attenuates activity-dependent immediate early gene induction. *Exp Neurol, 326*, 113098. https://doi.org/10.1016/j.expneurol.2019.113098

Steward, O., Yee, K. M., Metcalfe, M., Willenberg, R., Luo, J., Azevedo, R., Martin-Thompson, J. H., & Gandhi, S. P. (2021, Mar 31). Rostro-Caudal Specificity of Corticospinal Tract Projections in Mice. *Cereb Cortex, 31*(5), 2322-2344. https://doi.org/10.1093/cercor/bhaa338

Wang, Y., Wu, W., Wu, X., Sun, Y., Zhang, Y. P., Deng, L. X., Walker, M. J., Qu, W., Chen, C., Liu, N. K., Han, Q., Dai, H., Shields, L. B., Shields, C. B., Sengelaub, D. R., Jones, K. J., Smith, G. M., & Xu, X. M. (2018, Sep 12). Remodeling of lumbar motor circuitry remote to a thoracic spinal cord injury promotes locomotor recovery. *Elife, 7*. https://doi.org/10.7554/eLife.39016

Wang, Z., Maunze, B., Wang, Y., Tsoulfas, P., & Blackmore, M. G. (2018, Dec 5). Global Connectivity and Function of Descending Spinal Input Revealed by 3D Microscopy and Retrograde Transduction. *J Neurosci, 38*(49), 10566-10581. https://doi.org/10.1523/JNEUROSCI.1196-18.2018

Xiong, Q., Oviedo, H. V., Trotman, L. C., & Zador, A. M. (2012, Feb 1). PTEN regulation of local and long-range connections in mouse auditory cortex. *J Neurosci, 32*(5), 1643-1652. https://doi.org/10.1523/JNEUROSCI.4480-11.2012

Zukor, K., Belin, S., Wang, C., Keelan, N., Wang, X., & He, Z. (2013, Sep 25). Short hairpin RNA against PTEN enhances regenerative growth of corticospinal tract axons after spinal cord injury. *J Neurosci, 33*(39), 15350-15361. https://doi.org/10.1523/JNEUROSCI.2510-13.2013

CHAPTER 3:

Vector-mediated PTEN deletion in the adult dentate gyrus triggers growth of granule cells

ABSTRACT

Embryonic and early postnatal deletion of the gene phosphatase and tensin homolog (PTEN) results in neuronal hypertrophy, formation of aberrant neural networks and spontaneous seizures. Deletion of PTEN in mature neurons also causes neuronal growth, but it is unknown how this growth alters connectivity in mature circuits. Here, we explore consequences of deleting PTEN in a focal area of the dentate gyrus in adult male and female mice. PTEN deletion was accomplished by injecting AAV-Cre unilaterally into the dentate gyrus of double transgenic mice with lox-P sites flanking exon 5 of the PTEN gene and stop/flox tdTomato in the Rosa locus ($PTEN^{f/f}/Rosa^{tdTomato}$). Focal deletion led to progressive increases in the size of the dentate gyrus at the injection site, enlargement of granule cell bodies, and increases in dendritic length and caliber. Quantitative analysis of dendrites by Golgi staining revealed robust increases in spine numbers throughout the proximo-distal extent of the dendritic tree, indicating that dendritic growth is sufficient to induce new synapse formation by input neurons with intact PTEN expression. Laminar specificity of termination of inputs is maintained, however. Mossy fiber axons from PTEN-deleted granule cells expanded their terminal field in CA3 where PTEN expression was intact and supra-granular mossy fibers developed in some mice. These findings document that induction of growth of adult dentate

granule cells via persistent activation of mTOR triggers new innervation by input pathways and expanded innervation of targets of dentate granule cells, upending connectional homeostasis in fully mature hippocampal circuits.

INTRODUCTION

The phosphatase and tensin homolog (PTEN) gene is a well-known negative regulator of the mechanistic target of rapamycin (mTOR) pathway responsible for cell growth during development. Mutations affecting mTOR signaling, including PTEN mutations, have been implicated in both epilepsy and autism spectrum disorders (ASD) in humans, and some PTEN mutations are accompanied by macrocephaly, seizures, and reduced mental capacity (Conti et al., 2012; Jansen et al., 2015; Tilot et al., 2015; Zahedi Abghari et al., 2019).

Studies of PTEN deletion in transgenic mouse models using promoter-driven Cre/Lox systems report that loss of PTEN in developing neurons and glia lead to cellular hypertrophy and alterations in physiology associated with hyperexcitability. Cre expression driven by a glial fibrillary acidic protein (GFAP) promoter deletes PTEN in cortical, hippocampal, and cerebellar neurons and glia causing brain macrocephaly, neuronal hypertrophy, increased dendritic growth and spine density, seizures, and early mortality (Backman et al., 2001; Fraser et al., 2008; Fraser et al., 2004; Kwon et al., 2003; Kwon et al., 2001; Ljungberg et al., 2009; Wen et al., 2013). Cre expression driven by neuron-specific enolase (NSE) (Kwon et

al., 2006; Ogawa et al., 2007; Takeuchi et al., 2013; Zhou et al., 2009), or neuron-specific (NS) (Lugo et al., 2014; Sunnen et al., 2011) promotors lead to similar phenotypes.

The dentate gyrus has been a focus of interest for studies of the consequences of PTEN deletion because alterations in dentate gyrus circuitry are reported in various seizure disorders. Selective deletion of PTEN in immature proopiomelanocortin (POMC) expressing granule cells results in enlarged hippocampi, ectopic mossy fiber projections, altered excitatory-inhibitory balance, spontaneous seizures, and early mortality (Matsushita et al., 2016). A collection of studies from Danzer and collogues have reported that tamoxifen-induced PTEN deletion at postnatal day 14 specifically in newborn dentate granule cells also leads to neuronal hypertrophy and morphological features characteristic of temporal lobe epilepsy including ectopically located somata, ectopic mossy fiber projections, development of basal dendrites, enlarged apical dendrites, and increased spine densities (Arafa et al., 2019; LaSarge et al., 2016; LaSarge et al., 2015; Pun et al., 2012; Santos et al., 2017). Collectively, these data indicate that early life, promotor-driven PTEN deletion in the dentate gyrus results in pro-epileptic alterations to network connectivity (Althaus & Parent, 2012).

In contrast to developmental PTEN deletion, little is known about the consequences of PTEN deletion in fully mature neurons. Recent studies document that intracortical injections of AAV-Cre in fully mature transgenic $PTEN^{f/f}$ mice triggers growth of cortical neurons characterized by progressive increases in soma size and dendritic complexity (Gallent & Steward, 2018). PTEN knockdown in the adult rat cortex with AAV-shRNA targeted to PTEN also results in striking soma and nuclear enlargements (Steward et al., 2019). These

previous studies did not assess whether adult dendritic growth was accompanied by the formation of new synapses or circuits, and there were no overt physiological consequences including seizures (Gallent & Steward, 2018; Steward et al., 2019).

To gain insights into how growth of adult neurons alters connectivity, the present study assesses consequences of PTEN deletion in the fully mature hippocampal dentate gyrus. The hippocampus is an ideal model to study neuronal morphology and connectivity due to the highly specific laminar pattern of inputs and outputs. We use the same approach as previously used for cortical neurons involving focal injections of AAV-Cre in adult transgenic $PTEN^{f/f}$/Rosa reporter mice. This allows for focal PTEN deletion in dentate granule cells while preserving PTEN expression in input neurons and targets of granule cells. Focal rather than promoter-driven PTEN deletion allows us to answer three questions: 1) Does growth of dendrites trigger formation of new synapses by systems with intact PTEN expression? 2) Does dendritic growth disrupt the highly specific patterns of termination of input pathways? and 3) Does PTEN deletion trigger growth of axonal projections in target sites with intact PTEN expression?

MATERIALS AND METHODS

Experimental animals

Experiments involved four transgenic strains of mice developed in our local breeding colony. The first strain was generated by crossing PTEN-floxed mice containing lox-p flanked exon

5 of the PTEN gene (RRID: IMSR_JAX:004597) with ROSA26tdTomato reporter mice having a lox-P flanked STOP cassette in the Rosa locus upstream of a tandem dimer tomato (tdT) fluorescent protein sequence (RRID: IMSR_JAX:007905). This double transgenic strain is designated $PTEN^{f/f}/Rosa^{tdTomato}$. In these mice, transduction with AAV-Cre results in deletion of PTEN and expression of tdT in the same cells (Fig. 3.1A). Control mice ($Rosa^{tdTomato}$) only contain the floxed stop cassette before the tdT sequence. All studies involved mice that were homozygous at the transgenic loci. Two other lines were created by crossing these two strains with Thy1-eYFP mice, originally purchased from the Jackson Labs, to generate mice that were homozygous at the original loci, and heterozygous for Thy1- YFP. This strain was used for studies of input pathway tracing in adult mice, described below. For simplicity, these animals will be referred to as PTEN/tdT and tdT, regardless of their Thy1 expression. Because all strains were derived in our lab, they have different genetic backgrounds than the original mice available for purchase from Jackson Labs.

Surgical procedures, AAV-Cre injection into the dentate gyrus

All experimental procedures were approved by the Institutional Animal Care and Use Committee (IACUC) at the University of California, Irvine. Except where noted, most studies involved adult mice (at least 2 months of age at the time of AAV-Cre injection). For all surgical procedures, mice were anesthetized with Isoflurane (2-2.5%) and surgical duration was noted for each mouse. Anesthetized mice were placed in a stereotaxic device. Eyes were covered with Vaseline and the skin above the incision site was shaved and disinfected with Betadine. A scalp incision was made to expose the skull. A small cranial window was created

above the injection site. Using a 10µl Hamilton syringe with a pulled glass pipette tip, a single unilateral AAV2-Cre (Vector Bio Labs, 7011) injection was made at +1.3mm lateral and +2.2mm anterior to lambda at a depth of -1.6mm from the cortical surface. Each injection was 0.6µl in volume ($1x10^{12}$ GC/ml in 1xPBS with 5% glycerol) and was performed over 4 minutes. The glass pipette was left in place for another 2 minutes before removal. After injection, the incision site was sutured. Following completion of the surgery, mice were allowed to recover in a cage placed on a 37°C heating pad. Mice were allowed to survive for 2 weeks - 6 months post injection (Fig. 3.1B, Table 3.1).

Orthograde tracing of projections to the dentate gyrus from the entorhinal cortex and commissural/associational system

Studies of specificity of termination of hippocampal pathways involved mice that received injections of AAV-Cre on postnatal 19 or in adulthood (Table 3.1). One group of PTEN/tdT mice received AAV-Cre at p19 and then 11 weeks later, received unilateral injections of BDA into the ipsilateral entorhinal cortex to trace perforant path projections to the dentate gyrus or injections of AAV-ChR into the contralateral, ventral hippocampus to trace commissural projections (Fig. 3.6A, B). Injections were performed as described above using a Hamilton syringe with a pulled glass pipette. For the ipsilateral entorhinal cortex, three injections (0.5µl in volume for each injection) were made at +3.0mm lateral and -0.8mm anterior to lambda at a depth of -3.0, -2.0, and -1.0mm from the cortical surface. For the contralateral, ventral hippocampus, a single injection was made at -2.7mm lateral and -3.6mm posterior to

bregma at a depth of -3.2mm below the cortical surface. Mice were allowed to survive for 2.5 weeks post-tracer injections (13.5 weeks post AAV-Cre).

Another group of PTEN/tdT transgenic mice received BDA injections into the entorhinal cortex or ventral hippocampus between 7- and 8-months post AAV-Cre injection in adulthood (Fig. 3.7A, B). For the contralateral, ventral hippocampus, coordinates were the same as described above. For the ipsilateral entorhinal cortex, a single injection (0.5µl) was made at +3.0mm lateral and -0.2mm anterior to lambda at a depth of -3.0mm from the cortical surface. These mice were allowed to survive for 1-week post-tracer injection.

Tissue collection and histology

At each designated endpoint, mice received intraperitoneal injections of Fatal Plus and were intracardially perfused with 4% paraformaldehyde in phosphate buffer (PFA). Brains were dissected and post-fixed in 4% PFA for 48 hours, cryoprotected in 27% sucrose, and frozen in Tissue-Tek O.C.T. compound. Brains were then cryosectioned into 30µm sections and sections were stored in 1xPBS with 0.1% NaN_3 until processed for immunohistochemistry.

Sections spaced at 360µm intervals were processed for various histological markers (Table 3.1). For immunohistochemistry (IHC), sections were washed in 1xTBS (100mM Tris, pH 7.4 and 150mM NaCl) then quenched for endogenous peroxidase activity by incubation in 3% H_2O_2 for 15 minutes. Sections were then washed in 1xTBS and blocked in blocking buffer (1xTBS, 0.3% Triton X-100, 5% NDS) for 2 hours at room temperature. Sections were then

incubated overnight at room temperature in buffer containing primary antibodies (Table 3.2). Sections were then washed in 1xTBS, followed by a 2-hour incubation in buffer containing biotinylated donkey anti-rabbit IgG (1:250, Jackson ImmunoResearch, 711-065-152), then washed again. Visualization was accomplished through incubation in ABC reagent (Vectastain Elite kit, catalog #PK-6100; Vector Laboratories) and CARD amplification with Tyramide-FITC or Tyramide-AMCA. Sections were then mounted on 0.5% gelatin coated slides and counterstained with Hoechst (1µg/ mL).

Mice that received injections of BDA were perfused and prepared for histology as above. Briefly, sections washed in 1xTBS (100mM Tris, pH 7.4 and 150mM NaCl) then quenched for endogenous peroxidase activity by incubation in 3% H_2O_2 for 20 minutes. Sections were then washed in 1xTBS and incubated in 1xTBS with 0.1% Triton X-100 for 1 hour at room temperature. Sections were then incubated overnight at room temperature in ABC reagent (Vectastain Elite kit, catalog #PK-6100; Vector Laboratories), followed by CARD amplification with Tyramide-FITC or Tyramide-AMCA the following day.

Quantification of area/volume transduction

To determine vector transduction through the dentate gyrus, sections spaced 360µm apart were assessed for area of the granule cell layer occupied by tdTomato-positive granule cells. Briefly, images of the dentate gyrus were taken with a 10x objective using an Olympus AX80 microscope. Images were imported into NIH ImageJ FIJI, and a border was drawn around the Hoechst-positive dentate gyrus. The contour was then transferred to the tdT-labeled image.

The tdT-positive area within the contour was determined by thresholding the color image until the selected area matched the native red fluorescence. Area measurements gathered using tdT fluorescence were then used to estimate the volume of vector transduction for each animal using the Cavalieri method.

The percent of the granule cell layer that was tdT-positive was also calculated using the same sections in each mouse and included sections at the rostral and caudal ends of transduction without tdT expression. Data were plotted as the percent of the entire dentate gyrus that was transduced based on tdTomato expression for each animal at each time point. Percent transduction was further plotted through the length of the dentate gyrus. Due to slight variability in the anterior/ posterior positioning of each set of sections used for each animal, the section with the highest percent transduction was plotted as the transduction "core" with the remaining percentages plotted in sequential order for the rostral and caudal sections. Data were plotted as an average for all animals within a single endpoint group at each distance from the deletion core.

PTEN deletion measurements

PTEN deletion/expression was quantified at each time point in PTEN/tdT and tdT control mice. Briefly, one section per animal at the core of transduction and/or PTEN deletion was imaged at 10x magnification, as previously described. A 50μm x 50μm box delineating the region of interest (ROI) was drawn within the granule cell layer using the red channel to identify regions of tdT expression. A similar ROI was placed in the corresponding location

within the contralateral hippocampus. The mean grey value was then determined within each ROI in the green channel (PTEN fluorescence). Data is reported as the ratio of the mean grey values of the ipsilateral ROI to the corresponding contralateral ROI for each animal.

Hippocampal sub-region measurements

To assess changes in hippocampal subregion size over time, one set of sections from each mouse was stained for Cresyl violet. The section at the center of transduction was identified and 4x images of the ipsilateral and contralateral sides to AAV-Cre injection were taken and imported into ImageJ FIJI. Subregion area within the hippocampus (CA1, CA3, and dentate gyrus) were measured by manually outlining each structure. The dentate gyrus was defined by drawing a line connecting the lateral edges of the granule cell body layer. The area of the ipsilateral dentate gyrus was represented as a percentage of the contralateral dentate gyrus and as a percentage of the entire hippocampus. Dentate gyrus/hippocampal percent areas for the contralateral dentate gyrus in PTEN/tdT mice were similar at all timepoints, values were therefore combined. Finally, percent size of each individual subregion in relation to the entire hippocampus was calculated at 6 months post AAV-Cre injection in PTEN/tdT and tdT controls.

Dentate granule cell measurements

Cell body sizes were measured in regions of sparse and dense transduction. To measure granule cell body size over time in regions of sparse transduction, one set of sections for each

animal was assessed for native tdT expression and PTEN deletion was confirmed through immunohistochemistry, as above. Sections at the rostral end of the area of PTEN deletion were taken for cell size measurements where tdT labeled cells were more sparsely distributed and soma borders could be easily distinguished from surrounding non-transduced cells. Images were taken at 10x on an Olympus AX80 microscope and imported into ImageJ FIJI. Sampling was done by starting at the lateral end of the dorsal blade of the dentate gyrus and moving medially until 30 tdT expressing cells had been measured. The same process was done for animals in which localization of PTEN deletion was primarily in the ventral blade of the dentate gyrus.

A similar process was repeated at the core of transduction using Cresyl violet stained sections in order to determine cell size in regions of dense transduction. Here, 40x images were taken and imported into ImageJ. Sampling was done by measuring 30 cells within the granule cell layer within a 100μm^2 region of interest in the ipsilateral dentate gyrus, and the homologous regions in the contralateral granule cell layer. With both methods, cell size measurements were taken from both PTEN/tdT experimental animals and tdT controls. The mean cross-sectional area for PTEN deleted and control groups was determined by first averaging cell size measurements in individual mice, then averaging at each time point within each group so "n" for statistical purposes is number of animals.

Measurements of the thickness of the molecular layer were taken in the dorsal hippocampus at the core of transduction as a representation of dendritic length in both ipsilateral and contralateral sides in PTEN/tdT and tdT control mice.

Quantification of dendrite length, diameter, spine density, and spine morphology by Golgi-staining

For Golgi staining, mice that had received unilateral injections of AAV-Cre into the dentate gyrus as above were euthanized at 6 months post-AAV injection by intraperitoneal injection of Fatal Plus and were transcardially perfused with aldehyde fixative (sliceGolgi Kit, Bioenno Tech 003760). Brains were removed and placed in fixative for 3 hours followed immediately by sectioning on a vibratome into 200μm coronal sections. Free-floating sections were inspected using a fluorescence microscope to identify sections at the core of PTEN deletion by tdTomato expression, and these sections were then processed for Golgi impregnation using the sliceGolgi Kit. Briefly, slices were incubated in impregnation solution for 3 days at 37°C in the dark; the impregnation solution was changed after the first day. Following impregnation, sections were washed in 0.1M PBS-T, incubated in staining solution for 8 minutes, then washed again. Sections were then incubated in post staining solution for 4 minutes, washed, then mounted on gelatin coated slides. Mounted sections were dried overnight, dehydrated in 100% ethanol, cleared in xylenes, then cover slipped using Permount® mounting medium. Prepared slides were stored at room temperature in the dark until imaged.

Dendrite length was first determined in the ipsilateral and contralateral dentate gyrus. Z-stacks of granule cells were taken at 22.2x magnification at 1.0μm steps using a Keyence BZ-X800 microscope. Images of 10 granule cells per hemisphere were taken per animal (n=4 mice). Granule cells included had an observable cell body and had dendrites that terminated at or near the hippocampal fissure. Brightfield images were then imported into the Keyence

Analyzer Software for conversion into a greyscale image and creation of 2D projection images. Images were then imported into ImageJ where a single dendritic arbor was measured per granule cell. Measurements from the contralateral dentate gyrus in one animal were not included due to cutting of the distal end of dendrites during tissue processing resulting in incomplete extension toward the hippocampal fissure. Data are represented as the average dendritic length for each animal for each hemisphere and compared using t-test.

Spine density and dendrite diameters were taken within the inner, middle, and outer molecular layers of PTEN-deleted and PTEN-expressing neurons within the ipsilateral and contralateral hippocampi, respectively. Z-stacks of individual granule cells were taken under oil immersion at 60x magnification at 0.1μm steps using a Keyence BZ-X800 microscope. Care was taken to ensure that images contained the granule cell soma and attached apical dendrites within the overlying molecular layer. Imaging began at the lateral end of the dorsal blade and continued medially before progressing to the ventral blade from the apex of the dentate gyrus to the ventral lateral edge. Brightfield image stacks were then imported into the Keyence Analyzer Software for conversion into color-inverted, greyscale images, followed by deconvolution procedures and creation of 2D maximum contrast projection images. Finalized images were then imported into Oxford Instruments Imaris® software for detailed spine analysis using Filaments tracer module.

To determine dendritic segments selected for measurement, the dentate gyrus and granule cell layer were manually traced on 4x tdTomato images taken of the hippocampus prior to completion of the Golgi stain. These traces were then transposed onto 4x images taken of the

same tissue following Golgi staining. This process allowed for identification of borders between the granule cell layer and the molecular layer, as well as the hippocampal fissure. Actual measurements, however, were completed on the 60x images described above.

The inner molecular layer sample was the first 50μm from the granule cell border, the outer molecular layer sample was the first 50μm from the hippocampal fissure, and the middle molecular layer was 50μm centered around the midpoint between the granule cell layer and hippocampal fissure. Within each zone, Imaris Filaments software quantified spine density by calculating the number of protrusions within a 10μm section of dendritic segment. Segments within the inner molecular layer were measured from at least 10μm from the granule cell body or granule cell-molecular layer border. Segments in the outer molecular layer were measured from at least 10μm from the hippocampal fissure or dendrite terminal end. In each case, segments selected were easily differentiated from surrounding dendrites and did not contain any overlapping regions with other neurons or cell types. Only one measurement at each molecular layer zone was taken from a single neuron, but each measurement was not always possible from each neuron. Dendritic spines were defined as having greater than a 0.25μm spine head width and less that a 3μm spine length. Dendritic diameter was also averaged across the same 10μm segment. Data are represented as the average spine density or dendritic caliber from 10 segments per lamina for each individual animal.

Dendritic spines within each segment were further characterized as thin/filopodia, stubby, or mushroom using the Imaris filament software and each subtype was represented as a raw

number or density per 10μm segment length. Designations were determined by the Imaris filaments software. A thin spine was determined as having similar spine head and neck diameters, with spine length roughly 2.5x the neck diameter. Filipodia-like spines were not distinguished from thin spines and may therefore be included in this category. A stubby spine was designated as having a similar spine head and neck diameter, with spine length less that 2.5x the neck diameter. Finally, mushroom spines were identified as spines in which the diameter of the spine head was greater than or equal to 1.5x the diameter of the spine neck (Haws et al., 2014).

Assessment of mossy fiber projections

Sections stained for the zinc vesicular transporter, Znt3, at the core of the area of tdT expression were used to measure alterations to granule cell axonal projections (mossy fibers). Briefly, images of both the ipsilateral and contralateral dentate gyrus and CA3 were taken with a 10x objective using an Olympus AX80 microscope and images were imported into ImageJ FIJI. Measurements were taken of the thickness of the bundle containing mossy fibers upon exiting the hilus (blue line in Fig. 3.8A, B), and the thickness of the supra-pyramidal mossy fiber terminal field in *stratum lucidum* of CA3 (red line in Fig. 3.8A, B).

To detect supra-granular mossy fibers, Znt3 labeled sections at the core of transduction were used. Sections at each time point for both experimental and control animals were scored according to a modified scale described by (Hunt et al., 2009): 0=little to no Znt3 labeling in granule cell layer; 1=mild Znt3 labeling in granule cell layer; 2=moderate staining in the

granule cell layer and punctuate staining in inner molecular layer; 3=dense Znt3 labeling in inner molecular layer.

Statistical methods

Graphs were created and statistical analyses were performed using the GraphPad Prism Software. Except where noted, one-way analysis of variance (ANOVA) was used to compare measurements from the ipsilateral dentate gyrus in PTEN/tdT and tdT control groups and two-way ANOVA was used for comparisons between contralateral and ipsilateral hemispheres in PTEN/tdT mice. In each case, Sidak's multiple comparisons tests were used for detailed comparisons between groups. For all outcomes, the relationship between each measure and percent PTEN deletion at each endpoint were assessed by linear regression.

RESULTS

Patterns of transduction in the dentate gyrus following AAV-Cre injection in adult transgenic mice

Unilateral injections of AAV-Cre into the dentate gyrus of PTEN/tdT and tdT control mice led to robust transduction of dentate granule cells as revealed by tdT expression. Figure 3.1C illustrates tdT expression 2 months post-injection in sections taken at 360μm intervals through the hippocampus of a PTEN/tdT mouse. The area of transduction is characterized by a core in which most neurons are tdT-positive; overall intensity of labeling gradually

diminishes in the rostral and caudal directions as granule cells become more sparsely transduced (Fig. 3.1C). There was some variability in transduction between animals, despite use of consistent AAV-Cre titers, injection volumes, and coordinates. In most cases, granule cells were transduced in both dorsal and ventral blades of the dentate gyrus, but in some cases, transduction involved primarily either the dorsal or ventral blades. This variation is likely due to slight differences in the depth of the injection.

Transduction volume at different time points post-injection was determined by applying the Cavalieri principle to tdT-positive area measurements taken from sections spaced 360μm apart (Fig. 3.1D). The average volume of the transduced region was $5.91x10^6$ +/- $3.72x10^6$ μm^3 at 2 weeks and gradually increased over time to $1.21x10^7$ +/- $6.04x10^6$ μm^3 by 6 months. Although average volume of the transduced region was somewhat larger at longer intervals post-injection in PTEN/tdT mice, there was also greater variability in the values, and one-way ANOVA revealed no overall significant difference between time points [$F(4, 21) = 1.137$, $p= 0.3661$].

Transduction volume for tdT controls was $5.66x10^6$ +/- $2.58\ x10^6$ μm^3 at 6 months following transduction; one-way ANOVA revealed no significant difference in transduction volume between PTEN/tdT mice and tdT controls [$F(5, 25) = 1.562$, $p= 0.2073$]. The rostral to caudal spread of the transduced area appeared to be consistent across all cases, with tdTomato labeled cells evident across roughly 3.5mm of the dentate gyrus (Fig. 3.1F).

The percent area of the Hoechst-labeled dentate gyrus that was co-labeled with tdTomato was also measured throughout the entire length of the hippocampus in the same sections used for volume calculations and including sections at distal points from the injection core that may not contain any transduction (Fig. 3.1E, F). The percentage of the total ipsilateral dentate gyrus occupied by tdTomato in PTEN/tdT mice was 28.40% +/- 19.27% at 2 weeks, 35.00% +/- 12.37% at 1 month, 38.26% +/- 14.13% at 2 months, 40.19% +/- 25.58% at 4 months, 37.20% +/- 18.26% at 6 months, and 26.27% +/- 10.04% at 6 months in tdT controls. One-way ANOVA revealed no significant difference between timepoints in PTEN/tdT mice [$F(4,22) = 0.5379$, $p = 0.7094$] or when comparing PTEN/tdT mice to tdT controls [$F(5, 25) = 0.5344$, $p=0.7482$].

Time course of PTEN deletion and mTOR *in transduced granule cells*

To determine the timing of PTEN deletion and mTOR activation, we immunostained sections from mice at different time points post-injection for tdT, PTEN and pS6. Figure 3.2 illustrates that by 2-months post-injection, PTEN immunostaining was essentially absent in the area of tdT expression (compare Fig. 3.2A, D with Fig. 3.2B, E, which illustrate PTEN expression in the non-transduced, contralateral dentate gyrus). Quantification of PTEN fluorescence intensity (ipsilateral vs. contralateral dentate gyrus) at the core of transduction revealed decreases in PTEN immunostaining by 2 weeks and further decreases at longer time points (Fig. 3.2J). One-way ANOVA revealed an overall difference over time [$F(5, 24) = 40.94$, $p< 0.0001$], and Sidak's multiple comparisons test revealed a significant difference between the PTEN deleted dentate gyrus and controls at all time points (see legend to Figure 3.2 for

details). There were no apparent decreases in PTEN immunostaining in the area of transduction in tdT control mice (Fig. 3. 2C, F).

The canonical downstream marker of mTOR activation is activation of phosphorylation of ribosomal protein S6 (pS6) (Liu et al, 2010). Immunostaining using phospho-specific antibodies for pS6 (p235/236) revealed activation of S6 phosphorylation in most granule cells in the area of transduction at 2 months post-injection (Fig. 3.2G) and few pS6-positive granule cells in the contralateral dentate gyrus with intact PTEN expression (Fig. 3.2H). Similar activation of phospho-S6 was evident at all time points (not shown). There were no increases in immunostaining for pS6 in transduced granule cells in tdT controls (Fig. 3.2I).

Progressive enlargement of the PTEN-deleted dentate gyrus

One consequence of PTEN deletion was apparent enlargement of the dentate gyrus in the area of transduction involving increases in the width of the hilus and molecular layer. Figure 3.3 illustrates this effect in sections stained with Cresyl violet from tdT control and PTEN/tdT mice at 6 months post AAV-Cre (Fig. 3.3A, B). To quantify this, we measured the percent areas of the dentate gyrus, CA3 and CA1 in sections at the core of transduction stained for Cresyl violet. Percent area is used rather than absolute area because of variations in the rostro-caudal location of the core of transduction and the fact that the cross-sectional area of the dentate gyrus in coronal sections varied slightly in their rostro-caudal location.

As illustrated graphically in Figure 3.3C, there were progressive increases in the percent area occupied by the AAV-Cre-injected dentate gyrus in PTEN/tdT mice when represented as a percentage of the contralateral dentate gyrus with the initial increase being seen at 2 months post-injection and the largest increase being at 6 months. One-way ANOVA revealed a significant difference between PTEN/tdT and tdT controls [$F(5,25) = 10.56$, $p < 0.0001$].

Percentages for the control side contralateral to the injection remained constant (Fig. 3.3D, average of 28.22 +/- 2.63% across all time points) and were comparable to values in tdT controls (ipsi= 26.51 +/- 4.342%; contra= 29.10 +/- 2.133%) when dentate gyrus size was instead represented as a percentage of the entire hippocampus. Here, significant increases in the size of the dentate gyrus were observed at 4 months post injection. One-way ANOVA revealed a significant difference between the contralateral (PTEN intact) and ipsilateral (PTEN deleted) sides [$F(5,46) = 14.17$, $p < 0.0001$]. One-way ANOVA revealed further significance in relative percent size between the transduced, PTEN deleted dentate gyrus and the transduced dentate gyrus of tdT controls [$F(5,25) = 8.353$, $p < 0.0001$]. Of note, the extent of the increase in % area of the dentate gyrus was related to the total percent area of transduction (see Fig. 3.3E for r-squared values).

If there are increases in the percent area occupied by one sub-region of a structure, one would expect decreases in the percent area occupied by other subregions, and this trend was present. Figure 3.3F compares the percent area occupied by the dentate gyrus, CA1, and CA3 at 6 months post-injection in PTEN/tdT and tdT controls. Two-way ANOVA revealed a significant difference based on hippocampal subregions [$F(2,24) = 53.43$, $p < 0.0001$], and a

significant interaction [F (2,24) = 16.98, p< 0.0001], but no significant difference for PTEN expression state.

Progressive enlargement of dentate granule cell somata

Dentate granule cell bodies became notably larger over time following PTEN deletion. This was evident in areas of sparse tdTomato expression at the rostral and caudal ends of transduction where individual granule cell bodies could be discerned (Fig. 3.4A, B, 6m tdT control vs. 6m PTEN/tdT). To define the time course of the increases in cell size, we first measured the cross-sectional area of tdT-positive granule cells in regions of sparse transduction in tdT control vs. PTEN/tdT mice (Fig. 3.4E). Average cell size was slightly greater at 1 month (175.7 +/- 16.6μm^2 vs. 151.2 +/- 17.9μm^2 in tdT controls), increased dramatically between 1-2 months to 297.7 +/- 34.7μm^2, and then continued to increase gradually (323.4 +/- 24.8μm^2 at 4 months, and 369.1 +/- 45.8μm^2 at 6 months). One-way ANOVA revealed a significant difference between genotypes [F (5,25) = 58.69, p< 0.0001].

The boundaries of tdT-positive neurons were difficult to discern in regions of dense transduction, so soma size was assessed using Cresyl violet stained sections (Fig. 3.4G) comparing granule cell size ipsilateral vs. contralateral to the injections. This method allows for visualization of individual PTEN deleted cells in close proximity to one another, which is difficult with tdTomato expression (see granule cell layers in Fig. 3.4C, D). The time course and extent of the increases in soma size of PTEN-deleted granule cells was similar in Cresyl violet stained sections although values were about half of that with tdT labeling and

significant increases were first observed at 1 month post AAV-Cre injection (Fig. 3.4G). Two-way ANOVA comparing ipsilateral and contralateral sides in PTEN/tdT mice over time revealed significant differences for PTEN deletion status [$F(1,42) = 205.0$, $p < 0.0001$], and time post-injection [$F(4,42) = 13.35$, $p < 0.0001$], and a significant interaction [$F(4,42)=19.03$, $p<0.0001$]. Sidak's multiple comparisons test revealed significant differences between PTEN deleted and control granule cells at all time points from 1 to 6 months (See legend to Figure 3.4 for details on statistics). Comparisons of the size of Cresyl violet stained granule cells in the area of transduction in PTEN/tdT vs. control tdT mice confirmed increases in soma size (One-way ANOVA, [$F(5,25) = 29.84$, $p < 0.0001$]), and significant differences at all time points from 1 to 6 months by Sidak's multiple comparisons test (See legend to Figure 3.4 for details on statistics).

Of note, the measures of granule cell size in Cresyl violet stained material were about half that of tdT stained granule cells (roughly 70μm^2 vs. 150μm^2 in control neurons) although the % increases in size with PTEN deletion were comparable. One possible explanation is simply differential shrinkage during Cresyl violet staining vs. immunohistochemistry for tdT. Another explanation is that tdT labeling extends throughout the cytoplasm whereas ribosomes stained by Cresyl violet may be more concentrated near the nucleus making the apparent size of the cell appear smaller. Alternatively, it is actually the cell nucleus that is most heavily stained by Cresyl violet and granule cell bodies actually have relatively little cytoplasm so measurements may actually be of the nuclei rather than the cell body.

A previous study of PTEN-deleted adult-born granule cells reported that the extent of dendritic growth was greater in animals with a higher density of PTEN-deleted neurons (Arafa et al., 2019). This is noteworthy because it raises the possibility of non-cell intrinsic factors regulating growth. Accordingly, we assessed whether cell body enlargement was related to percent transduction. As illustrated in Fig. 3.4F, the extent of cell body enlargement correlated with percent transduction in regions of sparse transduction at 2 months post AAV-Cre, but not at later timepoints (see Fig. 3.4F for r^2 values). Similarly, regression analyses revealed a significant relationship between percent transduction and soma size in regions of dense transduction at 4 months post AAV-Cre injection (r^2=0.9655, Fig. 3.4H), but not 6 months (r^2=0.2821). Possible explanations for these trends are discussed below.

Increased apical dendrite length and caliber following PTEN deletion

In addition to increases in the overall size of the dentate gyrus and granule cell bodies, there appeared to be increases in the width of the molecular layer. In the normal dentate gyrus, granule cell apical dendrites extend to the boundary of the molecular layer, so increases in the width of the molecular layer could be a surrogate measure for increases in dendritic length. Accordingly, we measured the thickness of the molecular layer in regions of dense transduction in PTEN/tdT (Fig. 3.4D) and tdT control (Fig. 3.4C) mice. Because transduction did not always involve both blades of the dentate gyrus, these measurements were done only in mice with transduction of the dorsal blade.

Quantitative assessment confirmed our qualitative impression of increases in the width of the molecular layer in areas of PTEN deletion over time (Fig. 3.4I). Two-way ANOVA between the contralateral (PTEN expressing) and ipsilateral (PTEN deleted) molecular layers in PTEN/tdT mice revealed overall significance for PTEN deletion status [$F(1,40) = 53.6$, $p < 0.0001$], a significance difference over time [$F(4,40) = 17.77$, $p < 0.0001$], and a significant interaction [$F(4,40) = 8.929$, $p < 0.0001$]. Increases in the width of the molecular layer were also evident in comparisons of PTEN/tdT vs. control tdT mice (One-way ANOVA [$F(5,23) = 18.57$, $p < 0.0001$]. Post hoc comparisons by Sidak revealed significant differences at 4 and 6 months (See legend to Figure 3.4 for details on statistics). Interestingly, correlations between percent transduction and molecular layer thickness were inversely related at 4 and 6 months after PTEN deletion (Fig. 3.4J). This result may point to physical limitations placed on dendrite growth due to space availability or a lack of non-cell intrinsic factors regulating dendritic growth as documented by (Arafa et al., 2019).

As in the normal dentate gyrus, dendrites from PTEN deleted neurons extended to the border of the expanded molecular layer, confirming that the length of at least some dendrites must have increased. Interestingly, dendrites from PTEN-deleted granule cells also extended laterally along the edge of the molecular layer, suggesting continued growth even after the dendrite reached the boundary of the molecular layer. This could be best seen in regions of sparse transduction (arrowheads in Fig. 3.4B). This lateral extension differed from the situation for normal granule cells, whose dendrites typically terminate at the edge of the molecular layer (arrow in Fig. 3.4A). Although dendrites did extend laterally, few if any

dendrites from PTEN deleted granule cells extended across the hippocampal fissure into the stratum lacunosum-moleculare of CA1.

Although individual dendrites could be followed in areas of sparse transduction (Fig. 3.4A, B), it was challenging to reliably measure length and diameter of tdT labeled dendrites because tdTomato labeling was patchy within the dendrite. Additionally, it was not possible to distinguish individual dendrites at the core of the transduced area where growth appeared maximal (Fig. 3.4C, D). Accordingly, we used samples prepared for Golgi staining to compare the length of individual dendrites from PTEN-deleted granule cells at the core of transduction vs. PTEN expressing granule cells in the contralateral dentate gyrus at 6 months post deletion (Fig. 3.5A vs. 3.5B). We selected neurons with dendrites that could be followed from the cell body to the end of the molecular layer and measured one dendrite per neuron from 10 neurons in 4 mice. As expected, based on the increases in the width of the molecular layer reported above, dendrites of PTEN-deleted neurons were on average longer than controls in the contralateral dentate gyrus (Fig. 3.5C, t-test: df=5, t=3.953, p=0.0108).

Dendrites of PTEN-deleted neurons also appeared to be of larger caliber (compare PTEN-deleted dendrites in Fig. 3.5B, E with PTEN expressing dendrites in Fig. 3.5A, D). Thus, we assessed dendritic diameter from the same Golgi-stained sections, comparing dendrites in the area of transduction vs. the contralateral dentate gyrus. Examples of dendritic segments in the inner, middle, and outer molecular layers in the ipsilateral and contralateral dentate gyrus are illustrated in Figure 3.5; quantitative analyses revealed an approximately 2-fold increase in dendritic diameter (0.825μm vs. 1.47μm averaged across all laminae). In Figure

3.5F data from each mouse is represented as the average of the mean dendritic diameter from 10 individual, dendritic segments (10μm in length) in the inner, middle, and outer molecular layer; average dendritic caliber was greater in all 3 laminae (Two-way ANOVA was significant for PTEN expression state [$F(1,18) = 195.8$, $p < 0.0001$], but not for molecular layer or interaction, Sidak's multiple comparisons test $p < 0.0001$ for each layer).

Increased spine densities indicate new synapse formation onto PTEN deleted granule cells

An important feature of our model is that injections of AAV-Cre delete PTEN in a focal area of the dentate gyrus, but PTEN expression is intact in the cells of origin of the major input pathways. Thus, we were curious whether dendritic growth of PTEN-deleted neurons would be accompanied by new synapse formation by input pathways. As an indirect measure of synapses, we assessed spine densities on proximal, middle, and distal dendrites in the inner, middle, and outer molecular layer in the same Golgi-labeled segments measured for dendritic caliber (Fig. 3.5G). Middle and distal dendrites receive inputs from the entorhinal cortex via the perforant path whereas proximal dendrites receive input from the commissural/associational system. Elongation of dendrites without new synapse formation would be expected to lead to a decrease in spine density along the dendrite. Instead, our analysis revealed a dramatic increase in spine density throughout the length of the dendritic tree (two-way ANOVA for PTEN-deleted vs. controls [$F(1,18) = 50.98$, $p < 0.0001$], with no significance for molecular layer or interaction); Sidak's post hoc analysis revealed increases in spine density in all 3 laminae (see Figure 3.5 legend for statistics), suggestive of increased synapse formation onto PTEN deleted granule cells by otherwise normal input pathways.

Dendritic spines are often classified by their size and shape as an indication of their functional properties. During development, dendritic spines transition from thin to stubby, and then mature into a mushroom-like form. As a measure of functional maturity, we used the analysis program of Imaris to categorize spines as thin, stubby, or mushroom shaped in the inner, middle, and outer molecular layers in the same segments assessed for spine density and dendritic caliber. Our analysis revealed increases in the average number of thin spines in each of the three laminae, with no significance in the number of stubby or mushroom spines (two-way ANOVA for PTEN-deleted vs. controls [$F(2,12) = 24.91$, $p<0.0001$], for spine type [$F(2,12) = 77.13$, $p<0.0001$], for interaction [$F(1,12) = 44.74$, $p<0.0001$]). These suggest an increase in the density of functionally immature, thin spines following PTEN deletion. Preservation of the number of mushroom shaped spines over a given dendritic segment, indicates an increase in the total number of functionally mature spines across the elongated dendrite.

Preservation of segregation of afferent inputs in areas of PTEN deletion

An important reason for choosing the dentate gyrus for studies of connectivity is the extremely precise pattern of termination of input pathways, specifically the fact that the two major inputs to granule cells from the entorhinal cortex (the perforant path) and commissural/associational pathways terminate in non-overlapping laminae in the inner vs. outer molecular layers. This is an ideal setting in which to evaluate whether growth of postsynaptic neurons disrupts normal connectional specificity. To assess this, we used

orthograde tract tracing in mice that underwent PTEN deletion at p19 (Fig. 3.6A, B) and in adulthood (2 months, Fig 3.7A, B).

Figure 3.6C illustrates the pattern of termination of AAV-ChR labeled perforant path projections from the ipsilateral entorhinal cortex (green fluorescence) in the area of transduction (indicated by tdT fluorescence) at 13 weeks following PTEN deletion at p19. The terminal field of the perforant path is expanded in the middle molecular layer in the area of PTEN deletion (Fig. 3.6D) but there is a very precise boundary at the boundary with inner molecular (arrow) as in areas outside the zone of PTEN deletion (Fig. 3.6E).

Similarly, the precise pattern of termination of the BDA-labeled commissural pathway was also maintained in the area of transduction 13 weeks after PTEN deletion at p19. Figure 3.6F illustrates projections from the contralateral hippocampus (green) within the area of PTEN deletion (red). Again, higher magnification images reveal that afferents terminate within the inner molecular layer and rarely crossed the boundary into the granule cell layer or middle molecular layer (Fig. 3.6G, arrow), similar to commissural projections found in non-transduced regions within the ventral hippocampus (Fig. 3.6H, arrow). There was no obvious expansion of the terminal zone of commissural projections into the outer molecular layers in the area of transduction.

Dendritic length continues to increase with time after PTEN deletion, and so we were curious whether laminar specificity would still be maintained at longer intervals. For this, we assessed the pattern of termination of perforant path and commissural pathways 7.5 months

post AAV-Cre injections (Fig. 3.7A, B). As illustrated in Figure 3.7C, the terminal field of perforant path projections, although further expanded, was still restricted to the middle molecular layer with a sharp boundary at the edge of the inner molecular layer (Fig. 3.7D). For comparison, the pattern of termination outside the area of transduction is illustrated in (Fig. 3.7E). Similarly, the terminal field of commissural projections was expanded in the area of transduction, and axons appeared somewhat disorganized (Fig. 3.7F, G), but these axons were still largely restricted to the inner molecular layer (Fig. 3.7G) as in regions outside the area of PTEN deletion (Fig. 3.7H).

Expansion of mossy fiber laminae

PTEN deletion enables axon regeneration and enhances sprouting after injury, so we wondered whether deleting PTEN would trigger growth of granule cell axons. Granule cells project selectively to the stratum lucidum of CA3 where they synapse on pyramidal cells. To assess whether PTEN deletion led to expanded mossy fiber projections, sections were immunostained for the zinc vesicular transporter, Znt3, which is highly abundant in mossy fiber axons.

As illustrated in Figure 3.8, the mossy fiber terminal field in *stratum lucidum* was obviously thicker with PTEN deletion (compare Figure 3.8A vs. 3.8B, which compares mossy fiber projections at 6 months after AAV-Cre injection in tdT control vs. PTEN/tdT mouse, respectively). The same was true of the collection of mossy fibers as they leave the hilus, which we term the mossy fiber tract. To quantify this, we measured the width of the mossy

fiber terminal field in *stratum lucidum* of CA3 (SL, Fig. 3.8A, B red line) and the mossy fiber tract (Fig. 3.8A, B blue line).

For the mossy fiber terminal field in *stratum lucidum* A3 (Fig. 3.8E), two-way ANOVA revealed overall significant differences between ipsilateral vs. contralateral sides [F (1,36) = 6.042, p= 0.0189], significant difference over time post-deletion [F (4,36) = 11.26, p< 0.0001], and a significant interaction [F (4,36) = 5.576, p= 0.0013]. One-way ANOVA for the transduced dentate gyrus of PTEN/tdT mice vs. tdT controls was significant [F (5,20) = 10.52, p< 0.0001]. Of note, there was no evidence of ectopic mossy fiber growth into the *stratum radiatum* of the CA3, which suggests maintenance of appropriate targeting to PTEN expressing pyramidal cells by PTEN deleted granule cells despite expansion of their terminal field. Regression analyses indicated that enlargement of the mossy fiber tract terminal zone within the stratum lucidum was greater at 4 months post AAV-Cre injection in mice with higher percent transduction (Fig. 3.8F).

For the mossy fiber tract, quantitative analyses at different time points (Fig. 3.8C), revealed progressive increases in the thickness of the mossy fiber tract with time post-PTEN deletion. Two-way ANOVA was significant for ipsilateral vs. contralateral sides [F (1,36) = 14.03, p= 0.0006], and for time post-deletion [F (4,36) = 8.916, p< 0.0001], with significant interaction [F (4,36) = 2.731, p= 0.0440]. One-way ANOVA for the transduced dentate gyrus of PTEN/tdT vs. tdT controls was also significant [F (5,20) = 7.022, p= 0.0006]. Regression analyses indicated that the extent of the increase in mossy fiber tract thickness was greater at 4- and

6-months in cases with a higher percent transduction (Fig. 3.8D, see figure for r-squared values).

Delayed development of supra-granular mossy fibers in some mice

One finding in previous studies involving PTEN deletion in developing dentate granule cells was the growth of mossy fiber axons into the inner molecular layer, which is also present in rodent models of temporal lobe epilepsy. These supra-granular mossy fibers form excitatory recurrent collaterals with granule cells, which is thought to contribute to increased excitability (Althaus & Parent, 2012). Thus, we were curious whether PTEN deletion in adult mice would lead to similar ectopic projections.

Examination of Znt3 stained sections revealed supra-granular mossy fibers in some mice at long post-injection intervals (Fig. 3.8B, 3.9). To quantify these, we used a modified scoring system from (Hunt et al., 2009) where a score of 0 indicates no mossy fibers in the granule cell layer and a score of 3 indicates dense mossy fiber staining in the inner molecular layer (see methods and Figure 3.9 legend for complete scoring list).

There was no evidence of Znt3 labeling in either the granule cell or molecular layer at 2 weeks or 1-month post-AAV (Fig. 3.9A, higher magnification in F). At 2 months post-deletion, there was slight Znt3 labeling in the inner molecular layer in 1 of 6 mice (depicted in Fig. 3.9B, G). At 4 months, ectopic mossy fibers were more evident (Fig. 3.9C, H). Of 5 mice, Znt3 labeling in the granule cell layer was slight in one mouse (score of 1), but mild labeling

was found in the inner molecular layer of one mouse (score of 2), and dense Znt3 labeling in the inner molecular layer of another mouse (score of 3). Finally, by 6 months post PTEN deletion (Fig. 3.9D, I), 2 of 5 animals showed slight granule cell layer labeling, 1 of 5 animals displayed moderate granule cell layer labeling with mild labeling in the inner molecular layer, and 1 of 5 animals showed dense Znt3 labeling in the inner molecular layer. Interestingly, there were no obvious supra-granular mossy fibers at the rostral and caudal ends of transduction where PTEN deletion was more sparse; this suggests a relationship between density of PTEN deletion and formation of supra-granular mossy fibers. There were no ectopic mossy fibers in control tdT mice at 6 months post AAV-Cre injection (Fig. 3.9E, J). Graphical representation of this scoring is shown in Figure 3.9K. Further regression analyses indicate that the presence of supragranular mossy fibers progresses from 2 through 6 months post AAV-Cre injection and is most prevalent at later timepoints in cases with greater percent transduction (Fig. 3.9L).

DISCUSSION

This study confirms previous reports that deletion of PTEN in adult neurons triggers progressive growth of cell bodies and dendrites (Gallent & Steward, 2018) and extends the story by answering three questions: 1) Does dendritic growth induce new synapse formation by input pathways with intact PTEN expression; 2) Does dendritic growth alter specificity of termination of input pathways; and 3) Do axons from PTEN deleted neurons extend into ectopic sites. Using the model of unilateral deletion of PTEN in the dentate gyrus, we show

that dendritic growth is accompanied by spinogenesis, and presumably the formation of new synapses by input pathways in which PTEN expression is intact. Laminar specificity of afferent terminations is preserved. Mossy fiber terminal fields from PTEN-deleted neurons expand in CA3, and supragranular mossy fibers develop in some mice at late time points.

Growth due to PTEN deletion in adult neurons is initiated from a steady state of homeostatic size maintenance. During development, the brain increases in size, initially by cell proliferation and then by growth of axons, dendrites and synapses. The pace of brain growth slows as the brain matures and a steady state is achieved in the adult brain in which neurons have a characteristic size and morphology based on neuron type. In the adult brain, dendrites and synapses grow in response to neuronal activity, but overall, increases in synaptic strength or number are counterbalanced by homeostatic decreases of other synapses so that overall excitatory drive to a particular neuron is maintained (Maffei & Turrigiano, 2008; Turrigiano, 2008; Turrigiano & Nelson, 2004). Activation of mTOR via PTEN deletion re-initiates additive growth, upending homeostasis of dendritic size and synapse numbers.

Enlargement of mature granule cells following PTEN deletion

The time course of growth seen here is similar to the time course of growth of cortical neurons (Gallent & Steward, 2018). We document a new feature, however—that the time course of increases in cell size is faster in areas of dense transduction than in areas of sparse transduction. Specifically, increases in cell size were evident at 1 month after AAV-Cre

injection in regions of dense transduction, whereas increases in cell size were not statistically significant until 2 months in regions of sparse transduction. This difference suggests that cell growth is influenced by neighboring neurons in which PTEN has been deleted, consistent with previous studies involving shRNA-mediated PTEN knockdown (Luikart et al., 2011).

Although neuronal hypertrophy has been documented in early developmental PTEN deletion models (Kwon et al., 2001; Pun et al., 2012; Williams et al., 2015), the time course was faster than seen here. One interpretation is that time is required for transformation of mature neurons to a growth state whereas neurons are already growing during the developmental period. It remains to be determined whether growth induced by PTEN deletion continues indefinitely or whether it eventually slows down or stops entirely at a new steady state.

Dendritic growth in PTEN deleted granule cells

In the normal adult dentate gyrus, dendrites of granule cells extend to the edge of the molecular layer and stop. Similarly, in the core of the area of PTEN deletion, tdT labeled dendrites extended throughout the expanded thickness of the molecular layer. In areas of sparse transduction, where molecular layer thickness did not increase, some tdT-positive dendrites of PTEN deleted neurons extend laterally along the edge of the molecular layer rather than stopping at the edge. This indication of growth has also been reported in previous studies of promoter-driven PTEN deletion (Arafa et al., 2019).

Post synaptic dendritic growth is accompanied by spinogenesis

Dendrites of normal granule cells have a characteristic spine density of about 2 spines/μm. We wondered whether dendritic elongation would reduce spine density (same number of spines on longer dendrites) or whether new spines would form on elongated dendrites. Our analysis revealed that spine density was 1.5-fold higher on PTEN-deleted dendrites. Dendritic spines are the site of excitatory synapses, and although we did not determine whether every spine is innervated, our results strongly suggest that new synapses form on the elongated dendrites.

Of note, perforant path synapses, which innervate middle and distal dendrites, arise from neurons in the entorhinal cortex with intact PTEN expression. The inner 1/3 of the granule cell dendritic tree is innervated by synapses from the commissural/associational pathway, which originates from neurons in the hilus of the dentate gyrus in both hemispheres. Some hilar neurons in the area of transduction would be PTEN-deleted, but most of the cells of origin of the commissural/associational pathway retain PTEN expression. Thus, the additional spine synapses throughout the dendritic laminae come largely from neurons with intact PTEN expression.

Similar increases in spine numbers have been seen with developmental PTEN deletion (Luikart et al., 2011; Pun et al., 2012; Skelton, Frazel, et al., 2019; Skelton, Poquerusse, et al., 2019; Williams et al., 2015). Taken together, these results suggest that dendrites, at any developmental stage, control spine numbers, so increases in dendrite length and caliber due to PTEN deletion trigger addition of spines and presumably new synapse formation by input

pathways regardless of their PTEN expression state. This represents postsynaptic induction of synapse formation by otherwise mature neurons in an established network.

Spines are often categorized by size and shape into mushroom, thin, and stubby, and these shapes are thought to correlate with different functional properties. Thin spines are common during development and in adult brains are considered to be immature, whereas mushroom shaped spines are considered to be more mature. Our results reveal increases in the density of thin spines and no overall change in the density of mushroom shaped spines. The higher density of thin spines may indicate a continuing addition of new spines. Preservation of mushroom spines suggests an increase in the number of functionally mature spines along elongated dendrites. These results differ somewhat from previous studies involving promoter-driven PTEN deletion, in which increases in mushroom spine density were reported (Skelton, Poquerusse, et al., 2019). Differences in post-deletion interval or categorization method may account for differences between studies.

Preserved laminar specificity of input projections to PTEN deleted granule cells

The entorhinal cortex and commissural/associational pathway are the primary inputs to dentate granule cells. The middle and outer thirds of the molecular layer receive inputs from the medial and lateral entorhinal cortex respectively (the perforant path) and the inner molecular receives inputs from mossy cells in the hilus (the dentate commissural/associational pathway). Our tract tracing studies reveal that dendritic growth did not disrupt the normal specificity of these projections; both major afferent inputs still

terminate selectively in their normal laminae, although the width of the terminal fields increase along with the increases in the width of the molecular layer. It remains to be determined whether these pathways are the exclusive source of new synapses on dendritic spines. Studies of PTEN deletion in development suggest that PTEN deleted neurons may recruit input from more presynaptic partners (Skelton, Frazel, et al., 2019).

Expanded mossy fiber projections in CA3

Our results reveal increases in the thickness of the mossy fiber tract and terminal lamina in CA3, which has also been reported with developmental deletion (Amiri et al., 2012; Zhou et al., 2009). Although the mossy fiber lamina is thicker, mossy fibers are still limited to the proximal dendritic region of CA3 (*stratum lucidum*) and don't extend into *stratum radiatum*. It remains to be determined whether adult PTEN deletion alters the size, number, or spacing of mossy fiber boutons, as reported with PTEN deletion in adult born granule cells (LaSarge et al., 2015) and whether expansion of the mossy fiber terminal zone in CA3 alters the dendritic architecture of CA3 pyramidal cells.

Supra-granular mossy fibers present in some mice

Supra-granular mossy fibers are seen in embryonic and early postnatal PTEN deletion models (Amiri et al., 2012; Kwon et al., 2006; Pun et al., 2012; Sunnen et al., 2011), and were seen in 16% of mice at 2 months post-injection and 40% of our mice at 4-6 months. Importantly, supra-granular mossy fibers were only seen in PTEN-deleted animals at later

time points with greater than 40% transduction, which is a greater deletion burden than reported in promoter-driven models (Pun et al., 2012). Supra-granular mossy fibers are also a prominent feature in kainic acid and pilocarpine models of epilepsy, and are considered to indicate recurrent excitatory circuits that contribute to epileptogenesis.

Because the end result of the growth of adult granule neurons is similar morphologically to what is seen with early life PTEN deletion, it's reasonable to speculate that the physiological consequences would be similar, including increases in overall excitatory drive, changes in synaptic properties, and eventually development of spontaneous seizures (LaSarge et al., 2016; Luikart et al., 2011; Pun et al., 2012; Williams et al., 2015). Indeed, in a separate report, we document that most mice with unilateral PTEN deletion develop spontaneous generalized seizures at approximately 60 days post deletion. Thus, unilateral PTEN deletion in the dentate gyrus represents a new model, and new mechanism, of adult-onset epilepsy.

Table 3.1:

Mice used for histological analysis

Time post AAV-Cre	Age at time of injection	# PTEN/tdT mice	# tdT mice	Histology
2 weeks	9 weeks	n=4 (1M, 3F)		PTEN, n=4 pS6, n=4 Znt3, n=4 Cresyl violet, n=4
1 month	9 weeks	n=6 (3M, 3F)		PTEN, n=6 pS6, n=6 Znt3, n=6 Cresyl violet, n=6
2 months	9-10 weeks	n=6 (3M, 3F)		PTEN, n=6 pS6, n=6 Znt3, n=6 Cresyl violet, n=6
4 months	9 weeks	n=6 (3M, 3F) 1 excluded		PTEN, n=5 pS6, n=5 Znt3, n=5 Cresyl violet, n=5
6 months	8-9 weeks	n=14 (9M, 5F) 2 died 2 excluded	n=5 (2M, 3F)	PTEN, n=10 pS6, n=10 Znt3, n=10 Cresyl violet, n=10 Slice golgi, n=5
3.5 months	p19	n=2 (2F)		BDA, n=1 ChR, n=1
7-8 months	9-10 weeks	n=2 (2M)		BDA, n=2

Table 3.2:

Primary Antibody list

Antibody	Host	Vendor	RRID	Dilution
PTEN	Rabbit	Cell Signaling Technology, 9188	AB_2253290	1:250
pS6, Ser 235/236	Rabbit	Cell Signaling Technology, 4858	AB_916156	1:250
pS6, Ser 240/244	Rabbit	Cell Signaling Technology, 2215	AB_331682	1:250
Znt3	Rabbit	Millipore ABN994		1:1500

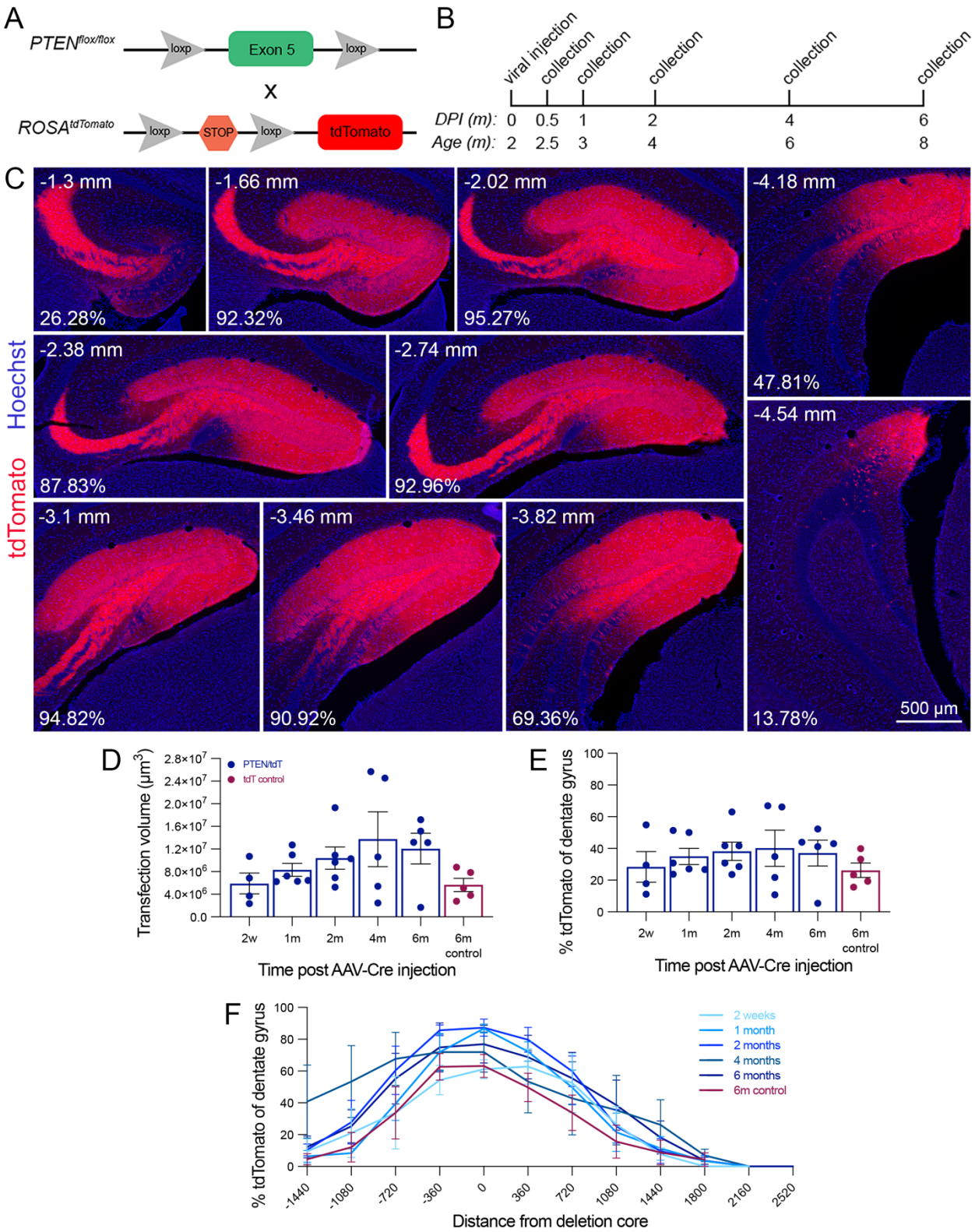
A
PTEN flox/flox
loxp
Exon 5
loxp
x
ROSA tdTomato
loxp
STOP
loxp
tdTomato
B
viral injection
collection
collection
collection
collection
collection
DPI (m): 0 0.5 1 2 4 6
Age (m): 2 2.5 3 4 6 8
C
Hoechst
tdTomato
-1.3 mm
26.28%
-1.66 mm
92.32%
-2.02 mm
95.27%
-4.18 mm
47.81%
-2.38 mm
87.83%
-2.74 mm
92.96%
-4.54 mm
-3.1 mm
94.82%
-3.46 mm
90.92%
-3.82 mm
69.36%
13.78%
500 µm
D
Transfection volume (µm3)
PTEN/tdT
tdT control
Time post AAV-Cre injection
2w
1m
2m
4m
6m
6m control
E
% tdTomato of dentate gyrus
Time post AAV-Cre injection
F
% tdTomato of dentate gyrus
2 weeks
1 month
2 months
4 months
6 months
6m control
Distance from deletion core

Figure 3.1. AAV-Cre transduction in the dentate gyrus of PTEN/tdT mice.

A) Diagram of lox-P flanked exon 5 transgene in $PTEN^{f/f}$ mice and lox-P flanked STOP cassette in the Rosa locus upstream of a tandem dimer tomato (tdT) fluorescent protein sequence. B) Experimental timeline: Adult PTEN/tdT and tdT control mice were unilaterally injected with AAV2-Cre into the dentate gyrus at 2 months of age. Animals were sacrificed for histological processing between 2 weeks and 6 months after injection. C) Example of granule cell transduction in a PTEN/tdT mouse 2 months after AAV-Cre injection in sections taken at 360μm intervals through the septo-temporal axis of the dentate gyrus (red= tdTomato, Blue= Hoechst). Approximate bregma coordinate based on physical distance is indicated in the top left corner and percent transduction of each section listed in bottom left corner. D) Transduction volume within the injected dentate gyrus between 2 weeks and 6 months following AAV-Cre injection in PTEN/tdT mice, and at 6 months in tdT control mice. E) Percent of entire ipsilateral dentate gyrus transduced by AAV-Cre at each time point. F) Percentage of the dentate gyrus occupied by tdT fluorescence throughout the dentate gyrus in PTEN/tdT mice and tdT control mice at 360μm intervals. An example of percent transduction in individual sections is shown in the bottom left corner in panel C.

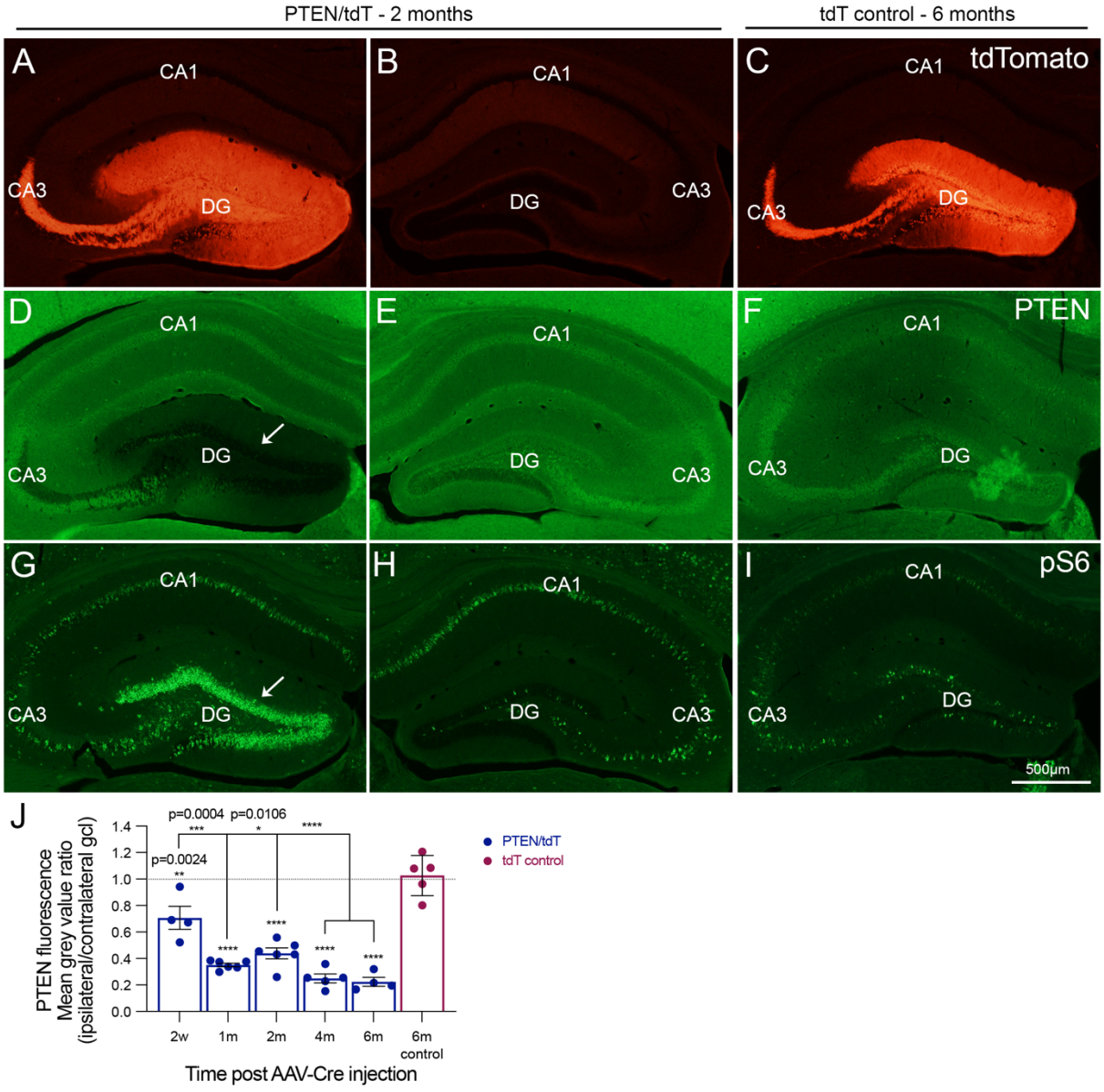
PTEN/tdT - 2 months
tdT control - 6 months
A
CA1
CA3
DG
B
CA1
DG
CA3
C
CA1
tdTomato
CA3
DG
D
CA1
CA3
DG
E
CA1
DG
CA3
F
CA1
PTEN
CA3
DG
G
CA1
CA3
DG
H
CA1
DG
CA3
I
CA1
pS6
CA3
DG
500µm
J
PTEN fluorescence
Mean grey value ratio
(ipsilateral/contralateral gcl)
p=0.0004
p=0.0106
p=0.0024
PTEN/tdT
tdT control
2w
1m
2m
4m
6m
6m control
Time post AAV-Cre injection

Figure 3.2. AAV-Cre-mediated PTEN deletion in the dentate gyrus of an adult PTEN/tdT mouse.

A) tdTomato fluorescence reveals area of focal transduction by AAV-Cre in the ipsilateral dentate gyrus of an experimental PTEN/tdT mouse at 2 months post AAV-Cre injection. B) Lack of tdTomato in the contralateral, non-injected dentate gyrus of the same animal. C) Area of transduction by AAV-Cre in a tdT control mouse. D) Area of PTEN deletion in the ipsilateral dentate gyrus corresponding to the area of tdT expression shown in panel A (arrows). Note the maintenance of PTEN expression in the CA1 and CA3 hippocampal subfields. E) PTEN expression on the contralateral side to injection. F) PTEN expression in the ipsilateral dentate gyrus of a tdT control mouse. G) Immunostaining for pS6 (Ser 235/236) reveals activation of S6 phosphorylation in the area of PTEN deletion (arrows). H) pS6 immunostaining on the contralateral side. I) pS6 immunostaining in transduced granule cells of a tdT control mouse. J) Ratio of PTEN fluorescence intensity between the granule cell layers of the ipsilateral and contralateral dentate gyri at various time points following AAV-Cre injection. Sidak's multiple comparisons test between the PTEN deleted dentate gyrus and controls (2 weeks; $p= 0.0024$, 1-6 months; $p< 0.0001$), and between 2 weeks post AAV-Cre and later time points (1 month; $p= 0.0004$, 2 months; $p= 0.0106$, 4 months; $p< 0.0001$, and 6 months; $p<0.0001$).

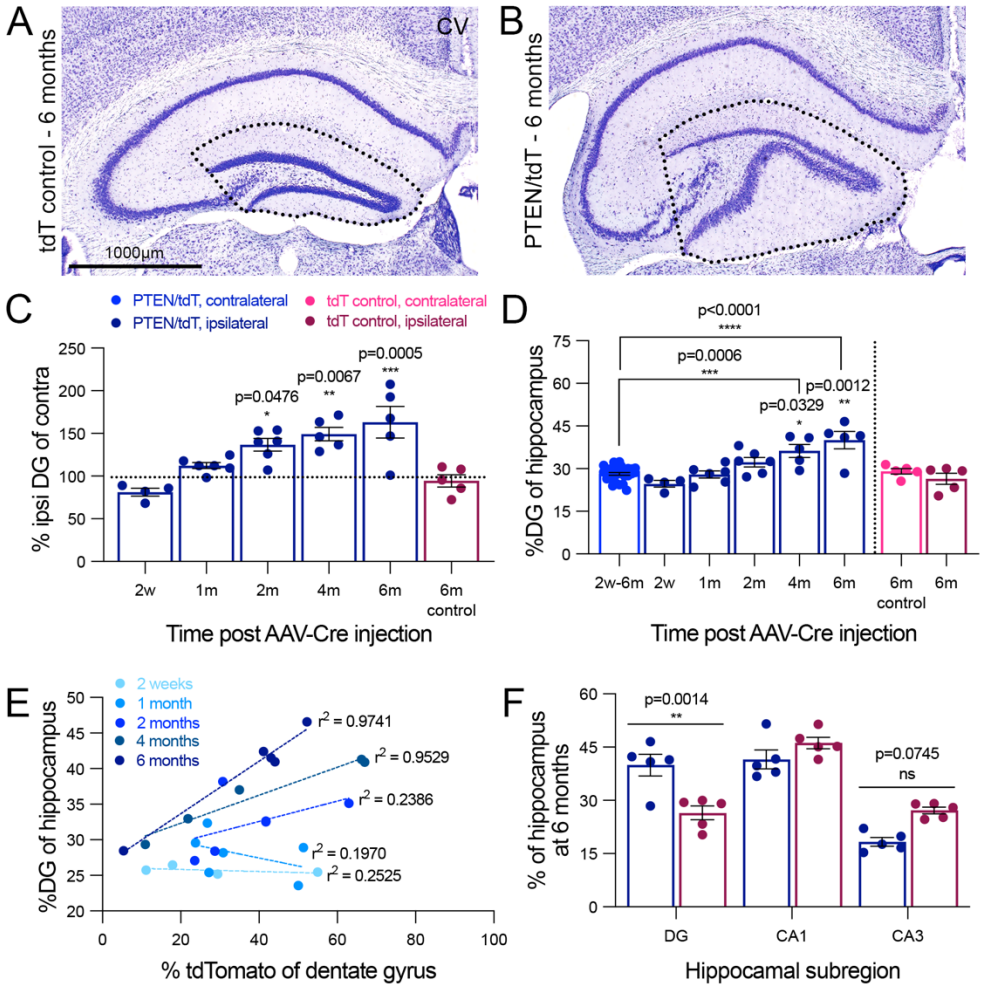
A
tdT control - 6 months
CV
1000µm
B
PTEN/tdT - 6 months
C
PTEN/tdT, contralateral
PTEN/tdT, ipsilateral
tdT control, contralateral
tdT control, ipsilateral
% ipsi DG of contra
p=0.0476
p=0.0067
p=0.0005
2w
1m
2m
4m
6m
6m control
Time post AAV-Cre injection
D
p<0.0001
p=0.0006
p=0.0012
p=0.0329
%DG of hippocampus
2w-6m
2w
1m
2m
4m
6m
6m control
6m control
Time post AAV-Cre injection
E
2 weeks
1 month
2 months
4 months
6 months
r² = 0.9741
r² = 0.9529
r² = 0.2386
r² = 0.1970
r² = 0.2525
%DG of hippocampus
% tdTomato of dentate gyrus
F
p=0.0014
p=0.0745
ns
% of hippocampus at 6 months
DG
CA1
CA3
Hippocamal subregion

Figure 3.3. Progressive enlargement of the dentate gyrus following PTEN deletion.

A-B) Representative Cresyl violet images of the ipsilateral hippocampus in control (A) and experimental (B) adult mice at 6 months following AAV-Cre injection. Note the enlarged dentate gyrus following PTEN deletion in PTEN/tdT mice. C) The ipsilateral dentate gyrus represented as a percentage of the contralateral dentate gyrus in PTEN/tdT and tdT control mice. Sidak's multiple comparisons test was significant at 2 months ($p=0.0476$), 4 months ($p=0.0067$), and 6 months ($p=0.0005$) for PTEN/tdT mice compared to controls. D) Percent area of the ipsilateral and contralateral hippocampus in PTEN/tdT and tdT controls occupied by the dentate gyrus at various time points following AAV-Cre injection. Note, there was no significant difference in area occupied by the contralateral dentate gyrus of PTEN/tdT mice therefore values have been combined. Sidak's multiple comparisons for the ipsilateral vs. contralateral dentate gyrus for PTEN/tdT mice were: 4 months ($p=0.0006$) and 6 months ($p<0.0001$). Further, Sidak's post hoc comparisons for PTEN/tdT vs. tdT controls were: 4 months ($p=0.0329$) and 6 months ($p=0.0012$). E) Correlation between the percentage of the entire dentate gyrus transduced by AAV-Cre (PTEN deletion area) and the relative percent size of the dentate gyrus measured in C. F) Percentage of hippocampal area occupied by each subregion at the core of transduction in control and PTEN-deleted animals at 6 months post AAV-Cre injection. Sidak's post hoc comparisons for PTEN/tdT and tdT control dentate gyrus: ($p=0.0014$), with no significant difference for CA1 and CA3.

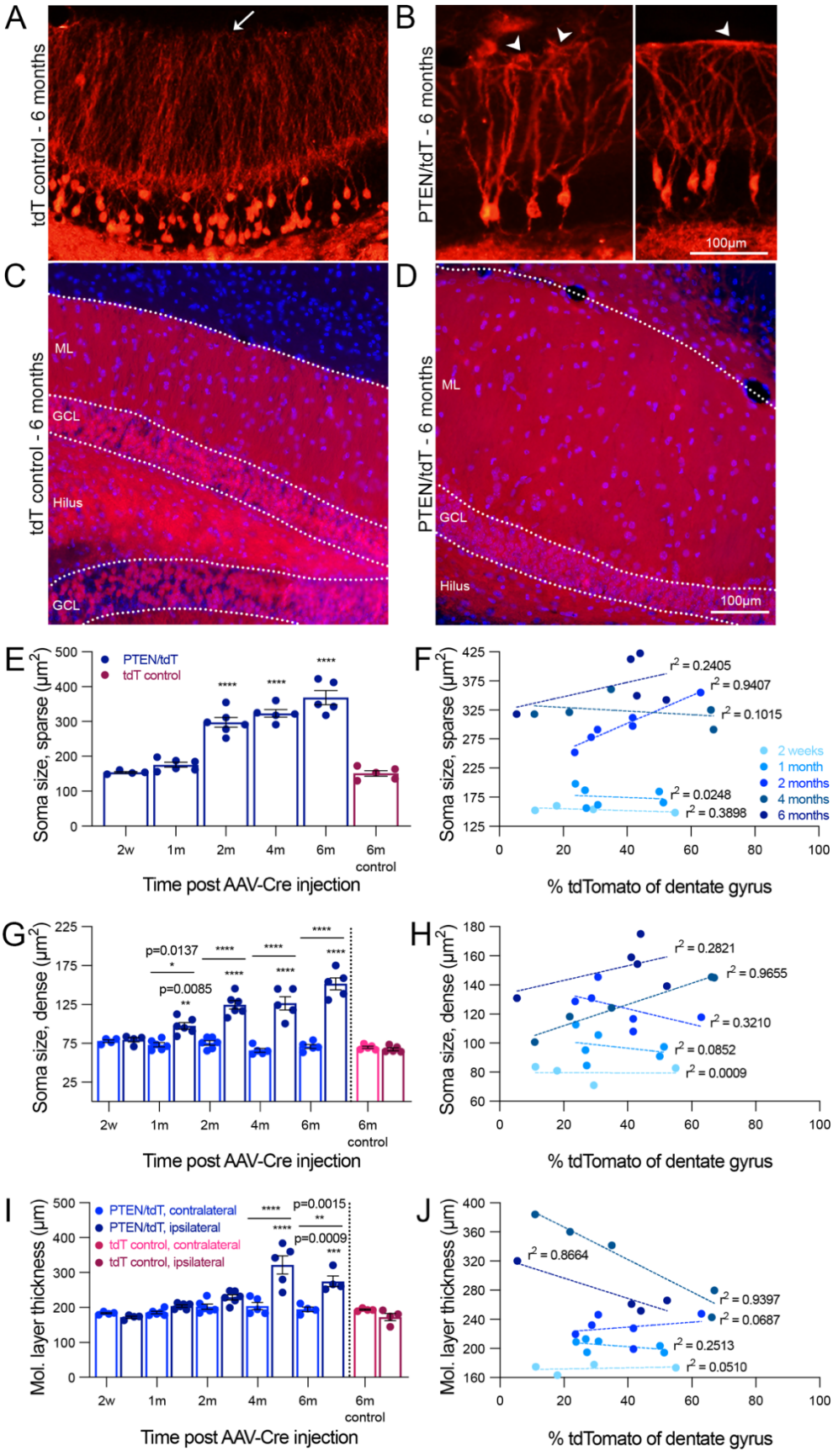
A
tdT control - 6 months
B
PTEN/tdT - 6 months
100μm
C
tdT control - 6 months
ML
GCL
Hilus
GCL
D
PTEN/tdT - 6 months
ML
GCL
Hilus
100μm
E
PTEN/tdT
tdT control
Soma size, sparse (μm²)
Time post AAV-Cre injection
2w
1m
2m
4m
6m
6m control
F
r² = 0.2405
r² = 0.9407
r² = 0.1015
r² = 0.0248
r² = 0.3898
2 weeks
1 month
2 months
4 months
6 months
Soma size, sparse (μm²)
% tdTomato of dentate gyrus
G
p=0.0137
p=0.0085
Soma size, dense (μm²)
Time post AAV-Cre injection
H
r² = 0.2821
r² = 0.9655
r² = 0.3210
r² = 0.0852
r² = 0.0009
Soma size, dense (μm²)
% tdTomato of dentate gyrus
I
PTEN/tdT, contralateral
PTEN/tdT, ipsilateral
tdT control, contralateral
tdT control, ipsilateral
p=0.0015
p=0.0009
Mol. layer thickness (μm)
Time post AAV-Cre injection
J
r² = 0.8664
r² = 0.9397
r² = 0.0687
r² = 0.2513
r² = 0.0510
Mol. layer thickness (μm)
% tdTomato of dentate gyrus

Figure 3.4. Growth of granule cells following PTEN deletion in PTEN/tdT mice.

A,B) Examples of tdTomato positive granule cells in tdT control (A) and PTEN/tdT (B) mice in regions of sparse transduction (6 months post-injection). Note enlarged somata and larger caliber dendrites in B. C-D) tdT expression in regions of dense transduction in tdT control (C) and PTEN/tdT mice (D). Note increased thickness of the molecular layer in D. E) Soma size from 5-6 PTEN/tdT and tdT control mice (30 neurons per mouse) at different time points post AAV injection. Sidak's comparisons at different times vs. control: 1 month ($p=0.0137$), 2 months ($p<0.0001$), 4 months ($p<0.0001$), and 6 months ($p<0.0001$). F) Relationship between percent PTEN deletion and soma size in regions of sparse transduction. G) Soma size in Cresyl violet stained sections from PTEN/tdT and tdT control mice in regions of dense transduction compared to contralateral, PTEN expressing granule cells. Sidak's post hoc comparisons for PTEN/tdT vs. tdT control mice were: 1 month ($p=0.0085$), and 2-6 months ($p<0.0001$), for PTEN/tdT ipsilateral vs. contralateral dentate gyrus were: 1 month ($p=0.0137$), and 2-6 months ($p<0.0001$). H) Relationship between percent PTEN deletion and soma size in regions of dense transduction in each timepoint. I) Thickness of ipsilateral and contralateral dentate molecular layers in PTEN/tdT and tdT control mice in regions of dense transduction. Note that in regions of sparse transduction, dendrites of PTEN-deleted granule cells extend laterally along the hippocampal fissure (arrowheads in B) whereas in tdT control mice, dendrites terminate at the edge of the molecular layer (arrow in A). Sidak's post hoc comparisons for PTEN/tdT vs. tdT control mice were: 4 months ($p<0.0001$) and 6 months ($p=0.0009$), for PTEN/tdT ipsilateral vs. contralateral dentate gyrus were: 4 month ($p<0.0001$) and 6 months ($p=0.0015$). J) Relationship between percent PTEN deletion and molecular layer thickness at each time.

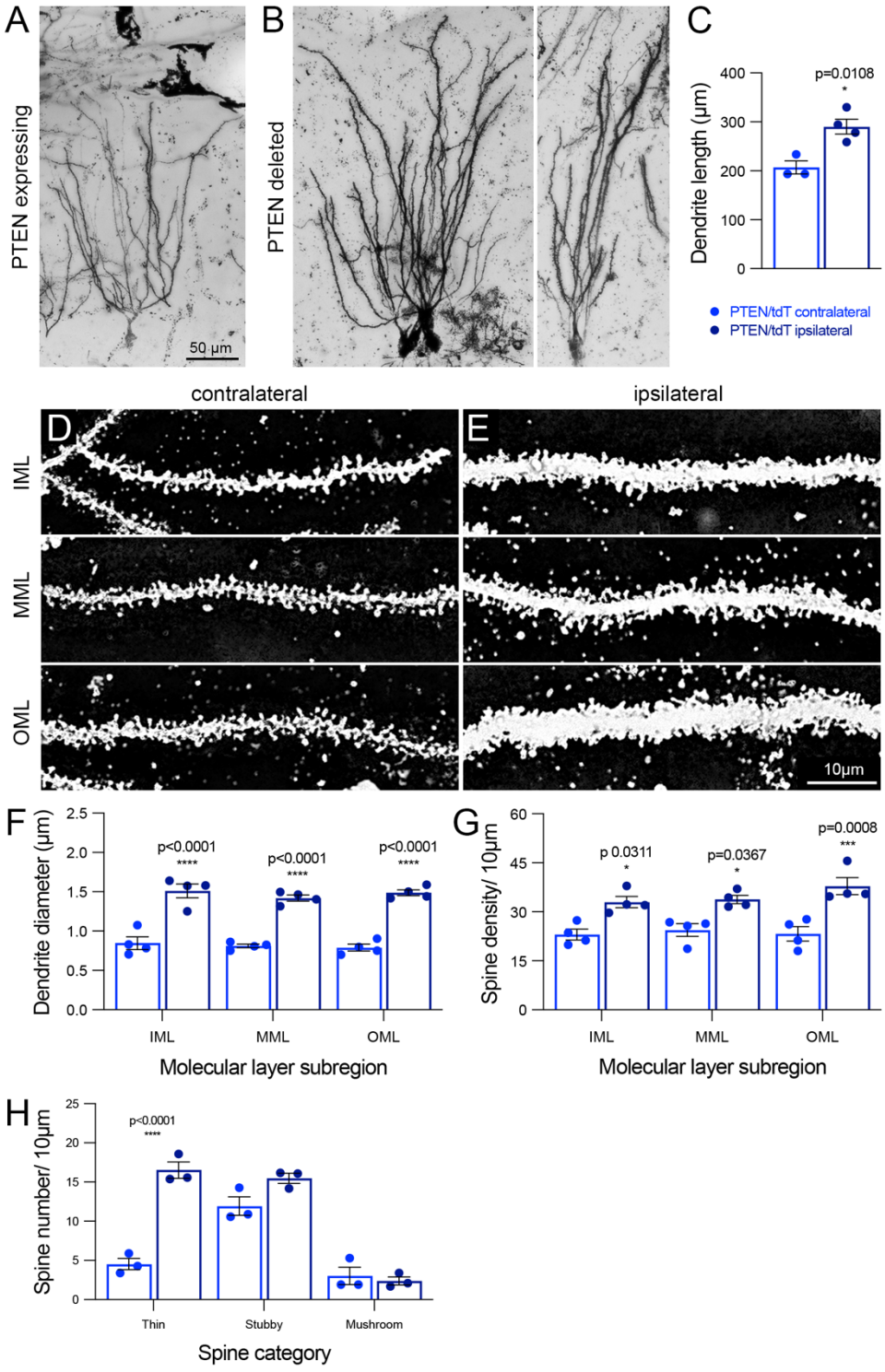
A
PTEN expressing
50 µm
B
PTEN deleted
C
Dendrite length (µm)
400
300
200
100
0
p=0.0108
*
PTEN/tdT contralateral
PTEN/tdT ipsilateral
contralateral
ipsilateral
D
E
IML
MML
OML
10µm
F
Dendrite diameter (µm)
2.5
2.0
1.5
1.0
0.5
0.0
p<0.0001
****
p<0.0001
****
p<0.0001
****
IML
MML
OML
Molecular layer subregion
G
Spine density/ 10µm
60
45
30
15
0
p 0.0311
*
p=0.0367
*
p=0.0008
***
IML
MML
OML
Molecular layer subregion
H
Spine number/ 10µm
25
20
15
10
5
0
p<0.0001
****
Thin
Stubby
Mushroom
Spine category

Figure 3.5. Assessment of dendrite length, diameter, and spine density at 6 months following PTEN deletion in adult PTEN/tdT mice.

A) Golgi stained, PTEN expressing granule cells in the dentate gyrus contralateral to AAV-Cre injection. B) Golgi stained, PTEN deleted granule cells in the ipsilateral dentate gyrus at 6 months after AAV-Cre injection. C) Average dendrite length from 10 granule cells measured in the ipsilateral (PTEN-deleted) and contralateral (PTEN-expressing) dentate gyrus of 4 mice ($p=0.0108$). D) Dendrites from PTEN expressing granule cells within the inner (top row), middle (center row), and outer (bottom row) molecular layers of the contralateral dentate gyrus. E) PTEN-deleted granule cell dendrites in the inner (top), middle (center), and outer (bottom) molecular layers in the ipsilateral dentate gyrus. F) Averaged mean dendrite diameters from 10μm segments within the inner, middle, and outer molecular layers from control and PTEN-deleted granule cells in the same 4 animals (10 measurements averaged per region for each animal). Sidak's multiple comparisons test at each of the three lamina: ($p<0.0001$). G) Spine density within the same 10μm dendritic segments shown in C (spine density in 10 segments averaged per region for each animal). Sidak's post hoc comparisons were: inner molecular layer ($p=0.0311$), middle molecular layer ($p=0.0367$), and outer molecular layer ($p=0.0008$). H) Average categorical spine number along a given dendritic segment. Each point represents the average number of spines per category in one of the three molecular layer lamina. Sidak's multiple comparisons test for each category: thin ($p<0.0001$), with no significance for stubby or mushroom spines.

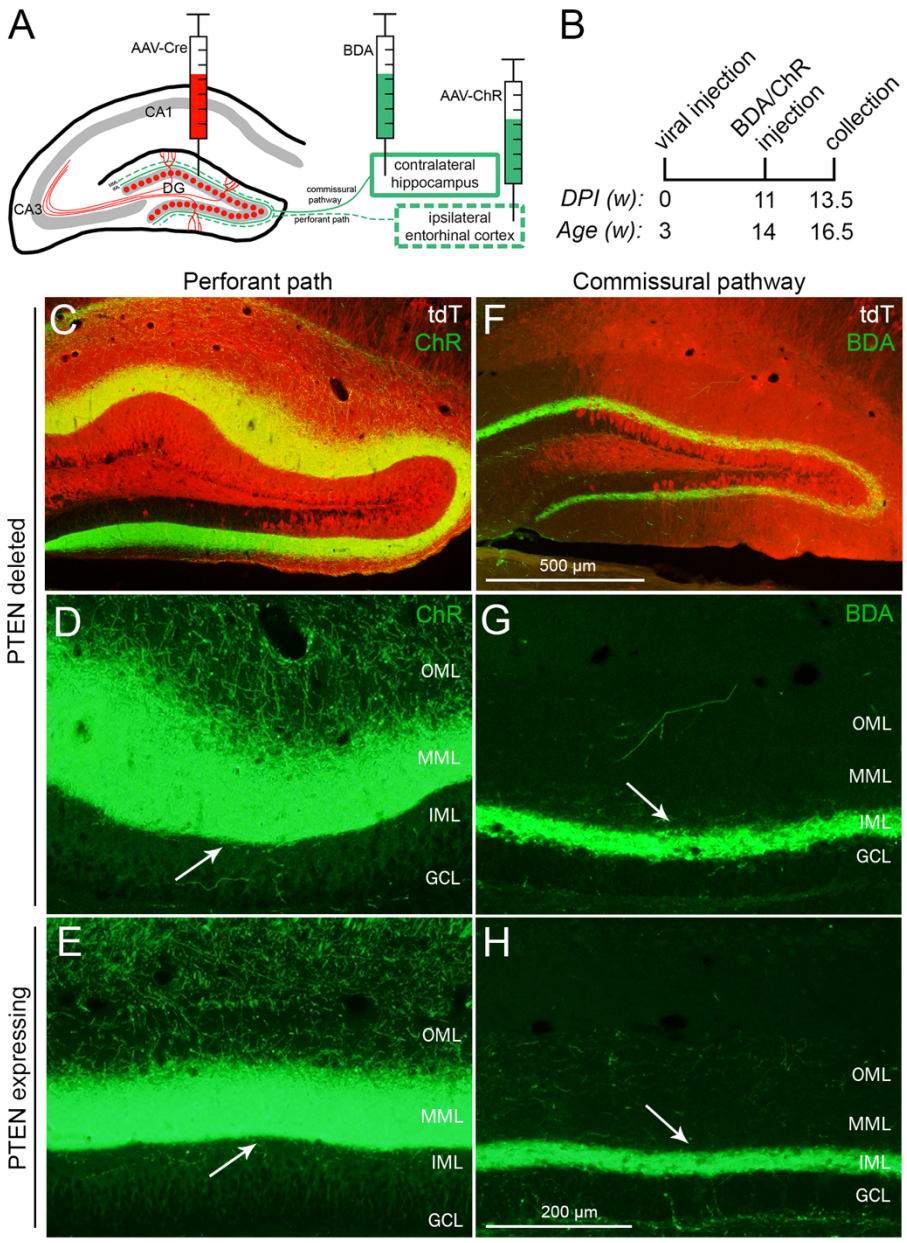
A
AAV-Cre
BDA
AAV-ChR
CA1
DG
CA3
commissural pathway
perforant path
contralateral hippocampus
ipsilateral entorhinal cortex
B
viral injection
BDA/ChR injection
collection
DPI (w): 0 11 13.5
Age (w): 3 14 16.5
Perforant path
Commissural pathway
PTEN deleted
PTEN expressing
C
tdT
ChR
F
tdT
BDA
500 µm
D
ChR
OML
MML
IML
GCL
G
BDA
OML
MML
IML
GCL
E
OML
MML
IML
GCL
H
OML
MML
IML
GCL
200 µm

Figure 3.6. Labeling of dentate granule cell input pathways following vector-mediated PTEN deletion in young PTEN/tdT mice.

A-B) Unilateral AAV-Cre injection in young mice at p19 results in PTEN deletion and tdT expression in dentate granule cells. This is followed by BDA injection into the contralateral, ventral hippocampus for labeling of commissural projections to the IML and AAV-ChR injections into the entorhinal cortex for labeling of perforant path projections to the MML at 11 weeks post AAV-Cre injection. C) Immunostaining for ChR (green) to label inputs from the ipsilateral entorhinal cortex within the area of PTEN deletion (red). D) Higher magnification of input pathways to the area of PTEN deletion shown in C. E) Perforant path projections to the ipsilateral, caudal dentate gyrus outside the area of PTEN deletion in C. Note that the precise boundary of perforant path projections at the border between the inner and middle molecular layers is maintained (arrow in D). F) Immunostaining for BDA (green) in the area of PTEN deletion (red) following tracer injection into the contralateral hippocampus for commissural pathway labeling. G) Higher magnification image of BDA labeled terminal projections in E reveals preservation of commissural pathway targeting to the dentate inner molecular layer and preservation of laminar borders (arrow). H) High magnification image of commissural projections to PTEN expressing dentate granule cells outside of the area of PTEN deletion.

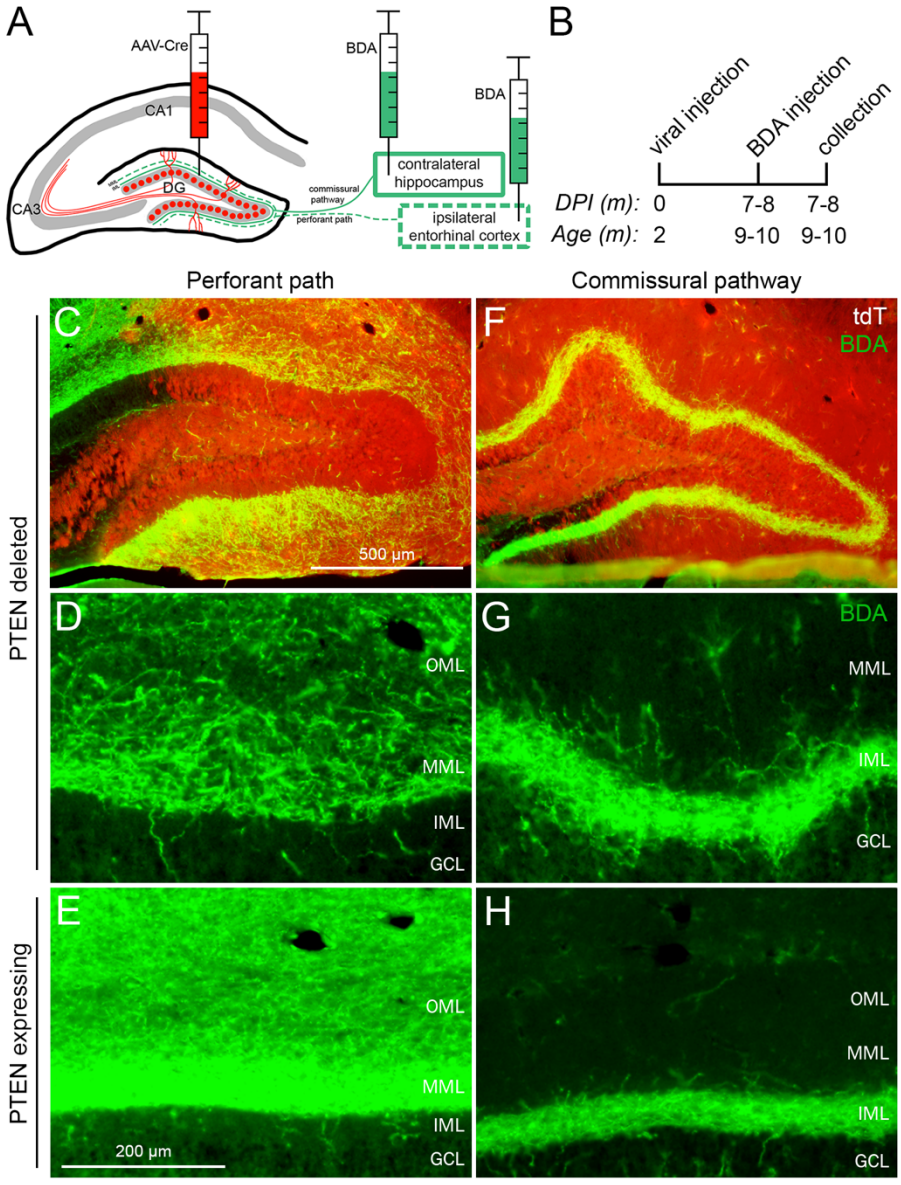
A
AAV-Cre
BDA
BDA
CA1
DG
CA3
commissural pathway
perforant path
contralateral hippocampus
ipsilateral entorhinal cortex
B
viral injection
BDA injection
collection
DPI (m): 0 7-8 7-8
Age (m): 2 9-10 9-10
Perforant path
Commissural pathway
PTEN deleted
PTEN expressing
C
F
tdT
BDA
500 µm
D
G
BDA
OML
MML
IML
GCL
E
H
200 µm

Figure 3.7. Dentate granule cell input pathway tracing following vector-mediated PTEN deletion in adult PTEN/tdT mice.

A-B) Unilateral AAV-Cre injection in adult mice is followed by BDA injections into the contralateral hippocampus or entorhinal cortex for labeling of commissural and perforant path projections, respectively, at 7-8 months following PTEN deletion. C) Immunostaining for BDA (green) to label inputs from the ipsilateral entorhinal cortex within the area of PTEN deletion (red). D) Higher magnification of input pathways to the area of PTEN deletion. E) Perforant path projections to the ipsilateral, caudal dentate gyrus outside the area of PTEN deletion. The precise boundary of perforant path projections at the border between the inner and middle molecular layers is largely maintained despite growth of apical dendrites in PTEN deleted granule cells. F) Immunostaining for BDA (green) in the area of PTEN deletion (red) following tracer injection into the contralateral hippocampus for commissural pathway labeling. G) Higher magnification image of BDA labeled terminal projections in F reveals preservation of commissural pathway targeting to the dentate inner molecular layer and relative preservation of laminar borders. H) High magnification image of commissural projections to PTEN expressing dentate granule cells outside of the area of PTEN deletion.

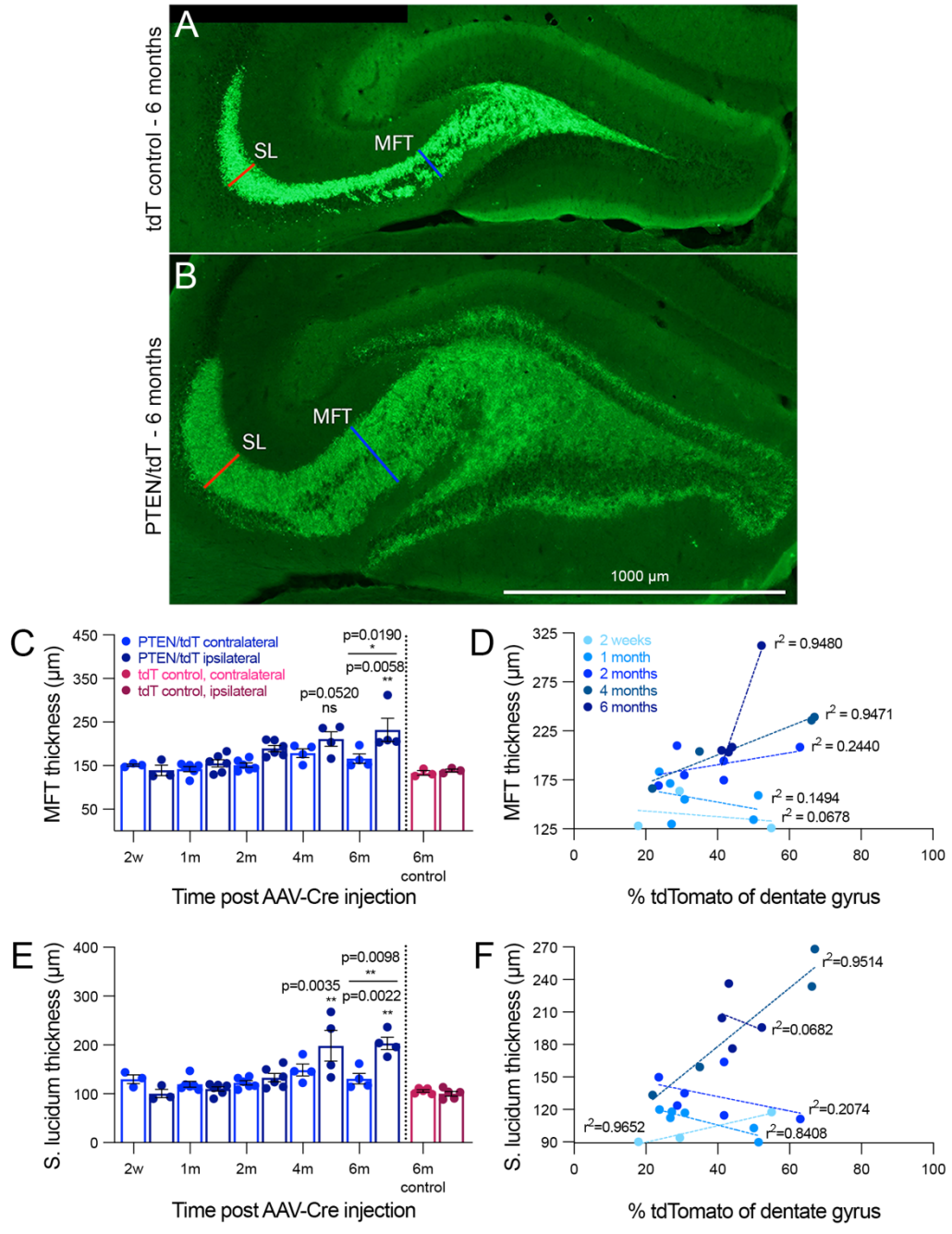
A
tdT control - 6 months
SL
MFT
B
PTEN/tdT - 6 months
SL
MFT
1000 µm
C
PTEN/tdT contralateral
PTEN/tdT ipsilateral
tdT control, contralateral
tdT control, ipsilateral
p=0.0190
*
p=0.0058
**
p=0.0520
ns
MFT thickness (µm)
450
350
250
150
50
2w
1m
2m
4m
6m
6m
control
Time post AAV-Cre injection
D
2 weeks
1 month
2 months
4 months
6 months
r² = 0.9480
r² = 0.9471
r² = 0.2440
r² = 0.1494
r² = 0.0678
MFT thickness (µm)
325
275
225
175
125
0
20
40
60
80
100
% tdTomato of dentate gyrus
E
p=0.0098
**
p=0.0035
**
p=0.0022
**
S. lucidum thickness (µm)
400
300
200
100
0
2w
1m
2m
4m
6m
6m
control
Time post AAV-Cre injection
F
r²=0.9514
r²=0.0682
r²=0.2074
r²=0.9652
r²=0.8408
S. lucidum thickness (µm)
270
240
210
180
150
120
90
0
20
40
60
80
100
% tdTomato of dentate gyrus

Figure 3.8. Mossy fiber tract enlargement following vector-mediated PTEN deletion.

A-B) Representative mossy fiber tract (Znt3) labeling in the ipsilateral hippocampus of control (A) and experimental (B) adult mice at 6 months following AAV-Cre injection. Note the areas of measurement for the mossy fiber tract (MFT, blue line) and the supra-pyramidal bundle located within the stratum lucidum (SL, red line). C) Thickness of ipsilateral and contralateral MFT in experimental and control animals at various time points following transduction. Sidak's multiple comparisons for ipsilateral and contralateral sides in PTEN/tdT mice: 6 months ($p=0.0190$). Post hoc comparisons for PTEN/tdT vs. tdT controls: 6 months ($p=0.0058$). D) Relationship between percent transduction and mossy fiber tract thickness in PTEN deleted animals. E) Thickness of ipsilateral and contralateral supra-pyramidal bundles within the SL in experimental and control animals. Sidak's multiple comparisons for ipsilateral vs. contralateral sides in PTEN/tdT mice: 6 months ($p=0.0098$). Post hoc comparisons for PTEN/tdT vs. tdT controls were: 4 months ($p=0.0035$) and 6 months ($p=0.0022$). Note, there was no evidence of uncontrolled mossy fiber growth into the stratum radiatum CA3 terminal zone. F) Correlation between percent PTEN deletion and SL thickness in PTEN/tdT mice.

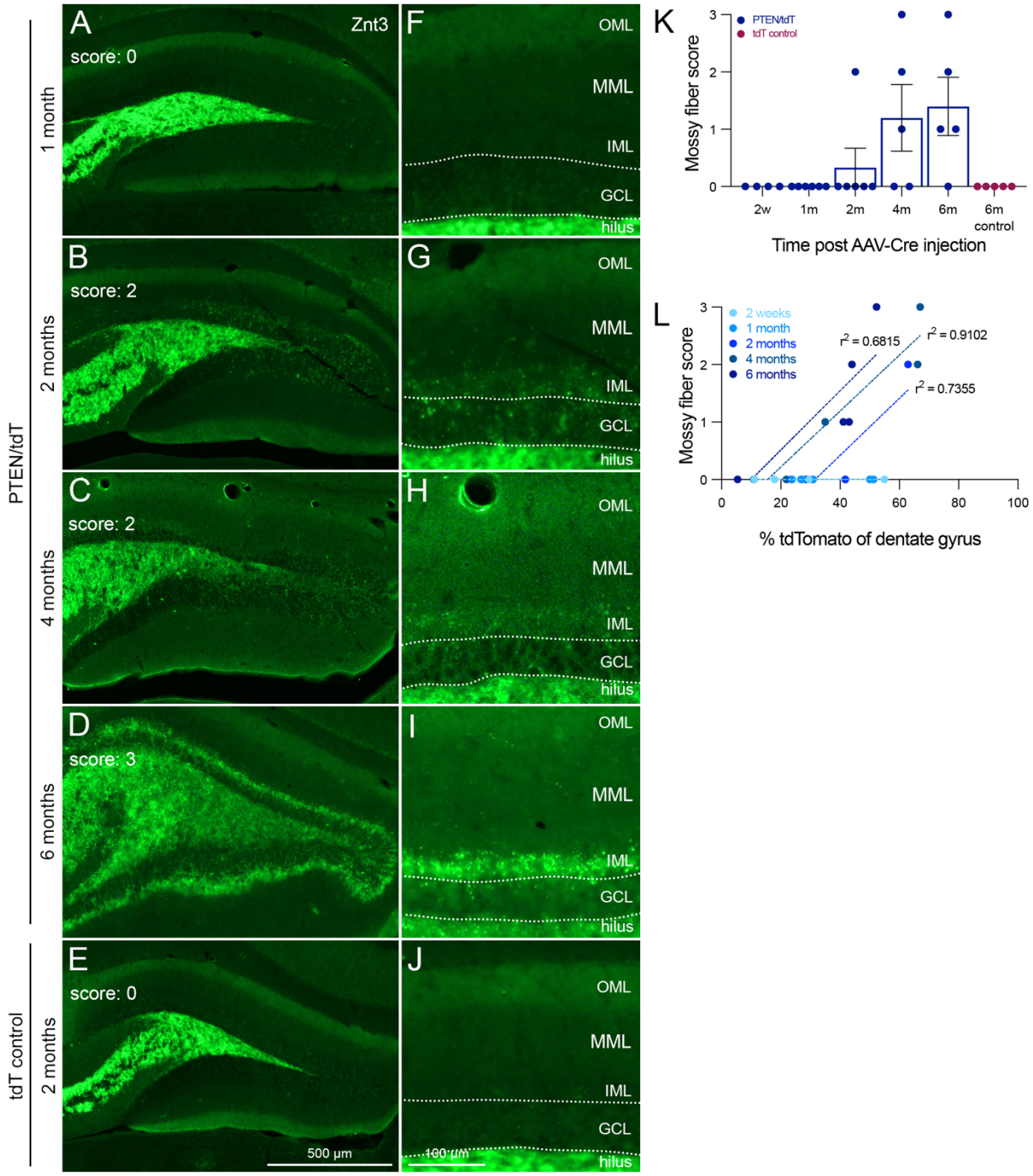
PTEN/tdT
tdT control
1 month
2 months
4 months
6 months
2 months
A
Znt3
score: 0
B
score: 2
C
score: 2
D
score: 3
E
score: 0
F
G
H
I
J
OML
MML
IML
GCL
hilus
500 µm
100 µm
K
PTEN/tdT
tdT control
Mossy fiber score
2w
1m
2m
4m
6m
6m control
Time post AAV-Cre injection
L
2 weeks
1 month
2 months
4 months
6 months
r2 = 0.6815
r2 = 0.9102
r2 = 0.7355
Mossy fiber score
% tdTomato of dentate gyrus

Figure 3.9. Mossy fiber labeling in the dentate gyrus following adult vector-mediated PTEN deletion.

A-D) Mossy fiber (Znt3) labeling on the side ipsilateral to AAV-Cre injection in PTEN/tdT mice between 1- and 6 months after PTEN deletion. Note progressive evidence of supra-granular mossy fibers over time in some mice. E) Znt3 mossy fiber labeling on the side ipsilateral to AAV-Cre injection in tdT control mice at 6 months post transduction. F-J) Higher magnification view of Znt3 labeling and lamina within the dentate gyrus shown in A-E. K) Mossy fiber score on the transduced side in experimental and control animals at each timepoint shows variability in the presence of supra-granular mossy fibers. Scoring examples are located in the top left corner in panels A-E. L) Correlation between percent transduction and mossy fiber score in PTEN deleted animals after AAV-Cre injection. Scoring scale: 0 - little to no Znt3 labeling in GCL, 1 - mild Znt3 labeling in GCL, 2 - moderate Znt3 labeling in GCL and mild labeling in IML, 3 - dense Znt3 labeling in IML.

REFERENCES

Althaus, A. L., & Parent, J. M. (2012, Sep 20). Pten-less dentate granule cells make fits. *Neuron, 75*(6), 938-940. https://doi.org/10.1016/j.neuron.2012.09.008

Amiri, A., Cho, W., Zhou, J., Birnbaum, S. G., Sinton, C. M., McKay, R. M., & Parada, L. F. (2012, Apr 25). Pten deletion in adult hippocampal neural stem/progenitor cells causes cellular abnormalities and alters neurogenesis. *J Neurosci, 32*(17), 5880-5890. https://doi.org/10.1523/JNEUROSCI.5462-11.2012

Arafa, S. R., LaSarge, C. L., Pun, R. Y. K., Khademi, S., & Danzer, S. C. (2019, Jan). Self-reinforcing effects of mTOR hyperactive neurons on dendritic growth. *Exp Neurol, 311*, 125-134. https://doi.org/10.1016/j.expneurol.2018.09.019

Backman, S. A., Stambolic, V., Suzuki, A., Haight, J., Elia, A., Pretorius, J., Tsao, M. S., Shannon, P., Bolon, B., Ivy, G. O., & Mak, T. W. (2001, Dec). Deletion of Pten in mouse brain causes seizures, ataxia and defects in soma size resembling Lhermitte-Duclos disease. *Nat Genet, 29*(4), 396-403. https://doi.org/10.1038/ng782

Conti, S., Condo, M., Posar, A., Mari, F., Resta, N., Renieri, A., Neri, I., Patrizi, A., & Parmeggiani, A. (2012, Mar). Phosphatase and tensin homolog (PTEN) gene mutations and autism: literature review and a case report of a patient with Cowden syndrome, autistic disorder, and epilepsy. *J Child Neurol, 27*(3), 392-397. https://doi.org/10.1177/0883073811420296

Fraser, M. M., Bayazitov, I. T., Zakharenko, S. S., & Baker, S. J. (2008, Jan 24). Phosphatase and tensin homolog, deleted on chromosome 10 deficiency in brain causes defects in synaptic structure, transmission and plasticity, and myelination abnormalities. *Neuroscience, 151*(2), 476-488. https://doi.org/10.1016/j.neuroscience.2007.10.048

Fraser, M. M., Zhu, X., Kwon, C. H., Uhlmann, E. J., Gutmann, D. H., & Baker, S. J. (2004, Nov 1). Pten loss causes hypertrophy and increased proliferation of astrocytes in vivo. *Cancer Res, 64*(21), 7773-7779. https://doi.org/10.1158/0008-5472.CAN-04-2487

Gallent, E. A., & Steward, O. (2018, May). Neuronal PTEN deletion in adult cortical neurons triggers progressive growth of cell bodies, dendrites, and axons. *Exp Neurol, 303*, 12-28. https://doi.org/10.1016/j.expneurol.2018.01.005

Haws, M. E., Jaramillo, T. C., Espinosa, F., Widman, A. J., Stuber, G. D., Sparta, D. R., Tye, K. M., Russo, S. J., Parada, L. F., Stavarache, M., Kaplitt, M., Bonci, A., & Powell, C. M. (2014, Apr 1). PTEN knockdown alters dendritic spine/protrusion morphology, not density. *J Comp Neurol, 522*(5), 1171-1190. https://doi.org/10.1002/cne.23488

Hunt, R. F., Scheff, S. W., & Smith, B. N. (2009, Feb). Posttraumatic epilepsy after controlled cortical impact injury in mice. *Exp Neurol, 215*(2), 243-252. https://doi.org/10.1016/j.expneurol.2008.10.005

Jansen, L. A., Mirzaa, G. M., Ishak, G. E., O'Roak, B. J., Hiatt, J. B., Roden, W. H., Gunter, S. A., Christian, S. L., Collins, S., Adams, C., Riviere, J. B., St-Onge, J., Ojemann, J. G., Shendure, J., Hevner, R. F., & Dobyns, W. B. (2015, Jun). PI3K/AKT pathway mutations cause a spectrum of brain malformations from megalencephaly to focal cortical dysplasia. *Brain, 138*(Pt 6), 1613-1628. https://doi.org/10.1093/brain/awv045

Kwon, C. H., Luikart, B. W., Powell, C. M., Zhou, J., Matheny, S. A., Zhang, W., Li, Y., Baker, S. J., & Parada, L. F. (2006, May 4). Pten regulates neuronal arborization and social interaction in mice. *Neuron, 50*(3), 377-388. https://doi.org/10.1016/j.neuron.2006.03.023

Kwon, C. H., Zhu, X., Zhang, J., & Baker, S. J. (2003, Oct 28). mTor is required for hypertrophy of Pten-deficient neuronal soma in vivo. *Proc Natl Acad Sci U S A, 100*(22), 12923-12928. https://doi.org/10.1073/pnas.2132711100

Kwon, C. H., Zhu, X., Zhang, J., Knoop, L. L., Tharp, R., Smeyne, R. J., Eberhart, C. G., Burger, P. C., & Baker, S. J. (2001, Dec). Pten regulates neuronal soma size: a mouse model of Lhermitte-Duclos disease. *Nat Genet, 29*(4), 404-411. https://doi.org/10.1038/ng781

LaSarge, C. L., Pun, R. Y., Muntifering, M. B., & Danzer, S. C. (2016, Dec). Disrupted hippocampal network physiology following PTEN deletion from newborn dentate granule cells. *Neurobiol Dis, 96*, 105-114. https://doi.org/10.1016/j.nbd.2016.09.004

LaSarge, C. L., Santos, V. R., & Danzer, S. C. (2015, Mar). PTEN deletion from adult-generated dentate granule cells disrupts granule cell mossy fiber axon structure. *Neurobiol Dis, 75*, 142-150. https://doi.org/10.1016/j.nbd.2014.12.029

Ljungberg, M. C., Sunnen, C. N., Lugo, J. N., Anderson, A. E., & D'Arcangelo, G. (2009, Jul-Aug). Rapamycin suppresses seizures and neuronal hypertrophy in a mouse model of cortical dysplasia. *Dis Model Mech, 2*(7-8), 389-398. https://doi.org/10.1242/dmm.002386

Lugo, J. N., Smith, G. D., Arbuckle, E. P., White, J., Holley, A. J., Floruta, C. M., Ahmed, N., Gomez, M. C., & Okonkwo, O. (2014). Deletion of PTEN produces autism-like behavioral deficits and alterations in synaptic proteins. *Front Mol Neurosci, 7*, 27. https://doi.org/10.3389/fnmol.2014.00027

Luikart, B. W., Schnell, E., Washburn, E. K., Bensen, A. L., Tovar, K. R., & Westbrook, G. L. (2011, Mar 16). Pten knockdown in vivo increases excitatory drive onto dentate granule cells. *J Neurosci, 31*(11), 4345-4354. https://doi.org/10.1523/JNEUROSCI.0061-11.2011

Maffei, A., & Turrigiano, G. (2008). The age of plasticity: developmental regulation of synaptic plasticity in neocortical microcircuits. *Prog Brain Res, 169*, 211-223. https://doi.org/10.1016/S0079-6123(07)00012-X

Matsushita, Y., Sakai, Y., Shimmura, M., Shigeto, H., Nishio, M., Akamine, S., Sanefuji, M., Ishizaki, Y., Torisu, H., Nakabeppu, Y., Suzuki, A., Takada, H., & Hara, T. (2016, Mar 10). Hyperactive mTOR signals in the proopiomelanocortin-expressing hippocampal neurons cause age-dependent epilepsy and premature death in mice. *Sci Rep, 6*, 22991. https://doi.org/10.1038/srep22991

Ogawa, S., Kwon, C. H., Zhou, J., Koovakkattu, D., Parada, L. F., & Sinton, C. M. (2007, Sep 7). A seizure-prone phenotype is associated with altered free-running rhythm in Pten mutant mice. *Brain Res, 1168*, 112-123. https://doi.org/10.1016/j.brainres.2007.06.074

Pun, R. Y., Rolle, I. J., Lasarge, C. L., Hosford, B. E., Rosen, J. M., Uhl, J. D., Schmeltzer, S. N., Faulkner, C., Bronson, S. L., Murphy, B. L., Richards, D. A., Holland, K. D., & Danzer, S. C. (2012, Sep 20). Excessive activation of mTOR in postnatally generated granule cells is sufficient to cause epilepsy. *Neuron, 75*(6), 1022-1034. https://doi.org/10.1016/j.neuron.2012.08.002

Santos, V. R., Pun, R. Y. K., Arafa, S. R., LaSarge, C. L., Rowley, S., Khademi, S., Bouley, T., Holland, K. D., Garcia-Cairasco, N., & Danzer, S. C. (2017, Dec). PTEN deletion increases hippocampal granule cell excitability in male and female mice. *Neurobiol Dis, 108*, 339-351. https://doi.org/10.1016/j.nbd.2017.08.014

Skelton, P. D., Frazel, P. W., Lee, D., Suh, H., & Luikart, B. W. (2019, Nov). Pten loss results in inappropriate excitatory connectivity. *Mol Psychiatry, 24*(11), 1627-1640. https://doi.org/10.1038/s41380-019-0412-6

Skelton, P. D., Poquerusse, J., Salinaro, J. R., Li, M., & Luikart, B. W. (2019, Dec 12). Activity-dependent dendritic elaboration requires Pten. *Neurobiol Dis, 134*, 104703. https://doi.org/10.1016/j.nbd.2019.104703

Steward, O., Coulibay, A., Metcalfe, M., Yonan, J. M., & Yee, K. M. (2019). AAVshRNA-mediated PTEN knockdown in adult neurons attenuates activity-dependent immediate early gene induction. *Exp Neurol*. https://doi.org/https://doi.org/10.1016/j.expneurol.2019.113098

Sunnen, C. N., Brewster, A. L., Lugo, J. N., Vanegas, F., Turcios, E., Mukhi, S., Parghi, D., D'Arcangelo, G., & Anderson, A. E. (2011, Nov). Inhibition of the mammalian target of rapamycin blocks epilepsy progression in NS-Pten conditional knockout mice. *Epilepsia, 52*(11), 2065-2075. https://doi.org/10.1111/j.1528-1167.2011.03280.x

Takeuchi, K., Gertner, M. J., Zhou, J., Parada, L. F., Bennett, M. V., & Zukin, R. S. (2013, Mar 19). Dysregulation of synaptic plasticity precedes appearance of morphological defects in a Pten conditional knockout mouse model of autism. *Proc Natl Acad Sci U S A, 110*(12), 4738-4743. https://doi.org/10.1073/pnas.1222803110

Tilot, A. K., Frazier, T. W., 2nd, & Eng, C. (2015, Jul). Balancing Proliferation and Connectivity in PTEN-associated Autism Spectrum Disorder. *Neurotherapeutics, 12*(3), 609-619. https://doi.org/10.1007/s13311-015-0356-8

Turrigiano, G. G. (2008, Oct 31). The self-tuning neuron: synaptic scaling of excitatory synapses. *Cell, 135*(3), 422-435. https://doi.org/10.1016/j.cell.2008.10.008

Turrigiano, G. G., & Nelson, S. B. (2004, Feb). Homeostatic plasticity in the developing nervous system. *Nat Rev Neurosci, 5*(2), 97-107. https://doi.org/10.1038/nrn1327

Wen, Y., Li, W., Choudhury, G. R., He, R., Yang, T., Liu, R., Jin, K., & Yang, S. H. (2013, Jun). Astroglial PTEN Loss Disrupts Neuronal Lamination by Dysregulating Radial Glia-guided Neuronal Migration. *Aging Dis, 4*(3), 113-126. https://www.ncbi.nlm.nih.gov/pubmed/23730527

Williams, M. R., DeSpenza, T., Jr., Li, M., Gulledge, A. T., & Luikart, B. W. (2015, Jan 21). Hyperactivity of newborn Pten knock-out neurons results from increased excitatory synaptic drive. *J Neurosci, 35*(3), 943-959. https://doi.org/10.1523/JNEUROSCI.3144-14.2015

Zahedi Abghari, F., Moradi, Y., & Akouchekian, M. (2019). PTEN gene mutations in patients with macrocephaly and classic autism: A systematic review. *Med J Islam Repub Iran, 33*, 10. https://doi.org/10.34171/mjiri.33.10

Zhou, J., Blundell, J., Ogawa, S., Kwon, C. H., Zhang, W., Sinton, C., Powell, C. M., & Parada, L. F. (2009, Feb 11). Pharmacological inhibition of mTORC1 suppresses anatomical, cellular, and behavioral abnormalities in neural-specific Pten knock-out mice. *J Neurosci, 29*(6), 1773-1783. https://doi.org/10.1523/JNEUROSCI.5685-08.2009

Chapter 4:

Rapamycin-mediated mTOR inhibition prevents and reverses neuronal growth of mature granule cells following PTEN deletion

ABSTRACT

Phosphatase and tensin homolog (PTEN) is a major negative regulator of the mechanistic target of rapamycin (mTOR) pathway. PTEN mutations are associated with neuronal hypertrophy, the formation of aberrant circuitry, and seizures in humans, with developmental animal models shedding light on mechanisms of disease. Recently, vector-mediated PTEN deletion in mature granule cells was reported to trigger a new, but slower wave of dramatic neuronal growth outside of the typical developmental period. Here, we assess if initiation and maintenance of this growth is dependent on sustained mTOR activity. Unilateral injections of AAV-Cre into the dentate gyrus of adult PTEN-floxed, Rosa-reporter mice resulted in focal PTEN deletion in mature granule cells. PTEN deleted granule cells displayed soma hypertrophy by 2 months after AAV-Cre injection, with growth of neuronal axons and dendrites by 4 months after PTEN deletion. To determine mechanism of action, one subset of mice was treated with the mTOR inhibitor, rapamycin, during the acute period after AAV-Cre injection and a second cohort of animals was treated at a delayed period after PTEN deletion. At each time period, rapamycin treatment reduced the phosphorylation of ribosomal protein S6 in PTEN deleted granule cells, suggesting effective inhibition of mTOR activity. Assessment of granule cell morphological features revealed that rapamycin

administration prevented the growth of granule cell somata and processes when given prior to the onset of significant change, as well as reversed neuronal hypertrophy when given after the onset of growth. These findings suggest that mTOR activation is required for the maintenance of morphological changes that occur as a result of PTEN deletion in mature neurons, and importantly suggests that inactivation of mTOR activity could ameliorate the negative consequences of neuronal PTEN mutations and other related TOR-opothies.

INTRODUCTION

The mechanistic target of rapamycin (mTOR) is a member of the PI3K (phosphoinositide-3-kinase)-Akt-mTOR signaling pathway responsible for various important cellular functions. mTOR is a serine-threonine kinase that becomes active in response to extracellular stimuli like growth factors. Briefly, receptor tyrosine kinase activation results in the conversion of phosphatidylinositol (4,5)-bisphosphate (PIP2) to phosphatidylinositol (3,4,5)-trisphosphate (PIP3) by phosphoinositide 3 kinase (PI3K). PIP3 leads to activation of Akt which inactivates the tuberous sclerosis complex (TSC1 and TCS2). Inactivation of TCS2 allows for activation of the Ras homolog enriched in brain protein (Rheb), which directly activates mTOR when bound. mTOR activation then results in downstream inactivation of the eIF4E binding protein 1 (4EBP1) and activation of the p70 ribosomal protein S6 kinase 1 (S6K1) for the initiation and promotion of protein translation. For more detail see review by (Switon et al., 2017). As such, mTOR is responsible for the regulation of cell growth, proliferation, metabolism, and survival during development through its kinase activity.

mTOR overactivation during development has been implicated in several disease models, termed TOR-opothies. Most notably are those that result from mutations in upstream negative regulators of mTOR, including TSC and the phosphatase and tensin homolog (PTEN) gene. PTEN is a lipid and protein phosphatase that acts to dephosphorylate PIP3 to PIP2, in opposition to PI3K activity. Such genetic mutations have been linked to the development of epilepsy, autism spectrum disorders, tumor formation, and reduced mental ability (Conti et al., 2012; Jansen et al., 2015; Switon et al., 2017; Tilot et al., 2015; Zahedi Abghari et al., 2019).

Various promotor-driven, PTEN-targeted animal models have been developed to model these disorders. Brain wide, neuron-specific PTEN deletion in embryonic and early postnatal development report brain and hippocampal macrocephaly, neuronal hypertrophy, seizures, and high mortality rates (Backman et al., 2001; Kazdoba et al., 2012; Kwon et al., 2006; Kwon et al., 2003; Kwon et al., 2001; Ljungberg et al., 2009; Lugo et al., 2014; Matsushita et al., 2016; Sunnen et al., 2011; Zhou et al., 2009). Additionally, PTEN deletion in postnatal adult born granule cells and differentiating neurons have revealed similar morphological and pro-excitatory changes to hippocampal circuitry (Arafa et al., 2019; Getz et al., 2016; LaSarge et al., 2016; LaSarge et al., 2015; Luikart et al., 2011; Pun et al., 2012; Santos et al., 2017; Skelton et al., 2019; Williams et al., 2015).

A handful of these studies have utilized the mTOR inhibitor, rapamycin, to investigate and confirm the mechanism of PTEN deletion through mTOR activation. Rapamycin, when bound to the cytosolic FK506 chaperone protein, FKBP12, form a complex that binds the FKBP-rapamycin binding (FRB) site on mTOR. Together, this results in physical blocking of mTOR's

catalytic domain, and therefore interference of its kinase activity (Tsang et al., 2007; Yang et al., 2013). Early administration of rapamycin following PTEN deletion has been reported to prevent the abnormal morphological and physiological properties that develop from overactive mTOR during these critical developmental periods, often leading to improved mortality rates and variable effects on seizure frequency and severity (Getz et al., 2016; Ljungberg et al., 2009; Matsushita et al., 2016; Pun et al., 2012; Sunnen et al., 2011; Zhou et al., 2009). Rapamycin, and specifically its rapalog Everolimus, have also shown beneficial, yet variable, effects on seizure frequency in humans with TSC-related mutations (Cardamone et al., 2014; Fukumura et al., 2015; Krueger et al., 2013; Kuki et al., 2018).

Recent reports from our lab suggest that vector-mediated PTEN deletion and knockdown in mature cortical motoneurons of adult mice and rats triggers progressive increases in soma size and dendritic complexity (Gallent & Steward, 2018; Steward et al., 2019). In Chapter 3, we expand these reports to include dramatic neuronal growth of somata, axons, and dendrites in mature granule cells of the dentate gyrus in adult mice. Additionally, we report increased synaptogenesis triggered by postsynaptic growth, with preservation of laminar specificity of most inputs to and from PTEN deleted granule cells from regions that maintain PTEN expression. Specifically, we report soma growth by 2 months after vector-mediated PTEN deletion, with progressive increases in soma, dendritic, and axonal growth by 4 months after PTEN deletion. Such a patterned timeline in our model allows us to answer two questions: 1) Is growth of mature neurons dependent on mTOR signaling? and 2) Is maintenance of mTOR activation required for sustained morphological change?

In the present study, we characterize the role of mTOR activity in the progression and stability of PTEN deletion-induced neuronal growth in mature granule cells. We utilize AAV-Cre injections into the dentate gyrus for focal, PTEN deletion in adult mice, followed by acute and delayed rapamycin administration. Assessment revealed that rapamycin administration prevented and reversed growth of mature granule cells revealing the dependence of PTEN deletion-induced growth in our model on persistent mTOR activation.

MATERIALS AND METHODS

Experimental animals

All experimental procedures were approved by the Institutional Animal Care and Use Committee (IACUC) at the University of California, Irvine. Experimental, triple transgenic mice were generated by breeding PTEN-floxed (RRID: IMSR_JAX:004597), $ROSA^{tdTomato}$ reporter mice (RRID: IMSR_JAX:007905) with Thy1-eYFP mice (Jackson Labs). Controls were double transgenic $Rosa^{tdT}$, Thy1-eYFP mice. Animals were homozygous for the PTEN and Rosa loci, but heterozygous for Thy1-YFP. For simplicity, these animals will be referred to as PTEN/tdT and tdT controls, regardless of their Thy1 expression. It is important to note that because these strains were developed in our lab, they have different genetic backgrounds than the original mice available for purchase.

AAV-Cre injection into the dentate gyrus

All mice were at least 2 months of age at the time of AAV-Cre injection. All surgical procedures were performed under 2-2.5% Isoflurane fixed to a stereotaxic device. A scalp incision was made to expose the skull and a small cranial window was created above the injection site. Using a 10µl Hamilton syringe with a pulled glass pipette tip, a single unilateral AAV2-Cre (Vector Bio Labs, 7011) injection was made at +1.3mm lateral and +2.2mm anterior to lambda at a depth of -1.6mm from the cortical surface. Each injection was 0.6µl in volume ($1x10^{12}$ GC/ml in 1xPBS with 5% glycerol) and was performed over 4 minutes, followed by an additional 2 minutes before the glass pipette was removed. After injection, the bone flap was replaced over the cranial window and the incision site was sutured. Mice survive between 2 and 4 months after injection (Table 4.1).

Rapamycin administration

Rapamycin was used to inhibit mTOR activity at various timepoints following PTEN deletion (Table 4.1). Rapamycin (LC Laboratories, R-5000) stocks of 40mg/mL in 100% EtOH were stored at 20°C until needed. Working solution (1mg/mL) was made in 4% ethanol, 5% tween 80, 5% PEG, and sterile saline immediately before use (Pun et al., 2012). Administration (6mg/kg or 10mg/kg) occurred for 8 weeks from 0 through 2 months (prevention only) and 2 through 4 months (prevention and reversal) following AAV-Cre injection into the dentate gyrus (Fig. 4.2A). Animals were sacrificed 3 hours after the final injection. No significant differences were found between mice treated with 6 or 10mg/kg rapamycin therefore

animals were combined. Vehicle and non-vehicle treated, PTEN-deleted animals were used for comparison.

Tissue collection and histology

Mice received intraperitoneal injections of Fatal Plus and were intracardially perfused with 4% paraformaldehyde in phosphate buffer (PFA). Brains were dissected and post-fixed in 4% PFA for 48 hours before being cryoprotected in 27% sucrose and frozen in Tissue-Tek O.C.T. compound. Brains were then cryosectioned into 30µm sections and stored in 1xPBS with 0.1% NaN_3 until processed for immunohistochemistry.

Sections spaced at 360µm intervals were processed for various histological markers. For immunohistochemistry (IHC), sections were washed in 1xTBS (100mM Tris, pH 7.4 and 150mM NaCl) then quenched for endogenous peroxidase activity by incubation in 3% H_2O_2 for 15 minutes. Sections were then washed in 1xTBS and blocked in blocking buffer (1xTBS, 0.3% Triton X-100, 5% NDS) for 2 hours at room temperature. Sections were then incubated overnight at room temperature in buffer containing primary antibodies (Table 4.2). Sections were then washed in 1xTBS, followed by a 2-hour incubation in buffer containing biotinylated donkey anti-rabbit IgG (1:250, Jackson ImmunoResearch, 711-065-152), then washed again. Visualization was accomplished through incubation in ABC reagent (Vectastain Elite kit, catalog #PK-6100; Vector Laboratories) and CARD amplification with Tyramide-AMCA. All sections were then mounted on 0.5% gelatin coated slides.

Quantification of percent transduction

To determine percent transduction through the dentate gyrus, sections spaced 360μm apart were assessed for percentage of the granule cell layer occupied by tdTomato-positive granule cells. Briefly, images of the dentate gyrus were taken with a 10x objective using an Olympus AX80 microscope. Images were imported into NIH ImageJ FIJI, and a border was drawn around the Hoechst-positive dentate gyrus. The contour was then transferred to the tdT-labeled image. The tdT-positive area within the contour was determined by thresholding the color image until the selected area matched the native red fluorescence. The percent of the granule cell layer that was tdT-positive was calculated for each section in each mouse. Sections outside of the transduced area that lacked tdTomato expression we included for determination of percent transduction of the entire ipsilateral dentate gyrus. Linear regressions were used for determination of correlations between percent transduction and outcome measures.

PTEN deletion and ribosomal protein S6 phosphorylation

The progression of PTEN deletion/expression has been previously determined in this model (Chapter 3). A similar process was completed for indirect quantification of ribosomal protein S6 phosphorylation following rapamycin administration. Briefly, one section per animal stained for pS6 and at the core of transduction and/or PTEN deletion was selected. 10x images of the ipsilateral and contralateral dentate gyri were taken and imported into ImageJ FIJI. A 50μm x 50μm box delineating the region of interest (ROI) was drawn within the granule cell layer using the red channel to identify regions of tdT expression within the

ipsilateral dentate gyrus. A similarly sized ROI was placed in the granule cell layer and stratum radiatum of the contralateral dentate gyrus. The mean grey value was then determined within each ROI in the blue channel (pS6 fluorescence). Data is reported as the ratio of the mean grey values between the ipsilateral and contralateral granule cell layers for each animal, as well as for each transduced dentate gyrus in relation to the contralateral stratum radiatum outside of the transduction area.

Dentate granule cell measurements

Granule cell body sizes were measured in sections at the rostral and lateral ends of PTEN deletion/transduction where tdT labeled cells were more sparsely located and soma borders could be easily distinguished from surrounding non-transduced cells. Images were taken at 10x and imported into ImageJ. Sampling was done by starting at the lateral end of the dorsal blade of the dentate gyrus and moving medially until 30 tdT expressing cells had been measured. Measurements of the thickness of the molecular layer were taken in the dorsal blade of the dorsal hippocampus at the core of transduction as a representation of dendritic length. Importantly, only measurements of the ipsilateral dentate gyrus were taken, as we have previously reported no effect of unilateral PTEN deletion on the contralateral dentate gyrus (Chapter 3).

A similar process was repeated at the core of transduction using Cresyl violet stained sections in order to determine the effect of rapamycin on neurons that maintain their PTEN expression in PTEN/tdT mice. Here, 44.4x images were taken on the Keyence BZ-X800

microscope and imported into ImageJ. Sampling was done by measuring 10 granule cells within a 100μm^2 region of interest in the ipsilateral dentate gyrus, and the homologous regions in the contralateral granule cell layer of PTEN/tdT mice treated with vehicle and rapamycin, as well as non-treated tdT control mice.

Assessment of mossy fiber projections

Sections at the core of transduction in PTEN/tdT and tdT control mice were used to measure alterations to granule cell axonal projections (mossy fibers) with and without rapamycin administration. Briefly, images of tdTomato-positive mossy fiber axons within the ipsilateral dentate gyrus and CA3 were taken with a 10x objective. Measurements were taken of the thickness of the laminae containing mossy fiber axons upon exiting the hilus (Fig. 4.7A-C, blue line) and the thickness of the supra-pyramidal mossy fiber bundle in *stratum lucidum* of CA3 (Fig. 4.7A-C, green line). Again, only measurements of the ipsilateral dentate gyrus were taken, as we have previously reported no effect of unilateral PTEN deletion on the contralateral dentate gyrus (Chapter 3).

To detect the presence of supra-granular mossy fibers, sections at the core of transduction were stained for the zinc vesicular transporter, Znt3. Sections from PTEN/tdT mice with and without rapamycin treatment, as well as tdT controls were scored as described by (Hunt et al., 2009): 0=little to no Znt3 labeling in granule cell layer; 1=mild Znt3 labeling in granule cell layer; 2=moderate staining in the granule cell layer and punctuate staining in inner molecular layer; 3=dense Znt3 labeling in inner molecular layer.

Statistical analysis

Graphpad Prism software was used for graphing and statistical analysis. One-way *ANOVA* with Sidak's post hoc comparisons were used for comparisons between the transduced dentate gyrus of PTEN/tdT mice and tdT controls. Two-way *ANOVA* with Sidak's multiple comparisons tests were used for comparisons between the ipsilateral, transduced dentate gyrus of PTEN deleted animals with and without rapamycin administration.

RESULTS

Rapamycin treatment results in weight loss in older animals.

Previous studies of rapamycin administration following embryonic or early postnatal PTEN deletion report slowed development and weight loss in young mice (Getz et al., 2016; Pun et al., 2012; Zhou et al., 2009). We therefore wondered if rapamycin administration would have similar effects in adult mice. Throughout the experimental duration, rapamycin-treated, PTEN-deleted mice appeared relatively healthy compared to vehicle and non-injected, PTEN-deleted animals. In Group 1, mice received rapamycin from 0 to 2 months after AAV-Cre injection, roughly 2 to 4 months of age (Fig. 4.1A). In contrast, Group 2 received rapamycin from 2 to 4 months after PTEN deletion (4-6 months of age). Mice in Group 1 did not show any effects of rapamycin administration on weight gain or maintenance, while older mice in Group 2 showed weight loss that lasted through the 8 weeks of rapamycin treatment, but remained above 90% of baseline weight (Fig. 4.1B). Two-way ANOVA was significant for treatment group [$F(2,518) = 206.8$, $p<0.000$], but not time. Sidak's post hoc

analysis revealed a significant difference between PTEN/tdT animals treated with rapamycin from 2-4 months after AAV-Cre injection vs. vehicle-injected, PTEN/tdT animals ($p<0.0001$) and vs. PTEN/tdT animals treated with rapamycin from 0-2 months ($p<0.0001$). There was no significant difference in body weight between PTEN/tdT Group 1 and vehicle treated mice.

Effective PTEN deletion and mTOR activation after AAV-Cre injection into PTEN/tdT mice

Unilateral injections of AAV-Cre into the dentate gyrus of mature PTEN/tdT mice resulted in transduction of granule cells and expression of tdTomato in the ipsilateral dentate gyrus (Fig. 4.2A). The areas of transduction were as previously described (Chapter 3), with a dense core of transduction which gradually decreases and becomes more sparse in the rostral and caudal directions. Immunostaining for PTEN revealed effective PTEN deletion in transduced, tdT expressing granule cells (Fig. 4.2C, arrow). Importantly, there was no evidence of decreased PTEN immunoreactivity in the contralateral dentate gyrus of PTEN/tdT mice (Fig. 4.2D) or in either dentate gyrus of tdT control mice (not shown). Immunostaining for the phospho-specific antibody for ribosomal protein S6, a canonical downstream marker of mTOR activation, revealed increased phosphorylation in PTEN-deleted granule cells (Fig. 4.2E, arrow). There was no increased immunostaining for pS6 in the non-injected, contralateral dentate gyrus of PTEN/tdT mice (Fig. 4.2F).

Reduced phosphorylation of ribosomal protein S6 after rapamycin administration

Rapamycin functions by directly inhibiting mTOR kinase activity. Assessment of the phosphorylation of ribosomal protein S6 can therefore be used as an indicator of effective mTOR inhibition in mice treated with rapamycin. Phospho-S6 was notably reduced in PTEN deleted granule cells from PTEN/tdT mice following rapamycin treatment during both acute and delayed administration periods. This was evident in sections stained for pS6 within the area of PTEN deletion for each group (Fig. 4.3 and Fig. 4.4).

PTEN deleted mice treated with rapamycin during the acute period after AAV-Cre injection (0-2 months) showed a prevention of S6 phosphorylation (Fig. 4.3D,E) compared to vehicle-treated, PTEN deleted mice assessed at the same period (Fig. 4.3A,B). Quantification of S6 phosphorylation in the ipsilateral dentate gyrus of PTEN/tdT mice revealed a significant increase in pS6 fluorescence following PTEN deletion that was reduced with rapamycin administration to levels comparable to controls when represented as a ratio of S6 phosphorylation in the contralateral dentate gyrus (Fig. 4.3G). One-way ANOVA comparing the ipsilateral dentate gyri of rapamycin-treated PTEN/tdT mice, vehicle-treated PTEN/tdT mice, and non-treated tdT controls was significant [$F(2,7) = 26.79$. $p=0.0005$], and significant differences between groups were evident by Sidak's multiple comparisons tests (see Figure 4.3 legend for details on statistics).

Two-way ANOVA (Fig. 4.3H) comparing pS6 immunoreactivity in ipsilateral and contralateral dentate gyri of PTEN/tdT mice as a ratio of the contralateral stratum radiatum was significant for hemisphere [$F(1,10) = 37.10$, $p=0.0001$], treatment group [$F(1,10) =$

22.40, p=0.0008], and interaction [F (1,10) = 13.52, p=0.0043] (see Figure 4.3 legend for details on post hoc comparisons). Importantly, there was no significant difference between the ipsilateral, rapamycin-treated (Fig. 4.3E), contralateral, rapamycin-treated (Fig. 4.3F), or contralateral, vehicle-treated (Fig. 4.3C) hemispheres in PTEN/tdT mice (Fig. 4.3H), revealing effective inhibition of mTOR activity by rapamycin in PTEN deleted neurons.

PTEN/tdT mice treated during the delayed period after PTEN deletion (2-4 months after AAV-Cre injection) showed reversal and prevention of further S6 phosphorylation in PTEN deleted granule cells (Fig. 4.4A,B vs. 4.4D,E). Levels in rapamycin treated mice were comparable to tdT controls. Similar to acute treatment, quantification of S6 phosphorylation in the ipsilateral dentate gyrus of PTEN/tdT mice (rapamycin and vehicle treated) vs. tdT controls (Fig. 4G) was significant by one-way ANOVA [F(2,10)= 12.29, p=0.0020], and Sidak's multiple comparisons revealed significant differences between groups (see Figure 4.4 legend for details on statistics).

Two-way ANOVA (Fig. 4.4H) comparing the ipsilateral and contralateral dentate gyrus of PTEN/tdT mice with the delayed treatment paradigm was, again, significant for hemisphere [F (1,16) = 17.64, p=0.0007], treatment group [F (1,16) = 4.653, p=0.0466], and interaction [F (1,16) = 13.17, p=0.0023], with significant differences by post hoc comparisons (see Figure 4.4 legend). S6 phosphorylation in the ipsilateral dentate gyrus of PTEN/tdT mice treated with rapamycin (Fig. 4.4E) was comparable to the contralateral dentate gyrus of the same mice (Fig. 4.4F) and the contralateral dentate gyrus of vehicle-treated PTEN/tdT mice (Fig. 4.4C). Together, these results show that rapamycin administration is able to effectively

inhibit downstream mTOR activity that results from PTEN deletion, regardless of the period at which it is given.

Prevention of granule cell somata hypertrophy with acute rapamycin administration

We have previously documented dramatic growth of mature granule cells in our model of vector-mediated PTEN deletion in adult mice (Chapter 3). To determine if growth of mature granule cells is dependent on mTOR signaling, mice were treated with rapamycin during the acute period (0-2 months) after PTEN deletion, a stage of active cell body growth. Granule cell soma size was then measured based on tdTomato expression in each group. As expected, PTEN deletion resulted in notable increases in soma size (Fig. 4.5A) compared to transduced granule cells from tdT controls (Fig. 4.5C). Granule cells from rapamycin-treated PTEN/tdT mice during this period were noticeably smaller, despite their PTEN-deletion state (Fig. 4.5B). Quantification of cell sizes from vehicle-treated PTEN/tdT mice were 302.3 +/- 4.187μm^2 at 2-months post AAV-Cre injection compared to cell size measurements of 153.5 +/- 11.33μm^2 from tdT controls, confirming growth of mature neurons following PTEN deletion. Cell sizes of PTEN-deleted granule cells treated with rapamycin were 213.5 +/- 23.58μm^2 when assessed at the same time point. Notably, while rapamycin administration effectively attenuated growth, soma size did not reach that of control, PTEN-expressing granule cells (Fig. 4.5F). One-way ANOVA was significant for 2-month PTEN/tdT vs. tdT control mice [$F(2,7) = 60.18$, $p<0.0001$], and Sidak's post hoc comparisons revealed significant differences between vehicle-treated PTEN/tdT, rapamycin-treated PTEN/tdT, and tdT control mice (see Figure 4.5 legend for details on statistics).

Reversal of granule cell somata hypertrophy with delayed rapamycin administration

We next wondered if maintenance of growth of mature granule cells requires sustained mTOR activation over time. Accordingly, PTEN/tdT mice underwent delayed rapamycin administration from 2 to 4 months after PTEN deletion, a time period at which granule cells already show significant increases in cell body size. Increases in granule cells size were persistent out to 4 months after AAV-Cre injection in PTEN/tdT mice (304.8 +/- 20.26μm^2, Fig. 4.5D) and delayed rapamycin administration resulted in notable decreases in cell body size (Fig. 4.5E), measuring 225.3 +/- 16.19μm^2. Despite such reductions, cell sizes still remained larger than those of tdT controls (Fig. 4.5F). One-way ANOVA was significant for 4-month PTEN/tdT vs. tdT control mice [$F(2,11) = 71.85$, $p<0.0001$], and Sidak's post hoc comparisons again revealed significant differences between vehicle-treated PTEN/tdT, rapamycin-treated PTEN/tdT, and tdT control mice (see Figure 4.5 legend for details on statistics).

When comparing PTEN/tdT mice across time and treatments, there was no significant difference between cell sizes of any rapamycin treated group (0-2 month vs. 2-4 month treatments). Importantly, there was a significant difference between 2-month, vehicle-treated mice and 4-month, rapamycin-treated mice, suggesting reversal of the growth that would have already occurred by 2 months after PTEN deletion when rapamycin treatment was initiated (Fig. 4.5F). Two-way ANOVA for comparison between PTEN/tdT mice with and without treatment at each timepoint (Fig. 4.5F) was significant for treatment [$F(1,4) = 90.18$, $p<0.0001$], but not for treatment period or interaction. Sidak's multiple comparisons

revealed significant differences between individual treatment groups (values located in red brackets joining individual bars in Fig. 4.5F, see figure legend for details on statistics).

Rapamycin administration does not alter cell size of PTEN expressing granule cells

In order to determine if rapamycin administration would alter soma size of non-transduced, PTEN expressing granule cells in PTEN/tdT mice, sections stained for Cresyl violet were used to measure soma size in the ipsilateral and contralateral dentate gyrus in all groups. There was no significant difference between cell size of PTEN-expressing granule cells in the contralateral dentate gyrus of rapamycin-treated or vehicle-treated PTEN/tdT mice, or when compared to granule cells from tdT controls (not shown). While we cannot entirely discount any effects of rapamycin in the mature brain, these data suggest that rapamycin is largely acting on PTEN deleted neurons in our model.

Rapamycin administration prevents dendritic growth after PTEN deletion

We have previously reported that significant increases in molecular layer thickness are not observed until 4 and 6 months after PTEN deletion in our model and are suggestive of increased length of granule cell apical dendrites (Chapter 3). We therefore wondered if delayed rapamycin administration would prevent this growth. Accordingly, the thickness of the molecular layer at the core of PTEN deletion was measured as an indirect assessment of apical dendrite length in mice treated with rapamycin from 2 to 4 months after AAV-Cre injection. Similar to our measurements of somata size with rapamycin treatment, delayed

rapamycin administration appeared to prevent dendritic growth in mature granule cells following PTEN deletion (Fig. 4.6D).

In vehicle-treated mice, PTEN deletion significantly increased the thickness of the molecular layer by 4 months post AAV-Cre injection to 369.1 +/- 17.20μm (Fig. 4.6B) compared to tdT control mice (211.4 +/-11.20μm, Fig. 4.6A). Mice with delayed rapamycin administration had noticeably reduced molecular layer thickness measurements at 272.0 +/- 12.04μm (Fig. 4.6C) compared to vehicle-treated mice. Importantly, molecular layer thickness of rapamycin treated mice remained significantly increased compared to tdT controls. One-way ANOVA was significant between groups [$F(2,7) = 88.32$, $p<0.0001$], with significant post hoc comparisons between vehicle-treated PTEN/tdT mice, rapamycin-treated PTEN/tdT mice, and tdT controls (See Figure 4.6 legend for post hoc comparisons).

Prevention of axonal enlargement with delayed rapamycin administration

In addition to postsynaptic effects of PTEN deletion, injections of AAV-Cre into PTEN/tdT mice also trigger enlargement of mossy fiber axon projections to the CA3 (Chapter 3). We were curious if delayed rapamycin administration would also prevent growth of granule cell axons. To assess this, the thickness of the mossy fiber tract was measured in two regions, the first at the point where both the supra and inferior pyramidal bundles initially exit the hilus (Fig. 4.7A-C, blue lines) and the second where the suprapyramidal bundle enters its terminal zone within the stratum lucidum of the CA3 (Fig. 4.7A-C, green lines).

At 4 months following AAV-Cre injection, PTEN/tdT mice had increased thickness of their mossy fiber tract bundle (Fig. 4.7B, blue line), expanding to 224.8 +/1 13.30μm following PTEN deletion compared to the 108.3 +/- 14.69μm mossy fiber tract thickness measured in tdT control mice (Fig. 4.7A, blue line). Rapamycin administration in PTEN/tdT mice from 2 to 4 months after AAV-Cre injection prevented mossy fiber tract enlargement, resulting in attenuated axonal expansion to 162.0 +/- 24.37μm (Fig. 4.7C, blue line), although still increased compared to measurements from controls (Fig. 4.7D). One-way ANOVA was significant between groups [$F(2,8) = 25.83$, $p=0.0003$] with significant post hoc comparisons (see Figure 4.7 legend for details).

Similarly, the thickness of the mossy fiber axon terminal zone, the stratum lucidum of the CA3, was increased to 206.3 +/- 24.17μm at 4 months after AAV-Cre injection in PTEN/tdT mice (Fig. 4.7B, green line) compared to 133.4 +/- 28.60μm in tdT controls (Fig. 4.7A, green line), with complete prevention of terminal zone enlargement with delayed rapamycin administration in PTEN/tdT mice (140.7 +/- 21.96μm, Fig. 4.7C, green line). Again, one-way ANOVA was significant between groups [$F(2,8) = 8.700$, $p=0.0098$] with significant post hoc comparisons between vehicle-treated PTEN/tdT mice vs. tdT controls and vs. rapamycin-treated mice. Interestingly, there was no significant difference between rapamycin-treated PTEN/tdT mice and tdT controls suggesting complete prevention of terminal zone enlargement (Fig. 4.7E).

Reduced mossy fiber sprouting with rapamycin administration

In Chapter 3, we report the formation of supragranular mossy fibers in some mice following PTEN deletion that is dependent on time post deletion and amount of PTEN deletion in the dentate gyrus. Again, we wondered if delayed rapamycin administration would prevent the formation of such aberrant circuitry. This was assessed in sections at the core of transduction and PTEN deletion stained for the zinc vesicular transporter, Znt3 (Fig. 4.8). In tdT control mice, Znt3 labeling was confined to the hilus and mossy fiber tract (Fig. 4.8A, score of 0). At 4 months post PTEN deletion in vehicle-treated mice, 2 of 4 mice assessed showed mild Znt3 labeling only in the granule cell layer (score of 1) and 1 of 4 mice showed moderate Znt3 labeling in the granule cell layer and mild labeling in the inner molecular layer (score of 2, Fig. 4.8B,D). Rapamycin treatment from 2 to 4 months after PTEN deletion appeared to completely prevent any granular or supragranular mossy fiber labeling in PTEN/tdT mice (Fig. 4.8C). A graph of mossy fiber scores for each mouse is shown in Figure 4.8D and representative images are labeled with corresponding mossy fiber scores in the bottom right of each panel.

There were positive correlations between mossy fiber score with percent transduction of the entire ipsilateral dentate gyrus (Fig. 4.8E) and the % transduction of the coronal section at the core of PTEN deletion (Fig. 4.8F). This is in agreement with our previous reports (Chapter 3) and suggests that mice with greater areas of PTEN deletion are more likely to have greater mossy fiber labeling outside of the hilus. Here we show that at least 8% of the unilaterally transduced dentate gyrus must be PTEN deleted for mossy fiber sprouting into the granule cell layer and 50% for supragranular mossy fibers in the inner molecular layer

(Fig. 4.8E). A greater range of PTEN deletion volumes will be required for a more detailed assessment of these correlations. Importantly, mice treated with rapamycin with percent PTEN deletion areas ranging from 2% to 42% showed no evidence of Znt3 labeling outside of the hilus. Any correlations in these animals were lost (Fig. 4.8E,F).

DISCUSSION

In the present study, administration of the mTOR inhibitor, rapamycin, was used to investigate the mechanisms of PTEN deletion-induced growth of mature neurons. Specifically, AAV-Cre was injected unilaterally into the dentate gyrus of mice containing a floxed exon 5 of the PTEN gene. In Chapter 3, we report that PTEN deletion in this model results in soma growth by 2 months after PTEN deletion, with progressive increases in soma, dendritic, and axonal size by 4 months after PTEN deletion. With this in mind, intraperitoneal injections of rapamycin were given during the acute (0-2 months) or delayed (2-4 months) period after AAV-Cre injection. Here we show that rapamycin administration is able to prevent and reverse the growth of granule cell somata and processes following PTEN deletion.

Prevention and reversal of neuronal growth with rapamycin administration

Rapamycin acts to specifically target mTORC1 activity, without effecting mTORC2, which is the pathway specifically activated following PTEN deletion (Getz et al., 2016). To our

knowledge, this is the first rodent study to investigate the consequence of long-term rapamycin administration following PTEN deletion in mature neuronal populations. Here we utilized an 8-week dosing paradigm, while previous studies have utilized dosing paradigms ranging from 2 (Ljungberg et al., 2009; Sunnen et al., 2011) to 4 weeks (Kwon et al., 2003; Zhou et al., 2009) in developmental deletion models. The use of longer treatment paradigms are perhaps more therapeutically relevant and require further investigation.

We first confirmed that vector-mediated PTEN deletion in the dentate gyrus of adult mice leads to a slow onset of soma growth by 2 months after injection and further growth of neuronal processes by 4 months after PTEN deletion. Acute rapamycin administration resulted in prevention of soma growth, while delayed rapamycin administration after the growth had already occurred was able to reverse the phenotype. Delayed rapamycin administration also resulted in prevention of apical dendrite lengthening and mossy fiber axon enlargement and prevented the occurrence of supragranular mossy fibers. These results are in agreement with previous reports in promoter driven, developmental models (Getz et al., 2016; Ljungberg et al., 2009; Matsushita et al., 2016; Sunnen et al., 2011; Zhou et al., 2009). The undetectable effect of rapamycin on PTEN expressing granule cells within the dentate gyrus suggests that mTOR may not be required for the maintenance of a morphological steady state under otherwise normal conditions in mature neurons, although this would require further investigation.

We have previously reported increased spine densities throughout the extent of elongated, PTEN deleted granule cell dendritic trees suggesting increased synapse formation triggered

by the post synaptic cell, as well as increased size of axon terminal zones within the CA3 (Chapter 3). The enlargement of neuronal process by 4 months after PTEN deletion shown in this report suggest possible increased connectivity with PTEN expressing pre- and post-synaptic partners. It will be important to assess a more chronically delayed rapamycin dosing paradigm beyond 4 months after PTEN deletion in our model to determine if continuous mTOR activation is required for preservation of these newly formed synaptic connections in an otherwise mature, but modified circuit. The limitations of rapamycin administration have been documented in the study of aberrant migration of PTEN deleted granule cells during early postnatal development, where rapamycin could prevent but not reverse mislamination within the dentate gyrus (Getz et al., 2016). These results could suggest that rapamycin may not be able to reverse or rectify all morphological phenotypes that occur as a result of PTEN deletion during either development or adulthood.

If reversal is possible, characterization of the time course by which mTOR activity is restored after termination of rapamycin treatment and the extent to which morphological changes re-occur would help to expand understanding of circuit plasticity in adulthood. Collectively, examining the regulation of neuronal hypertrophy and circuit changes at various stages following PTEN deletion allows for determination of the persistence of these morphological changes and their reliance on appropriately measured mTOR activation throughout life.

Incomplete prevention and reversal by rapamycin

Interestingly, rapamycin administration did not completely prevent or reverse the majority of the morphological outcomes assessed. Incomplete transition to baseline levels in our study could be due to the limitations of rapamycin activity, or simply be attributed to the dosing paradigm selected. Animals were injected once a day, five consecutive days a week, for a total of 8 weeks. Detailed pharmacological studies would be required to determine for how long each daily dose is effective over a 24-hour period and how large of an impact two days without treatment can have on the initiation and progression of growth. Alternatively, incomplete prevention and reversal could point to an mTOR-independent component to PTEN deletion-induced growth of mature neurons that involves a divergent PI3K-AKT path.

Functional consequence of mTOR activation and inhibition following PTEN deletion in adulthood

These initial findings suggest that growth of mature neurons in our model of vector-mediated PTEN deletion is dependent on mTOR signaling, and that maintenance of mTOR activation is required for sustained morphological change. One important factor that remains to be determined in our model of PTEN-deletion induced growth in the adult dentate gyrus is the effect on network function. The similarities between the morphological and circuit changes reported in our model and models of developmental PTEN deletion lend to the possibility that functional outcomes might also be similar, most notably the development of spontaneous seizures. If this were the case, investigation into how mTOR activation as a result of PTEN deletion, as well as mTOR inactivation at various time points by rapamycin,

might influence network function would help to elucidate mechanisms underlying possibly altered neuronal activity.

Long-term consequences of chronic rapamycin administration

The ability to regulate or control neuronal architecture or circuitry has important implications for mTOR-related disorders in humans where reduced connectivity and excitability would be advantageous. Understanding the long-term consequences of rapamycin administration to treat mTOR-related dysfunction in adulthood is, therefore, very important. Despite normal outward appearances, we document that older adult mice were more susceptible to weight loss compared to younger adult mice treated with rapamycin. Conversely, one might expect that rapamycin administration early in development might have detrimental effects on circuit formation or overall growth. A more intermittent treatment paradigm may be needed to determine the minimum dose required to positively ameliorate morphological and circuit abnormalities while maintaining proper health at any life stage.

Table 4.1:

Mice used for morphological assessments

Time post AAV-Cre	Age at time of injection	# PTEN/tdT mice	# tdT mice	Treatment group	Treatment duration
1 month	9 weeks		3 (3M)	n/a	n/a
2 months	9-10 weeks	4 (2M, 2F)		Vehicle	0-2 months (8 weeks)
2 months	9 weeks	4 (2M, 2F)		Rapamycin	0-2 months (8 weeks)
4 months	9-10 weeks	4 (4M)		Vehicle	2-4 months (8 weeks)
4 months	8-10 weeks	7 (6M, 1F)		Rapamycin	2-4 months (8 weeks)

Table 4.2:

Antibody list

Antibody	Host	Vendor	RRID	Dilution
PTEN	Rabbit	Cell Signaling Technology, 9188	AB_2253290	1:250
pS6, Ser 235/236	Rabbit	Cell Signaling Technology, 4858	AB_916156	1:250
pS6, Ser 240/244	Rabbit	Cell Signaling Technology, 2215	AB_331682	1:250
Znt3	Rabbit	Millipore ABN994		1:1500

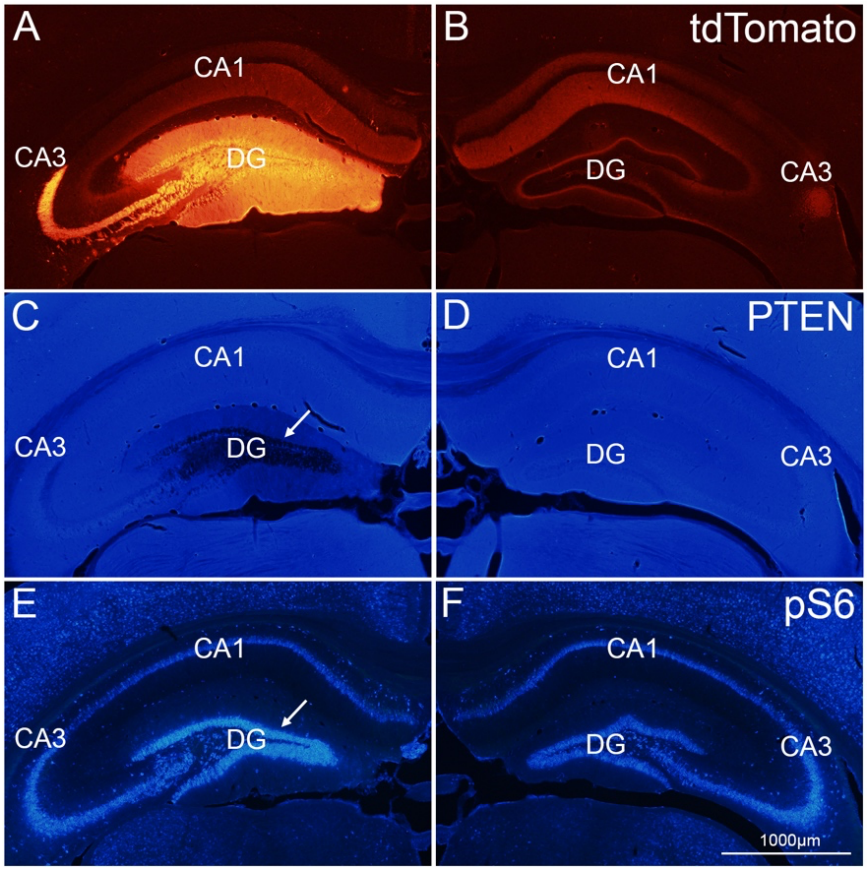
A
CA1
CA3
DG
B
tdTomato
CA1
DG
CA3
C
CA1
CA3
DG
D
PTEN
CA1
DG
CA3
E
CA1
CA3
DG
F
pS6
CA1
DG
CA3
1000μm

Figure 4.1. Unilateral, vector-mediated PTEN deletion in the dentate gyrus of adult PTEN/tdT mice. A) AAV-Cre injection results in transduction of mature granule cells of the dentate gyrus and expression of tdTomato in transduced granule cells. B) Lack of tdT expression in the contralateral dentate gyrus. C) Area of PTEN deletion in transduced granule cells if the dentate gyrus (arrow), with preservation of PTEN expression in the CA1 and CA3 regions. D) PTEN expression is maintained in the contralateral dentate gyrus. E) Increased phosphorylation of ribosomal protein S6 in PTEN deleted granule cells. F) pS6 levels in the contralateral dentate gyrus.

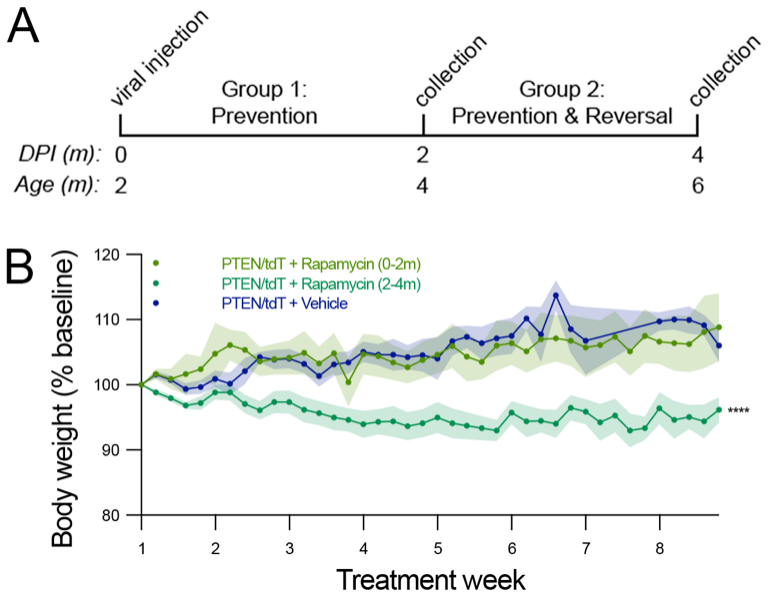
A
viral injection
Group 1:
Prevention
collection
Group 2:
Prevention & Reversal
collection
DPI (m): 0 2 4
Age (m): 2 4 6
B
PTEN/tdT + Rapamycin (0-2m)
PTEN/tdT + Rapamycin (2-4m)
PTEN/tdT + Vehicle
Body weight (% baseline)
120
110
100
90
80
****
1
2
3
4
5
6
7
8
Treatment week

Figure 4.2. Experimental design for rapamycin administration following unilateral PTEN deletion in adult PTEN/tdT mice. A) Mice were separated into two groups following PTEN deletion. Group 1 received rapamycin injections 5 times per week for 8 weeks (0-2 months) immediately after AAV-Cre injection for prevention of PTEN deletion induced morphological changes. Group 2 received 8 weeks of rapamycin injections from 2 to 4 months after PTEN deletion for prevention and reversal of growth. B) Mice in each group were weighed every day for determination of rapamycin and vehicle dose. Body weights are represented as percent change from baseline body weight on the first day of injection (mean +/- SEM) allowing for data to be compared across treatment week, independent of animal age.

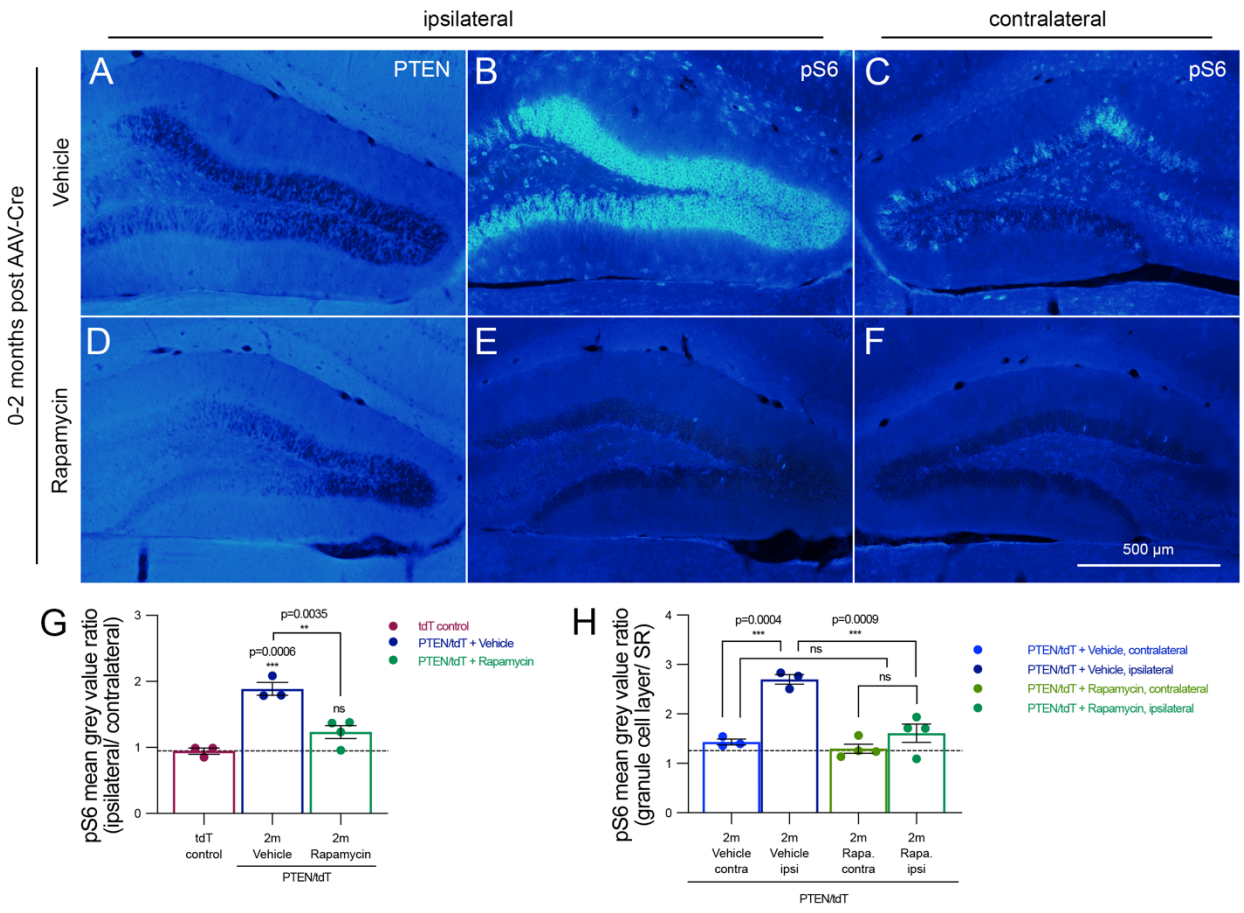
ipsilateral
contralateral
A
PTEN
B
pS6
C
pS6
D
E
F
500 µm
0-2 months post AAV-Cre
Vehicle
Rapamycin
G
pS6 mean grey value ratio (ipsilateral/ contralateral)
p=0.0035
**
p=0.0006
***
ns
tdT control
PTEN/tdT + Vehicle
PTEN/tdT + Rapamycin
tdT control
2m Vehicle
2m Rapamycin
PTEN/tdT
H
pS6 mean grey value ratio (granule cell layer/ SR)
p=0.0004
***
p=0.0009
***
ns
ns
PTEN/tdT + Vehicle, contralateral
PTEN/tdT + Vehicle, ipsilateral
PTEN/tdT + Rapamycin, contralateral
PTEN/tdT + Rapamycin, ipsilateral
2m Vehicle contra
2m Vehicle ipsi
2m Rapa. contra
2m Rapa. ipsi
PTEN/tdT

Figure 4.3. Acute rapamycin administration inhibits the phosphorylation of ribosomal protein S6 after vector-mediated PTEN deletion. A) Area of PTEN deletion in a vehicle-treated, PTEN/tdT mouse at 2 months after AAV-Cre injection. B) Increased phosphorylation of ribosomal protein S6 in PTEN deleted granule cells. C) pS6 immunoreactivity in the contralateral dentate gyrus of the same vehicle treated mouse. D) Area of PTEN deletion in a PTEN/tdT mouse treated with rapamycin from 0 to 2 months after AAV-Cre injection. E) Reduced S6 phosphorylation in the area of PTEN deletion following acute rapamycin administration. F) pS6 labeling in the contralateral dentate gyrus of the same mouse. G) Quantification of pS6 fluorescence intensity represented as a ratio of the ipsilateral and contralateral granule cell layers. Sidak's post hoc analysis: PTEN/tdT vehicle-treated mice vs. tdT controls ($p=0.0006$), PTEN/tdT vehicle-treated mice vs. PTEN/tdT rapamycin-treated mice ($p=0.0035$). H) Ratio of pS6 fluorescence between the granule cell layer within each hemisphere with the stratum radiatum of the contralateral hippocampus in PTEN/tdT mice. Sidak's post hoc comparisons: ipsilateral vs. contralateral, vehicle-treated ($p=0.0004$), ipsilateral, vehicle-treated vs. ipsilateral, rapamycin-treated ($p=0.0009$), ipsilateral, vehicle-treated vs. contralateral, rapamycin-treated ($p=0.0001$). Note that the horizontal dotted lines in G and H mark the average fluorescence in the ipsilateral dentate gyrus of tdT controls for each ratio.

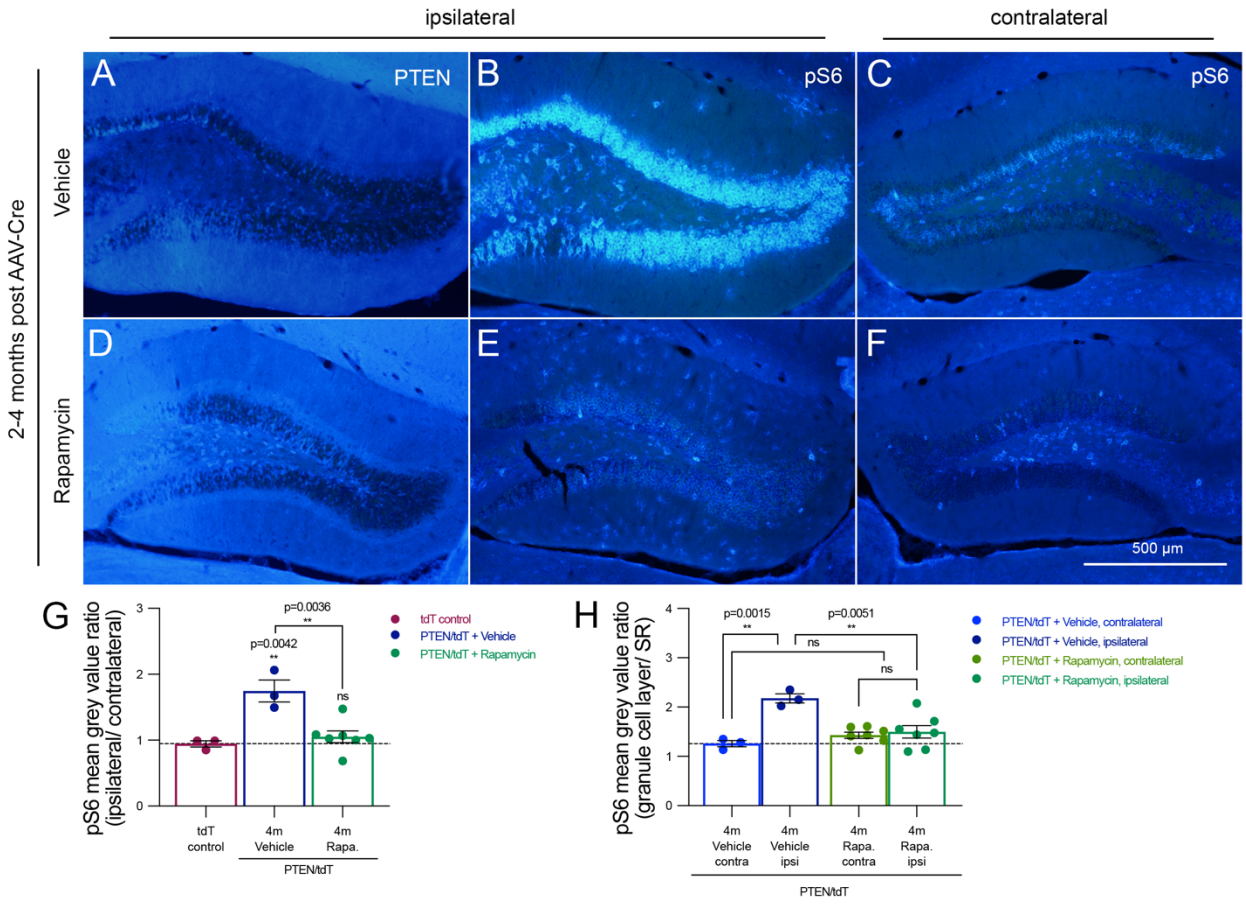
ipsilateral
contralateral
2-4 months post AAV-Cre
Vehicle
Rapamycin
A
PTEN
B
pS6
C
pS6
D
E
F
500 µm
G
pS6 mean grey value ratio (ipsilateral/ contralateral)
p=0.0042
**
p=0.0036
**
ns
tdT control
PTEN/tdT + Vehicle
PTEN/tdT + Rapamycin
tdT control
4m Vehicle
4m Rapa.
PTEN/tdT
H
pS6 mean grey value ratio (granule cell layer/ SR)
p=0.0015
**
p=0.0051
**
ns
ns
PTEN/tdT + Vehicle, contralateral
PTEN/tdT + Vehicle, ipsilateral
PTEN/tdT + Rapamycin, contralateral
PTEN/tdT + Rapamycin, ipsilateral
4m Vehicle contra
4m Vehicle ipsi
4m Rapa. contra
4m Rapa. ipsi
PTEN/tdT

Figure 4.4. Delayed rapamycin administration prevents further phosphorylation of ribosomal protein S6 following PTEN deletion. A) Maintenance of PTEN deletion in transduced granule cells of a vehicle-treated, PTEN/tdT mouse at 4 months after AAV-Cre injection. B) Prolonged phosphorylation of ribosomal protein S6 in PTEN deleted granule cells in the same mouse. C) pS6 immunoreactivity in the contralateral dentate gyrus. D) Area of PTEN deletion in a PTEN/tdT mouse treated with rapamycin from 2-4 months after AAV-Cre injection. E) Reduced S6 phosphorylation in the area of PTEN deletion following delayed rapamycin administration in the same mouse. F) pS6 labeling in the contralateral dentate gyrus. G) Quantification of pS6 fluorescence intensity represented as a ratio of the ipsilateral and contralateral granule cell layers at 4 months after AAV-Cre injection. Sidak's post hoc comparisons: PTEN/tdT, vehicle-treated mice vs. tdT controls ($p=0.0042$) and PTEN/tdT, vehicle-treated mice vs PTEN/tdT, rapamycin-treated mice ($p=0.0036$). H) Ratio of pS6 fluorescence between the granule cell layer within each hemisphere with the stratum radiatum of the contralateral hippocampus in PTEN/tdT mice. Sidak's post hoc comparisons: ipsilateral vs. contralateral, vehicle-treated ($p=0.0015$), ipsilateral, vehicle-treated vs. ipsilateral, rapamycin-treated ($p=0.0051$), ipsilateral, vehicle-treated vs. contralateral, rapamycin-treated ($p=0.0022$). Note that the horizontal dotted lines in G and H mark the average fluorescence in the ipsilateral dentate gyrus of tdT controls for each ratio.

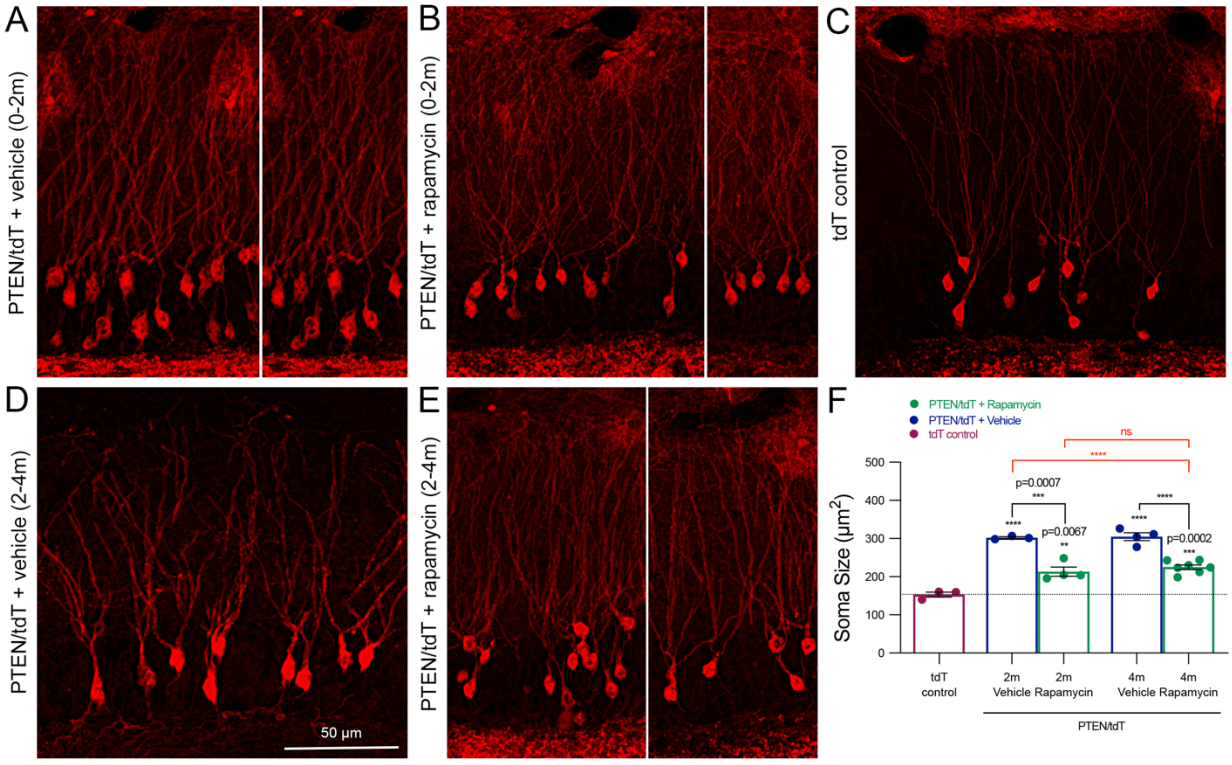
A
PTEN/tdT + vehicle (0-2m)
B
PTEN/tdT + rapamycin (0-2m)
C
tdT control
D
PTEN/tdT + vehicle (2-4m)
50 µm
E
PTEN/tdT + rapamycin (2-4m)
F
PTEN/tdT + Rapamycin
PTEN/tdT + Vehicle
tdT control
Soma Size (µm²)
500
400
300
200
100
0
ns
****
p=0.0007
***
p=0.0067
**
p=0.0002
***
tdT control
2m Vehicle
2m Rapamycin
4m Vehicle
4m Rapamycin
PTEN/tdT

Figure 4.5. Rapamycin administration prevents and reverses growth of mature granule cells after vector-mediated PTEN deletion. A) Representative images of tdTomato-expressing, PTEN-deleted granule cells from two PTEN/tdT mice treated with vehicle from 0 to 2 months after AAV-Cre injection. B) tdTomato expressing granule cells from PTEN/tdT mice treated during the same period with rapamycin showing prevention of somata growth. C) Transduced, PTEN-expressing granule cells from a tdT control mouse. D) Representative images of PTEN deleted granule cells from a mouse treated with vehicle from 2 to 4 months after AAV-Cre injection. E) PTEN deleted granule cells from two PTEN/tdT mice treated with rapamycin from 2 to 4 months after PTEN deletion. F) Soma cross sectional area from 3-7 experimental animals (30 neurons per mouse) treated with rapamycin or vehicle during acute and delayed periods after AAV-Cre injection. The horizontal dotted line marks the average soma size of tdT control mice. Sidak's multiple comparisons test for tdT vs. 2-month PTEN/tdT mice (values in black directly above bars): tdT controls vs. 2-month vehicle-treated ($p<0.0001$), tdT controls vs. 2-month rapamycin-treated ($p=0.0067$), and 2-month vehicle-treated vs. 2-month rapamycin-treated ($p=0.0007$). Sidak's multiple comparisons test for tdT vs. 4-month PTEN/tdT mice (values in black directly above bars): tdT controls vs. 4-month vehicle-treated ($p<0.0001$), tdT controls vs. 4-month rapamycin-treated ($p=0.0002$), and 4-month vehicle-treated vs. 4-month rapamycin-treated ($p=0.0007$). Sidak's comparisons for PTEN/tdT mice (red brackets joining individual bars): 2-month vehicle-treated vs. 4-month rapamycin-treated ($p=0.0001$).

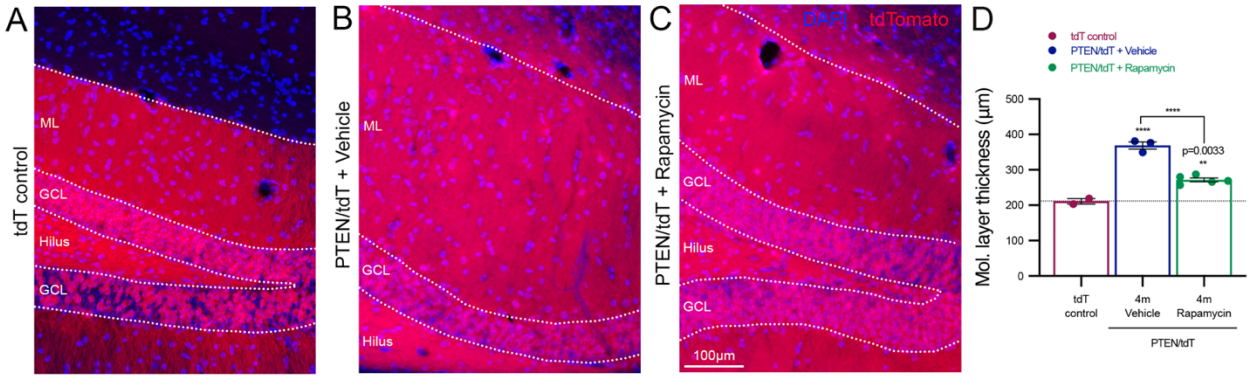
A
tdT control
ML
GCL
Hilus
GCL
B
PTEN/tdT + Vehicle
ML
GCL
Hilus
C
DAPI
tdTomato
PTEN/tdT + Rapamycin
ML
GCL
Hilus
GCL
100μm
D
tdT control
PTEN/tdT + Vehicle
PTEN/tdT + Rapamycin
Mol. layer thickness (μm)
500
400
300
200
100
0
****
****
p=0.0033
**
tdT control
4m Vehicle
4m Rapamycin
PTEN/tdT

Figure 4.6. Delayed rapamycin administration prevents lengthening of apical dendrites and increased molecular layer thickness following PTEN deletion in PTEN/tdT mice. A) Transduced molecular layer from a tdT control mouse. B) Representative image of a vehicle-treated, PTEN/tdT mouse at the core of transduction showing increased molecular layer thickness following PTEN deletion. C) tdT-labeled molecular layer in a PTEN/tdT mouse treated with rapamycin from 2-4 months after PTEN deletion. D) Quantification of molecular layer thickness in the dorsal blade of PTEN/tdT vehicle- and rapamycin-treated mice compared to tdT non-treated controls. The horizontal dotted line marks the average molecular layer thickness of tdT control mice. Sidak's post hoc comparisons: vehicle-treated PTEN/tdT mice vs. tdT non-treated controls ($p<0.0001$), vehicle-treated PTEN/tdT vs. rapamycin-treated PTEN/tdT mice ($p<0.0001$), and rapamycin-treated PTEN/tdT mice vs. tdT controls ($p=0.0033$).

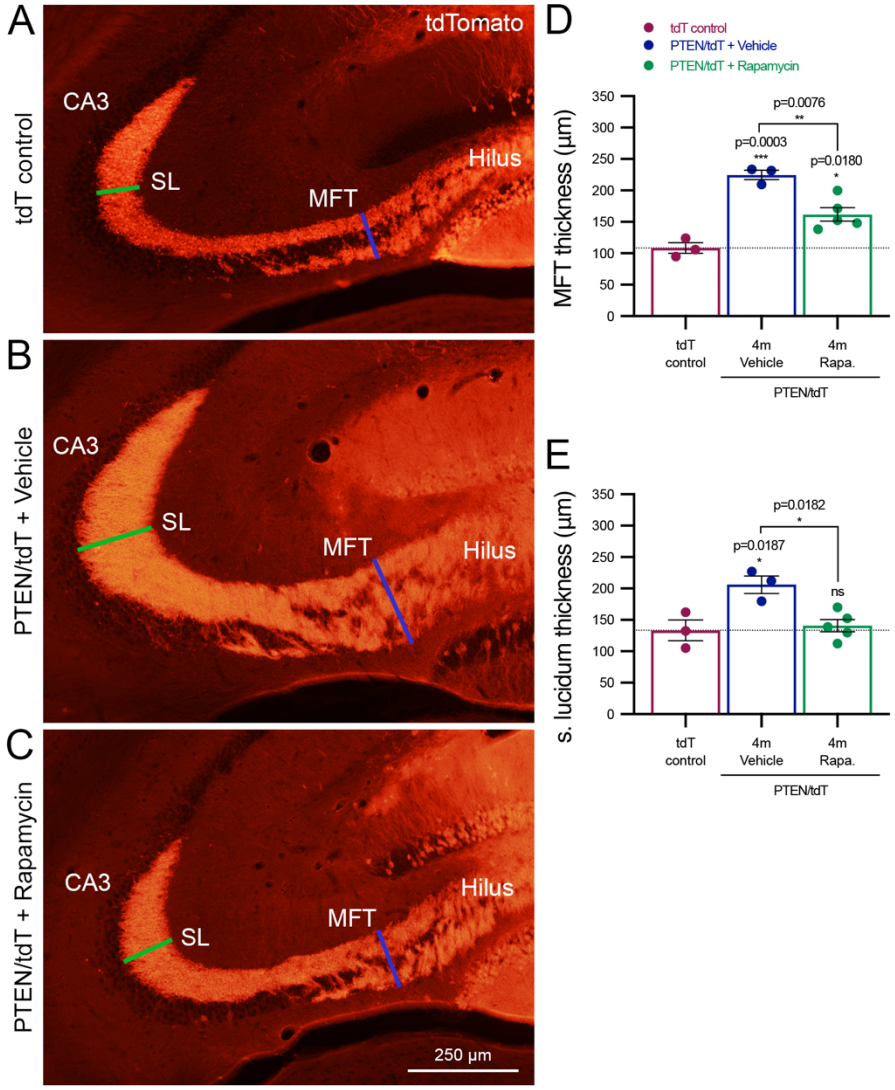
A
tdTomato
tdT control
CA3
SL
MFT
Hilus
B
PTEN/tdT + Vehicle
CA3
SL
MFT
Hilus
C
PTEN/tdT + Rapamycin
CA3
SL
MFT
Hilus
250 µm
D
tdT control
PTEN/tdT + Vehicle
PTEN/tdT + Rapamycin
MFT thickness (µm)
p=0.0076
**
p=0.0003
***
p=0.0180
*
tdT control
4m Vehicle
4m Rapa.
PTEN/tdT
E
s. lucidum thickness (µm)
p=0.0182
*
p=0.0187
*
ns
tdT control
4m Vehicle
4m Rapa.
PTEN/tdT

Figure 4.7. Prevention of axonal enlargement with delayed rapamycin administration following PTEN deletion in PTEN/tdT mice. A) Transduced mossy fiber axons expressing tdTomato from a tdT control mouse. B) Enlarged mossy fiber axons from a PTEN/tdT mouse at 4 months after PTEN deletion. C) Representative mossy fiber axons from a PTEN/tdT mouse at 4 months after AAV-Cre injection following delayed rapamycin administration. D) Quantification of mossy fiber tract thickness (blue line) in the ipsilateral dentate gyrus of each group. Sidak's post hoc comparisons: vehicle-treated PTEN/tdT mice vs. tdT non-treated controls ($p=0.0003$), vehicle-treated PTEN/tdT vs. rapamycin-treated PTEN/tdT mice ($p=0.0076$), and rapamycin-treated PTEN/tdT mice vs. tdT controls ($p=0.0180$). E) Quantification of mossy fiber tract thickness within the stratum lucidum of the CA3 (green line) in the same animals. Sidak's post hoc comparisons: vehicle-treated PTEN/tdT mice vs. tdT non-treated controls ($p=0.0187$) and vehicle-treated PTEN/tdT vs. rapamycin-treated PTEN/tdT mice ($p=0.0182$). Note, the horizontal dotted lines in D and E mark the average mossy fiber axon thickness from tdT control mice at each location.

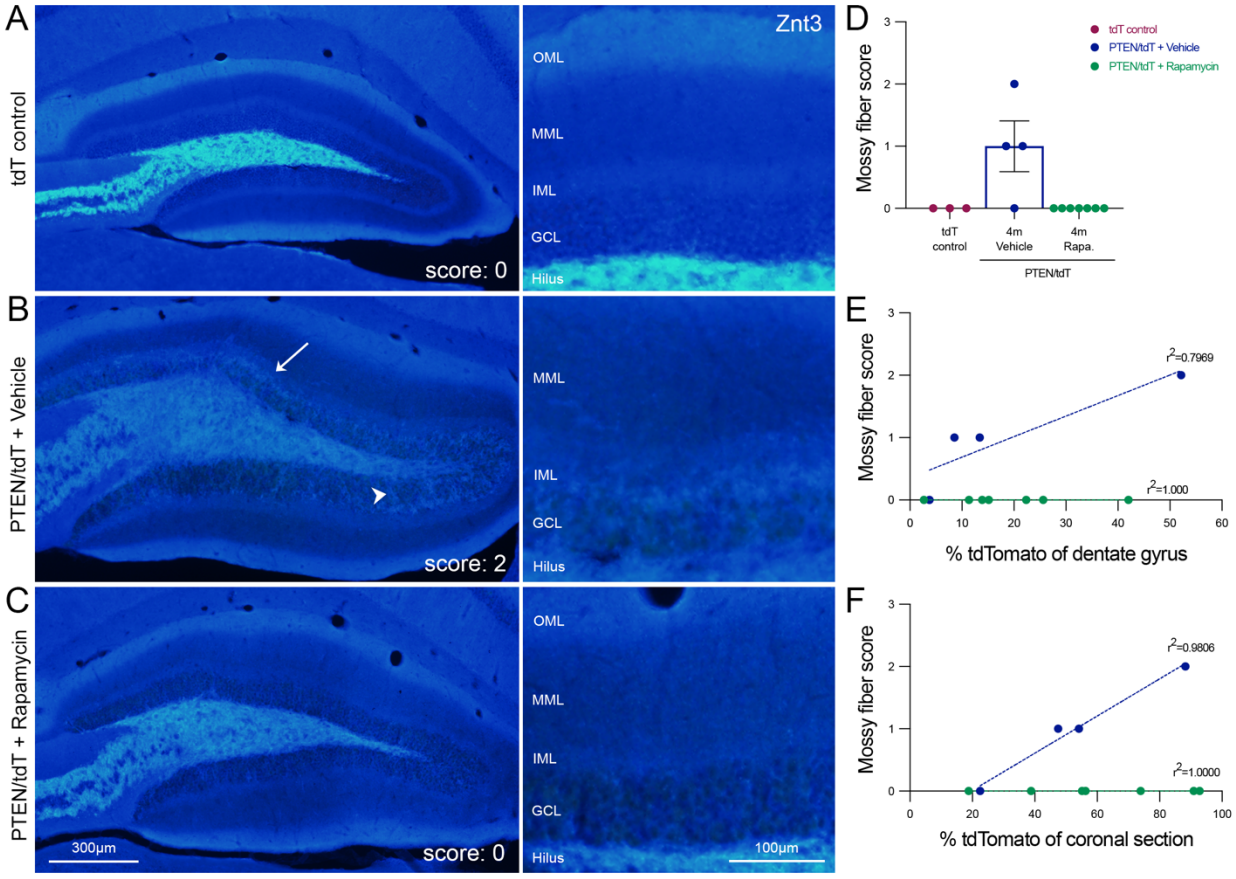
A
tdT control
Znt3
OML
MML
IML
GCL
Hilus
score: 0
B
PTEN/tdT + Vehicle
MML
IML
GCL
Hilus
score: 2
C
PTEN/tdT + Rapamycin
OML
MML
IML
GCL
Hilus
300μm
score: 0
100μm
D
Mossy fiber score
tdT control
PTEN/tdT + Vehicle
PTEN/tdT + Rapamycin
tdT control
4m Vehicle
4m Rapa.
PTEN/tdT
E
Mossy fiber score
r2=0.7969
r2=1.000
% tdTomato of dentate gyrus
F
Mossy fiber score
r2=0.9806
r2=1.0000
% tdTomato of coronal section

Figure 4.8. Rapamycin administration reduces mossy fiber sprouting in areas of dense PTEN deletion. A) Mossy fiber labeling (Znt3) on the side ipsilateral to AAV-Cre injection in a tdT control mouse. B) Mossy fiber axons in the dentate gyrus of a PTEN-deleted, PTEN/tdT mouse at 4 months post AAV-Cre injection showing Znt3 labeling in the granule cell layer (ventral blade, arrowhead) and in the inner molecular layer of the dorsal blade (arrow) resulting in a score of 2. C) Lack of mossy fiber labeling in the granule cell layer and inner molecular layer of a PTEN/tdT mouse treated with rapamycin from 2 to 4 months post AAV-Cre injection. Note that higher magnification images from each animal are shown in the right column. D) Mossy fiber score in the transduced dentate gyrus of tdT controls and PTEN/tdT mice treated with either vehicle or rapamycin. E) Correlation between percent transduction of the ipsilateral dentate gyrus and mossy fiber score in PTEN deleted animals following treatment. F) Correlation between percent transduction at the core of PTEN deletion and mossy fiber score. Scoring scale: 0 - little to no Znt3 labeling in GCL, 1 - mild Znt3 labeling in GCL, 2 - moderate Znt3 labeling in GCL and mild labeling in IML, 3 - dense Znt3 labeling in IML.

REFERENCES

Arafa, S. R., LaSarge, C. L., Pun, R. Y. K., Khademi, S., & Danzer, S. C. (2019, Jan). Self-reinforcing effects of mTOR hyperactive neurons on dendritic growth. *Exp Neurol, 311*, 125-134. https://doi.org/10.1016/j.expneurol.2018.09.019

Backman, S. A., Stambolic, V., Suzuki, A., Haight, J., Elia, A., Pretorius, J., Tsao, M. S., Shannon, P., Bolon, B., Ivy, G. O., & Mak, T. W. (2001, Dec). Deletion of Pten in mouse brain causes seizures, ataxia and defects in soma size resembling Lhermitte-Duclos disease. *Nat Genet, 29*(4), 396-403. https://doi.org/10.1038/ng782

Cardamone, M., Flanagan, D., Mowat, D., Kennedy, S. E., Chopra, M., & Lawson, J. A. (2014, May). Mammalian target of rapamycin inhibitors for intractable epilepsy and subependymal giant cell astrocytomas in tuberous sclerosis complex. *J Pediatr, 164*(5), 1195-1200. https://doi.org/10.1016/j.jpeds.2013.12.053

Conti, S., Condo, M., Posar, A., Mari, F., Resta, N., Renieri, A., Neri, I., Patrizi, A., & Parmeggiani, A. (2012, Mar). Phosphatase and tensin homolog (PTEN) gene mutations and autism: literature review and a case report of a patient with Cowden syndrome, autistic disorder, and epilepsy. *J Child Neurol, 27*(3), 392-397. https://doi.org/10.1177/0883073811420296

Fukumura, S., Watanabe, T., Takayama, R., Minagawa, K., & Tsutsumi, H. (2015, Aug). Everolimus Treatment for an Early Infantile Subependymal Giant Cell Astrocytoma With Tuberous Sclerosis Complex. *J Child Neurol, 30*(9), 1192-1195. https://doi.org/10.1177/0883073814544703

Gallent, E. A., & Steward, O. (2018, May). Neuronal PTEN deletion in adult cortical neurons triggers progressive growth of cell bodies, dendrites, and axons. *Exp Neurol, 303*, 12-28. https://doi.org/10.1016/j.expneurol.2018.01.005

Getz, S. A., DeSpenza, T., Jr., Li, M., & Luikart, B. W. (2016, Sep). Rapamycin prevents, but does not reverse, aberrant migration in Pten knockout neurons. *Neurobiol Dis, 93*, 12-20. https://doi.org/10.1016/j.nbd.2016.03.010

Hunt, R. F., Scheff, S. W., & Smith, B. N. (2009, Feb). Posttraumatic epilepsy after controlled cortical impact injury in mice. *Exp Neurol, 215*(2), 243-252. https://doi.org/10.1016/j.expneurol.2008.10.005

Jansen, L. A., Mirzaa, G. M., Ishak, G. E., O'Roak, B. J., Hiatt, J. B., Roden, W. H., Gunter, S. A., Christian, S. L., Collins, S., Adams, C., Riviere, J. B., St-Onge, J., Ojemann, J. G., Shendure, J., Hevner, R. F., & Dobyns, W. B. (2015, Jun). PI3K/AKT pathway mutations cause a spectrum of brain malformations from megalencephaly to focal cortical dysplasia. *Brain, 138*(Pt 6), 1613-1628. https://doi.org/10.1093/brain/awv045

Kazdoba, T. M., Sunnen, C. N., Crowell, B., Lee, G. H., Anderson, A. E., & D'Arcangelo, G. (2012). Development and characterization of NEX- Pten, a novel forebrain excitatory neuron-specific knockout mouse. *Dev Neurosci, 34*(2-3), 198-209. https://doi.org/10.1159/000337229

Krueger, D. A., Wilfong, A. A., Holland-Bouley, K., Anderson, A. E., Agricola, K., Tudor, C., Mays, M., Lopez, C. M., Kim, M. O., & Franz, D. N. (2013, Nov). Everolimus treatment of refractory epilepsy in tuberous sclerosis complex. *Ann Neurol, 74*(5), 679-687. https://doi.org/10.1002/ana.23960

Kuki, I., Kawawaki, H., Okazaki, S., Ehara, E., Yoshida, Y., Kunihiro, N., & Matsusaka, Y. (2018, May). Efficacy and safety of everolimus in patients younger than 12months with congenital subependymal giant cell astrocytoma. *Brain Dev, 40*(5), 415-420. https://doi.org/10.1016/j.braindev.2018.01.001

Kwon, C. H., Luikart, B. W., Powell, C. M., Zhou, J., Matheny, S. A., Zhang, W., Li, Y., Baker, S. J., & Parada, L. F. (2006, May 4). Pten regulates neuronal arborization and social interaction in mice. *Neuron, 50*(3), 377-388. https://doi.org/10.1016/j.neuron.2006.03.023

Kwon, C. H., Zhu, X., Zhang, J., & Baker, S. J. (2003, Oct 28). mTor is required for hypertrophy of Pten-deficient neuronal soma in vivo. *Proc Natl Acad Sci U S A, 100*(22), 12923-12928. https://doi.org/10.1073/pnas.2132711100

Kwon, C. H., Zhu, X., Zhang, J., Knoop, L. L., Tharp, R., Smeyne, R. J., Eberhart, C. G., Burger, P. C., & Baker, S. J. (2001, Dec). Pten regulates neuronal soma size: a mouse model of Lhermitte-Duclos disease. *Nat Genet, 29*(4), 404-411. https://doi.org/10.1038/ng781

LaSarge, C. L., Pun, R. Y., Muntifering, M. B., & Danzer, S. C. (2016, Dec). Disrupted hippocampal network physiology following PTEN deletion from newborn dentate granule cells. *Neurobiol Dis, 96*, 105-114. https://doi.org/10.1016/j.nbd.2016.09.004

LaSarge, C. L., Santos, V. R., & Danzer, S. C. (2015, Mar). PTEN deletion from adult-generated dentate granule cells disrupts granule cell mossy fiber axon structure. *Neurobiol Dis, 75*, 142-150. https://doi.org/10.1016/j.nbd.2014.12.029

Ljungberg, M. C., Sunnen, C. N., Lugo, J. N., Anderson, A. E., & D'Arcangelo, G. (2009, Jul-Aug). Rapamycin suppresses seizures and neuronal hypertrophy in a mouse model of cortical dysplasia. *Dis Model Mech, 2*(7-8), 389-398. https://doi.org/10.1242/dmm.002386

Lugo, J. N., Smith, G. D., Arbuckle, E. P., White, J., Holley, A. J., Floruta, C. M., Ahmed, N., Gomez, M. C., & Okonkwo, O. (2014). Deletion of PTEN produces autism-like behavioral deficits and alterations in synaptic proteins. *Front Mol Neurosci, 7*, 27. https://doi.org/10.3389/fnmol.2014.00027

Luikart, B. W., Schnell, E., Washburn, E. K., Bensen, A. L., Tovar, K. R., & Westbrook, G. L. (2011, Mar 16). Pten knockdown in vivo increases excitatory drive onto dentate granule cells. *J Neurosci, 31*(11), 4345-4354. https://doi.org/10.1523/JNEUROSCI.0061-11.2011

Matsushita, Y., Sakai, Y., Shimmura, M., Shigeto, H., Nishio, M., Akamine, S., Sanefuji, M., Ishizaki, Y., Torisu, H., Nakabeppu, Y., Suzuki, A., Takada, H., & Hara, T. (2016, Mar 10). Hyperactive mTOR signals in the proopiomelanocortin-expressing hippocampal neurons cause age-dependent epilepsy and premature death in mice. *Sci Rep, 6*, 22991. https://doi.org/10.1038/srep22991

Pun, R. Y., Rolle, I. J., Lasarge, C. L., Hosford, B. E., Rosen, J. M., Uhl, J. D., Schmeltzer, S. N., Faulkner, C., Bronson, S. L., Murphy, B. L., Richards, D. A., Holland, K. D., & Danzer, S. C. (2012, Sep 20). Excessive activation of mTOR in postnatally generated granule cells is sufficient to cause epilepsy. *Neuron, 75*(6), 1022-1034. https://doi.org/10.1016/j.neuron.2012.08.002

Santos, V. R., Pun, R. Y. K., Arafa, S. R., LaSarge, C. L., Rowley, S., Khademi, S., Bouley, T., Holland, K. D., Garcia-Cairasco, N., & Danzer, S. C. (2017, Dec). PTEN deletion increases hippocampal granule cell excitability in male and female mice. *Neurobiol Dis, 108*, 339-351. https://doi.org/10.1016/j.nbd.2017.08.014

Skelton, P. D., Frazel, P. W., Lee, D., Suh, H., & Luikart, B. W. (2019, Nov). Pten loss results in inappropriate excitatory connectivity. *Mol Psychiatry, 24*(11), 1627-1640. https://doi.org/10.1038/s41380-019-0412-6

Steward, O., Coulibay, A., Metcalfe, M., Yonan, J. M., & Yee, K. M. (2019). AAVshRNA-mediated PTEN knockdown in adult neurons attenuates activity-dependent immediate early gene induction. *Exp Neurol*. https://doi.org/https://doi.org/10.1016/j.expneurol.2019.113098

Sunnen, C. N., Brewster, A. L., Lugo, J. N., Vanegas, F., Turcios, E., Mukhi, S., Parghi, D., D'Arcangelo, G., & Anderson, A. E. (2011, Nov). Inhibition of the mammalian target of rapamycin blocks epilepsy progression in NS-Pten conditional knockout mice. *Epilepsia, 52*(11), 2065-2075. https://doi.org/10.1111/j.1528-1167.2011.03280.x

Switon, K., Kotulska, K., Janusz-Kaminska, A., Zmorzynska, J., & Jaworski, J. (2017, Jan 26). Molecular neurobiology of mTOR. *Neuroscience, 341*, 112-153. https://doi.org/10.1016/j.neuroscience.2016.11.017

Tilot, A. K., Frazier, T. W., 2nd, & Eng, C. (2015, Jul). Balancing Proliferation and Connectivity in PTEN-associated Autism Spectrum Disorder. *Neurotherapeutics, 12*(3), 609-619. https://doi.org/10.1007/s13311-015-0356-8

Tsang, C. K., Qi, H., Liu, L. F., & Zheng, X. F. (2007, Feb). Targeting mammalian target of rapamycin (mTOR) for health and diseases. *Drug Discov Today, 12*(3-4), 112-124. https://doi.org/10.1016/j.drudis.2006.12.008

Williams, M. R., DeSpenza, T., Jr., Li, M., Gulledge, A. T., & Luikart, B. W. (2015, Jan 21). Hyperactivity of newborn Pten knock-out neurons results from increased excitatory synaptic drive. *J Neurosci, 35*(3), 943-959. https://doi.org/10.1523/JNEUROSCI.3144-14.2015

Yang, H., Rudge, D. G., Koos, J. D., Vaidialingam, B., Yang, H. J., & Pavletich, N. P. (2013, May 9). mTOR kinase structure, mechanism and regulation. *Nature, 497*(7448), 217-223. https://doi.org/10.1038/nature12122

Zahedi Abghari, F., Moradi, Y., & Akouchekian, M. (2019). PTEN gene mutations in patients with macrocephaly and classic autism: A systematic review. *Med J Islam Repub Iran, 33*, 10. https://doi.org/10.34171/mjiri.33.10

Zhou, J., Blundell, J., Ogawa, S., Kwon, C. H., Zhang, W., Sinton, C., Powell, C. M., & Parada, L. F. (2009, Feb 11). Pharmacological inhibition of mTORC1 suppresses anatomical, cellular, and behavioral abnormalities in neural-specific Pten knock-out mice. *J Neurosci, 29*(6), 1773-1783. https://doi.org/10.1523/JNEUROSCI.5685-08.2009

CHAPTER 5:

PTEN deletion in the adult dentate gyrus results in the development of a seizure prone circuit

ABSTRACT

Previous studies have reported that embryonic and early postnatal promotor-driven deletion of the phosphatase and tensin homolog (PTEN) gene results in neuronal hypertrophy, aberrant hyperexcitable circuitry, seizures, and high mortality rates, possibly due to sudden death during seizures. We previously documented that focal, vector-mediated PTEN deletion in mature granule cells of the adult dentate gyrus triggers dramatic growth of cell bodies, dendrites, and axons, in a manner reminiscent of what is seen with early postnatal PTEN deletion. Here, we assess the functional consequences of PTEN deletion in the adult dentate gyrus, specifically, whether focal PTEN deletion leads to the development of spontaneous seizures. PTEN deletion was accomplished by injecting AAV-Cre either bilaterally or unilaterally into the dentate gyrus of double transgenic PTEN-floxed, ROSA reporter mice. Recording electrodes were then implanted in the hippocampus to record continuous EEG with simultaneous video recordings in the home cage. Continuous video-EEG monitoring revealed onset of spontaneous electrographic and behavioral seizures beginning after 2 months post-AAV-Cre injection. Seizures occurred in the majority of mice with either unilateral or bilateral PTEN deletion, and some mice died during the seizures. There was no obvious hippocampal neuron death as is seen with excitotoxin-induced

epileptogenesis but supra-granular mossy fibers were seen in some mice. Our findings reveal that focal unilateral deletion of PTEN in the dentate gyrus in fully mature mice is sufficient to lead to the progressive development of an epileptic circuit that eventually generates generalized spontaneous seizures. This presents a new model for studies of adult onset epileptogenesis.

INTRODUCTION

Mechanistic target of rapamycin (mTOR) is a serine-threonine kinase involved in many important features of cellular function, including cellular growth and proliferation during development. Mutations in genes involved in mTOR signaling during development, termed TORopathies, have been implicated in neurological disorders, including epilepsy, autism, and intellectual disability in humans (Switon et al., 2017). Increasing investigation into developmental animal models has strengthened the link between disruptions of mTOR signaling and physiological dysfunction. Mutations of the phosphatase and tensin homolog (PTEN) gene, an important upstream negative regulator of the mTOR pathway, are one cause of TORopathies, motivating studies of consequences of such mutations in animal models.

Previous studies investigating the consequences of embryonic and early postnatal PTEN deletion have largely focused on alterations to neuronal morphology, connectivity, and function in the hippocampus due to its accepted role in epileptogenesis. Embryonic PTEN deletion has been reported to cause brain and neuronal hypertrophy accompanied by

progressive seizure severity and early mortality (Backman et al., 2001; Kwon et al., 2003; Kwon et al., 2001; Ljungberg et al., 2009; Sunnen et al., 2011). Early postnatal promoter-driven PTEN deletion models have expanded on this, characterizing alterations to neuronal morphology in the dentate gyrus, including enlarged granule cell bodies, increased dendrite complexity, and aberrant expansion of mossy fiber axon connectivity (Arafa et al., 2019; LaSarge et al., 2015; Matsushita et al., 2016; Pun et al., 2012). Physiological consequences of such morphological changes have been reported to include the formation of hyperexcitable, pro-epileptic networks (LaSarge et al., 2016; Luikart et al., 2011; Santos et al., 2017; Skelton et al., 2019; Takeuchi et al., 2013; Williams et al., 2015).

Our lab has reported that both AAV-Cre mediated PTEN deletion in PTEN-floxed adult mice (Gallent & Steward, 2018) and AAV-shRNA mediated PTEN knockdown in adult rats (Steward et al., 2019) results in a striking growth phenotype in mature cortical neurons. More recently, we have expanded our results to include alterations to neuronal morphology and connectivity in the mature dentate gyrus of adult mice. Injections of AAV-Cre into the dentate gyrus of adult PTEN-floxed mice resulted focal PTEN deletion, triggering the enlargement of granule cell bodies, elongation of dendrites, robust formation of new synapses on elongated dendritic segments, and expansion of mossy fiber terminal fields in target areas (Chapter 3). In this collection of studies, casual observations did not reveal spontaneous behavioral seizures out to 6 months following PTEN deletion, and there were no sudden deaths that might have been due to seizures. Importantly, however, abnormal physiological activity including electrographic seizures, cannot be excluded without continuous recording and monitoring.

The present study assessed the functional consequences of focal PTEN deletion in the adult dentate gyrus using continuous video-EEG. Here we show that bilateral or unilateral vector-mediated PTEN deletion in PTEN-floxed, ROSA reporter mice leads to the development of spontaneous seizures beginning around 2 months after AAV-Cre injection, with three verified example of sudden death during a seizure. Our model of unilateral and focal PTEN deletion, therefore, provides a unique opportunity to establish a novel model of adult-onset temporal lobe epilepsy (TLE) in which the pathophysiology is initiated by a localized focus within the hippocampus.

MATERIALS AND METHODS

Experimental mice

Experiments involved four transgenic strains of mice developed in our local breeding colony. The first strain was generated by crossing PTEN-floxed mice containing lox-p flanked exon 5 of the PTEN gene (RRID: IMSR_JAX:004597) with ROSA26tdTomato reporter mice having a lox-P flanked STOP cassette in the Rosa locus upstream of a tandem dimer tomato (tdT) fluorescent protein sequence (RRID: IMSR_JAX:007905). This double transgenic strain is designated $PTEN^{f/f}/Rosa^{tdTomato}$. Control mice ($Rosa^{tdTomato}$) only contain the floxed stop cassette before the tdT sequence. All studies involved mice that were homozygous at the transgenic loci. As a way to label individual neurons and their dendrites without special staining, we created two other lines by crossing $PTEN^{f/f}/Rosa^{tdTomato}$ and control mice ($Rosa^{tdTomato}$) with Thy1-eYFP mice, originally purchased from the Jackson Labs, to generate

mice that were homozygous PTEN$^{f/f}$/Rosa^{tdTomato}, and heterozygous for Thy1- YFP. For simplicity, these mice will be referred to as PTEN/tdT and tdT, regardless of their Thy1 expression.

Surgical procedure: AAV-Cre injections into the dentate gyrus

All experimental procedures were approved by the Institutional Animal Care and Use Committee (IACUC) at the University of California, Irvine. Studies involved adult mice (at least 2 months of age at the time of AAV-Cre injection). For all surgical procedures, mice were anesthetized with Isoflurane (2-2.5%). Anesthetized mice were placed in a stereotaxic device. Eyes were covered with Vaseline and the skin above the incision site was shaved and disinfected with Betadine. A scalp incision was made to expose the skull. A small cranial window was created above the injection site. Using a 10µl Hamilton syringe with a pulled glass pipette tip, either a single unilateral or bilateral injection of AAV2-Cre (Vector Bio Labs, 7011) or AAV2-GFP (Vector Bio Labs, 7004) was made at +/-1.3mm lateral and +2.2mm anterior to lambda at a depth of -1.6mm from the cortical surface. Each injection was 0.6µl in volume ($1x10^{12}$ GC/ml in 1xPBS with 5% glycerol) and was performed over 4 minutes. The glass pipette was left in place for another 2 minutes before removal. After injection, the bone flap was replaced over the cranial window and the incision site was sutured. Following completion of the surgery, mice were allowed to recover in a cage placed on top of a 37°C heating pad. Surgeries were performed in four separate iterations, termed Squads, three injected with AAV-Cre and a fourth injected with AAV-GFP (Table 5.1).

Surgical procedure: Bilateral and unilateral intrahippocampal EEG probe placement

At 4-6 weeks post AAV-Cre injection, mice underwent a second procedure for placement of either bilateral or unilateral intrahippocampal electrodes. Mice were anesthetized with Isoflurane (2-2.5%) and placed in a stereotaxic device. Eyes were covered with Vaseline, scalp hair was removed with Nair, and skin was disinfected with Betadine and ethanol. A scalp incision was made to expose the skull and the skull was cleaned and dried with a 30% hydrogen peroxide solution. Two burr holes were placed in the skull above the hippocampus in each hemisphere at +/-1.6mm lateral and -1.9 posterior to bregma. Twisted wire electrodes were placed at a depth of -3.0 to -2.2mm below the brain surface (P Technologies, E363/2-2TW/SPC). For mice with a unilateral EEG probe, the electrode was placed into the right hippocampus, contralateral to AAV-Cre injection. Another 2 burr holes were created above on the left side of the cerebellum and right frontal cortex for placement of ground screw electrodes (P technologies, E363/20). Each electrode was then placed into a 6-channel pedestal (P Technologies, MS363). Electrodes, screws, pedestals, and wiring were held in place using a combination of cyanoacrylate and dental cement for creation of a head cap. Following completion of the surgery, mice were allowed to recover in a cage placed on a 37°C heating pad. Information regarding animal numbers, attrition and exclusions are listed in Table 5.1.

Continuous video EEG recordings

At 6-8 weeks post AAV-Cre injection and 1-2 weeks following electrode placement, mice were transferred into plexiglass cages and attached to a commutator to allow for free

movement during video-EEG recording. Continuous recordings and videos were collected using the Lab Chart EEG analysis software (versions 7 and 8, AD Instruments). Bilateral recordings were made in mice that received bilateral electrodes. In mice that received unilateral injections and unilateral electrodes, recordings were made on the side contralateral to the injection. Information on recording durations for each Squad of mice is listed in Tables 5.2-5.5.

Rapamycin administration

A pilot study was carried out in a small subset of mice in Squads 1 and 2 (n=4) to explore whether seizures depended on continuous activation of mTOR. For this, mice received injections of rapamycin (6mg/kg i.p., LC laboratories) for variable durations after AAV-Cre injection. Rapamycin administration did not produce any notable effect on seizure frequency during the administration period in the small subset of mice assessed (not shown).

EEG analysis and scoring

Scoring of EEG recordings was done blind to animal group. Recordings were scanned for 3 main features to identify a seizure: 1) seizure begins from a baseline EEG, 2) seizure begins with progressive increases in wave amplitude, and 3) seizure activity is followed by a period of post-ictal depression characterized by a dramatic decrease in EEG amplitude. Both ipsilateral and contralateral EEG recordings were scored, when available. Data are represented as cumulative number of seizures for each individual animal over time.

Tissue collection and histology

At designated endpoints (Tables 5.2-5.5), mice received intraperitoneal injections of Fatal Plus and were intracardially perfused with 4% paraformaldehyde in phosphate buffer (PFA). Brains were dissected and post-fixed in 4% PFA for 48 hours before being cryoprotected in 27% sucrose and frozen in Tissue-Tek O.C.T. compound. Brains were then cryosectioned into 30µm sections and sections were stored in 1xPBS with 0.1% NaN_3 until processed for immunohistochemistry. For mice that were found dead, brains were drop-fixed in 4% PFA and then prepared as above. The area of transduction was visualized by tdTomato expression in $PTEN^{f/f}/Rosa^{tdTomato}$ and ($Rosa^{tdTomato}$) mice that received AAV-Cre and GFP expression in mice that received AAV-GFP.

Collections of sections spaced at 360µm intervals were processed for various histological markers. For immunohistochemistry (IHC), sections were washed in 1xTBS (100mM Tris, pH 7.4 and 150mM NaCl) then quenched for endogenous peroxidase activity by incubation in 3% H_2O_2 for 15 minutes. Sections were then washed in 1xTBS and blocked in blocking buffer (1xTBS, 0.3% Triton X-100, 5% NDS) for 2 hours at room temperature. Sections were then incubated overnight at room temperature in buffer containing primary antibodies for rabbit anti-PTEN (1:250, Cell Signaling Technology 9188, RRID: AB_2253290), rabbit anti-pS6 Ser235/236 (1:250, Cell Signaling Technology 4858, RRID: AB_916156), rabbit anti-Znt3 (1:1500, Millipore ABN994) and rabbit anti-cFos (1:1000, Millipore ABE457, RRID: AB_2631318). Sections were then washed in 1xTBS, followed by a 2-hour incubation in buffer containing biotinylated donkey anti-rabbit IgG (1:250, Jackson ImmunoResearch, 711-065-152), then washed again. Visualization was accomplished through incubation in

ABC reagent (Vectastain Elite kit, catalog #PK-6100; Vector Laboratories) and CARD amplification with Tyramide-FITC or AMCA. Sections stained for rabbit anti-GFP (1:1500, Novus NB600-308, RRID:10003058) were visualized using Alexa fluor-488 (1:250, Invitrogen A21206). All sections were then mounted on 0.5% gelatin coated slides and counterstained with Hoechst (1µg/mL).

Extent of transduction of the dentate gyrus

To determine the percent area of transduction through the dentate gyrus, sections spaced 360µm apart (8-10 sections per mouse) were assessed for percentage of the granule cell layer occupied by tdTomato-positive granule cells. Briefly, images of the dentate gyrus were taken with a 10x objective using an Olympus AX80 microscope. Images were imported into NIH ImageJ FIJI, and a border was drawn around the Hoechst-positive granule cell layer. The contour was then transferred to the tdT-labeled image. The tdT-positive area within the contour was determined by thresholding the color image until the selected area matched the native red fluorescence. The percent of the granule cell layer that was tdT-positive was then calculated for each section in each mouse, and included rostral and caudal sections without any notable transduction. Data are plotted as percent transduction through the length of the dentate gyrus at 360µm intervals and percentage transduction of the entire dentate gyrus for each mouse.

Granule cell size measurements

Cell body sizes were measured in regions of dense transduction. One set of sections for each mouse was stained with Cresyl violet and a separate set of sections was assessed for the region PTEN deletion through immunohistochemistry and visualization of tdTomato, as described above. A single section at the core of PTEN deletion and transduction was taken for cell size measurements. Images of Cresyl violet sections were taken at 44.4x at 1μm step size using the Keyence BZ-X800 microscope and imported into ImageJ FIJI. Sampling was done by measuring 30 cells within the granule cell layer within a 1000μm^2 region of interest in the ipsilateral dentate gyrus, and the homologous regions in the contralateral granule cell layer. The mean cross-sectional area for PTEN deleted and PTEN expressing granule cells was determined by first averaging cell sizes from individual mice, then averaging for each hemisphere.

Measurements of the thickness of the molecular layer were taken at the core of transduction using 10x images taken on an Olympus AX80 microscope as a representation of dendritic length on both ipsilateral and contralateral sides in PTEN/tdT mice.

Assessment of mossy fiber projections

To assess alterations in granule cell axonal projections (mossy fibers), sections were immunostained for the zinc transporter Znt3. Images of both the ipsilateral and contralateral dentate gyrus were taken with a 10x objective using an Olympus AX80 microscope and

imported into ImageJ FIJI. Measurements were taken of the thickness of the laminae containing mossy fibers upon exiting the hilus in both ipsilateral and contralateral sides.

To detect supra-granular mossy fibers, the same Znt3 labeled sections at the core of transduction were used. Sections were scored as described by (Hunt et al., 2009): 0=little to no Znt3 labeling in granule cell layer; 1=mild Znt3 labeling in granule cell layer; 2=moderate staining in the granule cell layer and punctuate staining in inner molecular layer; 3=dense Znt3 labeling in inner molecular layer.

Statistical methods

Graphs were created and statistical analyses were performed using GraphPad Prism Software. Two-way analysis of variance (ANOVA) was used for comparisons between contralateral and ipsilateral hemispheres in PTEN/tdT mice. Sidak's multiple comparisons tests were used for multiple comparisons between groups. Relationships between measures and percent PTEN deletion were assessed by linear regression.

RESULTS

Effective PTEN deletion in PTEN/tdT mice following unilateral and bilateral AAV-Cre injections into the dentate gyrus

Injections of AAV-Cre into the dentate gyrus of PTEN/tdT mice at 2 months of age resulted in transduction of mature granule cells. Figure 5.1 illustrates representative images of mice with bilateral and unilateral AAV-Cre injections collected between 2 and 4 months after injection. Figures 5.1A and 5.1B depict the regions of granule cell transduction following bilateral AAV-Cre injection based on tdTomato expression. In both dentate gyri, PTEN immunostaining was absent in the area of tdT expression (Fig. 5.1C,D). Immunostaining for the downstream marker of mTOR activation, phosphorylation of ribosomal protein S6 (pS6), revealed activation of S6 phosphorylation in the region of PTEN deletion (Fig. 5.1E,F).

Figures 5.1I and 5.1J depict the regions of transduction following unilateral injection of AAV-Cre into the left dentate gyrus (compare tdT expression in Fig. 5.1I with the lack of tdT expression in the contralateral, non-injected dentate gyrus in Fig. 5.1J). As expected, PTEN deletion was confirmed by lack of immunostaining in transduced, tdT-positive granule cells (Fig. 5.1K), but remained intact in granule cells of the contralateral, non-injected dentate gyrus (Fig. 5.1L). Increases in immunostaining for pS6 was evident on the side of PTEN deletion (Fig. 5.1M) in comparison to the contralateral dentate gyrus (Fig. 5.1N).

Spontaneous seizures develop following bilateral PTEN deletion

Squad 1, Bilateral PTEN deletion with bilateral EEG recording: Promoter-driven PTEN deletion in the developing brain and selectively in newborn granule cells of the dentate gyrus has been reported to trigger the development of seizures resulting in high mortality rates (Kwon et al., 2001; Matsushita et al., 2016; Pun et al., 2012). Because deletion is driven by a

promoter, deletion is throughout the dentate gyri of both hemispheres. To determine if bilateral but focal PTEN deletion in mature granule cells of the adult dentate gyrus results in pro-epileptic alterations to circuit function, recording electrodes were implanted bilaterally into the hippocampi 4-6 weeks after bilateral injections of AAV-Cre. Figure 1G,H illustrate examples of recording electrode tracks.

Animal attrition and exclusions: In Squad 1 (Table 5.1), 1 mouse died prior to the EEG electrode placement surgery; tissue for this mouse was unavailable for postmortem analysis because the mouse was found dead and the carcass was disposed of. Two of 11 mice (18%) died at 3 and 4 days after electrode probe placement but prior to the initiation of EEG recordings. For 1 mouse, tissue was unavailable for analysis because the mouse was found dead and the carcass was disposed of. For the remaining mouse, the brain was drop-fixed and was prepared for histology, which revealed appropriate transduction of granule cells in both hemispheres, with no transduction of other hippocampal subregions. The cause of death in these mice is unknown given that death occurred prior to initiation of EEG/video recordings. Another 1 of 11 mice (9%) experience seizures during their recording period but was excluded following tissue analysis due to a large brain lesion of unknown origin that may have influenced seizure onset and incidence.

Seizure onset and incidence: Of the 5 mice that were included for analysis of seizure incidence, 4 mice (80%) developed spontaneous electrographic and behavioral seizures at an average of 90.25 +/- 28.02 days post AAV-Cre injection. These mice experienced an average of 28.5 +/- 12.61 seizures over the recording period (Fig. 5.2A, Table 5.2). Mice with

bilateral PTEN deletion exhibited seizures that originated in either hippocampus (Fig. 5.2B,C), all of which developed beyond 2 months after PTEN deletion. It is noteworthy that the frequency (Fig. 5.2A) of the developing seizures did not increase over time, displaying clustered periods both with and without seizure activity. This is in contrast to reports of developmental PTEN deletion that increase in frequency and severity over time (Kwon et al., 2001). In this cohort, one mouse with bilateral PTEN deletion died at 147 days post AAV-Cre injection during a seizure, after exhibiting a total of 12 seizures during the recording period (Fig. 5.2A, animal 329-21).

Interestingly, all mice that were recorded beyond 2 months after PTEN deletion developed seizures, suggesting a possible critical period for development of a seizure prone circuit. Two of 11 mice (18%) were recorded, but tissue was collected early at the two-month time point to verify electrode placement (Table 5.1). Whether these 2 mice would have displayed seizures had they been recorded for longer periods of time is unknown, so these two mice were excluded from the calculation of seizure incidence.

Patterns of AAV-Cre transduction in PTEN/tdT mice with bilateral PTEN deletion: There was some variability in transduction efficacy despite the use of consistent stereotaxic coordinates, injection parameters, and vector titers. Table 5.2 provides detailed descriptions of the pattern of transduction and PTEN deletion in each mouse, specifically the accuracy of transduction of the dentate gyrus and the transduction of other hippocampal subregions. Three mice with bilateral transduction also had mild transduction of the CA1 region in one or both hippocampi, one mouse had bilateral transduction in which targeting in the right

hippocampus was predominately in the CA1 region, and one mouse with bilateral transduction displayed mild transduction of the left CA1, and targeting in the right hippocampus predominately of the CA1. Of note, this final animal is the one that died as a result of a verified seizure. It remains to be determined how these variations and patterns of PTEN deletion impact circuit and network function.

Spontaneous seizures develop following unilateral PTEN deletion

Squad 2: Unilateral PTEN deletion with bilateral EEG recording: Temporal lobe epilepsy in humans often develops from a unilateral seizure focus. To determine if unilateral PTEN deletion is sufficient for seizure development, we carried out a pilot study in which 6 mice received unilateral injections of AAV-Cre into the dentate gyrus followed by placement of bilateral intrahippocampal electrodes. Figures 5.1O and P illustrate electrode tracks in a mouse with unilateral PTEN deletion.

Animal attrition, exclusions, and patterns of transduction: Three of 6 mice (50%) were excluded from analysis due to death (two mice at 1- and 47-days post EEG implantation surgery) or due use of the incorrect electrode (Table 5.1). Mice included in analysis (n=3, Table 5.3), as well as mice with tissue available postmortem, all displayed appropriate and well targeted transduction of only the dentate gyrus. In these cases, PTEN expression was retained in both the CA1 and CA3.

Seizure onset and incidence: In Squad 2, 2 of 3 mice (67%) developed spontaneous seizures at an average of 67.5 +/- 0.707 days post AAV-Cre injection, having an average of 43 +/- 11.31 seizures over the recording period (Fig. 5.3A). In mice with unilateral PTEN deletion, seizures were consistently initiated in the PTEN deleted dentate gyrus and then propagated to the contralateral, PTEN-expressing dentate gyrus (Fig. 5.3B,C). Seizures were clustered, did not increase in frequency over time, and began after 2 months post PTEN deletion. In this cohort, animal 305-1 displayed the greatest number of total seizures over time, eventually dying suddenly at 87 days post injection during a seizure, having a total of 51 seizures during the recording period.

Spontaneous seizures develop following unilateral PTEN deletion with contralateral EEG probe placement

Squad 3, unilateral PTEN deletion with unilateral EEG recording: It was noteworthy that several mice in Squads 1 and 2 died suddenly, and in 2 cases, death occurred during a verified seizure. In our previous studies of anatomical consequences of PTEN deletion in the adult dentate gyrus, in which mice survived up to 6 months after PTEN deletion (Chapter 3), no behavioral seizures were observed and there was only one instance of sudden death. Because we had not previously seen such mortality rates in mice with PTEN deletion but no implanted recording electrodes, we wondered whether PTEN deletion and injury due to electrode placement within the same regions could synergistically trigger more severe seizures resulting in increased incidence of sudden death.

To address this, PTEN/tdT mice (Squad 3, Tables 5.1 and 5.4) received unilateral injections of AAV-Cre into the dentate gyrus followed by unilateral EEG electrode placement into the contralateral dentate gyrus (Fig. 5.4G,H). As above, AAV-Cre injection resulted in expression of tdTomato in transduced granule cells in the ipsilateral dentate gyrus (Fig. 5.4A vs. 5.4B), PTEN deletion in transduced cells alone (Fig. 5.4C vs. 5.4D), and activation of S6 phosphorylation in PTEN deleted granule cells (Fig. 5.4E vs. 5.4F). Notably, in Squad 2, seizures recorded in mice with unilateral AAV-Cre injections were always initiated in the PTEN deleted dentate gyrus and consistently propagated to the contralateral hippocampus (Fig. 5.3B,C). Therefore, in this paradigm seizures recorded in the contralateral dentate gyrus are presumed to have propagated from the contralateral PTEN deleted dentate gyrus.

Seizure onset and incidence: Mice were recorded for 4 months post injection. Of the 7 mice recorded, all went on to display spontaneous seizures of varying frequency (Table 5.4, Fig. 5.5). As above, the average time to first seizure in this cohort of mice was after the 2-month critical period (69.29 +/- 5.68 days) with an average of 28.29 +/- 24.56 seizures over the recording period. One mouse died suddenly at 77 days post AAV-Cre injection during a seizure, having had a total of 12 seizures (Fig. 5.5A, animal 69-29). While not an entirely isolated circuit, this paradigm mostly eliminates the possibility of a two-hit theory of seizure initiation in our model, strongly supporting the conclusion that unilateral PTEN deletion in the mature dentate gyrus is sufficient to result in the formation of a circuit that eventually leads to spontaneous electrographic and behavioral seizures.

Unilateral or bilateral AAV-GFP injections do not trigger seizures

As a control for the possibility that injections of a control AAV with intrahippocampal EEG probe placement would be sufficient to lead to spontaneous seizures, PTEN/tdT mice received unilateral or bilateral injections of AAV-GFP into the dentate gyrus followed by continuous video EEG recordings (Table 5.5). A total of 6 mice were included in Squad 4, all survived each surgical procedure, but 2 mice (33%) were eventually excluded due to mistargeted viral transduction following anatomical analysis (Table 5.1). Figure 5.6 illustrates representative images from a mouse with unilateral AAV-GFP injections recorded for 100 days post injection. In Figure 5.6A, GFP transduction can be seen throughout the dentate gyrus (green) and is lacking in the contralateral, non-injected dentate gyrus (Fig. 5.6B). Regardless of injection location, PTEN expression remains intact in both hemispheres (Fig. 5.6C,D) and pS6 levels are comparable on the two sides of the brain (Fig. 5.6E,F). Following bilateral EEG placement (Fig. 5.6G,H) and continuous recording, no spontaneous electrographic or behavioral seizures were detected in these control AAV-GFP injected PTEN/tdT mice (Fig. 5.6I).

Amount of PTEN deletion correlates with seizure outcomes

Given the variability in the timing of seizure onset and seizure frequency, we wondered if the amount of PTEN deletion in each animal influenced seizure outcomes. The mice with electrodes positioned contralateral to the PTEN deleted dentate gyrus in Squad 3 allowed for detailed assessment of area of PTEN deletion without the complication of an implanted recording electrode. The area of transduction in these mice was characterized by a core in

which most cells were tdT-positive, with transduction diminishing in the rostral and caudal directions (Fig. 5.7A). The average percent area transduced throughout the entire length of the dentate gyrus of PTEN/tdT mice was 36.16 +/- 6.79% (Fig. 5.7B).

Interestingly, percent transduction was correlated with the total number of seizures in each mouse (r^2=0.6395) where total number of seizures experience over the recording period was greater in mice with larger areas of PTEN deletion within the dentate gyrus (Fig. 5.7C). In this cohort of mice, 2 of 7 mice had mild transduction of CA1 pyramidal cells (Table 5.4); seizure number in these mice was within the range of the mice with transduction limited to the dentate gyrus, suggesting that transduction of a small area of CA1 did not alter seizure development.

Enlargement of granule cell bodies and processes after PTEN deletion

As in our other studies, a notable consequence of PTEN deletion was the enlargement of granule cell bodies and processes at roughly 4 months post AAV-Cre injection. Figure 5.8A illustrates the enlargement of granule cell somata in the ipsilateral dentate gyrus (left) when compared to granule cells in the contralateral, PTEN-expressing dentate gyrus (right) in Cresyl violet stained sections. We have previously used this method to measure the cell size of granule cells near one another, specifically in regions of dense transduction. Soma cross sectional area was 127.5 +/- 15.93 μm^2 for PTEN deleted granule cells and 67.96 +/- 14.19μm^2 for PTEN expressing granule cells (Fig. 5.8B).

Enlargement of cell body size was accompanied by increases in the width of the molecular layer (Fig. 5.8D). We have previously confirmed that measurements of molecular layer thickness can serve as an indicator of apical dendrite length, given that dendrites typically extend to the hippocampal fissure. Molecular layer thickness was 315.9 +/- 44.94μm in the PTEN deleted dentate gyrus and 194.7 +/- 21.02μm in the contralateral dentate gyrus (Fig. 5.8E), confirming PTEN-deletion induced expansion of dendritic arbors.

To assess whether PTEN deletion led to expansion of mossy fiber projections to the CA3, sections at the core of transduction were stained for the zinc vesicular transporter, Znt3. As illustrated in Figure 5.8G, the collection of mossy fibers as they exit the hilus was notably thicker in the PTEN deleted dentate gyrus compared to the contralateral, PTEN-expressing dentate gyrus (MFT, red lines). Mossy fiber tract thickness was 196.8 +/- 19.3μm in the ipsilateral dentate gyrus and 135.0 +/- 14.8μm in the contralateral dentate gyrus (Fig. 5.8H).

Two-way ANOVA for all 3 parameters, collectively, revealed an overall significance for ipsilateral vs. contralateral sides [$F(1,29) = 96.63$, $p<0.0001$], a significance for measurement location [$F(2,29) = 120.6$, $p<0.0001$], and a significant interaction [$F(2,29) = 5.816$, $p=0.0075$]. Sidak's multiple comparisons tests were also significant for somata, molecular layer, and mossy fiber tract measurements (see Figure 5.8 legend for statistics). No correlations were found between somata or process measurements and total seizure number for each animal (Fig. 5.8C,F,I).

Development of supra-granular mossy fibers following PTEN deletion

The growth of mossy fiber axons into the inner molecular layer, which indicates the formation of recurrent excitatory connections amongst granule cells, is a hallmark of different models of temporal lobe epilepsy (Althaus & Parent, 2012). We have previously reported the presence of supra-granular mossy fibers in some mice assessed at 4 months post PTEN deletion with greater than 40% transduction of the dentate gyrus (Chapter 3). We were therefore curious if similar ectopic projections would be seen in mice that display spontaneous seizures.

To quantify this, we used a modified scoring system from (Hunt et al., 2009) where a score of 0 indicates no mossy fibers in the granule cell layer and a score of 3 indicates dense mossy fiber staining in the inner molecular layer (Chapter 3). Sections stained for Znt3 at the core of PTEN deletion for each mouse, as well as the contralateral dentate gyrus were assessed according to this metric.

At 4 months post deletion (Fig. 5.9A), 3 of 6 mice showed slight Znt3 labeling in the granule cell layer (score of 1), 2 of 6 mice displayed moderate granule cell layer labeling with mild labeling in the inner molecular layer (score of 2), and 1 of 6 mice showed dense Znt3 labeling in the inner molecular layer (score of 3). Collectively 50% of mice (n=3) developed at least moderate Znt3 labeling in the inner molecular layer (Fig. 5.9B). All 3 mice had greater than 35% transduction of the dentate gyrus, although a fourth mouse that fit these criteria only showed Znt3 labeling in the granule cell layer. Regression analysis of the relationship between percent transduction and mossy fiber score revealed positive relationship

(r^2=0.4563). Of note, mice with higher mossy fiber scores experienced a greater total number of seizures over the recording period (Fig. 5.9C, r^2=0.6244).

Immunocytochemical evidence for seizures in mice without electrode implantation

The combined evidence above leaves little doubt that a focal area of PTEN deletion in the dentate gyrus of mature mice leads to the development of spontaneous seizures over time. The only small caveat is the implantation of a recording electrode, which could in theory act synergistically with PTEN deletion to increase excitability. As indirect evidence that seizures do occur following focal PTEN deletion, here we describe incidental findings of increased neuronal activation in a mouse without implanted recording electrodes that was part of our anatomical study (Chapter 4) in which tissue was collected 4-month post AAV-Cre injection. Of note, we did not observe or record for behavioral seizures in this mouse.

Prolonged neuronal activation has been reported during and after seizure activity in mouse models of temporal lobe epilepsy (Peng & Houser, 2005), and has been associated with increased markers of mTOR signaling (Ahmed et al., 2021). Typically, increases in the phosphorylation of ribosomal protein S6 in our model are confined to the region of PTEN deletion, and do not extend to regions of PTEN expression within the same dentate gyrus, or in the contralateral dentate gyrus (examples in Fig. 5.1E,F, Fig. 5.1M,N, Fig. 5.4E,F). Here, a single mouse showed striking increases in pS6 immunoreactivity in regions within and beyond the area of PTEN deletion (see area of PTEN deletion in Fig. 5.10A and pS6 immunoreactivity within and outside of the area of transduction outlined in Fig. 5.10C).

Similarly, PTEN expressing granule cells in the contralateral dentate gyrus (Fig. 5.10B) also displayed increased pS6 (Fig. 5.10D).

Further assessment of cFOS expression in both hemispheres revealed increased expression in the ipsilateral dentate gyrus (Fig. 5.10E) and as well as the contralateral dentate gyrus (Fig. 5.10F). Unilateral AAV-Cre injection into Rosa control mice did not trigger any notable increases in cFOS expression within the region of transduction (outline in Fig. 5.10G). Similarly, PTEN deletion alone did not lead to increases in cFOS-positive granule cells indicating neuronal activation (transduction zone outline in Fig. 5.10H). While this mouse was not directly monitored for seizures, such notable increases in pS6 and cFOS immunoreactivity throughout the hippocampus suggest the possibility that tissue was collected within hours after a seizure event.

DISCUSSION

In the present study, we characterize functional consequences of vector-mediated PTEN deletion in mature granule cells of the adult dentate gyrus focusing on whether focal PTEN deletion led to the development of spontaneous seizures. For this, AAV-Cre was injected into the dentate gyrus of mice carrying a floxed exon 5 PTEN gene allowing Cre-mediated PTEN deletion. We monitored for seizures by continuous video-EEG recordings analyzing electrographic and behavioral seizures. As in our other studies, PTEN deletion in adult neurons triggers progressive growth of granule cell bodies, axons, and dendrites (Gallent &

Steward, 2018)(Chapter 3), and appearance of spontaneous electrographic and behavioral seizures beginning around 2 months post-PTEN deletion. Of note, seizures developed even with focal, unilateral PTEN deletion in involving about 20-40% of the dentate gyrus on the injected side.

Focal PTEN deletion is sufficient for the development of a seizure-prone circuit

The key finding of the present report that focal, unilateral PTEN deletion in mature granule cells of the dentate gyrus is sufficient to trigger spontaneous seizures in adult mice extends our understanding of functional consequences of persistent mTOR activation in neurons. Previous developmental studies have reported that embryonic and early postnatal brain-wide or cell type specific PTEN deletion triggers seizures that begin around 4 to 10 weeks of age and increase in frequency and severity over time (Kwon et al., 2001; Matsushita et al., 2016; Pun et al., 2012). In these studies, there was also increased early mortality. Sudden death can occur during different types of seizures in mice due to respiratory arrest. While our previous work has extensively documented growth of mature neurons in the cortex (Gallent & Steward, 2018; Steward et al., 2019) and dentate gyrus (Chapter 3) following vector-mediated PTEN deletion, we had not previously observed spontaneous seizures or instances of sudden death in these models. However, to rule out the occurrence of spontaneous seizures requires appropriate monitoring (EEG with combined video recording).

Here, we report the results of two pilot studies to develop the approach in which mice underwent bilateral and unilateral PTEN deletion in the dentate gyrus followed by continuous video-EEG monitoring with bilateral, intrahippocampal electrodes. The first pilot study with bilateral PTEN deletion and bilateral recording revealed that 80% of the mice developed spontaneous electrographic and behavioral seizures beginning after 2 months. Notably, seizures were initiated in either hippocampus in mice with bilateral PTEN deletion. In the second pilot study, mice with unilateral PTEN deletion were implanted with bilateral recording electrodes. In this cohort, 67% of mice developed seizures that were consistently initiated in the PTEN deleted dentate gyrus and then propagated to the contralateral side.

The two pilot studies set the stage for the final study, in which mice received unilateral injections of AAV-Cre and recording electrodes were positioned on the contralateral side. This approach was to control for the possibility of a "two-hit theory" of epileptogenesis where the combination of PTEN deletion and injury due to electrode placement fostered the formation of a seizure-prone circuit. Importantly, all mice in this cohort developed spontaneous seizures beginning after 2 months post-deletion. The results from this cohort confirm that unilateral PTEN deletion in granule cells of the mature dentate gyrus is sufficient to result in the development of a circuit that leads to spontaneous electrographic and behavioral seizures.

Critical period for pro-epileptic alterations to hippocampal circuitry

Of the 15 mice with PTEN deletion recorded across three squads, 13 mice (87%) went on to display spontaneous seizures. Interestingly, in all mice, seizures began after 2 months post-PTEN deletion. This delayed onset of spontaneous seizures suggests some progressive network modification that occurs over a generally similar time period as the anatomical alterations including growth of granule cell bodies, dendrites, and mossy fiber axons.

Anatomical assessments of mice in the present study confirm our other studies. PTEN deleted granule cells bodies were about 190% larger than PTEN expressing granule cells in the contralateral, PTEN expressing dentate gyrus. Similar to previous reports, growth of granule cell bodies was accompanied by a 160% increase in apical dendrite length and 145% expansion of mossy fiber axon bundles. This indication of growth at both presynaptic and postsynaptic ends suggests increased connectivity with target PTEN-expressing pyramidal cells within the CA3 and with projection neurons from the entorhinal cortex and contralateral hippocampus, respectively. This assumption is supported by a 1.5-fold increase in spinogenesis on mature granule cells and enlargement of granule cell terminal zones in the CA3 reported in the same PTEN deletion model (Chapter 3). However, linear regression analysis did not confirm a relationship between any of these outcomes and total seizure number experienced by each mouse. Therefore we cannot entirely rule in or rule out the possibility that progressive growth of mature granule cells might influence seizure development.

The development of supragranular mossy fibers, although controversial, are often associated with the development of epilepsy and have been noted in early PTEN deletion models (Amiri et al., 2012; Kwon et al., 2006; Pun et al., 2012; Sunnen et al., 2011). In our previous reports, we document that 16% of mice at 2 months and 40% of mice at 4 and 6 months after PTEN deletion show mossy fiber labeling in the inner molecular layer. Here, we report that while all mice developed seizures and showed evidence of mossy fiber labeling outside of the hilus (including the granule cell layer and inner molecular layer), only 50% of mice showed moderate to dense labeling in the inner molecular layer, which would indicate the formation of a recurrent excitatory circuit. Interestingly, mice that experience a greater number of seizures during the recording period were more likely to have a greater percent transduction (percent PTEN deletion) of the dentate gyrus and higher mossy fiber score. While the presence of supragranular mossy fibers may not be required for the development of seizures in this model, as also reported by others (Pun et al., 2012), we cannot exclude the possibility of its contribution to seizure progression over time.

One caveat to these assumptions is that measurements were taken at 4 months post AAV-Cre injection, well after seizures are initiated at 2 months. In our previous assessments, granule cell body increases are the only significant change at this time point (Chapter 3). Detailed assessments of synaptogenesis with pre- and postsynaptic partners (spinogenesis and mossy fiber bouton number and structure) at earlier timepoints would be required to determine if these factors may impact circuit function prior to significant changes in process length and caliber. Additionally, it would be important to determine if intrinsic neuronal modifications might occur prior to structural changes to influence granule cell behavior.

Sudden death during seizures

Seizures in these cases were clustered in nature and did not increase in frequency over time. Of the 13 mice that developed seizures, 3 eventually died during a seizure (23%). This is in contrast to developmental reports of high mortality rates averaging around 2 months of age in some cases that result from increasing seizure severity (Kwon et al., 2003; Kwon et al., 2001; Matsushita et al., 2016; Pun et al., 2012; Sunnen et al., 2011). These differences in mortality rates may suggest that seizures in our model are less severe, and thus less likely to lead to respiratory arrest. Other possibilities include some compensatory mechanisms, or established network properties in more mature circuits that might attenuate disease advancement. Detailed scoring of seizures in our model would be required to make any such conclusions. Curiously, the survival rates reported here differ from our previous observations in the same PTEN deletion model (Chapter 3). Analysis of such variable mortality rates requires further investigation.

One important caveat was the contribution of other hippocampal subregions to circuit modification based on variability in intra-dentate injections of AAV-Cre. Here we thoroughly report patterns of transduction in mice recorded, describing cases in which transduction of the CA1 might contribute to functional outcomes. Importantly, this concern in mostly negated given that 7 mice with well targeted unilateral PTEN deletion (2 with bilateral electrodes and 5 with contralateral electrode placement) also developed seizures. Additionally, transduction of the CA1 in addition to the dentate gyrus did not always produce seizures in animals recorded, nor did it result in a greater number of seizures in those that

did develop epileptiform activity. Instead, mice with well targeted unilateral PTEN deletion often displayed the greatest number of collective seizures during the recording period.

New model of epileptogenesis and adult-onset epilepsy

Temporal lobe epilepsy (TLE) is the most common type of epilepsy found in humans, characterized by a single seizure focus typically within the hippocampus. The development of TLE is often defined by an initial insult or injury that may or may not trigger a seizure, followed by a latent period in which no seizures occur, and ending with the onset of epilepsy in which patients display spontaneous seizures. Various laboratory models have been developed to investigate and advance our understanding of epileptogenesis, including models of brain injury, hypoxia and ischemia, kindling, and chemical convulsants (for full review see (Buckmaster, 2004)). Here, we show that PTEN deletion in the mature dentate gyrus is followed by a period of neuron and circuit reorganization that results in the formation of a seizure prone circuit, much like the progression of events seen in TLE. It will be important, however, to determine how PTEN deletion in this setting alters the function, survival, and organization of other cell types within the hippocampus, including inhibitory interneurons, excitatory hilar mossy cells, and newborn granule cells that might contribute to the development of spontaneous seizures. Together, we suggest that PTEN deletion in the adult dentate gyrus provides a unique opportunity to investigate a new model of adult-onset temporal lobe epilepsy in which the seizure epicenter is isolated to a single focus.

ACKNOWLEDGMENTS

I would like to thank Dr. Tallie Z. Baram from the University of California, Irvine for collaborating on this chapter of the dissertation and without whom the EEG work would not have been possible. Thank you to Kevin D. Chen for assistance with EEG surgical procedures and analysis. Thank you to Karla McHale for additional assistance with EEG scoring.

Table 5.1:

Animal numbers, attrition, and exclusions

Squad	Vector	AAV Group	Died post AAV Sx	Died post EEG Sx	Excluded post death/perfusion	Final numbers
1	AAV-Cre	Bilateral, n=11	n=1	n=2	n=1, large brain lesion n=2, ended recording early	n=5
2	AAV-Cre	Unilateral, n=6	n=0	n=2	n=1, incorrect EEG probe	n=3
3	AAV-Cre	Unilateral, n=7	n=0	n=0	n=0	n=7
4	AAV-GFP	Unilateral, n=3 Bilateral, n=3	n=0 n=0	n=0 n=0	n=1, AAV missed n=1, AAV missed	n=4

Table 5.2:

Squad 1, Bilateral PTEN-deleted mice with bilateral electrode placement used for EEG recordings

Animal	Strain	AAV-Cre location	EEG location	DPIs recorded	DPI first seizure	Total # seizures	DPI died/ sacrificed
307-8	PTEN/tdT	Bilateral ^	Bilateral	43-113	65	42	113
307-9	PTEN/tdT	Bilateral +	Bilateral	43-113	79	27	113
329-20	PTEN/tdT	Bilateral ^	Bilateral	42-174	87	33	190
329-21	PTEN/tdT	Bilateral ^+	Bilateral	42-148	130	12	S.D. 147
329-22	PTEN/tdT	Bilateral ^	Bilateral	42-201	n/a	0	201

^ Bilateral injection with mild/moderate transduction of one/both CA1
+ Bilateral injection with one injection mistargeted to CA1
S.D.= seizure-related death

Table 5.3:

Squad 2, Unilateral PTEN-deleted mice with bilateral electrode placement used for EEG recordings

Animal	Strain	AAV-Cre location	EEG location	DPIs recorded	DPI first seizure	Total # seizures	DPI died/ sacrificed
305-1	PTEN/tdT	Unilateral	Bilateral	43-86	67	51	S.D. 87
329-18	PTEN/tdT	Unilateral	Bilateral	42-190	68	35	190
329-19	PTEN/tdT	Unilateral	Bilateral	42-174	n/a	0	174

S.D.= seizure-related death

Table 5.4:

Squad 3, Unilateral PTEN-deleted mice with contralateral electrode placement used for EEG recordings

Animal	Strain	AAV-Cre location	EEG location	DPIs recorded	First Seizure	Total # seizures	DPI died/ sacrificed
68-25	PTEN/tdT/Thy1	Unilateral	contralateral	56-127	71	9	127
68-26	PTEN/tdT/Thy1	Unilateral	contralateral	56-127	71	40	127
68-27	PTEN/tdT/Thy1	Unilateral	contralateral	56-127	68	72	127
68-28	PTEN/tdT/Thy1	Unilateral	contralateral	59-113	61	23	113
69-29	PTEN/tdT/Thy1	Unilateral	contralateral	59-77	76	12	S.D. 77
69-30	PTEN/tdT/Thy1	Unilateral ^	contralateral	59-127	75	41	127
69-31	PTEN/tdT/Thy1	Unilateral ^	contralateral	62-127	63	1	127

^ Unilateral dentate gyrus injection with mild/moderate transduction of CA1
S.D.= seizure-related death

Table 5.5:

Squad 4, Control mice used for EEG recordings

Animal	Strain	AAV-GFP location	EEG location	DPIs recorded	First seizure	Total # seizures	DPI sacrificed
322-13	PTEN/tdT	Unilateral	Bilateral	44-100	n/a	0	100
323-16	PTEN/tdT	Unilateral	Bilateral	44-100	n/a	0	100
322-14	PTEN/tdT	Bilateral	Bilateral	44-100	n/a	0	100
323-17	PTEN/tdT	Bilateral	Bilateral	44-100	n/a	0	100

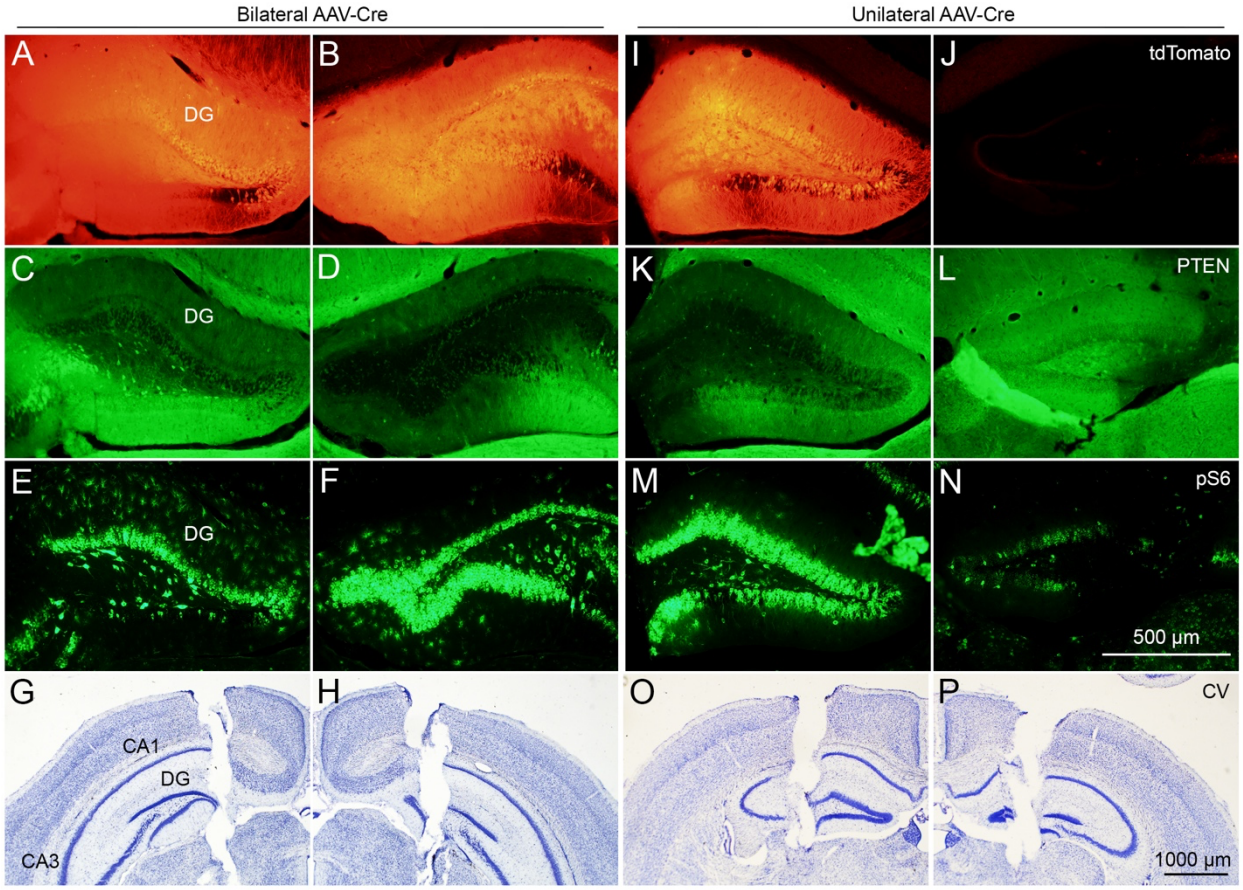
Bilateral AAV-Cre
Unilateral AAV-Cre
A
DG
B
I
J
tdTomato
C
DG
D
K
L
PTEN
E
DG
F
M
N
pS6
500 µm
G
CA1
DG
CA3
H
O
P
CV
1000 µm

Figure 5.1. Effective PTEN deletion and mTOR activation in PTEN/tdT mice following bilateral and unilateral AAV-Cre injections into the dentate gyrus.

A-B) tdTomato expression in transduced granule cells of the dentate gyrus in both left and right hemispheres following bilateral AAV-Cre injection in a PTEN/tdT mouse. C-D) Successful PTEN deletion in tdT positive granule cells. E-F) Increased phosphorylation of ribosomal protein S6 in PTEN deleted granule cells. G-H) Cresyl violet stain sections reveal bilateral electrode placement into the hippocampus. I-J) tdT expression in the transduced dentate gyrus (left) and lack of tdT expression in the non-injected dentate gyrus (right) of a PTEN/tdT mouse following unilateral AAV-Cre injection. K-L) PTEN deletion in the ipsilateral dentate gyrus. Note, the preservation of PTEN expression in the contralateral dentate gyrus. M-N) pS6 immunoreactivity in the PTEN deleted and PTEN expressing dentate gyrus of the same mouse. O-P) Location of bilateral, intrahippocampal electrodes in the same mouse.

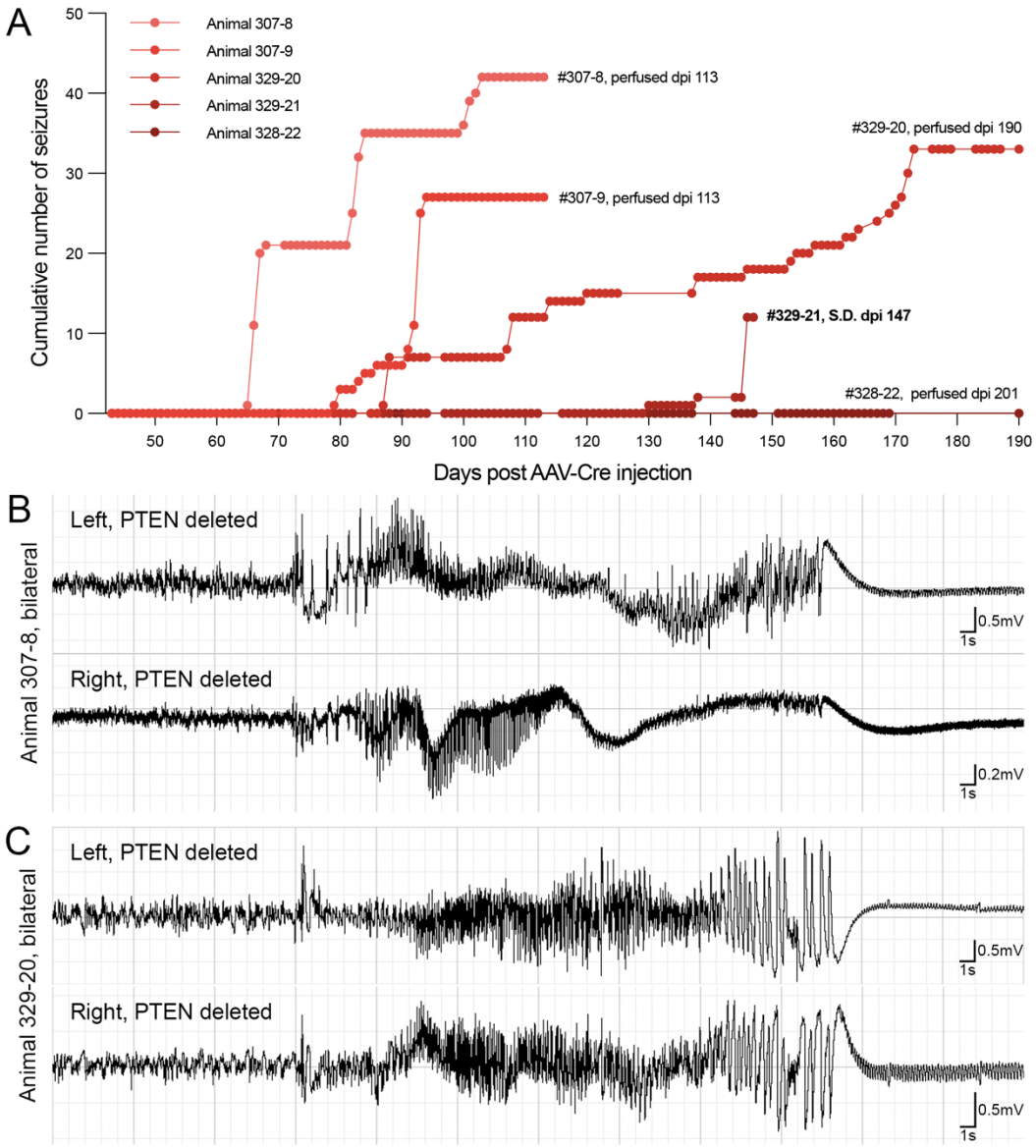
A
Animal 307-8
Animal 307-9
Animal 329-20
Animal 329-21
Animal 328-22
#307-8, perfused dpi 113
#329-20, perfused dpi 190
#307-9, perfused dpi 113
#329-21, S.D. dpi 147
#328-22, perfused dpi 201
Cumulative number of seizures
Days post AAV-Cre injection
B
Animal 307-8, bilateral
Left, PTEN deleted
Right, PTEN deleted
0.5mV
0.2mV
1s
C
Animal 329-20, bilateral
Left, PTEN deleted
Right, PTEN deleted
0.5mV
1s

Figure 5.2. EEG recordings in PTEN/tdT mice (Squad 1) following bilateral AAV-Cre injections into the dentate gyrus.

A) Cumulative number of seizures for each mouse over time following bilateral PTEN deletion. B-C) Representative EEG recordings from two mice with bilateral PTEN deletion in the dentate gyrus. Note the typical progression of seizures activity in both hippocampi followed by a period of post ictal suppression.

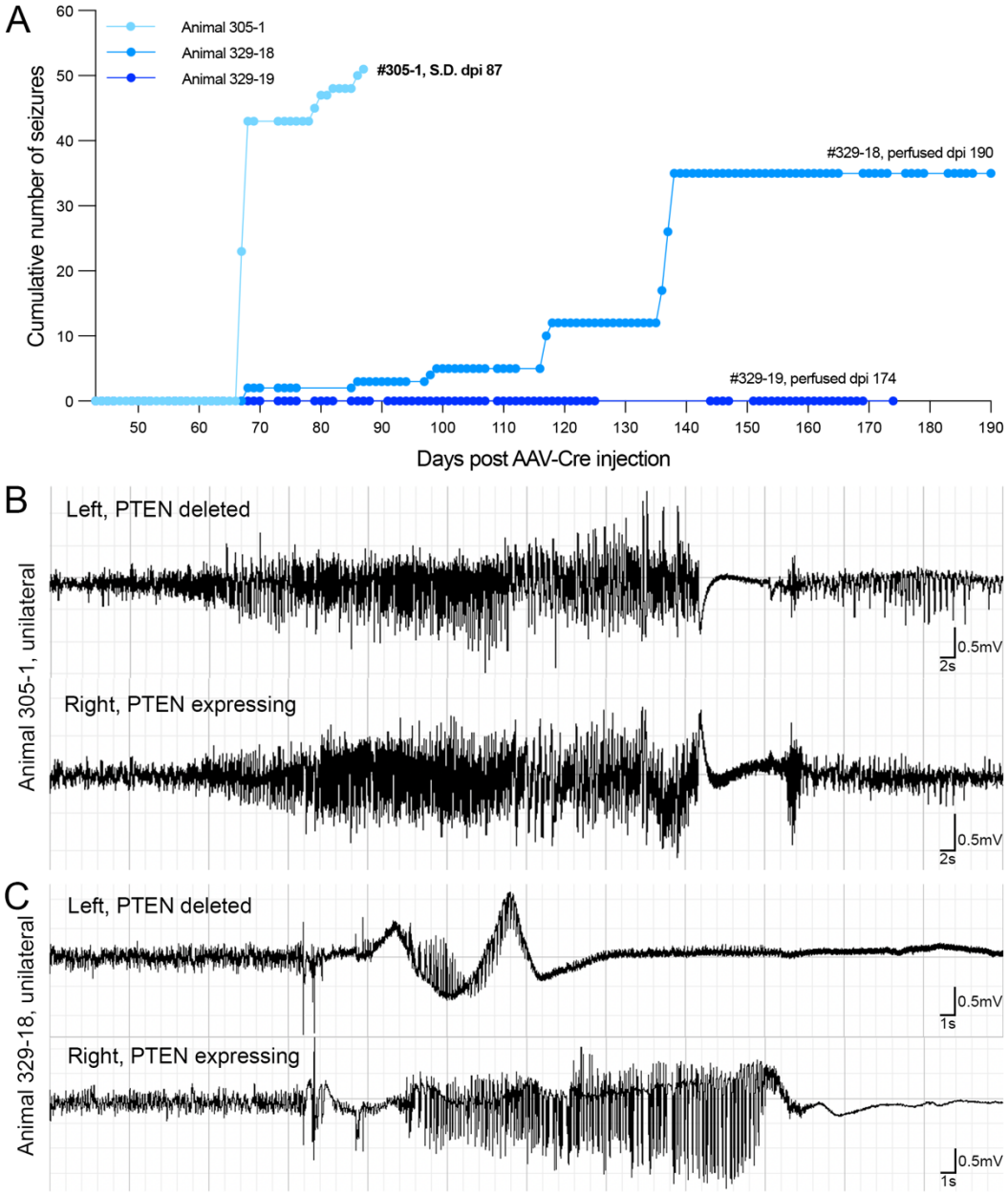
A
Animal 305-1
Animal 329-18
Animal 329-19
#305-1, S.D. dpi 87
#329-18, perfused dpi 190
#329-19, perfused dpi 174
Cumulative number of seizures
Days post AAV-Cre injection
B
Left, PTEN deleted
Right, PTEN expressing
Animal 305-1, unilateral
0.5mV
2s
C
Left, PTEN deleted
Right, PTEN expressing
Animal 329-18, unilateral
0.5mV
1s

Figure 5.3. EEG recordings in PTEN/tdT mice (Squad 2) following unilateral AAV-Cre injections into the dentate gyrus.

A) Cumulative number of seizures for each mouse over time with unilateral PTEN deletion. B-C) Representative EEG recordings from two mice with unilateral PTEN deletion in the dentate gyrus. Note, seizure activity is initiated in the PTEN deleted hippocampus then propagates to the contralateral, PTEN expressing hippocampus.

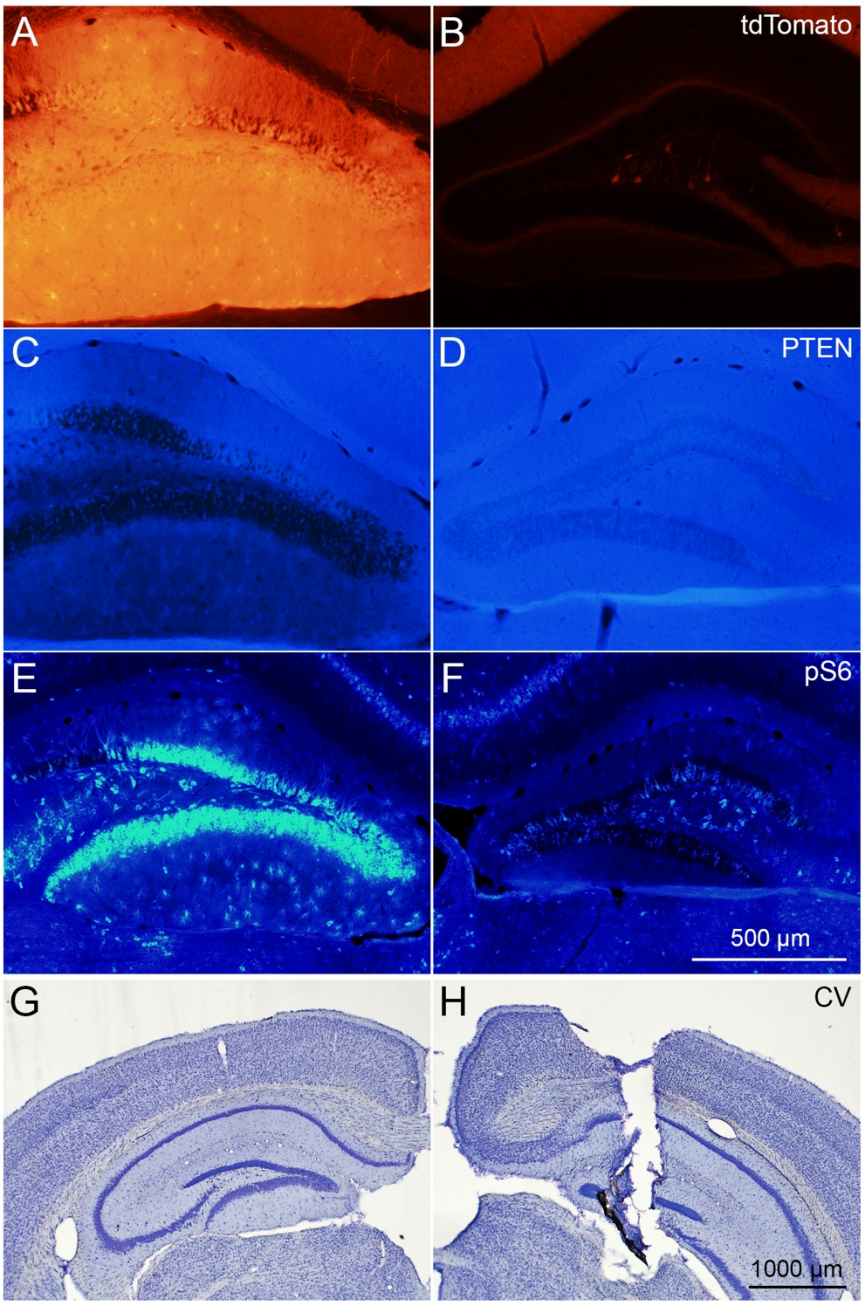
A
B
tdTomato
C
D
PTEN
E
F
pS6
500 µm
G
H
CV
1000 µm

Figure 5.4. Unilateral PTEN deletion in the dentate gyrus of a PTEN/tdT mouse (Squad 3) with EEG placement in the contralateral dentate gyrus.

A) tdTomato expression in transduced granule cells of the ipsilateral dentate gyrus following unilateral AAV-Cre injection into a PTEN/tdT mouse. B) Lack of tdT expression in non-transduced cells in the contralateral dentate gyrus. C) PTEN deletion in tdT positive granule cells. D) Preservation of PTEN expression in the contralateral dentate gyrus. E) Increased phosphorylation of ribosomal protein S6 in PTEN deleted granule cells. F) pS6 immunoreactivity in the contralateral dentate gyrus. G) Cresyl violet stained section at the core of transduction and PTEN deletion. H) Cresyl violet stain section showing unilateral electrode placement into the contralateral hippocampus.

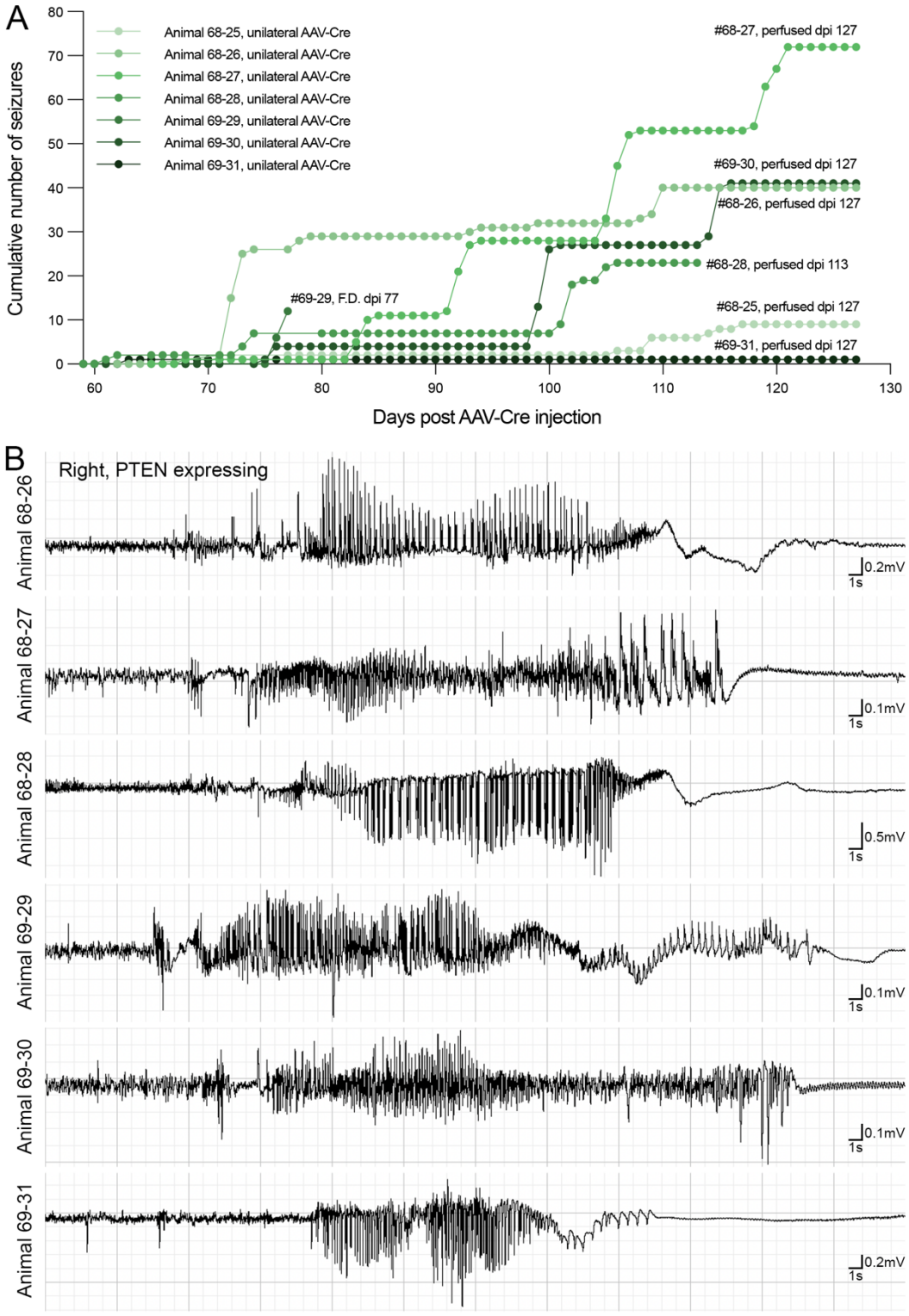
A
Cumulative number of seizures
Days post AAV-Cre injection
Animal 68-25, unilateral AAV-Cre
Animal 68-26, unilateral AAV-Cre
Animal 68-27, unilateral AAV-Cre
Animal 68-28, unilateral AAV-Cre
Animal 69-29, unilateral AAV-Cre
Animal 69-30, unilateral AAV-Cre
Animal 69-31, unilateral AAV-Cre
#68-27, perfused dpi 127
#69-30, perfused dpi 127
#68-26, perfused dpi 127
#68-28, perfused dpi 113
#68-25, perfused dpi 127
#69-31, perfused dpi 127
#69-29, F.D. dpi 77
B
Right, PTEN expressing
Animal 68-26
Animal 68-27
Animal 68-28
Animal 69-29
Animal 69-30
Animal 69-31
0.2mV
0.1mV
0.5mV
1s

Figure 5.5. EEG recordings in PTEN/tdT mice (Squad 3) following unilateral AAV-Cre injections into the dentate gyrus and placement of EEG electrode into contralateral hippocampus.

A) Cumulative number of seizures recorded in the contralateral, PTEN-expressing dentate gyrus for each mouse over time. B) Representative EEG recordings from all mice with unilateral PTEN deletion in the dentate gyrus.

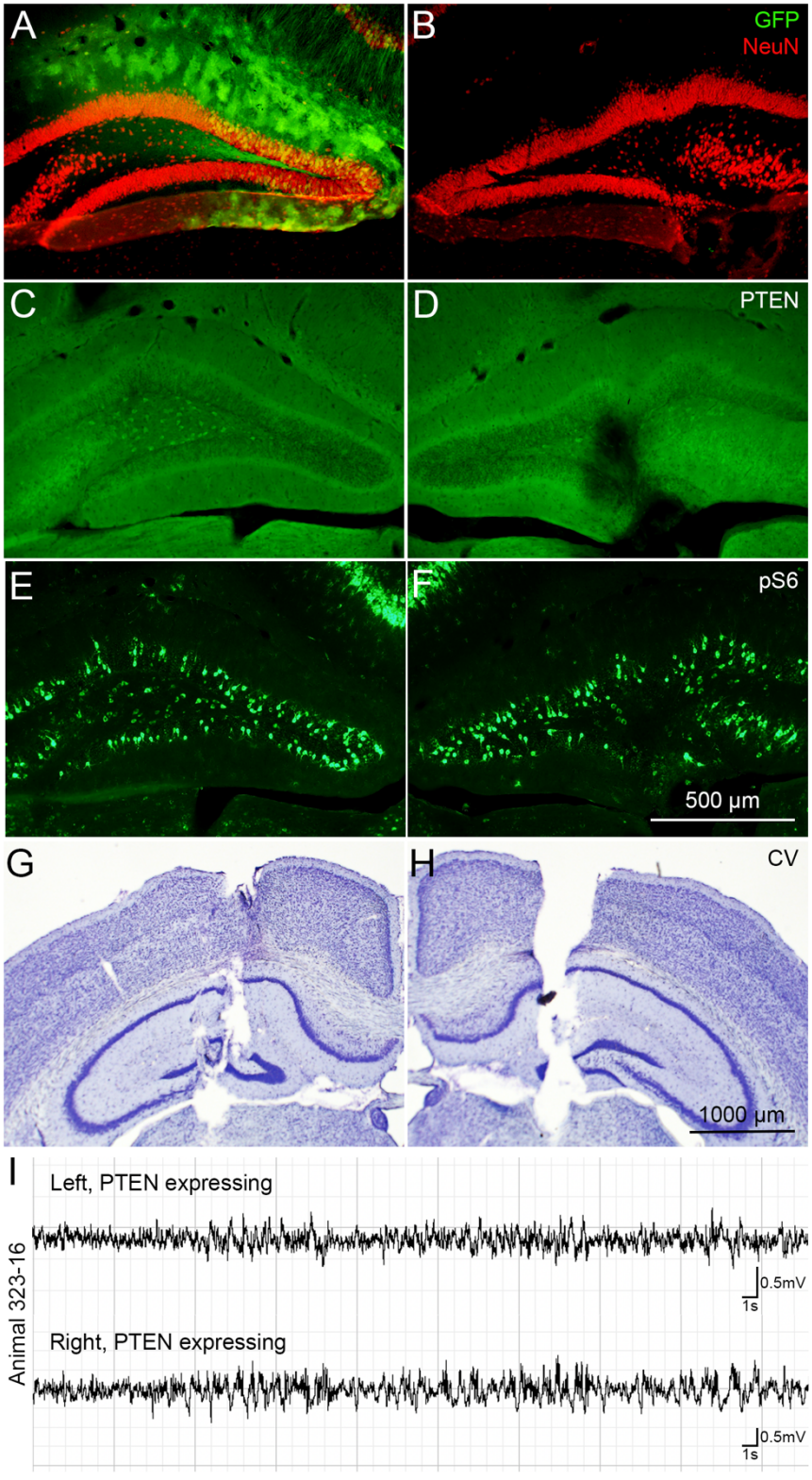
A
B
GFP
NeuN
C
D
PTEN
E
F
pS6
500 µm
G
H
CV
1000 µm
I
Left, PTEN expressing
Animal 323-16
0.5mV
1s
Right, PTEN expressing
0.5mV
1s

Figure 5.6. EEG recordings following AAV-GFP injection into the dentate gyrus of PTEN/tdT mice (Squad 4).

A) GFP expression in the ipsilateral (left) dentate gyrus of a PTEN/tdT mouse following unilateral AAV-GFP injection into the dentate gyrus. B) Lack of GFP expression in the contralateral dentate gyrus. C-D) Preservation of PTEN expression in both hippocampi following unilateral AAV-GFP injection. E-F) pS6 immunoreactivity in the same control mouse. G-H) Cresyl violet stained sections show placement of bilateral electrodes in a control mouse. I) Representative EEG recordings from a control mouse.

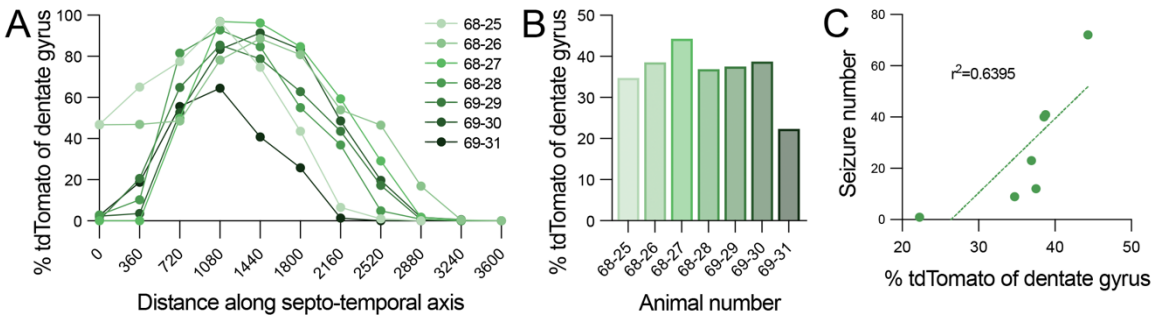
A
% tdTomato of dentate gyrus
100
80
60
40
20
0
0
360
720
1080
1440
1800
2160
2520
2880
3240
3600
Distance along septo-temporal axis
68-25
68-26
68-27
68-28
69-29
69-30
69-31
B
% tdTomato of dentate gyrus
50
40
30
20
10
0
68-25
68-26
68-27
68-28
69-29
69-30
69-31
Animal number
C
Seizure number
80
60
40
20
0
r2=0.6395
20
30
40
50
% tdTomato of dentate gyrus

Figure 5.7. Relationship between PTEN deletion of the dentate gyrus and seizure number.

A) Percent transduction of granule cells based on tdTomato expression by AAV-Cre over the septo-temporal axis of the ipsilateral dentate gyrus for each mouse in Squad 3. B) Percent transduction of the entire ipsilateral dentate gyrus of the same mice. C) Relationship between percent transduction of the dentate gyrus for each mouse and cumulative number of seizures reported over the recording period.

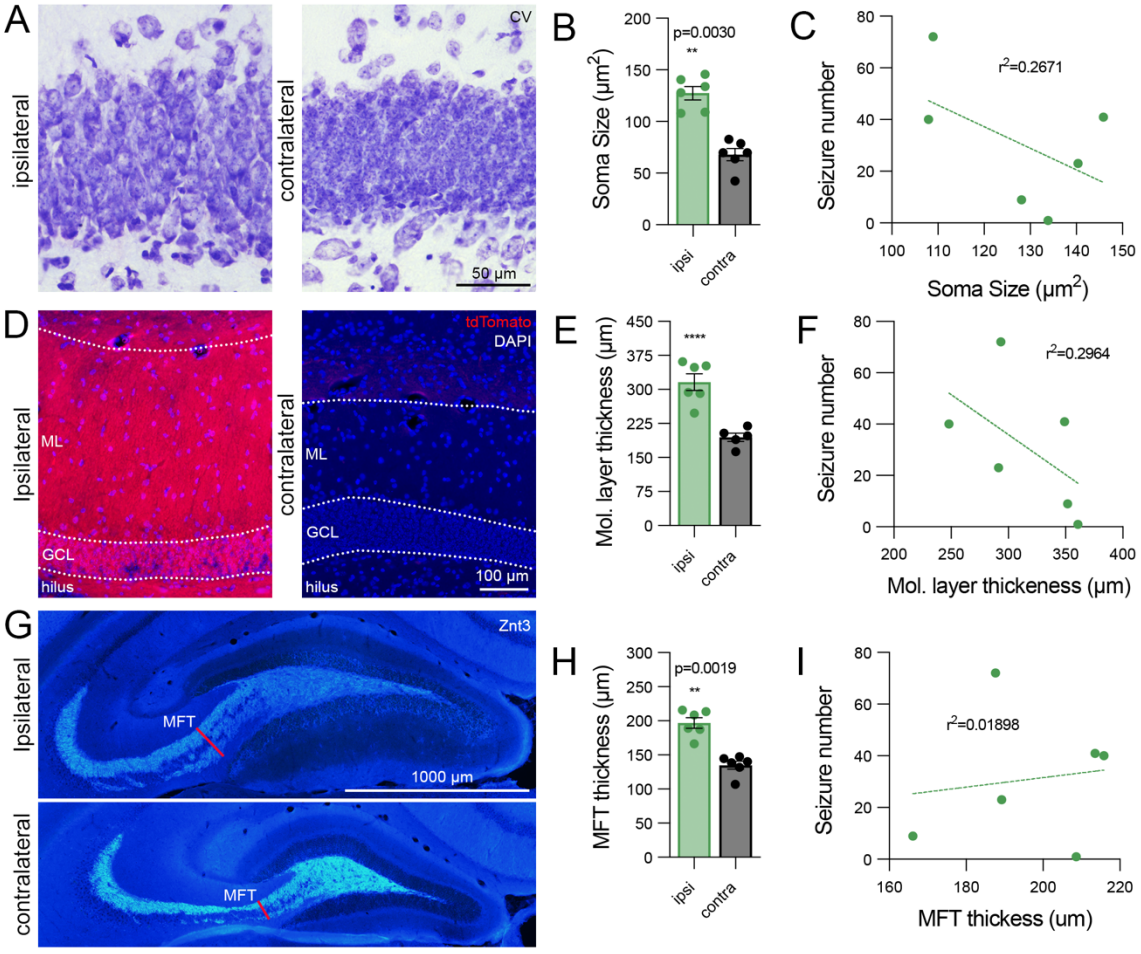
A
ipsilateral
contralateral
CV
50 µm
B
Soma Size (µm²)
p=0.0030
**
ipsi
contra
C
Seizure number
r²=0.2671
Soma Size (µm²)
D
Ipsilateral
contralateral
ML
GCL
hilus
tdTomato
DAPI
100 µm
E
Mol. layer thickness (µm)
****
F
Seizure number
r²=0.2964
Mol. layer thickeness (µm)
G
Ipsilateral
contralateral
Znt3
MFT
1000 µm
H
MFT thickness (µm)
p=0.0019
**
I
Seizure number
r²=0.01898
MFT thickess (um)

Figure 5.8. PTEN deletion triggers growth of granule cell bodies and processes.

A) Representative Cresyl violet stained sections from the ipsilateral (left) and contralateral (right) dentate gyrus showing enlarged granule cell bodies. B) Average cell body size from the ipsilateral and contralateral dentate gyrus. Note each dot represents the average of 30 granule cells for an individual mouse. Sidak's multiple comparisons for ipsilateral vs. contralateral sides in PTEN/tdT mice: $p=0.0030$. C) Relationship between soma size and seizure number for each animal. D) Images of the molecular layer from the ipsilateral and contralateral dentate gyrus from the same mouse showing enlargement of the molecular layer, suggestive of increased apical dendrite length. E) Molecular layer thickness measured at the core of transduction for each mouse and the corresponding contralateral molecular layer. Sidak's multiple comparisons for ipsilateral vs. contralateral sides in PTEN/tdT mice: $p<0.0001$. F) Relationship between molecular layer thickness and seizure number. G) Znt3 labeling in the ipsilateral and contralateral dentate gyrus reveals enlargement of mossy fiber tract projections to the CA3. H) Measurements of mossy fiber tract thickness as it exits the hilus for each mouse (red lines labeled MFT in G). Sidak's multiple comparisons for ipsilateral vs. contralateral sides in PTEN/tdT mice: $p=0.0019$. I) Relationship between mossy fiber tract thickness and seizure number.

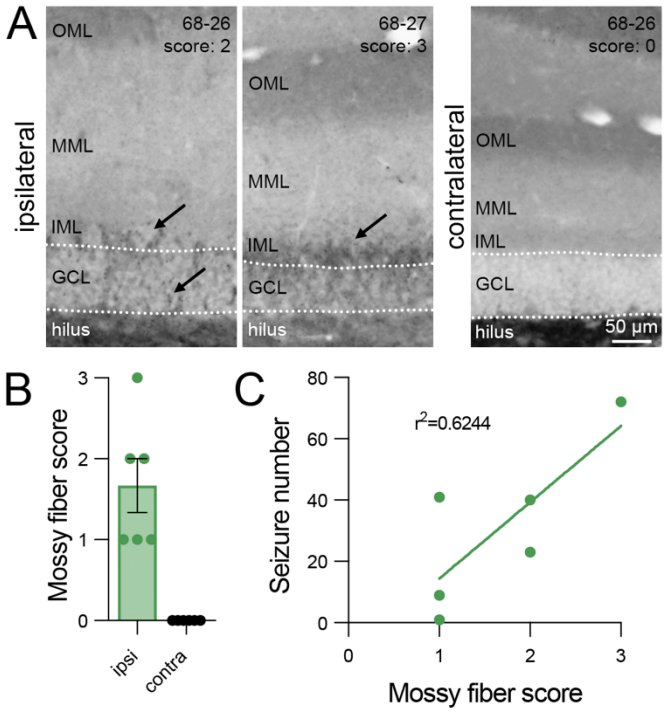
A
ipsilateral
OML
MML
IML
GCL
hilus
68-26
score: 2
68-27
score: 3
contralateral
68-26
score: 0
50 µm
B
Mossy fiber score
ipsi
contra
C
Seizure number
r2=0.6244
Mossy fiber score

Figure 5.9. Presence of supragranular mossy fiber following PTEN deletion correlates with seizure number for each animal.

A) Znt3 labeling in the granule cell layer and inner molecular layer reveals presence of supragranular mossy fibers following PTEN deletion that are not present in the contralateral dentate gyrus. B) Mossy fiber score for the transduced and contralateral dentate gyrus of each mouse shows variability in the presence of supra-granular mossy fibers. Note representative scores are depicted in the top right corner of panel I. C) Relationship between mossy fiber score and seizure number. Scoring scale: 0 - little to no Znt3 labeling in GCL, 1 - mild Znt3 labeling in GCL, 2 - moderate Znt3 labeling in GCL and mild labeling in IML, 3 - dense Znt3 labeling in IML.

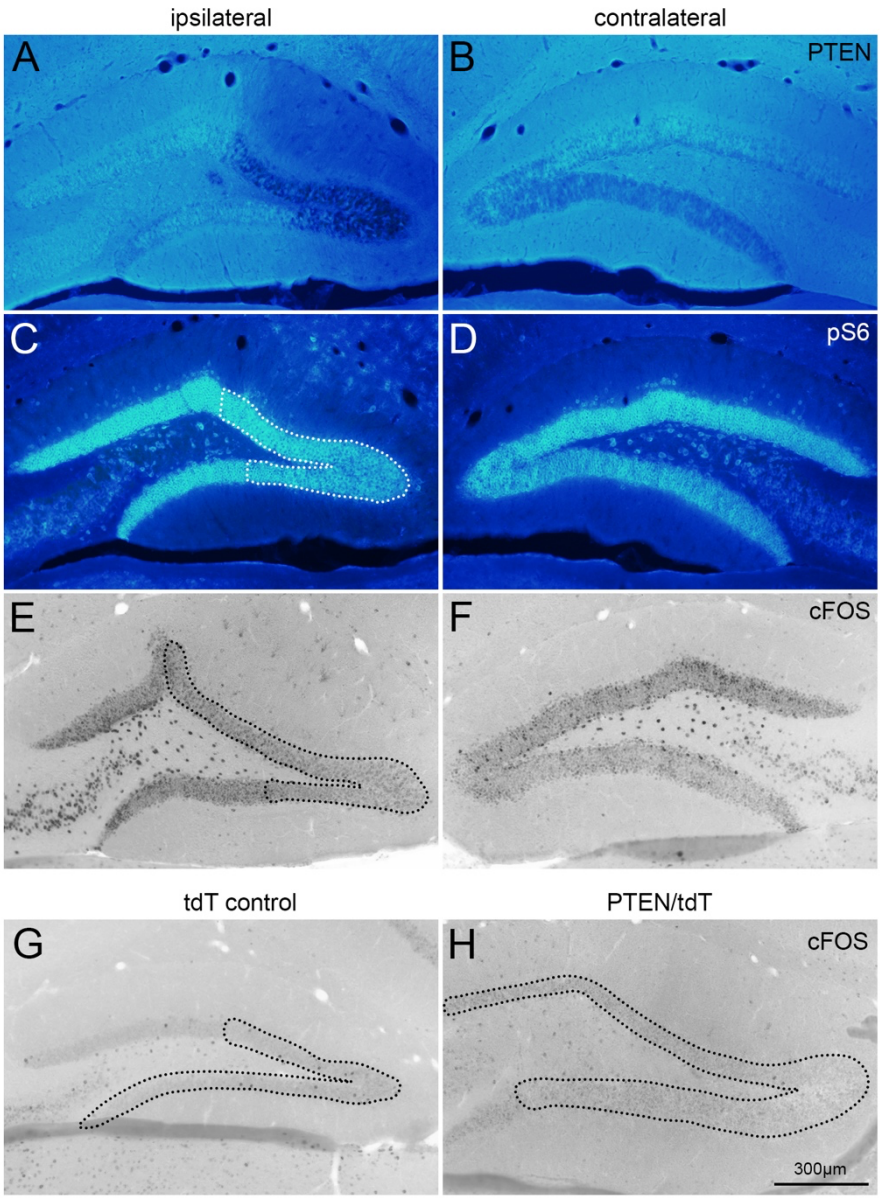
ipsilateral
contralateral
A
B
PTEN
C
D
pS6
E
F
cFOS
tdT control
PTEN/tdT
G
H
cFOS
300µm

Figure 5.10. cFOS expression in the dentate gyrus of PTEN/tdT and control mice at 4 months following unilateral AAV-Cre injection.

A) Effective PTEN deletion in the ipsilateral dentate gyrus of a PTEN/tdT mouse at 4 months after AAV-Cre injection. B) PTEN expression is maintained in the contralateral dentate gyrus. C) Increased phosphorylation of ribosomal protein S6 in the area of PTEN deletion (outlined in white) and in PTEN expression granule cells of the ipsilateral dentate gyrus. D) Increased phospho S6 in the contralateral dentate gyrus of the same mouse. E) Ipsilateral dentate gyrus of the same PTEN/tdT mouse showing increased cFos expression within and beyond the regions of PTEN deletion. F) Increased cFos expression in the contralateral dentate gyrus. G) Injections of AAV-Cre in a tdT control mouse do not result in increased cFOS expression (area of transduction outlined in black). H) PTEN deletion alone does not trigger increased cFOS expression (area of transduction and PTEN deletion outlined in black).

REFERENCES

Ahmed, M. M., Carrel, A. J., Cruz Del Angel, Y., Carlsen, J., Thomas, A. X., Gonzalez, M. I., Gardiner, K. J., & Brooks-Kayal, A. (2021). Altered Protein Profiles During Epileptogenesis in the Pilocarpine Mouse Model of Temporal Lobe Epilepsy. *Front Neurol, 12*, 654606. https://doi.org/10.3389/fneur.2021.654606

Althaus, A. L., & Parent, J. M. (2012, Sep 20). Pten-less dentate granule cells make fits. *Neuron, 75*(6), 938-940. https://doi.org/10.1016/j.neuron.2012.09.008

Amiri, A., Cho, W., Zhou, J., Birnbaum, S. G., Sinton, C. M., McKay, R. M., & Parada, L. F. (2012, Apr 25). Pten deletion in adult hippocampal neural stem/progenitor cells causes cellular abnormalities and alters neurogenesis. *J Neurosci, 32*(17), 5880-5890. https://doi.org/10.1523/JNEUROSCI.5462-11.2012

Arafa, S. R., LaSarge, C. L., Pun, R. Y. K., Khademi, S., & Danzer, S. C. (2019, Jan). Self-reinforcing effects of mTOR hyperactive neurons on dendritic growth. *Exp Neurol, 311*, 125-134. https://doi.org/10.1016/j.expneurol.2018.09.019

Backman, S. A., Stambolic, V., Suzuki, A., Haight, J., Elia, A., Pretorius, J., Tsao, M. S., Shannon, P., Bolon, B., Ivy, G. O., & Mak, T. W. (2001, Dec). Deletion of Pten in mouse brain causes seizures, ataxia and defects in soma size resembling Lhermitte-Duclos disease. *Nat Genet, 29*(4), 396-403. https://doi.org/10.1038/ng782

Buckmaster, P. S. (2004, Oct). Laboratory animal models of temporal lobe epilepsy. *Comp Med, 54*(5), 473-485. https://www.ncbi.nlm.nih.gov/pubmed/15575361

Gallent, E. A., & Steward, O. (2018, May). Neuronal PTEN deletion in adult cortical neurons triggers progressive growth of cell bodies, dendrites, and axons. *Exp Neurol, 303*, 12-28. https://doi.org/10.1016/j.expneurol.2018.01.005

Hunt, R. F., Scheff, S. W., & Smith, B. N. (2009, Feb). Posttraumatic epilepsy after controlled cortical impact injury in mice. *Exp Neurol, 215*(2), 243-252. https://doi.org/10.1016/j.expneurol.2008.10.005

Kwon, C. H., Luikart, B. W., Powell, C. M., Zhou, J., Matheny, S. A., Zhang, W., Li, Y., Baker, S. J., & Parada, L. F. (2006, May 4). Pten regulates neuronal arborization and social interaction in mice. *Neuron, 50*(3), 377-388. https://doi.org/10.1016/j.neuron.2006.03.023

Kwon, C. H., Zhu, X., Zhang, J., & Baker, S. J. (2003, Oct 28). mTor is required for hypertrophy of Pten-deficient neuronal soma in vivo. *Proc Natl Acad Sci U S A, 100*(22), 12923-12928. https://doi.org/10.1073/pnas.2132711100

Kwon, C. H., Zhu, X., Zhang, J., Knoop, L. L., Tharp, R., Smeyne, R. J., Eberhart, C. G., Burger, P. C., & Baker, S. J. (2001, Dec). Pten regulates neuronal soma size: a mouse model of Lhermitte-Duclos disease. *Nat Genet, 29*(4), 404-411. https://doi.org/10.1038/ng781

LaSarge, C. L., Pun, R. Y., Muntifering, M. B., & Danzer, S. C. (2016, Dec). Disrupted hippocampal network physiology following PTEN deletion from newborn dentate granule cells. *Neurobiol Dis, 96*, 105-114. https://doi.org/10.1016/j.nbd.2016.09.004

LaSarge, C. L., Santos, V. R., & Danzer, S. C. (2015, Mar). PTEN deletion from adult-generated dentate granule cells disrupts granule cell mossy fiber axon structure. *Neurobiol Dis, 75*, 142-150. https://doi.org/10.1016/j.nbd.2014.12.029

Ljungberg, M. C., Sunnen, C. N., Lugo, J. N., Anderson, A. E., & D'Arcangelo, G. (2009, Jul-Aug). Rapamycin suppresses seizures and neuronal hypertrophy in a mouse model of cortical dysplasia. *Dis Model Mech, 2*(7-8), 389-398. https://doi.org/10.1242/dmm.002386

Luikart, B. W., Schnell, E., Washburn, E. K., Bensen, A. L., Tovar, K. R., & Westbrook, G. L. (2011, Mar 16). Pten knockdown in vivo increases excitatory drive onto dentate granule cells. *J Neurosci, 31*(11), 4345-4354. https://doi.org/10.1523/JNEUROSCI.0061-11.2011

Matsushita, Y., Sakai, Y., Shimmura, M., Shigeto, H., Nishio, M., Akamine, S., Sanefuji, M., Ishizaki, Y., Torisu, H., Nakabeppu, Y., Suzuki, A., Takada, H., & Hara, T. (2016, Mar 10). Hyperactive mTOR signals in the proopiomelanocortin-expressing hippocampal neurons cause age-dependent epilepsy and premature death in mice. *Sci Rep, 6*, 22991. https://doi.org/10.1038/srep22991

Peng, Z., & Houser, C. R. (2005, Aug 3). Temporal patterns of fos expression in the dentate gyrus after spontaneous seizures in a mouse model of temporal lobe epilepsy. *J Neurosci, 25*(31), 7210-7220. https://doi.org/10.1523/JNEUROSCI.0838-05.2005

Pun, R. Y., Rolle, I. J., Lasarge, C. L., Hosford, B. E., Rosen, J. M., Uhl, J. D., Schmeltzer, S. N., Faulkner, C., Bronson, S. L., Murphy, B. L., Richards, D. A., Holland, K. D., & Danzer, S. C. (2012, Sep 20). Excessive activation of mTOR in postnatally generated granule cells is sufficient to cause epilepsy. *Neuron, 75*(6), 1022-1034. https://doi.org/10.1016/j.neuron.2012.08.002

Santos, V. R., Pun, R. Y. K., Arafa, S. R., LaSarge, C. L., Rowley, S., Khademi, S., Bouley, T., Holland, K. D., Garcia-Cairasco, N., & Danzer, S. C. (2017, Dec). PTEN deletion increases hippocampal granule cell excitability in male and female mice. *Neurobiol Dis, 108*, 339-351. https://doi.org/10.1016/j.nbd.2017.08.014

Skelton, P. D., Frazel, P. W., Lee, D., Suh, H., & Luikart, B. W. (2019, Nov). Pten loss results in inappropriate excitatory connectivity. *Mol Psychiatry, 24*(11), 1627-1640. https://doi.org/10.1038/s41380-019-0412-6

Steward, O., Coulibay, A., Metcalfe, M., Yonan, J. M., & Yee, K. M. (2019). AAVshRNA-mediated PTEN knockdown in adult neurons attenuates activity-dependent immediate early gene induction. *Exp Neurol*. https://doi.org/https://doi.org/10.1016/j.expneurol.2019.113098

Sunnen, C. N., Brewster, A. L., Lugo, J. N., Vanegas, F., Turcios, E., Mukhi, S., Parghi, D., D'Arcangelo, G., & Anderson, A. E. (2011, Nov). Inhibition of the mammalian target of rapamycin blocks epilepsy progression in NS-Pten conditional knockout mice. *Epilepsia, 52*(11), 2065-2075. https://doi.org/10.1111/j.1528-1167.2011.03280.x

Switon, K., Kotulska, K., Janusz-Kaminska, A., Zmorzynska, J., & Jaworski, J. (2017, Jan 26). Molecular neurobiology of mTOR. *Neuroscience, 341*, 112-153. https://doi.org/10.1016/j.neuroscience.2016.11.017

Takeuchi, K., Gertner, M. J., Zhou, J., Parada, L. F., Bennett, M. V., & Zukin, R. S. (2013, Mar 19). Dysregulation of synaptic plasticity precedes appearance of morphological defects in a Pten conditional knockout mouse model of autism. *Proc Natl Acad Sci U S A, 110*(12), 4738-4743. https://doi.org/10.1073/pnas.1222803110

Williams, M. R., DeSpenza, T., Jr., Li, M., Gulledge, A. T., & Luikart, B. W. (2015, Jan 21). Hyperactivity of newborn Pten knock-out neurons results from increased excitatory synaptic drive. *J Neurosci, 35*(3), 943-959. https://doi.org/10.1523/JNEUROSCI.3144-14.2015

Chapter 6:

Summary and Conclusions

For many years it was believed that the adult brain was something "fixed, ended and immutable". Previous reports from our lab have combated this notion, showing that modulation of the phosphatase and tensin homolog (PTEN) gene in the cortex of adult mice and rats triggers robust regeneration of injured axons following spinal cord injury (Danilov & Steward, 2015; Lewandowski & Steward, 2014; Liu et al., 2010) and delayed, but gradual growth of uninjured cortical motoneuron cell bodies and dendrites over time (Gallent & Steward, 2018). The present report expands on previous work to investigate the consequences of PTEN deletion in mature neuronal populations, demonstrating that the transition to a growth permissive state in adulthood is not unique to cortical motoneurons alone and that growth of mature neurons can influence the connectivity and function of otherwise established circuits.

Collectively, we demonstrate that focal, vector-mediated PTEN deletion in the hippocampal dentate gyrus of adult, PTEN-floxed mice results in dramatic and progressive growth of mature granule cell bodies, dendrites, and axons. We found that presynaptic dendritic growth triggers adult synaptogenesis and increased connectivity with PTEN-expressing presynaptic inputs and that expansion of axonal projections triggers similar increases in connectivity with PTEN-expressing target neurons. Further, we show that growth of mature neurons is dependent on sustained signaling through the mechanistic target of rapamycin

(mTOR) pathway and that prolonged PTEN deletion is sufficient to elicit the formation of a seizure prone circuit. This body of work serves to advance understanding of plasticity within mature neuronal populations and the brain in adulthood.

The most widely agreed upon feature of PTEN deletion in embryogenesis and at early postnatal periods is cellular hypertrophy characterized by rapid growth of neuronal cell bodies (Kwon et al., 2001; Matsushita et al., 2016; Pun et al., 2012; Zhou et al., 2009). Up until recently, it was unknown if mature neurons that had undergone the full extent of development were capable of similar growth. In 2011, a paper by Luikart et al. were the first to show that shRNA-mediated PTEN knockdown in the dentate gyrus of adult mice resulted in a slower onset of neuronal enlargement by 4 months post knockdown compared to younger neuronal populations which showed significant increases by 2 weeks (Luikart et al., 2011). Our lab corroborated such results, assessing neuronal sizes from 3 to 15 months post vector-mediated PTEN deletion in cortical motoneurons of adult mice. Here, significant increases in cell size were also observed beginning at 4 months post PTEN deletion (Gallent & Steward, 2018).

In Chapter 3, we report a slightly less delayed, but similarly progressive growth of granule cell bodies in the adult dentate gyrus in regions of both sparse and dense PTEN deletion. Interestingly, increases in cell size were noted at 1 month after AAV-Cre injection in regions of dense transduction, while significant increases in cell size were not observable until 2 months in regions of sparse transduction. To our knowledge, this is the first account of the influence of PTEN deletion density on the time course of neuronal cell body enlargement.

Other reports have suggested that viral load was predicative of the extent of morphological change based on the fluorescence intensity observed within individually labeled cells (Luikart et al., 2011).

In our model, these results may suggest one of two scenarios. The first, that the growth of PTEN deleted neurons in regions of sparse transduction is initially attenuated or delayed by their surrounding PTEN expressing neighbors. That attenuation, however, is within limits, as PTEN deleted neurons in regions of sparse transduction show a slightly greater percent increase in size (240%) by 6 months after deletion compared to control neurons, possibly due to a greater availability of space. The second scenario suggests an initial boosting of growth potential amongst neighboring PTEN deleted granule cells when near one another, as seen in regions of dense transduction. This initial boost then leads to a competition for space, limiting the overall increase at the latest time point assessed (220%). In either case, the volume or amount of PTEN deletion correlated with soma size during periods of more noticeable growth (2 and 4 months after PTEN deletion), but was lost by 6 months, which may suggest a limit of this progressive growth state. Assessment of time points beyond 6 months would be required to determine if PTEN deleted neurons eventually reach a new steady state, or if growth is continuous throughout life.

Interestingly, our results in combination with a recent report suggest that the neighbor effect may be largely unidirectional, where the growth potential of PTEN deleted neurons can be altered by both PTEN deleted and expressing neurons in their surroundings, but not in reverse. Specifically, PTEN deletion in adult born granule cells does not appear to

dramatically alter the morphology or physiology of nearby PTEN expressing granule cells regardless of the extent of deletion (LaSarge et al., 2019). The growth of cell bodies after PTEN deletion therefore may not be cell autonomous, with neighboring cells able to influence growth potential and in effect influence functional outcomes within the network.

The dramatic cell body growth documented was accompanied by increases in the thickness of the molecular layer and increased length and caliber of granule cell apical dendrites at 4 and 6 months after PTEN deletion. An unexpected finding was the inverse relationship between extent of PTEN deletion and molecular layer thickness at later timepoints that has not been observed following developmental PTEN deletion (Arafa et al., 2019). One possible interpretation could be physical limitations placed on dendrite growth due to space availability in adulthood. In support of this are maintenance of the percent area occupied by the CA1 at the core of PTEN deletion, as well as the preservation of cortical thickness (by observation).

A key finding of this report is that dramatic elongation of dendrites on mature granule cells triggered synapse formation by PTEN expressing input pathways. Much of our understanding of synaptogenesis has been derived from studying the vertebrate neuromuscular junction, where the initial trigger for synapse formation appears to be from the presynaptic axon. In this context, an axon first approaches a newly formed myotube where together they create a naïve, but functional connection. During this time, multiple axons converge on several muscles until a process of synapse elimination occurs, resulting in the stabilization of a single one-to-one connection (Brown et al., 1976; Hall & Sanes, 1993;

Personius & Balice-Gordon, 2002; Redfern, 1970; Sanes & Lichtman, 1999). While in-depth investigation of the neuromuscular junction has set the groundwork for understanding synapse formation and elimination, it is noteworthy that these events occur outside of the central nervous system and involve connections between a presynaptic neuron and a non-neuronal, postsynaptic cell.

In early development of the dentate gyrus, synaptogenesis between neuron-neuron pairs occurs during periods of more or less simultaneous pre- and postsynaptic growth. The first evidence of filipodia-like protrusions on developing granule cell dendrites can be seen between postnatal days 2 and 3, with spine densities continuing to increase as granule cells mature and dendritic arbors reach the hippocampal fissure by days 7 through 9 (Jones et al., 2003). Studies of synaptogenesis in this region using electron microscopy report the greatest increase in synapse number between 4 and 11 days (Crain et al., 1973). Initial projections from the entorhinal cortex first reach the outer molecular layer of the dentate gyrus in late embryogenesis (Super & Soriano, 1994), at a timepoint where the presence of granule cells are few and far between. This would suggest that axonal targeting might be regulated by factors unrelated to their later interactions with granule cells. Contrary to this, inputs projecting to the middle molecular layer from the entorhinal cortex have been reported at postnatal day 3 (Fricke & Cowan, 1977) and commissural/ associational inputs to the inner molecular layer have been seen at postnatal day 4 (Loy et al., 1977). The near-simultaneous growth of afferent inputs into these layers along with the first appearance of postsynaptic spines and synapses, blur the origins of synaptogenesis during development.

In the special case of adult born granule cells, neuronal stem cells located within the subgranular zone of the dentate gyrus differentiate and integrate into the pre-existing circuit. As spine densities increase on these new neurons and dendrites extend through the granule cell layer and into the molecular layer, their protrusions gravitate towards pre-existing synapses. The resulting multi-synapse is transient, as one postsynaptic partner is eventually eliminated (Toni & Schinder, 2015; Toni et al., 2007). These data suggest that spine formation on adult born granule cells induces a presynaptic change when forming synapses with pre-existing axon terminals, resulting in synapse elimination and remodeling.

Our assessment of Golgi-stained granule cells at 6 months post deletion revealed a 1.5-fold increase in spine densities characterized by an increase in the number of immature spines and a preservation of the number of mature, mushroom-shaped spines suggestive of adult synaptogenesis. These results of increased spine densities are in line with developmental PTEN deletion models (Luikart et al., 2011; Pun et al., 2012; Skelton, Frazel, et al., 2019; Skelton, Poquerusse, et al., 2019; Williams et al., 2015). We propose that dendrites, at any developmental stage, are capable of tight control over their spine content, where intrinsically induced changes to dendrite length and caliber are the main driver for synapse formation by presynaptic afferent terminals.

Importantly, the laminar specificity of input projections from the entorhinal cortex and contralateral hippocampus expand but maintain appropriate targeting at long post-deletion time points despite elongation of dendrites and increased synapse formation. While other studies have used physiological outcomes to show increased connectivity within major

hippocampal pathways at the level of the synapse (LaSarge et al., 2016; Luikart et al., 2011; Santos et al., 2017; Williams et al., 2015), here we provide the first visual evidence of appropriate targeting and preservation of input pathways to distinct lamina within the dentate gyrus over time. It will be of interest to determine if projection neurons form axon collaterals within their given terminal fields to accommodate such dendritic growth.

In addition to enlarged apical dendrites, we document increases in the thickness of the mossy fiber tract, as also reported in developmental deletion (Amiri et al., 2012; Zhou et al., 2009). Importantly, axons from PTEN deleted granule cells maintain appropriate projections to their terminal zone within the stratum lucidum of the CA3, with the presence of supragranular mossy fibers in some mice a long post-injection time points. What remains to be determined is whether PTEN deletion alters the size, number, or spacing of excitatory mossy fiber boutons in mature granule cells. A recent paper reports increases in mossy fiber axon size and spacing of boutons in PTEN deleted, adult born granule cells with preservation of bouton volume (LaSarge et al., 2015). In contrast, PTEN knockdown in young neurons has been reported to increase bouton volume along with axonal enlargement (Luikart et al., 2011). Both cases imply increased synaptic strength and connections onto CA3 pyramidal cells. In our model, the enlargement of the mossy fiber terminal zone in the CA3 suggests increased connectivity with and alterations to the dendritic architecture of CA3 pyramidal cells that remain PTEN expressing. Modification of this kind would suggest that focal PTEN deletion is sufficient to induce structure change in PTEN expressing neurons and adult synaptogenesis with both pre- and post-synaptic partners.

In Chapter 4 we present evidence for the reliance of initiation and maintenance of growth in mature neurons on sustained mTOR activation. mTOR activity was inhibited through prolonged administration of rapamycin at acute and delayed periods after PTEN deletion. mTOR inhibition was confirmed through reductions in the phosphorylation of ribosomal protein S6 in PTEN deleted granule cells. First, we demonstrate that rapamycin administration during the acute and delayed periods after PTEN deletion prevented and reversed growth of granule cell bodies, respectively. Delayed rapamycin administration also functioned to prevent dendritic and axonal growth, as well as prevent the formation of recurrent excitatory networks by invasion of mossy fiber axons into the inner molecular layer. Rapamycin administration and mTOR inhibition before the onset of neuronal growth therefore prevented increases in connectivity with granule cell pre- and postsynaptic partners. Further investigations will be required to determine the stability of this increased connectivity once it is formed through even further delayed periods of mTOR inactivation, something that has yet to be directly assessed in current literature. These results would have important, yet opposing, implications for network connectivity and function dependent on the model and region of PTEN deletion assessed, as will be addressed in follow up discussions.

The studies outlined in Chapter 5 demonstrate that unilateral PTEN deletion in mature granule cells of the dentate gyrus is sufficient for the development of a seizure prone circuit. To date, promotor-driven models that report seizures and high mortality rates in mice involve PTEN deletion in both hippocampi or in multiple structures throughout the developing brain (Kwon et al., 2001; Matsushita et al., 2016; Pun et al., 2012). To our

knowledge, this is the first study to report seizures following PTEN deletion not only in adulthood, but as a result of unilateral PTEN deletion. Whether unilateral or bilateral, we show that 87% of mice recorded went on to develop spontaneous seizures with initiation of seizure activity occurring beyond 2 months post injection. The delayed onset of spontaneous seizures suggests a critical period of morphological and circuit modification.

Our studies are the first to suggest that the overall extent of PTEN deletion is predictive of seizure outcomes, and not just anatomical change. Unexpectedly, increases in soma, dendrite, and axonal size did not correlate with the cumulative number of seizures experienced by an individual mouse. We did find that the increasing presence of mossy fibers outside of the hilus and within the inner molecular layer were indicative of increased seizure numbers. Although not obviously predictive or required for seizure onset as also suggested by others (Pun et al., 2012), it is possible that the abnormal presence of supragranular mossy fibers might influence the progression of seizure outcomes over time.

The implications of the current report are two-fold. The first is the possible creation of a new model of adult-onset seizures. Temporal lobe epilepsy (TLE) in humans is characterize by a single focus of seizure initiation, most often located within the hippocampus. The development of seizures in these cases is characterized by an initial insult or seizure, a latent period is which circuit modifications are thought to occur, and a resulting period of spontaneous seizures (Buckmaster, 2004). Here we show a similar timeline of events following unilateral PTEN deletion in which mice go on to display spontaneous seizures beyond 2 months after PTEN deletion. While most of our significant morphological outcomes

are reported after the development of seizures, it will be important to characterize how connectivity at the synaptic level is altered within the observed 2-month critical window.

This model also provides a unique opportunity to explore how targeted PTEN deletion in mature granule cells alters the function and survival of other cell types within the hippocampus, including hilar mossy cells and inhibitory interneurons. Both the loss of hilar mossy cells, which is implicated in mossy fiber sprouting (Hester & Danzer, 2013), and the loss of local inhibitory interneurons (LaSarge et al., 2021) have been implicated in increased network excitability following PTEN deletion in adult born granule cells in young mice. Early administration of rapamycin following PTEN deletion during development has been reported to prevent abnormal morphology with variable effects on seizure frequency and severity (Getz et al., 2016; Ljungberg et al., 2009; Matsushita et al., 2016; Pun et al., 2012; Sunnen et al., 2011; Zhou et al., 2009). While preventative rapamycin administration would be expected to have similar functional results in our model in adults, as seen by our morphological assessments, it will be important to determine the solidity of increased connectivity at later time points once established. Specifically, if reversal of connectivity is possible in mature but altered circuits and if any reversal would positively ameliorate abnormal network function.

The second implication of the current report sends us back to models of injury. To date, PTEN deletion has resulted in an unmatched ability for intrinsic induction of recovery following spinal cord injury. Again, previous reports in our lab and by others have demonstrated the therapeutic potential of PTEN modulation in various models resulting in impressive axon

regeneration and functional recovery (Danilov & Steward, 2015; Du et al., 2015; Lewandowski & Steward, 2014; Liu et al., 2010; Zukor et al., 2013). In addition to axonal dieback, injured neurons also display cell body and dendritic atrophy (Nielson et al., 2011; Wang et al., 2018). In Chapter 2, we confirm the growth of uninjured cortical motoneurons and dendrites in the adult using a novel retrograde vector that selectively transduces layer V cortical motoneurons when injected into the spinal cord (Metcalfe et al., 2022; Steward et al., 2021). The potential of PTEN deletion to induce growth of neuronal cell bodies, axons, and dendrites provides a unique opportunity to improve connectivity at multiple levels throughout the central nervous system after trauma. Curiously, our assessment of axonal and dendritic growth occurs at delayed periods after PTEN deletion in dentate granule cells. In contrast, the functional improvements following PTEN deletion in spinal cord injury often plateau within weeks after injury. This discrepancy could suggest cell-type specific regulation of process growth that will be essential to define in the context of injured and uninjured cortical motoneurons.

Additionally, we demonstrate that PTEN deletion in the mature dentate gyrus triggers spontaneous seizures over time. To date, we have not observed any obvious evidence of seizures or pathology in PTEN deleted mice with spinal cord injuries or following prolonged PTEN deletion in the cortex of uninjured mice. Appropriate functional monitoring is required to define the network effects of PTEN deletion at the level of the cortex. If adverse long-term effects are observed in an injury model, methods that allow for variable modulation of PTEN expression over time would prove advantageous. In this regard, temporary PTEN hypofunction would be valuable during periods of active regeneration or recovery, but no

longer necessary at later time points when abnormal physiological activity might occur. Again, it will be important to determine the stability of increased connectivity in our hippocampal model through rapamycin-induced mTOR inhibition. If adult synaptogenesis and connectivity are reversed following methods for PTEN reinstatement or mTOR inactivation, this could be instead detrimental to recovery efforts following injury.

Remarkably, it is still unknown how the transcriptional profile of neurons is altered after PTEN deletion and mTOR activation, or if PTEN deletion in a single population influences the expression profiles of its microenvironment or synaptic partners. Characterization of the transcriptional profile of PTEN deleted neurons in various neuronal populations is essential to elucidate the mechanism of deletion-induced outcomes and identify other potential therapeutic targets. This could allow us to harness the benefits of downstream PTEN modulation and mTOR activation while hopefully circumventing possible negative outcomes. Together, our results further unravel the potential plasticity of mature neuronal populations and established circuits in the brain, and reveal that loss of PTEN can greatly influence functional outcomes in the adult central nervous system.

To summarize our findings:

- PTEN deletion in mature dentate gyrus granule cells triggers persistent mTOR activation
- PTEN deletion in the adult dentate gyrus initiates growth of neuronal cell bodies, axons, and dendrites

- Postsynaptic dendritic growth is sufficient to drive increased synapse formation by input pathways that maintain their PTEN expression
- Presynaptic axonal enlargement results in increased connectivity with PTEN expressing postsynaptic targets
- Laminar specificity of input and output projections is maintained
- Initiation and maintenance of neuronal growth requires sustained mTOR activation
- Focal, unilateral PTEN deletion in mature granule cells of the adult dentate gyrus results in the formation of a seizure prone circuit

REFERENCES

Amiri, A., Cho, W., Zhou, J., Birnbaum, S. G., Sinton, C. M., McKay, R. M., & Parada, L. F. (2012, Apr 25). Pten deletion in adult hippocampal neural stem/progenitor cells causes cellular abnormalities and alters neurogenesis. *J Neurosci, 32*(17), 5880-5890. https://doi.org/10.1523/JNEUROSCI.5462-11.2012

Arafa, S. R., LaSarge, C. L., Pun, R. Y. K., Khademi, S., & Danzer, S. C. (2019, Jan). Self-reinforcing effects of mTOR hyperactive neurons on dendritic growth. *Exp Neurol, 311*, 125-134. https://doi.org/10.1016/j.expneurol.2018.09.019

Brown, M. C., Jansen, J. K., & Van Essen, D. (1976, Oct). Polyneuronal innervation of skeletal muscle in new-born rats and its elimination during maturation. *J Physiol, 261*(2), 387-422. https://doi.org/10.1113/jphysiol.1976.sp011565

Buckmaster, P. S. (2004, Oct). Laboratory animal models of temporal lobe epilepsy. *Comp Med, 54*(5), 473-485. https://www.ncbi.nlm.nih.gov/pubmed/15575361

Crain, B., Cotman, C., Taylor, D., & Lynch, G. (1973, Dec 7). A quantitative electron microscopic study of synaptogenesis in the dentate gyrus of the rat. *Brain Res, 63*, 195-204. https://doi.org/10.1016/0006-8993(73)90088-7

Danilov, C. A., & Steward, O. (2015, Apr). Conditional genetic deletion of PTEN after a spinal cord injury enhances regenerative growth of CST axons and motor function recovery in mice. *Exp Neurol, 266*, 147-160. https://doi.org/10.1016/j.expneurol.2015.02.012

Du, K., Zheng, S., Zhang, Q., Li, S., Gao, X., Wang, J., Jiang, L., & Liu, K. (2015, Jul 1). Pten Deletion Promotes Regrowth of Corticospinal Tract Axons 1 Year after Spinal Cord Injury. *J Neurosci, 35*(26), 9754-9763. https://doi.org/10.1523/JNEUROSCI.3637-14.2015

Fricke, R., & Cowan, W. M. (1977, May 15). An autoradiographic study of the development of the entorhinal and commissural afferents to the dentate gyrus of the rat. *J Comp Neurol, 173*(2), 231-250. https://doi.org/10.1002/cne.901730203

Gallent, E. A., & Steward, O. (2018, May). Neuronal PTEN deletion in adult cortical neurons triggers progressive growth of cell bodies, dendrites, and axons. *Exp Neurol, 303*, 12-28. https://doi.org/10.1016/j.expneurol.2018.01.005

Getz, S. A., DeSpenza, T., Jr., Li, M., & Luikart, B. W. (2016, Sep). Rapamycin prevents, but does not reverse, aberrant migration in Pten knockout neurons. *Neurobiol Dis, 93*, 12-20. https://doi.org/10.1016/j.nbd.2016.03.010

Hall, Z. W., & Sanes, J. R. (1993, Jan). Synaptic structure and development: the neuromuscular junction. *Cell, 72 Suppl*, 99-121. https://doi.org/10.1016/s0092-8674(05)80031-5

Hester, M. S., & Danzer, S. C. (2013, May 22). Accumulation of abnormal adult-generated hippocampal granule cells predicts seizure frequency and severity. *J Neurosci, 33*(21), 8926-8936. https://doi.org/10.1523/JNEUROSCI.5161-12.2013

Jones, S. P., Rahimi, O., O'Boyle, M. P., Diaz, D. L., & Claiborne, B. J. (2003). Maturation of granule cell dendrites after mossy fiber arrival in hippocampal field CA3. *Hippocampus, 13*(3), 413-427. https://doi.org/10.1002/hipo.10121

Kwon, C. H., Zhu, X., Zhang, J., Knoop, L. L., Tharp, R., Smeyne, R. J., Eberhart, C. G., Burger, P. C., & Baker, S. J. (2001, Dec). Pten regulates neuronal soma size: a mouse model of Lhermitte-Duclos disease. *Nat Genet, 29*(4), 404-411. https://doi.org/10.1038/ng781

LaSarge, C. L., Pun, R. Y., Muntifering, M. B., & Danzer, S. C. (2016, Dec). Disrupted hippocampal network physiology following PTEN deletion from newborn dentate granule cells. *Neurobiol Dis, 96*, 105-114. https://doi.org/10.1016/j.nbd.2016.09.004

LaSarge, C. L., Pun, R. Y. K., Gu, Z., Riccetti, M. R., Namboodiri, D. V., Tiwari, D., Gross, C., & Danzer, S. C. (2021, May). mTOR-driven neural circuit changes initiate an epileptogenic cascade. *Prog Neurobiol, 200*, 101974. https://doi.org/10.1016/j.pneurobio.2020.101974

LaSarge, C. L., Pun, R. Y. K., Gu, Z., Santos, V. R., & Danzer, S. C. (2019, Nov). Impact of mTOR hyperactive neurons on the morphology and physiology of adjacent neurons: Do PTEN KO cells make bad neighbors? *Exp Neurol, 321*, 113029. https://doi.org/10.1016/j.expneurol.2019.113029

LaSarge, C. L., Santos, V. R., & Danzer, S. C. (2015, Mar). PTEN deletion from adult-generated dentate granule cells disrupts granule cell mossy fiber axon structure. *Neurobiol Dis, 75*, 142-150. https://doi.org/10.1016/j.nbd.2014.12.029

Lewandowski, G., & Steward, O. (2014, Jul 23). AAVshRNA-mediated suppression of PTEN in adult rats in combination with salmon fibrin administration enables regenerative growth of corticospinal axons and enhances recovery of voluntary motor function after cervical spinal cord injury. *J Neurosci, 34*(30), 9951-9962. https://doi.org/10.1523/JNEUROSCI.1996-14.2014

Liu, K., Lu, Y., Lee, J. K., Samara, R., Willenberg, R., Sears-Kraxberger, I., Tedeschi, A., Park, K. K., Jin, D., Cai, B., Xu, B., Connolly, L., Steward, O., Zheng, B., & He, Z. (2010, Sep). PTEN deletion enhances the regenerative ability of adult corticospinal neurons. *Nat Neurosci, 13*(9), 1075-1081. https://doi.org/10.1038/nn.2603

Ljungberg, M. C., Sunnen, C. N., Lugo, J. N., Anderson, A. E., & D'Arcangelo, G. (2009, Jul-Aug). Rapamycin suppresses seizures and neuronal hypertrophy in a mouse model of cortical dysplasia. *Dis Model Mech, 2*(7-8), 389-398. https://doi.org/10.1242/dmm.002386

Loy, R., Lynch, G., & Cotman, C. W. (1977, Feb). Development of afferent lamination in the fascia dentata of the rat. *Brain Res, 121*(2), 229-243. https://doi.org/10.1016/0006-8993(77)90149-4

Luikart, B. W., Schnell, E., Washburn, E. K., Bensen, A. L., Tovar, K. R., & Westbrook, G. L. (2011, Mar 16). Pten knockdown in vivo increases excitatory drive onto dentate granule cells. *J Neurosci, 31*(11), 4345-4354. https://doi.org/10.1523/JNEUROSCI.0061-11.2011

Matsushita, Y., Sakai, Y., Shimmura, M., Shigeto, H., Nishio, M., Akamine, S., Sanefuji, M., Ishizaki, Y., Torisu, H., Nakabeppu, Y., Suzuki, A., Takada, H., & Hara, T. (2016, Mar 10). Hyperactive mTOR signals in the proopiomelanocortin-expressing hippocampal neurons cause age-dependent epilepsy and premature death in mice. *Sci Rep, 6*, 22991. https://doi.org/10.1038/srep22991

Metcalfe, M., Yee, K. M., Luo, J., Martin-Thompson, J. H., Gandhi, S. P., & Steward, O. (2022, Apr). Harnessing rAAV-retro for gene manipulations in multiple pathways that are interrupted after spinal cord injury. *Exp Neurol, 350*, 113965. https://doi.org/10.1016/j.expneurol.2021.113965

Nielson, J. L., Strong, M. K., & Steward, O. (2011, Oct 1). A reassessment of whether cortical motor neurons die following spinal cord injury. *J Comp Neurol, 519*(14), 2852-2869. https://doi.org/10.1002/cne.22661

Personius, K. E., & Balice-Gordon, R. J. (2002, Oct). Activity-dependent synaptic plasticity: insights from neuromuscular junctions. *Neuroscientist, 8*(5), 414-422. https://doi.org/10.1177/107385802236970

Pun, R. Y., Rolle, I. J., Lasarge, C. L., Hosford, B. E., Rosen, J. M., Uhl, J. D., Schmeltzer, S. N., Faulkner, C., Bronson, S. L., Murphy, B. L., Richards, D. A., Holland, K. D., & Danzer, S. C. (2012, Sep 20). Excessive activation of mTOR in postnatally generated granule cells is sufficient to cause epilepsy. *Neuron, 75*(6), 1022-1034. https://doi.org/10.1016/j.neuron.2012.08.002

Redfern, P. A. (1970, Aug). Neuromuscular transmission in new-born rats. *J Physiol, 209*(3), 701-709. https://doi.org/10.1113/jphysiol.1970.sp009187

Sanes, J. R., & Lichtman, J. W. (1999). Development of the vertebrate neuromuscular junction. *Annu Rev Neurosci, 22*, 389-442. https://doi.org/10.1146/annurev.neuro.22.1.389

Santos, V. R., Pun, R. Y. K., Arafa, S. R., LaSarge, C. L., Rowley, S., Khademi, S., Bouley, T., Holland, K. D., Garcia-Cairasco, N., & Danzer, S. C. (2017, Dec). PTEN deletion increases hippocampal granule cell excitability in male and female mice. *Neurobiol Dis, 108*, 339-351. https://doi.org/10.1016/j.nbd.2017.08.014

Skelton, P. D., Frazel, P. W., Lee, D., Suh, H., & Luikart, B. W. (2019, Nov). Pten loss results in inappropriate excitatory connectivity. *Mol Psychiatry, 24*(11), 1627-1640. https://doi.org/10.1038/s41380-019-0412-6

Skelton, P. D., Poquerusse, J., Salinaro, J. R., Li, M., & Luikart, B. W. (2019, Dec 12). Activity-dependent dendritic elaboration requires Pten. *Neurobiol Dis, 134*, 104703. https://doi.org/10.1016/j.nbd.2019.104703

Steward, O., Yee, K. M., Metcalfe, M., Willenberg, R., Luo, J., Azevedo, R., Martin-Thompson, J. H., & Gandhi, S. P. (2021, Mar 31). Rostro-Caudal Specificity of Corticospinal Tract Projections in Mice. *Cereb Cortex, 31*(5), 2322-2344. https://doi.org/10.1093/cercor/bhaa338

Sunnen, C. N., Brewster, A. L., Lugo, J. N., Vanegas, F., Turcios, E., Mukhi, S., Parghi, D., D'Arcangelo, G., & Anderson, A. E. (2011, Nov). Inhibition of the mammalian target of rapamycin blocks epilepsy progression in NS-Pten conditional knockout mice. *Epilepsia, 52*(11), 2065-2075. https://doi.org/10.1111/j.1528-1167.2011.03280.x

Super, H., & Soriano, E. (1994, Jun 1). The organization of the embryonic and early postnatal murine hippocampus. II. Development of entorhinal, commissural, and septal connections studied with the lipophilic tracer DiI. *J Comp Neurol, 344*(1), 101-120. https://doi.org/10.1002/cne.903440108

Toni, N., & Schinder, A. F. (2015, Dec 4). Maturation and Functional Integration of New Granule Cells into the Adult Hippocampus. *Cold Spring Harb Perspect Biol, 8*(1), a018903. https://doi.org/10.1101/cshperspect.a018903

Toni, N., Teng, E. M., Bushong, E. A., Aimone, J. B., Zhao, C., Consiglio, A., van Praag, H., Martone, M. E., Ellisman, M. H., & Gage, F. H. (2007, Jun). Synapse formation on neurons born in the adult hippocampus. *Nat Neurosci, 10*(6), 727-734. https://doi.org/10.1038/nn1908

Wang, Y., Wu, W., Wu, X., Sun, Y., Zhang, Y. P., Deng, L. X., Walker, M. J., Qu, W., Chen, C., Liu, N. K., Han, Q., Dai, H., Shields, L. B., Shields, C. B., Sengelaub, D. R., Jones, K. J., Smith, G. M., & Xu, X. M. (2018, Sep 12). Remodeling of lumbar motor circuitry remote to a thoracic spinal cord injury promotes locomotor recovery. *Elife, 7*. https://doi.org/10.7554/eLife.39016

Williams, M. R., DeSpenza, T., Jr., Li, M., Gulledge, A. T., & Luikart, B. W. (2015, Jan 21). Hyperactivity of newborn Pten knock-out neurons results from increased excitatory synaptic drive. *J Neurosci, 35*(3), 943-959. https://doi.org/10.1523/JNEUROSCI.3144-14.2015

Zhou, J., Blundell, J., Ogawa, S., Kwon, C. H., Zhang, W., Sinton, C., Powell, C. M., & Parada, L. F. (2009, Feb 11). Pharmacological inhibition of mTORC1 suppresses anatomical, cellular, and behavioral abnormalities in neural-specific Pten knock-out mice. *J Neurosci, 29*(6), 1773-1783. https://doi.org/10.1523/JNEUROSCI.5685-08.2009

Zukor, K., Belin, S., Wang, C., Keelan, N., Wang, X., & He, Z. (2013, Sep 25). Short hairpin RNA against PTEN enhances regenerative growth of corticospinal tract axons after spinal cord injury. *J Neurosci, 33*(39), 15350-15361. https://doi.org/10.1523/JNEUROSCI.2510-13.2013